CHIPPING AND BREAKAGE OF CARBIDE TOOLS

CHIPPING AND BREAKAGE OF CARBIDE TOOLS

by

ZAHER A. M. MASOOD, B.Sc. (Eng.)

A Thesis

Submitted to the School of Graduate Studies

in Partial Fulfilment of the Requirements

for the Degree

Master of Engineering

McMaster University

May, 1976

TO MY MOTHER

MASTER OF ENGINEERING (1976) McMaster University
(Mechanical Engineering) Hamilton, Ontario

TITLE: Chipping and Breakage of Carbide Tools

AUTHOR: Zaher Abdel Meged Masood,
B.Sc. (Production Eng.)
(Alexandria University, Alexandria, Egypt)

SUPERVISOR: Professor J. Tlusty

NUMBER OF PAGES: xv, 201

SCOPE AND CONTENTS:

The purpose of this project was to study the failure mechanisms of carbide tools in turning operations due to fracture of the cutting edge. The study consisted of a combination of turning tests, examination of fracture surfaces and an analysis of the stresses in the tool as produced by the cutting force. Thermal stresses are so far not considered. It is concluded that chipping is a ductile failure due to high shear stresses at the cutting edge and breakage is brittle fracture originating at the rake face at a local maximum of tensile stress.

For the finite element stress analysis a new method of successively refining mesh while diminishing the analysed area is introduced which is rather effective and economical in that all computation except for the final field is done only once for various loading cases.

ACKNOWLEDGEMENTS

My sincere gratitude and thanks are due to Dr. J. Tlusty for providing constant guidance and inspiration throughout the study.

The author also expresses his appreciation to Ms. BettyAnne Bedell and Ms. Barbara Eastman for typing the manuscript.

I gratefully acknowledge the financial assistance from the National Research Council of Canada and McMaster University.

TABLE OF CONTENTS,

		Page
CHAPTER 1	INTRODUCTION	1
CHAPTER 2	BASIC CHARACTERISTICS OF SINTERED CARBIDES AND SUMMARY OF KNOWLEDGE FOUND IN BIBLIOGRAPHY ON BREAKAGE OF CARBIDE TOOLS	4
2.1	Basic Characteristics of Sintered Carbide Tool Materials	4
2.1.1	Introduction	4
2.1.2	Method of Manufacturing Carbides	5
2.2	Failure of Carbide Tools	16
2.2.1	Tool Wear and Tool Failure Mechanisms	16
2.2.2	Parameters Affecting the Stresses in a Tool	19
	a) Thermally induced stresses	19
	b) Stresses generated by the cutting force	24
2.3	Parameters Significant for Failure of Cemented Carbides	26
2.3.1	Introduction	26
2.3.2	The Relation Between Fracture Toughness and the Material Parameters	27
2.3.3	Structural Parameters and their Influence on the Stress Distribution in the Binder Phase of Cemented Carbides	29
2.3.4	Standard Test Method for Measuring Material Properties	34
2.3.5	The Development of Test Method	36

		2.3.6 Introduction of Tool Fracture Classification System	38
CHAPTER 3		EXPERIMENTAL RESULTS	46
	3.1	Introduction	46
	3.2	Test Equipment and Materials	46
		3.2.1 Machine Tool	46
		3.2.2 Tool	46
		3.2.3 Workpiece	47
	3.3	Cutting Tests	50
	3.4	Fractography	75
	3.5	Fracture Mechanisms for Sintered Carbides	75
		3.5.1 Transgranular Fracture	75
		3.5.2 Intergranular Fracture	75
	3.6	Evaluation of Test Results	79
		3.6.1 Type of Fracture	79
		3.6.2 Chipping	79
		3.6.3 Breakage	82
CHAPTER 4		ANALYSIS OF STRESSES	95
	4.1	Introduction	95
	4.2	Definition of the Problem	95
	4.3	Stress Analysis of the Tool	112
		4.3.1 Solution Using Elementary Beam Theory (Cantiliver Beam in Bending)	112
		4.3.2 Solutions Using the Finite Element Technique	118
		A - Single step method	118
		B - Stepwise sub-dividing and refining method	146
CHAPTER 5		CONCLUSIONS	156

REFERENCES		159
APPENDIX A	Analysis of Stresses Using the Single Step Method	161
APPENDIX B	Resulting Stresses in the Case of Zero Rake Angle and No Flank Wear (a = 0.0 inch)	168
APPENDIX C	Derivation of the Replacement Matrix Used in the Method Suggested by Tlusty	178
APPENDIX D	Computer Program Used for Calculation of the Replacement Matrix in the First Step	182
APPENDIX E	Computer Program for Calculation of the Stresses in the Fifth Step	189

LIST OF TABLES

		Page
Table 1	Key properties of hard metal carbides	6
Table 2	Solubility of carbides in iron	8
Table 3	Chemical composition and hardness of wickaloy grades	47
Table 4	Chemical composition and hardness of steels 4340, 1040	50
Table 5	Test results in case of continuous cutting using tool number 1-a	51
Table 6	Test results in case of continuous cutting using tool number 1-b	53
Table 7	Test results in case of continuous cutting using tool number 1-c	54
Table 8	Test results in case of continuous cutting using tool number 2-a,b	55
Table 9	Test results in case of continuous cutting using tool number 3	56
Table 10	Test results in case of continuous cutting using tool number 4-a	57
Table 11	Test results in case of continuous cutting using tool number 4-b,c	58
Table 12	Test results in case of continuous cutting using tool number 5	59
Table 13	Test results in case of continuous cutting using tool number 6	60
Table 14	Test results in case of continuous cutting using tool number 7-a	61
Table 15	Test results in case of continuous cutting using tool number 7-b	62
Table 16	Test results in case of continuous cutting using tool number 8	63
Table 17	Test results in case of continuous cutting using tool number 9-a,b,c	65

Table 18 Test results in case of continuous cutting using tool number 10-a,b,c, 11 66

Table 19 Test results in case of interrupted cutting using tool number 1 67

Table 20 Test results in case of interrupted cutting using tool number 2-a,b 68

Table 21 Test results in case of interrupted cutting using tool number 3, 4 69

Table 22 Summary of tests results in case of continuous cutting 71

Table 23 Summary of tests results in case of interrupted cutting 73

Table 24 Chemical composition of the etcher used for removing the iron 82

LIST OF FIGURES

		Page
Figure 1.	Structure of WC-Co Combination	10
Figure 2.	The frequency of occurrence of narrow and wide particle size distribution as a function of spherical diameter in microns.	10
Figure 3.	Transverse rupture strength of sintered carbide as a function of mean grain size for various types of distributions.	11
Figure 4.	Hardness of straight tungsten carbide-cobalt grades (Adamas grades) as a function of cobalt content and grain size.	13
Figure 5.	Transverse rupture strength of straight tungsten carbide-cobalt grades as a function of cobalt content and grain size.	14
Figure 6.	Transverse rupture strength of sintered carbides at elevated temperature, according to Kreimer.	15
Figure 7.	Tool wear features	17
Figure 8.	Temperatures in the workpiece in the chip	21
Figure 9a,b	Tensile stresses in the tool	25
Figure 10.	The mean free path λ versus fracture toughness after results from Gurland and Pairkh	28
Figure 11.	The mean free path λ versus fracture toughness ε_{fT} for a number of carbide tool materials.	30
Figure 12.	Transverse rupture strength (σ_{fT}) as a function of mean free path for various compositions.	31
Figure 13.	The influence of grain size on tensile strength (σ_{fT}) and fracture strain (ε_{fT}) for straight carbides.	31
Figure 14.	a) Geometry of the Bridgman model b) Analogue for the structure of cemented carbides.	33

Figure 15.	The ultimate uniaxial strain (ε_{ft}, tensile test) as a function of d_{av}/λ_{av}	35
Figure 16.	The ultimate uniaxial strain (ε_{fT}, bending test) vs. the ratio d_{av}/λ_{av} for a number of commercial grades	35
Figure 17.	Distribution of stresses of a diametrical loaded circular disc.	37
Figure 18.	Stress distribution across the diagonals of a diagonally loaded square specimen.	39
Figure 19.	Safety chart of the chipping at low cutting speed.	41
Figure 20.	Typical location and appearance of various types of fatigue cracks.	43
Figure 21.	Fatigue tool life of P20 tungsten carbide determined by the chipping starting on the flank and or the chipping starting on the rake face.	44
Figure 22.	Example of breakage (Tool grade K7H)	45
Figure 23.	Dimensions of the tool	48
Figure 24.	Microstructure of K7H carbide grade	48
Figure 25.	Microstructure of K45 carbide grade	49
Figure 26.	Microstructure of WP5 carbide grade	49
Figure 27.	Microstructure of WP6 carbide grade	49
Figure 28.	Optical micrograph showing a transgranular crack	76
Figure 29.	Types of intergranular fracture	78
Figure 30.	Optical micrograph showing an intergranular crack	78
Figure 31.	Chipping of the edge (K45 tool grade)	80
Figure 32-a	Stereo picture of chipping area at the nose of the tool, WP6	81

Figure 32-b	Chipping area near to the tool nose WP6	81
Figure 33-a	Chipping area after etching, WP6	83
Figure 33-b	Chipping area after etching, K45	83
Figure 34-a	Crack on the rake face of K7H carbide grade	84
Figure 34-b	End of the same crack as figure 34-a with high magnification	84
Figure 35-a	Microcrack on the rake face of K45 carbide grade tool	86
Figure 35-b	Stereo view of the same microcrack as figure 35-a	86
Figure 36-a	Microcrack on the rake face of the same tool as figure 35	87
Figure 36-b	Microcrack with high magnification, K45 tool grade	87
Figure 37.	Fracture surface at K7H carbide grade tool	88
Figure 38.	Fracture surface of the same tool as figure 37 taken from another view	88
Figure 39.	Fracture surface of K7H carbide grade tool	89
Figure 40.	Fracture surface of K45 carbide grade tool	89
Figure 41.	Stereo picture of fracture surface of K45 carbide grade tool	90
Figure 42.	Fracture surface of K45 carbide grade tool	90
Figure 43.	Stereo picture of fracture surface WP6	91
Figure 44.	Stereo picture of fracture surface WP6	92
Figure 45.	Stereo picture of fracture surface WP5	93
Figure 46-a	The load distribution (normal and shear loads) on the rake face and on the flank	97

Figure 46-b	Mesh used in the Finite Element Computation (single step method)	98
Figure 47.	Diagrammatical representation of the problem	100
Figure 48.	The area of interest (B) with refined mesh and imposed the displacement boundary conditions (δ_b)	103
Figure 49.	The area of interest (B) with refined mesh and imposed a very stiff springs (K_b) and external force (F_b) on boundary b	106
Figure 50.	Substructures A and B	108
Figure 51.	Stepwise and subdividing and refining method (Tlusty's approach)	111
Figure 52-a	Normal stress contours using the classical solution	113
Figure 52-b	Maximum principal stress contours using the classical solution	114
Figure 52-c	Minimum principal stress contours using the classical solution	115
Figure 52-d	Maximum shear stress contours using the classical solution	116
Figure 52-e	Direction of maximum principal stresses and maximum shear stresses using the classical solution	117
Figure 53-a	Computed maximum principal stress in the loading region	119
Figure 53-b	Computed maximum principal stress in the tool and tool holder	120
Figure 54.	Computed minimum principal stress in the loading region	121
Figure 55.	Computed maximum shear stress in the loading region	122
Figure 56-a	Directions at maximum principal stress and at maximum shear stress in the loading region	126

Figure 56-b	Directions of maximum principal stress and at maximum shear stress in the tool	127
Figure 57.	Computed maximum principal stress in the loading region	131
Figure 58.	Computed minimum principal stress in the loading region	132
Figure 59.	Computed maximum shear stress in the loading region	133
Figure 60.	Computed maximum principal stress in the loading region	134
Figure 61.	Computed minimum principal stress in the loading region	135
Figure 62.	Computed maximum shear stress in the loading region	136
Figure 63-a	Computed maximum principal stress in the loading region	138
Figure 63-b	Computed maximum principal stress in the tool and tool holder	139
Figure 64.	Computed minimum principal stress in the loading region	140
Figure 65.	Computed maximum shear stress in the loading region	141
Figure 66-a	Computed maximum principal stress in the loading region	142
Figure 66-b	Computed maximum principal stress in the tool and tool holder	143
Figure 67.	Computed minimum principal stress in the loading region	144
Figure 68.	Computed maximum shear stress in the loading region	145
Figure 69.	Dimensions of the fifth step (loading region)	147
Figure 70.	Computed maximum principal stress in the loading region	148

Figure 71. Computed minimum principal stress in the loading region 149

Figure 72. Computed maximum shear stress in the loading region 150

Figure 73. Computed maximum principal stress in the loading region 152

Figure 74. Computed minimum principal stress in the loading region 153

Figure 75. Computed maximum shear stress in the loading region 154

CHAPTER 1

INTRODUCTION

Tool wear in metal cutting is characterized by a number of various features. Flank wear and crater wear are accepted as a regular phenomenon. They grow rather uniformly with the time of cutting. Chipping of the edge and breakage are both irregular phenomena and their development is difficult to predict and they should be avoided completely if possible. Breakage is the most dangerous of all the various tool wear features because it may lead to damage of the workpiece and/or of the machine.

Sintered carbides are one of the most important cutting tool materials. They offer an unsurpassed combination of hardness and strength. Therefore, many attempts have been made to evaluate the significant parameters resulting in failure of sintered carbides.

In the present work an attempt has been made to study the mechanisms of chipping and breakage of carbide tools.

Failure of steel cutting grade carbide tools due to the fracture of the cutting edge was investigated in turning operations. Three types of work material were used (steel 1040, steel 4340 and steel 4340 hardened and tempered to 380 BHN. The purpose was to try and correlate tool failure with an analysis of the stresses in the tool caused by the

cutting force. Thermal effects have so far been neglected. The study consisted of metal cutting tests (continuous and interrupted) in which tools were tested until they failed due to fracture.

The study of fracture in sintered carbides on a microscopic scale has been limited mainly to the optical examination of surface cracks on the intersection of fracture surfaces with polished surfaces. The large depth of focus of the Scanning Electron Microscope has permitted the examination of fractured surfaces. The fractured surfaces of the carbide tools were examined and a stereo picture for both chipping and breakage were obtained and examined to investigate the fracture phenomena of each. The stress distribution on the tool and on a special area of interest (tool wedge) was carried out using the Finite Element Method. The method is especially useful for stress analysis problems which cannot be solved by classical theory. The problem is mainly the analysis of local stresses in the tool wedge. The computations were carried out using two different methods of mesh generation. The first method was named "The Single Step Method" in which the computation work was carried out in one step. Also, a stepwise subdividing and refining method was used for investigating the stresses in the tool wedge. Using this method the computation work was carried out in a number of steps ending with the area of interest with a very fine mesh in which stresses could be obtained in great detail.

A new algorithm was developed which makes it possible

to investigate stresses at various loads without repeating these successive steps of computation.

By comparing the cutting test results, analysis of fractures surfaces and the stress fields, it was concluded that chipping is a ductile failure due to shear stresses close to the cutting edge while breakage is a brittle fracture phenomenon originating at a certain distance from the cutting edge. It is assumed that the work will be continued to include the temperature effects.

CHAPTER 2

BASIC CHARACTERISTICS OF SINTERED CARBIDES AND SUMMARY OF KNOWLEDGE FOUND IN BIBLIOGRAPHY ON BREAKAGE OF CARBIDE TOOLS

2.1 Basic Characteristics of Sintered Carbide Tool Materials

2.1.1 Introduction

Tungsten carbide was discovered by Moissan in about 1890. However, at that time it was of no value as a cutting tool material, since fabrication into cutting tools was not possible due to decomposition at the high temperatures required for sintering. A solution to this problem was found by Schroter in 1923 when he mixed tungsten carbide with cobalt powder, the mixture being sintered at about 1320^{o}C (melting point of cobalt). The actual cutting tool material was introduced around 1933 by Krupp in Germany under the name of Widia. The name implies "like diamond". Although it actually is by far not as hard as diamond, the sintered WC with Co binder offered and practically offers still today an unsurpassed combination of hardness and strength. It was its ability to retain high hardness up to temperatures of 800^{o}C to 1000^{o}C compared to high speed steels which lose substantially their hardness at temperatures in the range of 500 ^{o}C to 700^{o}C which made it an instant success in machining non-ferrous materials and cast iron. However, it was soon discovered that in machining steel it suffered from severe

cratering on the rake face. This was remedied by the introduction, almost a decade later, of the complex tungsten carbide and titanium carbide (WC + TiC). In spite of some recent developments in tool materials sintered carbides are still the most important cutting tool materials.

2.1.2 Method of Manufacturing Carbides

Based on powder metallurgy techniques, the procedures to manufacture sintered carbides for tools are:

1. Tungsten oxide reduced by hydrogen results in tungsten powder.
2. Milling of tungsten with carbon (lamp black), blending in fine mixture in a ball mill, heating and carburizing.
3. Ball milling (several days) together with cobalt.
4. Waxing to impart some coehesion and lubrication.
5. Cold compacting at pressures up to 60,000 psi using dies of alloy steel. Dies must be larger to account for shrinkage during subsequent sintering.
6. Presintering (816^{o}C) in hydrogen, removing the lubricant, shaping, and machining if necessary.
7. Sintering (at temperatures in the range of 1370^{o}C to 1593^{o}C) in hydrogen or in a vacuum, so the cobalt melts and tungsten carbide dissolves partly in cobalt, diffuses and forms a strong matrix.

In items 1 to 7 any oxidation should be prevented.

Densification occurs by liquid phase sintering above the melting point of the binder phase (1320°C) [1]. The process takes place in three overlapping stages:

1. Rearrangement of the particles into a dense packing by particle transport under the influence of the surface tension of the liquid.
2. Solution and reprecipitation of WC in and out of the liquid resulting in further densification and particle growth.
3. Coalesence and welding of carbide particles, which may interfere with further densification.

Various types of hard metallic carbides have been considered for cutting tools. The hardness and melting point values for a number of them are assembled in Table 1, in a sequence of decreasing hardness.

TABLE 1. KEY PROPERTIES OF HARD METAL CARBIDES

Material		Microhardness (kg/sq.mm)	Melting Point (F)	(C)	Theoretical Density (g/cm^3)
TiC	Titanium carbide	3200	5790	3200	4.94
VC	Vanadium carbide	2950	5125	2830	5.71
HfC	Hafnium carbide	2700	7030	3890	12.76
ZrC	Zirconium carbide	2560	6380	3530	6.56
CbC	Columbium carbide	2400	6330	3500	7.80
Cr_3C_2	Chromium carbide	2280	3440	1895	6.66
WC	Tungsten carbide	2080	4710	2600	15.67
Mo_2C	Molybdenum carbide	1950	4850	2400	9.18
TaC	Tantalum carbide	1790	6835	3780	14.50

Brief comments can be made regarding their individual practical usefulness [2].

- Titanium Carbide (TiC) is essential to be added to tungsten carbide to impart crater resistance for machining steel as cutting speed increases.
- Vanadium Carbide (VC) has never been properly cemented together to form a strong body and is used only, to a small extent, as an additive to control grain growth.
- Hafnium Carbide (HfC) is expensive and has only recently become available in quantity conditions. This applies also to Zirconium Carbide (ZrC). Neither of these appears to be suitable as a cemented carbide except as an additive.
- Columbium Carbide (CbC), which also has been used as an additive to control grain growth and to improve crater resistance in steel machining grades, is generally associated with Tanalum Carbide (TaC).
- Chromium Carbide (Cr_3C_2) cannot be properly bonded or cemented and, therefore, is used only, to a limited extent, as an additive for grain growth control.

Thus the two most important classes remain to be the "straight" grades of WC-Co combination and the "steel cutting" grades of (WC + TiC, WC) - Co combination. In order to understand their properties, Table 2 shows the affinity of the various carbides to iron [3].

TABLE 2. SOLUBILITY OF CARBIDES IN IRON

Carbide	Solubility in Iron at 1250°C
Tungsten Carbide (WC)	7%
Titanium Carbide (TiC)	Less than $\frac{1}{2}$%
50/50 TiC/WC solid solution	$\frac{1}{2}$%
Tantalum Carbide	$\frac{1}{2}$%

Tungsten Carbide easily dissolves in iron. Therefore, when machining steel rather extensive diffusion occurs on the rake face of the tool over which the hot chip is sliding. The underside of the chip is freshly generated non-contaminated steel and the tool material readily dissolves in it and a crater is generated on the face of the tool. Because the chip slides away and continuously a new chip surface is created no saturation by the diffusing WC can occur and the diffusion rate is kept high. In machining cast iron this does not occur because cast iron is already rather saturated with carbon. This would not occur with TiC which, therefore, would be very crater resistant.

However, similarly as with iron, WC is rather well soluble in cobalt while TiC is not. In the structure of the WC-Co combination the WC grains are bonded together by a thin intermediate layer of, actually, solid solution of WC in Co (Fig. 1).

This is what makes the bond so strong. There is an ideally thin layer of the (WC + Co) bond which gives the best

strength. A thick layer would be in the middle almost pure Co with much less strength.

Actually, in order to obtain a good uniformly thin uninterrupted layer it is important that high uniformity of grain size be maintained. Graphs in Figures 2 and 3 illustrate this, reproduced from [1].

In Figure 2, two types of grain size distributions are shown, one wide and one narrow, both centered on 4 microns diameter. In Figure 3 the transverse rupture strength of sintered carbide is shown as a function of mean grain size for various types of distributions. It is seen that the narrow distribution gives up to 400,000 psi strength and exceeds that of the wider distribution by about 15%.

It is understood that a bond layer which is too thin leads to harder, however, more brittle grades. A thicker layer of Co, which is more ductile than WC imparts the material better impact resistance.

Because of the bad solubility of TiC in Co a sintered material of a TiC-Co combination would have very little strength. Therefore the steel cutting grades are made either as a combination of complex (WC + TiC) carbides with up to 50% TiC content and Co, or complex (WC + TiC) carbides, simple WC carbides and Co (the three-phase carbide).

In both the basic classes of straight and steel cutting grades the amount of cobalt content influences both hardness and strength. Actually, in general, the hardness of a sintered carbide is determined by the carbide grains while its strength is determined by the strength of the binder.

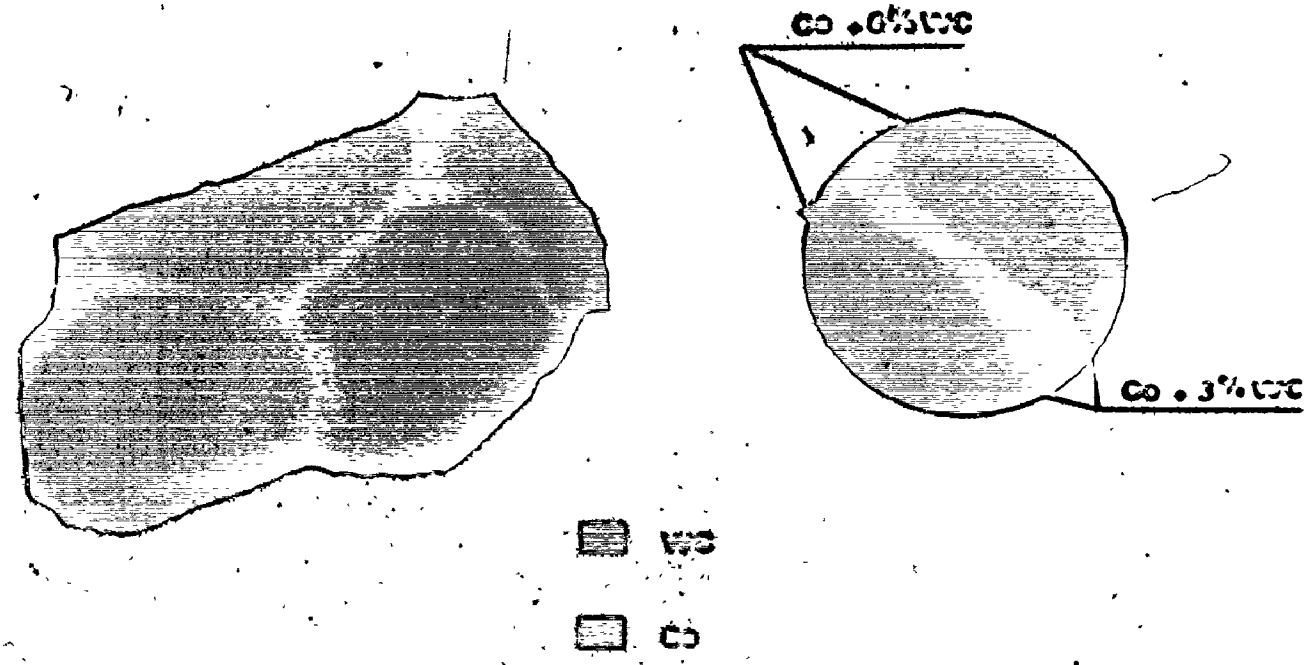

Figure 1. Structure of WC-Co Combination.

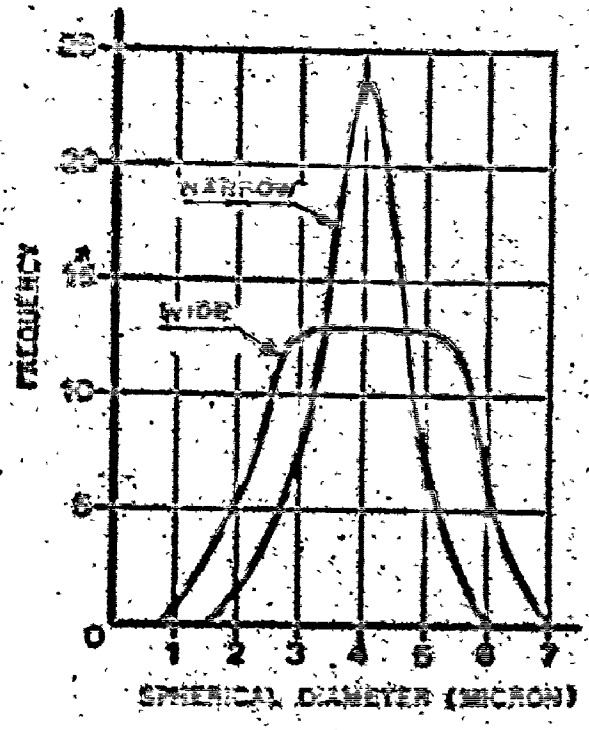

Figure 2. The Frequency of Occurrence of Narrow and Wide Particle Size Distril a Fi of

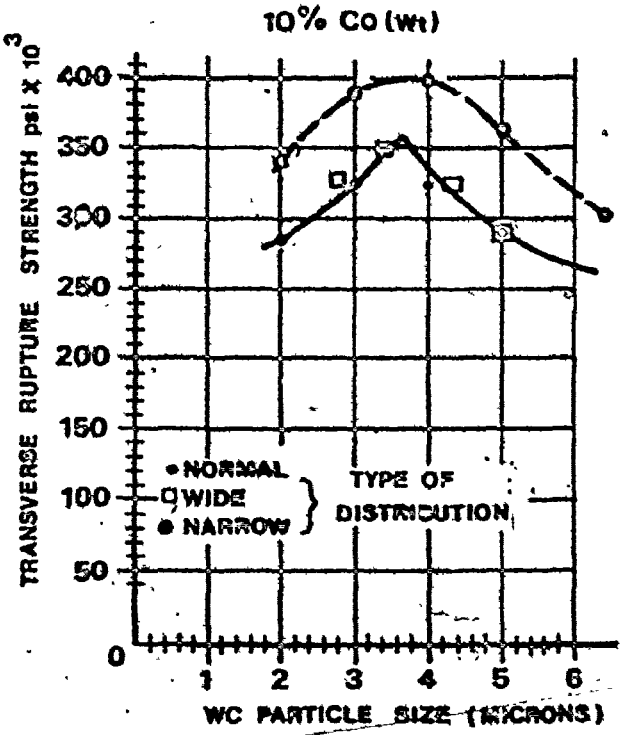

Figure 3. Transverse Rupture Strength of Sintered Carbide as a Function of Mean Grain Size for Various Types of Distributions.

Therefore, naturally, with the increase of cobalt content hardness decreases and strength increases (the latter up to a certain percentage, 15 to 20 wt.%). The grain size has an influence too.

The effect of cobalt content on hardness is shown in Figure 4 and on transverse rupture strength in Figure 5 [2]. In this respect it is fair to include also the effect of temperature. Thus, the comparison of strength of the various classes of sintered carbides inclusive effect of temperature is shown in Figure 6 reproduced from [4], based on [5].

It is seen that in general, and especially so at room temperature, the straight grades are the strongest ones and they are about 1.5 times stronger than the three-phase carbides. With temperature the straight grades lose hardness faster than the complex grades and they are equally strong at 500°C. At higher temperatures the straight grades are again much better.

Thus, while the addition of TiC strongly improves crater resistance it leads to some loss of strength. Therefore, recently new developments were based on:

a) Coating a thin layer (5 microns) of purely TiC on a strong WC-Co combination base.

b) Developing sintered carbide of TiC and MoC with Ni as a binder.

The solution a) is being rather widely accepted while the material b) is still rather limited in practical

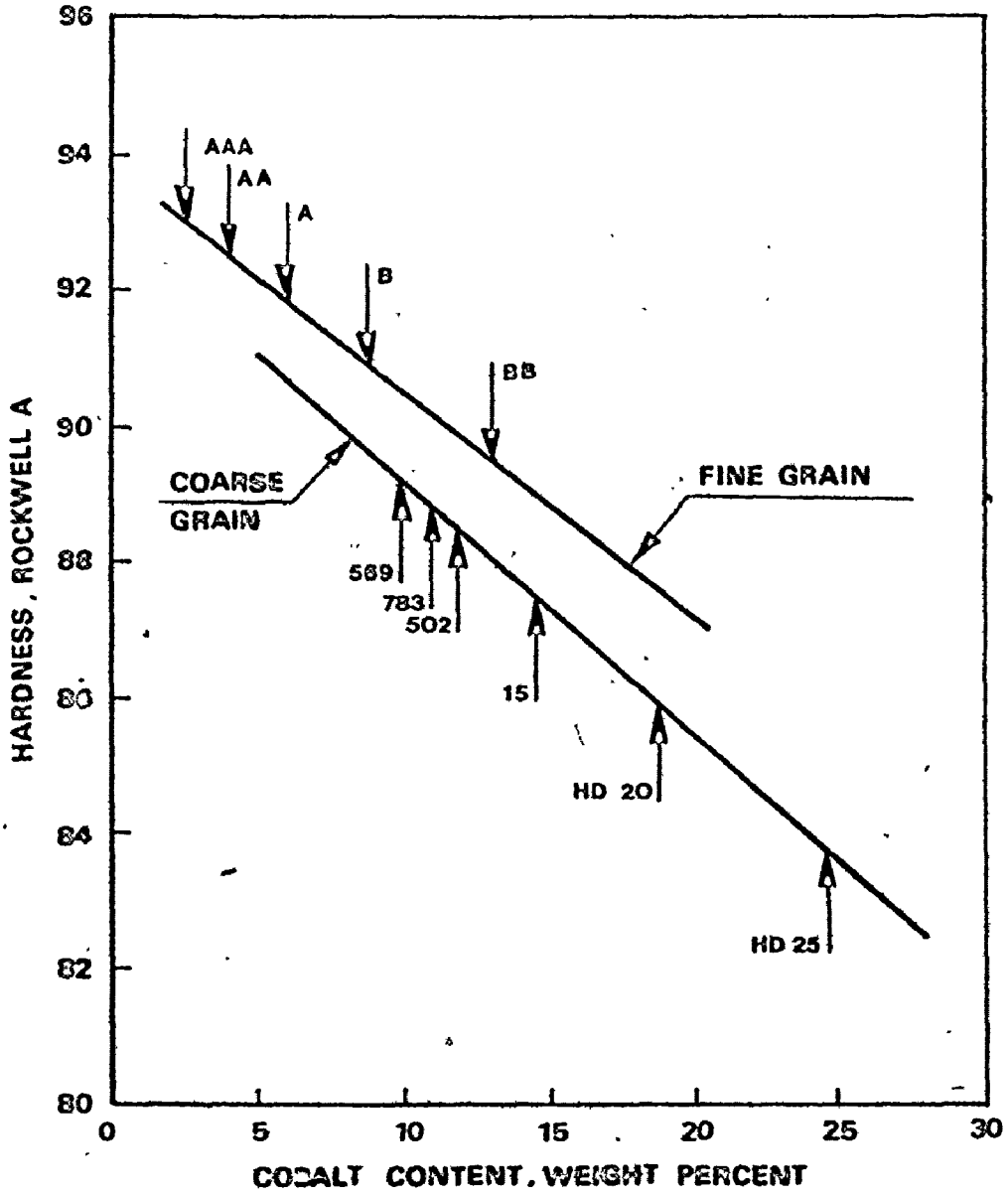

Figure 4. Hardness of Straight Tungsten Carbide-Cobalt Grades (Adamas Grades) as a Function of Cobalt Content and Grain Size.

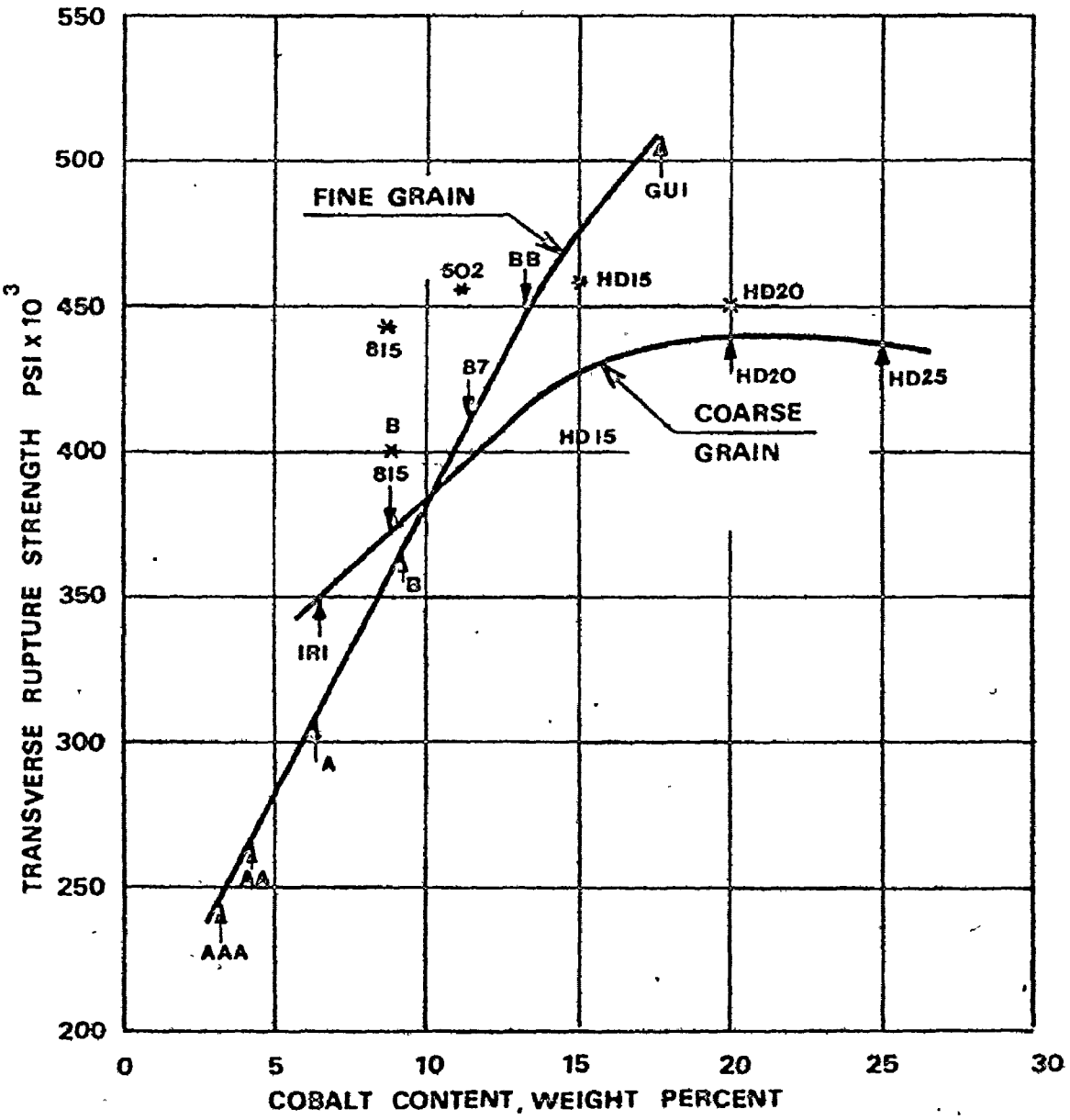

Figure 5. Transverse Rupture Strength of Straight Tungsten Carbide-Cobalt Grades as a Function of Cobalt Content and Grain Size.

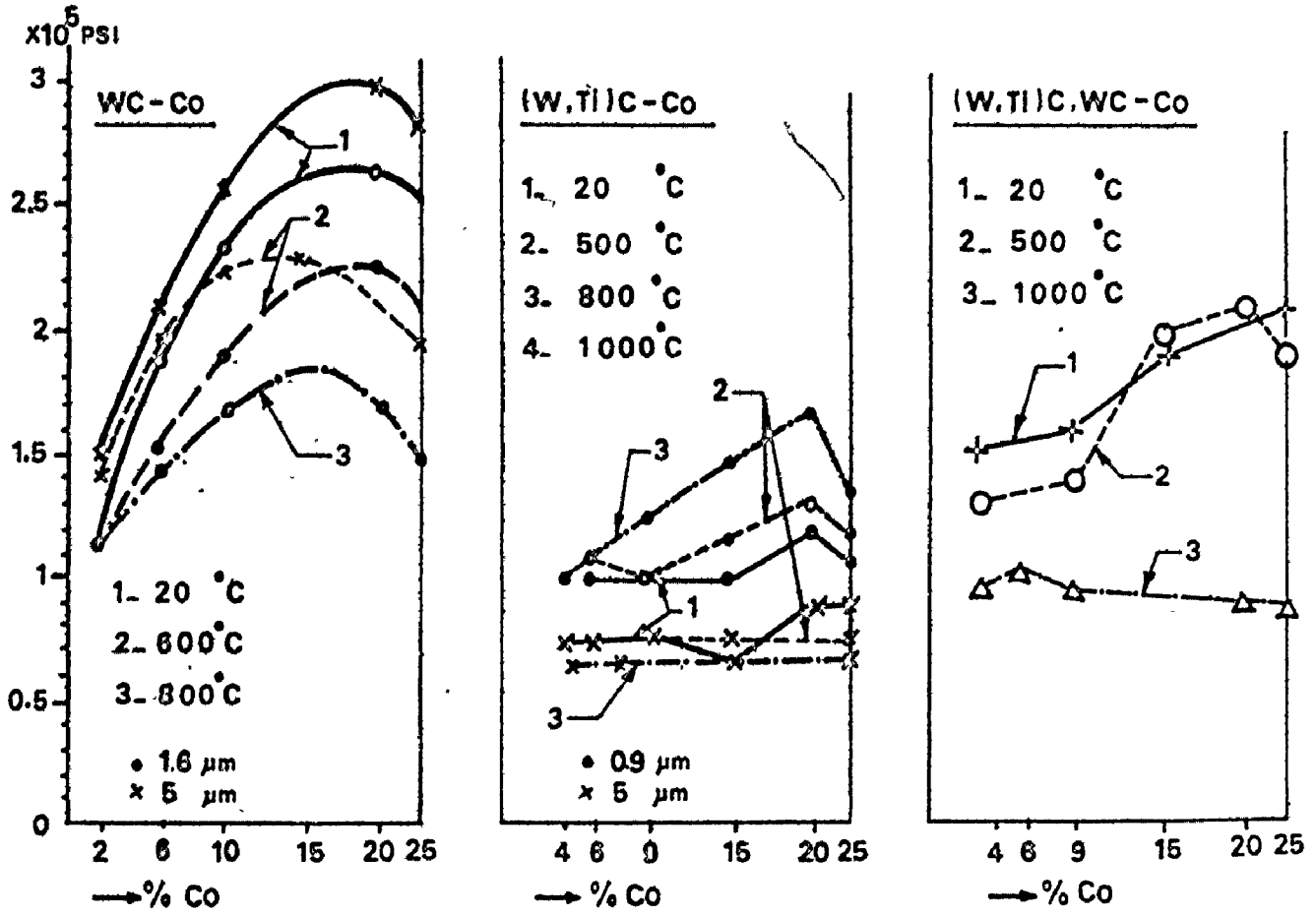

Figure 6. Transverse Rupture Strength of Sintered Carbides at Elevated Temperature, According to Kreimer.

applications.

Other recent developments in cutting tool materials were non-carbides like Borazon (cubic boron nitride) and UCON (an alloy of Columbium (Cb), Titanium (Ti) and Tungsten (W); nitrided at its surface.)

2.2 Failure of Carbide Tools

2.2.1 Tool Wear and Tool Failure Mechanisms

Tool wear in metal cutting is characterized by a number of various features which are diagrammatically summarized in Figure 7 [4].

There the flank wear FW may be distinguished which is caused by the rubbing of the workpiece material on the flank, i.e., on the relief side of the main cutting edge, of the nose radius and of a part of the secondary edge, crater wear CW which is due to the sliding of the chip on the rake face of the tool, the notch N which develops on the main cutting edge at the point which cuts the surface of the workpiece, chipping CH of the edge, cracks CR which may be parallel with or transversal to the cutting edge, breakage BR of the tool nose, plastic deformation PD of the tool nose.

Of all these forms of wear the flank wear FW is always present and it is accepted as the regular phenomenon. The flank wear width increases rather regularly with the time of cutting. Flank wear is usually accepted as the criterion for tool life which is considered terminated when flank wear width reaches a certain limit value. The crater wear CW is another rather regular phenomenon. It does not occur always but

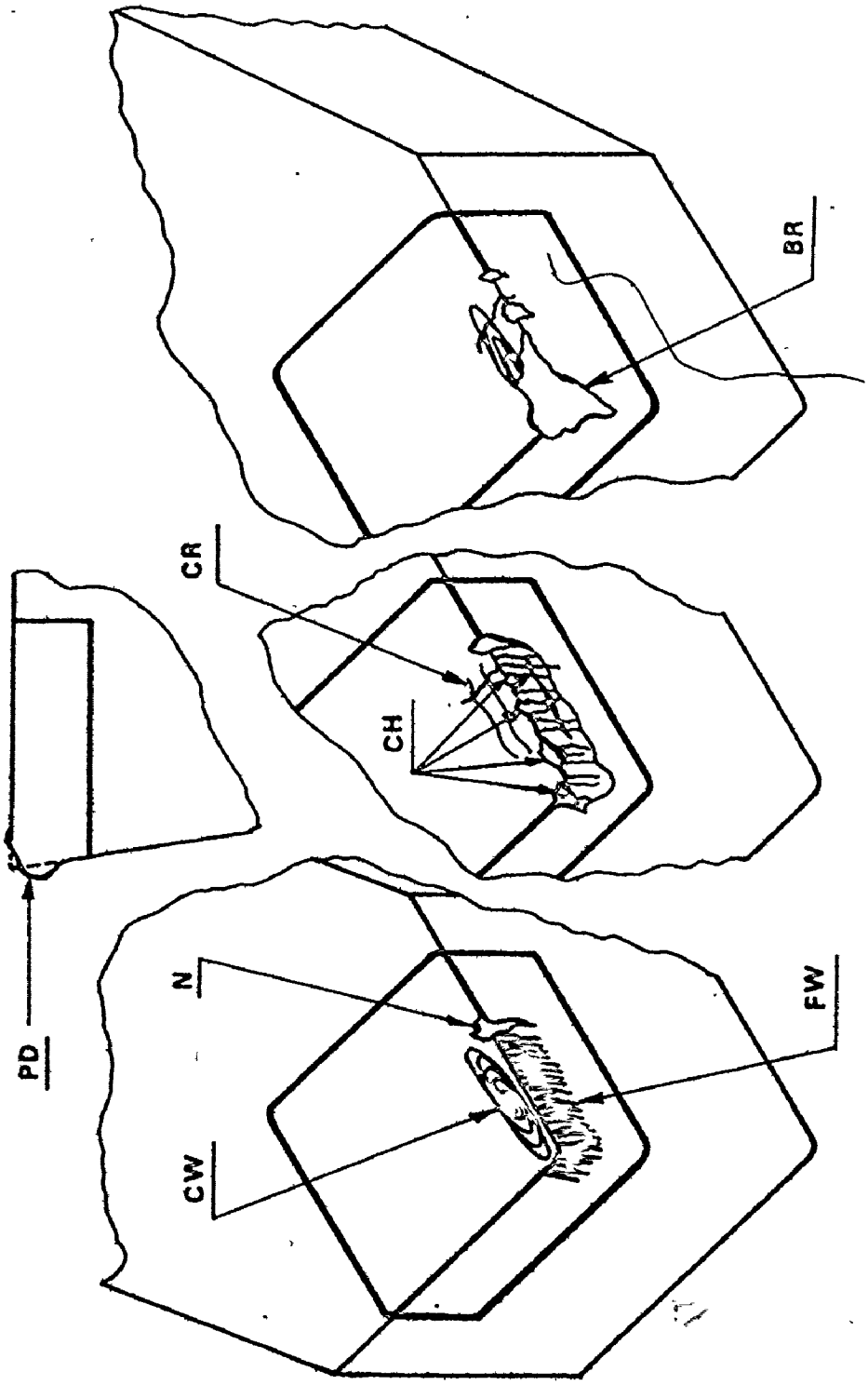

Figure 7. Tool Wear Features.

whenever it does it also grows rather uniformly with time. The time of cutting during which both FW and CW will not exceed an unwanted value can be fairly well predicted.

All the other mentioned phenomena are rather irregular and their development is difficult to predict and they should be avoided completely if possible by a suitable choice of tool material, tool geometry and cutting conditions, mainly of cutting speed and feed (chip thickness). Chipping of the edge and breakage might be considered both to be phenomena of primarily brittle fracture and differ mainly by their magnitude and they are related to the phenomenon of cracks. On the contrary, plastic deformation is mainly associated with the loss of compressive strength of the tool material at high cutting temperatures. Breakage is the most dangerous of all the various tool wear features because it may lead to damage of the workpiece and/or of the machine. Breakage and chipping as brittle fractures develop from macrocracks which result from interlinking of microcracks originating in points where the tensile stress exceeds the tensile strength. More precisely, it is recently recognized that the limit is imposed on tensile strain rather than on tensile stress which, of course, involves the modulus of elasticity of the material concerned. An ultimate admissible tensile stress value could be obtained once the modulus of elasticity is given.

Brittle fracture is a rather probabilistic phenomenon and it depends very much on the existence of cracks and voids in the material prior to its stressing. In this instance it

very often depends strongly on the surface quality of the stressed specimen. However, it is found that breakage of carbide tools is also affected by fatigue and consequently the specimens fail at lower stress values if the stress is of a periodically variable nature as, for example, in interrupted cutting. This shows that breakage is not purely brittle in character.

Chipping occurs close to the cutting edge where a very high temperature is developed. The binder (cobalt) would lose its strength and becomes ductile to a certain degree due to the high temperature generated during the cut. The results obtained using the finite element technique agreed rather well with those of Loladze [6]. Both of them showed compressive stresses near the cutting edge contact area between chip and tool and almost no tensile stresses responsible for the brittle fracture are found. Chipping is thus considered as being more of a ductile than brittle fracture phenomenon.

2.2.2 Parameters Affecting the Stresses in a Tool

As mentioned earlier, brittle fracture fundamentally is associated with tensile stresses. In a tool these may be due to two basically different causes:

a) The thermal load

b) The load by the cutting force

a) Thermally induced stresses

When the tool starts cutting a high temperature

develops very quickly on the rake face due to the contact with the chip which has been heated as a result of plastic work in the shear zone and also due additionally to the friction work (or, more precisely due to the plastic flow in the layer of the chip which is close to the rake face of the tool) and the flank of the tool heats up as well due to friction between the machined surface and the tool. Subsequently, as part of the heat is conducted away through the insert and, further through the holder, the temperature inside the insert increases too. In a short time the temperature field in the insert reaches a steady balanced state. A typical example of temperatures in the chip and workpiece as are obtained in machining steel with carbide tools is given in Figure 8. In this example the maximum temperature on the rake face of the tool reached 750°C. During the heating up period of the tool when the outer parts of the insert expand more than the inside, compression stresses only are produced in the insert.

However, when the tool stops cutting its outside is cooled first by air or by cutting fluid, and the cooling of the interior follows later. The outer parts are shrinking and tensile stresses are created. These are greater when cooling is efficient. Therefore, use of coolants is not recommended in high speed machining with carbides.

Tlusty [4] shows that the important parameters which influence the resistance to thermal shock are the Coefficient of Thermal Expansion α and Thermal Conductivity K. It is

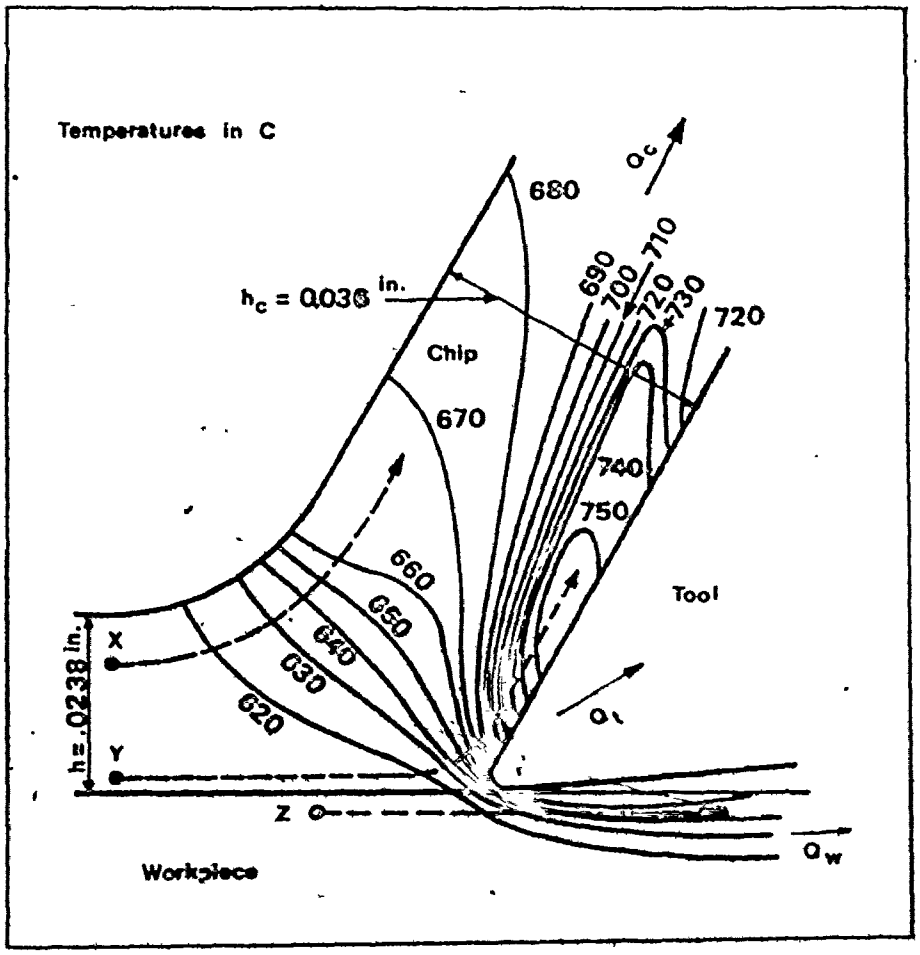

Figure 8. Temperatures in the Workpiece and in the Chip.

obvious that the greater is α, the greater stress is induced by a given temperature gradient because of greater differences of expansion of the corresponding layers of the tool. For a given heat flux the temperature gradients in the tool will be smaller for materials with better conductivity K.

Various authors define then the resistance to thermal shock in various ways but always it is proportional to the ratio of K/α.

The formula of Kals [7] is:

$$R_t = \epsilon_f \frac{K}{\alpha} \quad , \quad \epsilon_f = \alpha \Delta\theta \tag{2.1}$$

where ϵ_f is the ultimate tensile strain of the given material.

The thermal stress of a clamped tool-bit can be expressed by:

$$\sigma_\theta = \alpha \Delta\theta \ . \ E \tag{2.2}$$

So, let the thermal load be characterized by a heat flux ϕ per unit area then:

$$\frac{\Delta\theta}{L} = \frac{\phi}{K} \tag{2.3}$$

where L = length of thermal path

ϕ = heat flux

$$\therefore \quad \sigma_\theta = \frac{\alpha E}{K} \phi L \tag{2.4}$$

In this equation the thermal stress sensitivity S_t is

represented by $\frac{\alpha E}{K}$ which is not just simply the inverse of R_t because it involves also the modulus of elasticity E.

The parameter which is of greatest importance for breakage either due to the cutting force or due to the thermal stress is the tensile strength or the ultimate tensile strain. This parameter is generally measured by means of a bending test and the values of maximum tensile stress induced in this test at the fracture load are called the Transverse Rupture Strength, TRS.

Data on Transverse Rupture Strength of various types of carbides at various temperatures may be found in the book of Kreimer [5]. From this reference the graphs given in Figure 6 are compiled. In these graphs the values of TRS are plotted with respect to the Co content in the sintered carbide and the various curves apply to different temperatures in the range of room temperature of 20°C up to 800°C and 1000°C respectively. In the two first graphs also, the effect of carbide grain size is shown using very fine grain and rather coarse grain types.

Briefly, the TRS of all kinds of carbide grades depends strongly on the content of cobalt, the best percentage of which is between 15 and 20 wt. %. The "straight" grades are much stronger than the steel cutting grades at room temperature but they start losing the strength with increasing temperature above about 500°C.

The steel cutting grades are less sensitive to increased temperature and the strength of certain of these grades actually improves and attains a maximum at about 500°C

to 800°C and is almost equal to the strength of the straight grades in this temperature range.

b) Stresses generated by the cutting force

There have been attempts to experimentally determine the distribution of stresses in the tool loaded by the cutting force. Several authors used a method where photoelastic analysis was applied to a tool made of transparent plastic which was used to cut lead at rather low cutting speeds (at higher speeds the plastic would lose its strength due to the temperature generated during the cut). One of these investigators was Loladze [6].

In Figure 9-a a typical example is shown of the distribution of stress on the rake face of a tool with 10° positive rake angle. The stress is plotted in relation to the distance y from the cutting edge and C is the length of contact between the chip and the rake face. For $y < C$ the stress is compressive with a maximum value at the distance $y = 0.4C$. For $y > C$ the stress is tensile with a maximum at $y = 2C$. Loladze investigated the effect of the rake angle on the value of maximum tensile stress which in general was found proportional to the chip thickness a.

In Figure 9-b the relative value of the maximum tensile stress as measured in photoelastic fringe orders is plotted versus chip thickness a (inch) for rake angles: 1) $+20^{\circ}$, 2) 0°, 3) -20°.

It is seen that the maximum tensile stress was found to be about seven times lower for $\alpha = -20^{\circ}$ than for $\alpha = 20^{\circ}$.

(a)

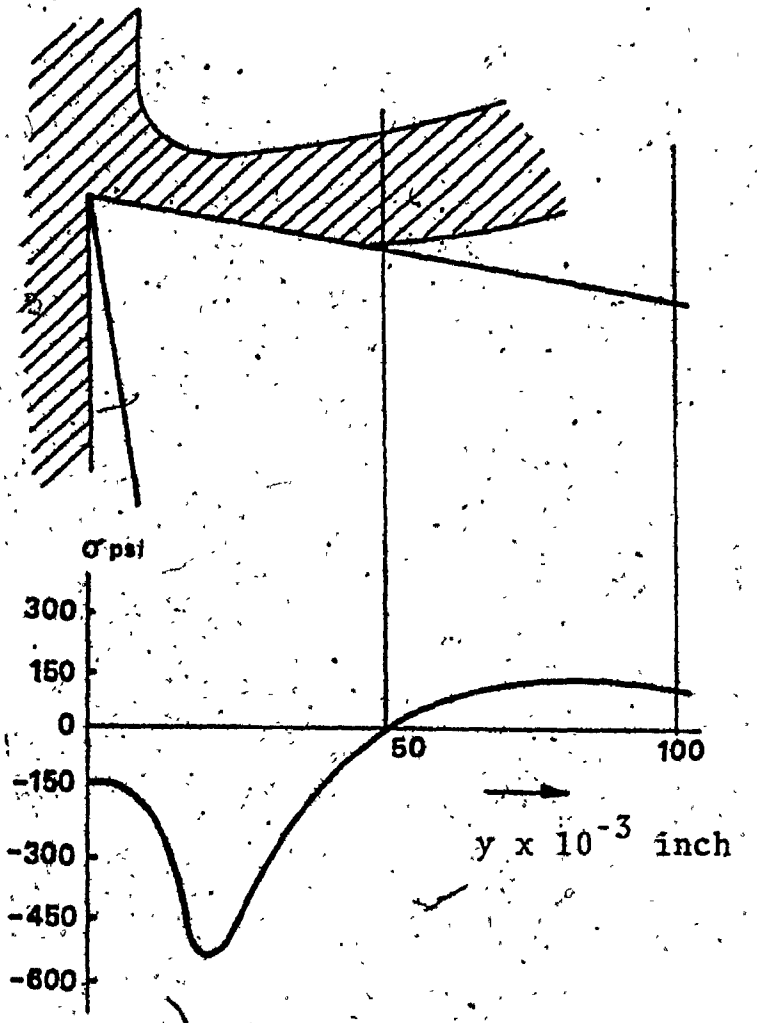

(b)

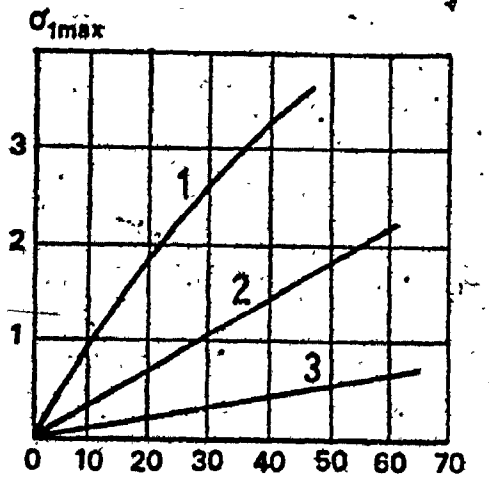

Figure 9(a), (b). Tensile Stresses in the Tool.

A very systematic work in this area was carried out by Primus, [8]. He used glass tools to machine aluminum and a diamond tool to machine various steels and, again, applied photoelastic analysis. He did not evaluate stresses in the tool but concentrated on determining the distribution of the cutting load on the rake and flank faces.

2.3 Parameters Significant for Failure of Cemented Carbides

2.3.1 Introduction

Brittle fracture of cemented carbides is an important factor in cutting tool performance. It has been observed that the strength and toughness of cemented carbides are predominantly influenced by grain size and the thickness of the binder layer. Some investigators have determined a significant dependence of strength on the isostatic stress component. This dependence was found to increase with a decreasing percentage of the binder content.

An attempt has been made by Kals [9] to evaluate the ratio of the effective stress ($\bar{\sigma}$) and the maximum tensile stress (σ) component within the binder ($C = \bar{\sigma}/\sigma$) in relation to strength.

It has been shown that the ultimate tensile strain can be related to C. In turn, the parameter C is dependent on structural parameters.

Recently, Shaw et al. [10] came to the conclusion that the maximum tensile strain criterion is a reliable tool for predicting brittle fracture. However, measurement of

small strain is substantially more difficult than the measurement of load. Subsequently the ultimate strain is preferentially derived from $\varepsilon_f = \frac{\sigma_f}{E}$. There is more evidence that ε_f is an adequate parameter for brittle material.

From the results of Gurland and Parikh [11] it appears that ε_f may satisfy as a criterion for fracture toughness of cemented carbides when the carbide contents exceed 60%.

Hatano [12] and Brands [13], who examined the influence of the deformation rate and the isostatic stress component on brittle fracture respectively, concluded that the ultimate uniaxial strain (ε_f) rather than the fracture strength (σ_f) is the reliable brittle failure criterion. Brands showed that brittle failure occurs irrespective of the state of stress when the maximum elastic strain

$$\varepsilon_1 = \frac{1}{E}\{\sigma_1 - \nu(\sigma_2 + \sigma_3)\} \qquad (2.5)$$

reaches a critical value.

This would mean that the combined principal stresses rather than the maximum uniaxial stress determines failure.

2.3.2 The Relation between Fracture Toughness and the Material Parameters

Examining experimental results obtained by Gurland and Parikh, it has been observed that a pure exponential relationship exists between fracture toughness in bending ε_{fT} and the mean free path between the carbides, i.e., the average value of the thickness of the binder layer (Figure 10).

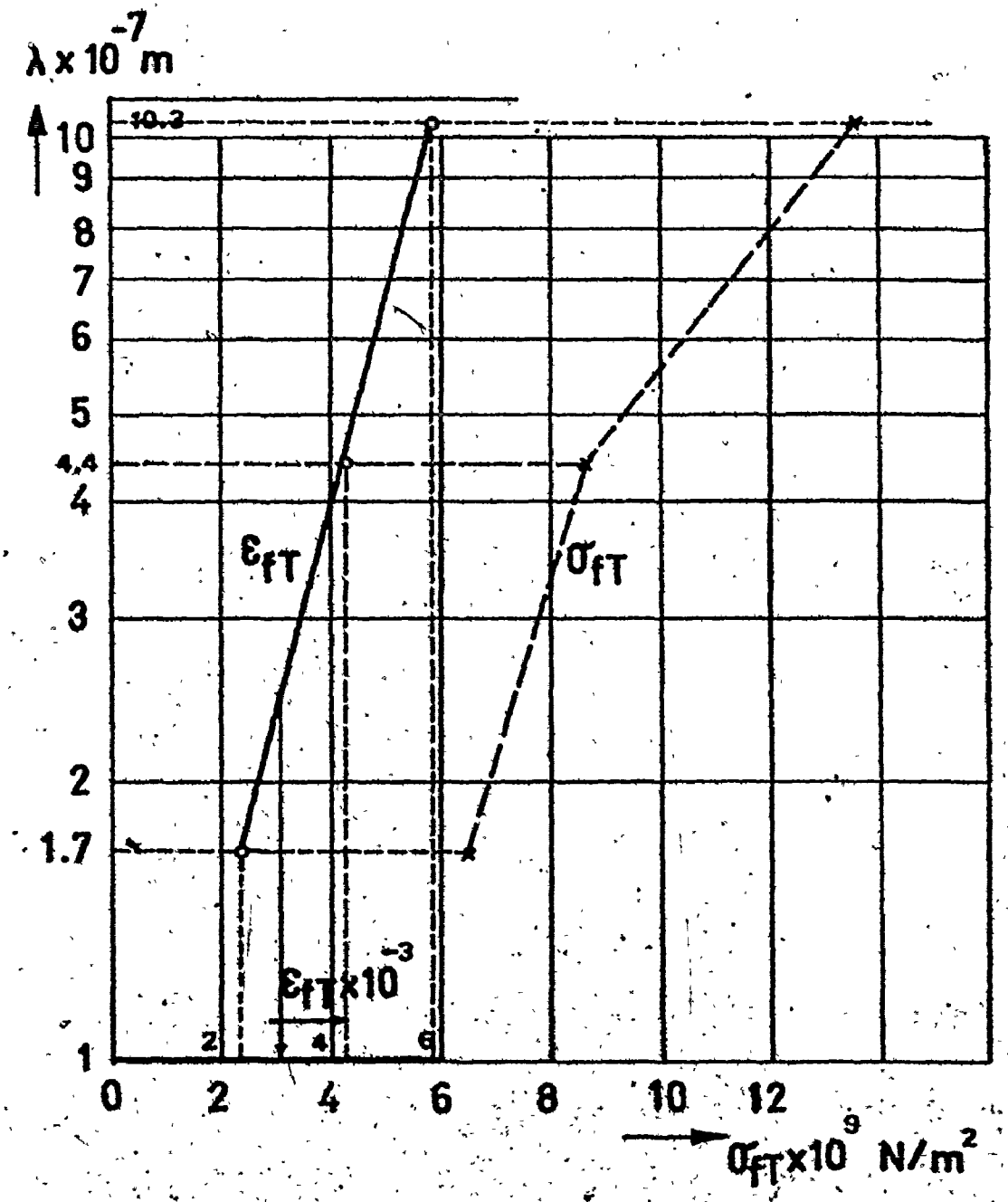

Figure 10. The Mean Free Path λ Versus Fracture Toughness after Results from Gurland and Parikh.

lb/in^2 = .6895 N/m^2

Figure 11 taken from Liebowitz [11] shows that this behaviour can be confirmed for various sintered carbide grades quoted by their corresponding ISO denotations. The values of mean free paths have been calculated from the average particle size d1 and the composition of the material G, assuming cubic grains

$$\lambda = d1 \left(\sqrt[3]{\frac{1}{G}} - 1 \right) \qquad (2.6)$$

The author concludes that:

a) Fracture toughness is mainly controlled by the mechanical properties of the binder and by the mean free path between grains.

b) The mechanical properties of the carbides (TiC, TaC, NbC, CrC_2, WC) do not have any significant influence on fracture toughness.

Gurland and Parikh [11] have shown that strength increases with increasing values of the mean free path λ. However, beyond $\lambda = 0,45\ \mu$ when the influence of plastic deformation becomes important, the trend is reversed (Figure 12).

From the work of Doi et al. [14], Figure 13, it appears that there is a systematic increase in rupture strength with a decrease in grain size.

2.3.3 Structural Parameters and their Influence on the Stress Distribution in the Binder Phase of Cemented Carbides

Although a relationship between structural and

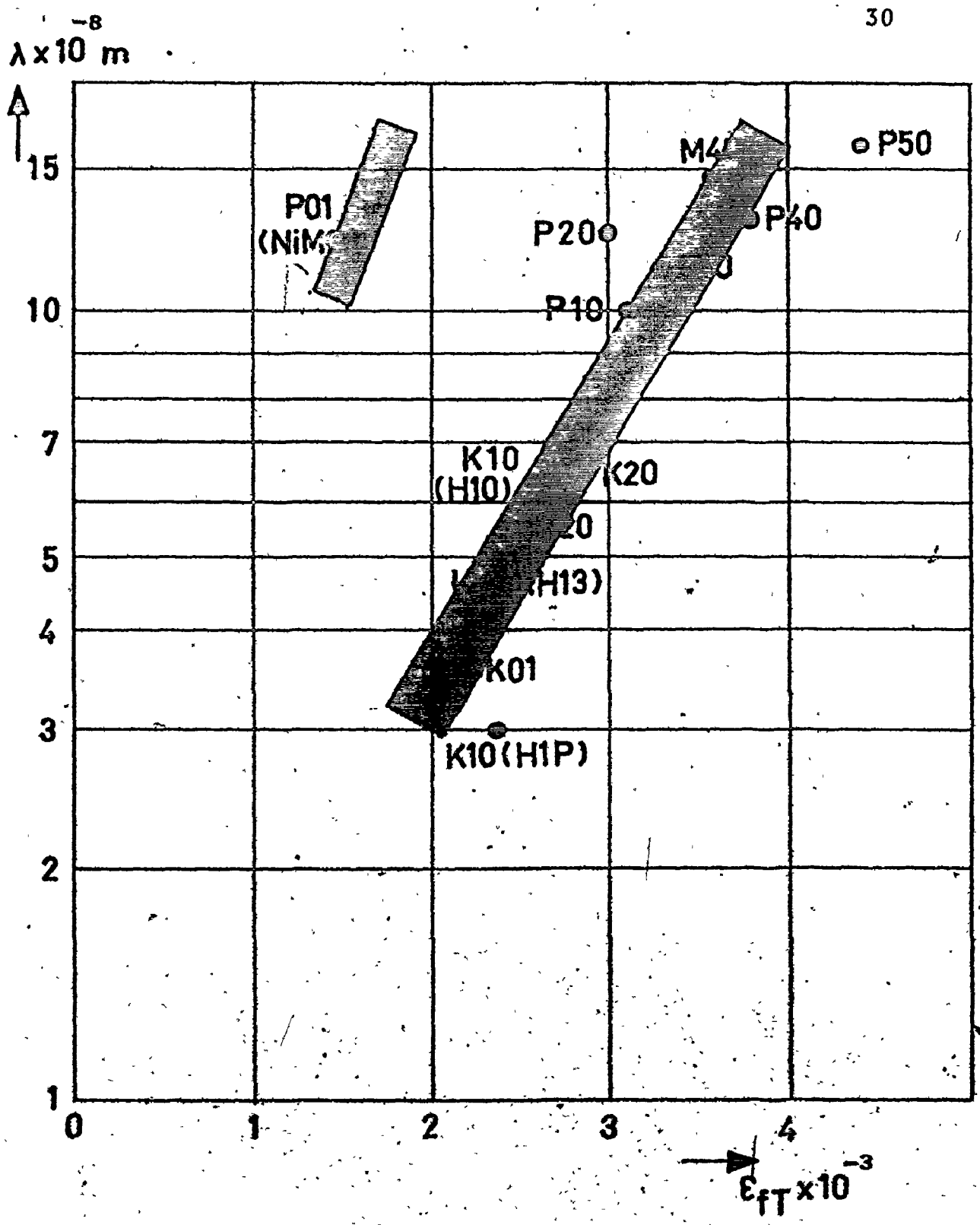

Figure 11. The Mean Free Path λ Versus Fracture Toughness ε_{fT} for a Number of Carbide Tool Materials.

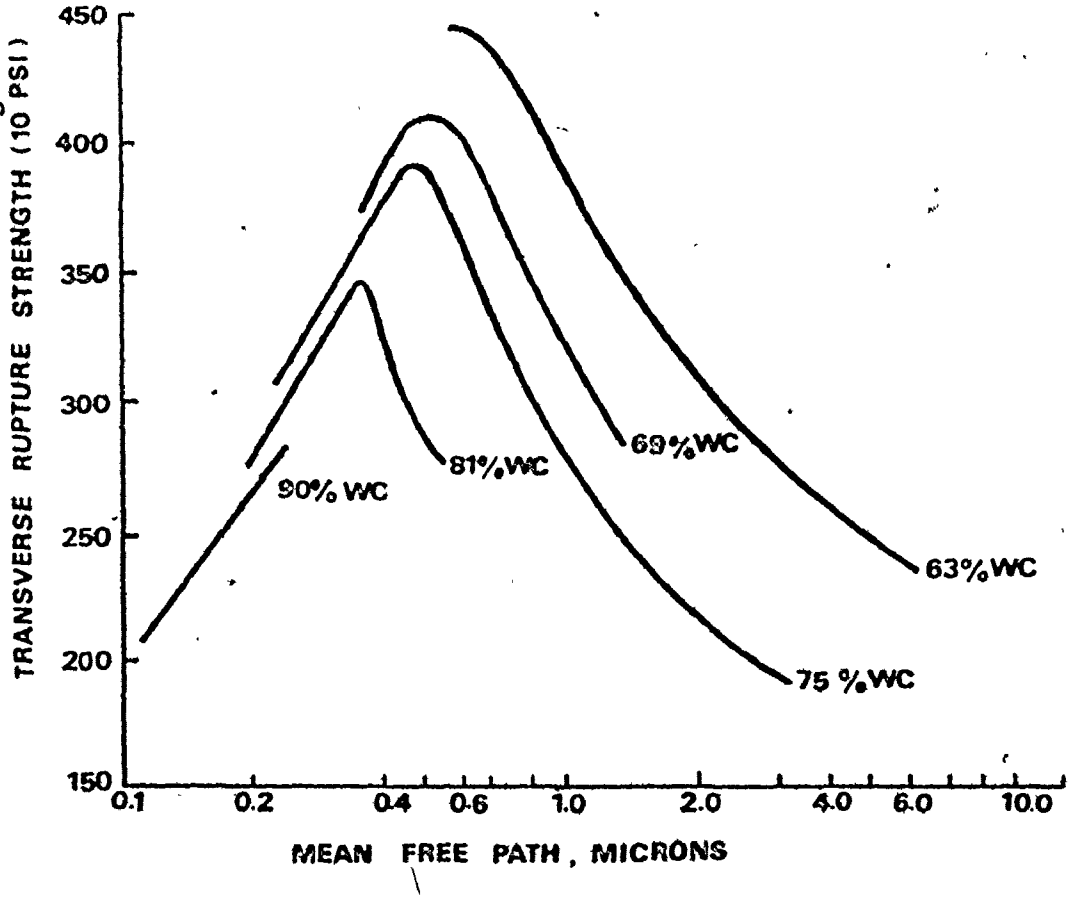

Figure 12. Transverse Rupture Strength (σ_{fT}) as a Function of Mean Free Path for Various Compositions.

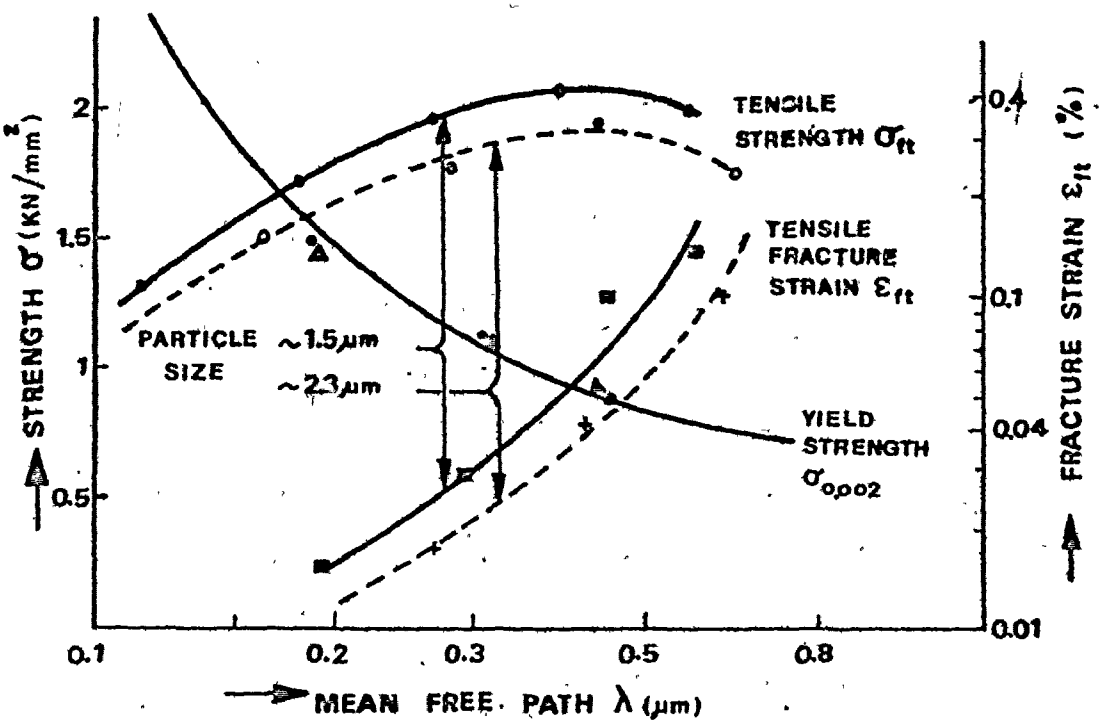

Figure 13. The Influence of Grain Size on Tensile Strength (σ_{fT}) and Fracture Strain (ε_{fT}) for Straight Carbides.

strength parameters exists, there remains the need for determining a generally applicable structural parameter which would uniquely quantify the fracture behaviour of cemented carbides. Bridgman [15] derived the relation

$$\frac{\bar{\sigma}}{\tilde{\sigma}_z} = C_B = [(1 + \frac{2h}{R}) \ln (1 + \frac{R}{2h})]^{-1} \qquad (2.7)$$

with applying the model of Figure 14-a which shows a toroidal-shaped reduction area characterized by the ratio $\frac{R}{h}$ and assuming a three-dimensional state of stress. This relationship explains the results of tensile tests at high strain values ($\bar{\sigma}$ stands for the effective stress, whilst $\tilde{\sigma}_z$ represents the average value of the axial tensile stress related to the true area). The factor C_B is known as the Bridgman factor.

Close examination of the structure of cemented carbides was carried out by Kals and Gielisse [9]. This examination reveals, both on the surface and in the bulk (particularly in and around voids and pores) specific detail that is geometrically comparable to the tensile test situation of Figure 14-a. It seems therefore justified to adopt the analogue model of Figure 14-b, where it will be noticed that $d_{av}/2$ substitutes for R, whilst half the average value of the mean free path $\lambda_{av}/2$ represents a fair minimum value of the radius. Generally, the occurrence of intergranular voids is less frequent than is suggested in Figure 14-b. Putting the average effective distance between the voids equal to K d_{av}, an expression analogous to Equation (2.7) is

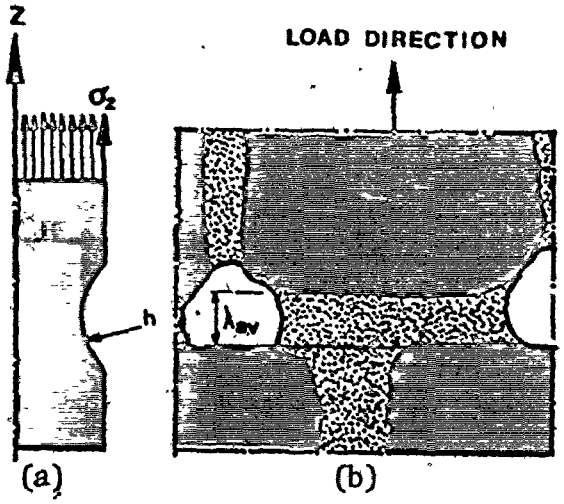

Figure 14. (a) Geometry of the Bridgman Model.
(b) Analogue for the Structure of Cemented Carbides.

arrived at:

$$\left(\frac{\bar{\sigma}}{\sigma_z}\right)_{z=0} = C = \left[\left(1 + \frac{2\lambda_{av}}{Kd_{av}} \ln\left(1 + \frac{Kd_{av}}{2/\lambda_{av}}\right)\right)\right]^{-1} \qquad (2.8)$$

The factor K depends upon the density of the voids. Its value will be largely determined by specific material processing conditions.

The ratio d_{av}/λ_{av} is a structural parameter and the potential significance of it to failure, in terms of the ultimate uniaxial strain is shown in Figures 15 and 16.

The use of tensile test analogue gives rise to the following five statements:

1. Necking phenomenon in a tensile specimen
2. Plastic flow in the carbide intergranular layer is localized and concentrated in the immediate vicinity of the voids.
3. The Bridgman factor has not been verified for values of R/h exceeding 10.
4. Maximum tensile stress occurs at the surface, so the test result depends very strongly on the surface roughness of the specimen.
5. Brittle fracture being a probabilistic feature, it depends strongly on the volume under stress, i.e., practically on the size of the specimen.

2.3.4 Standard Test Method for Measuring Material Properties

A proposal is found for the introduction of a new

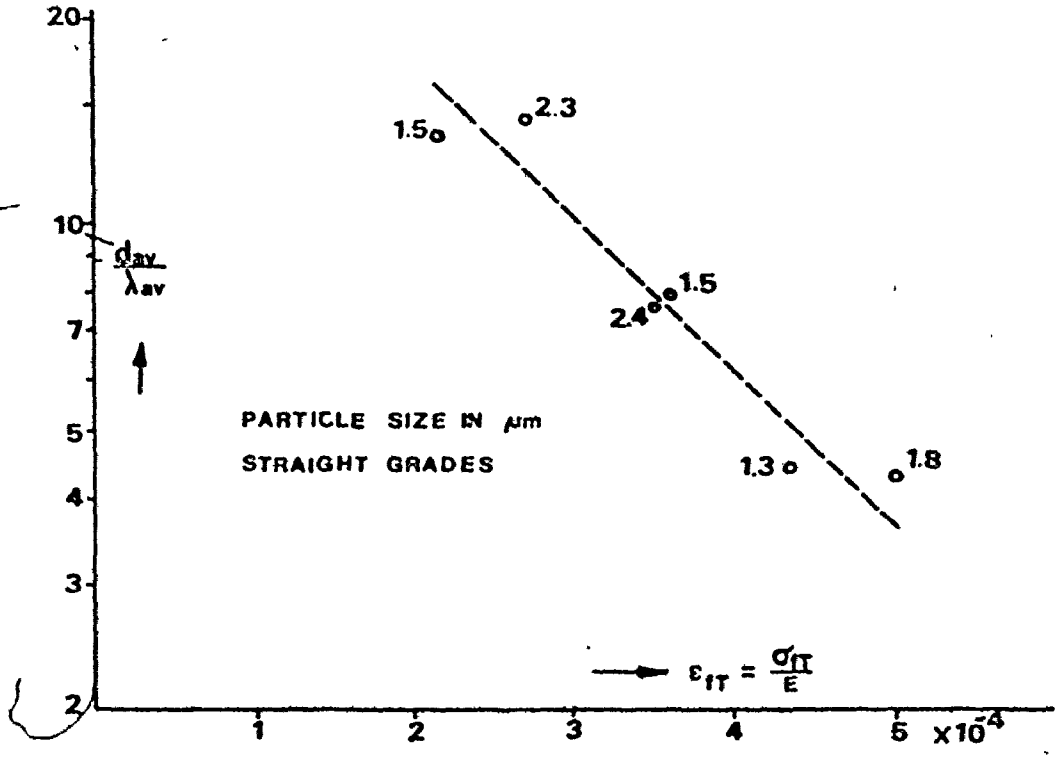

Figure 15. The Ultimate Uniaxial Strain (ε_{ft}, Tensile Test) as a Function of d_{av}/λ_{av}.

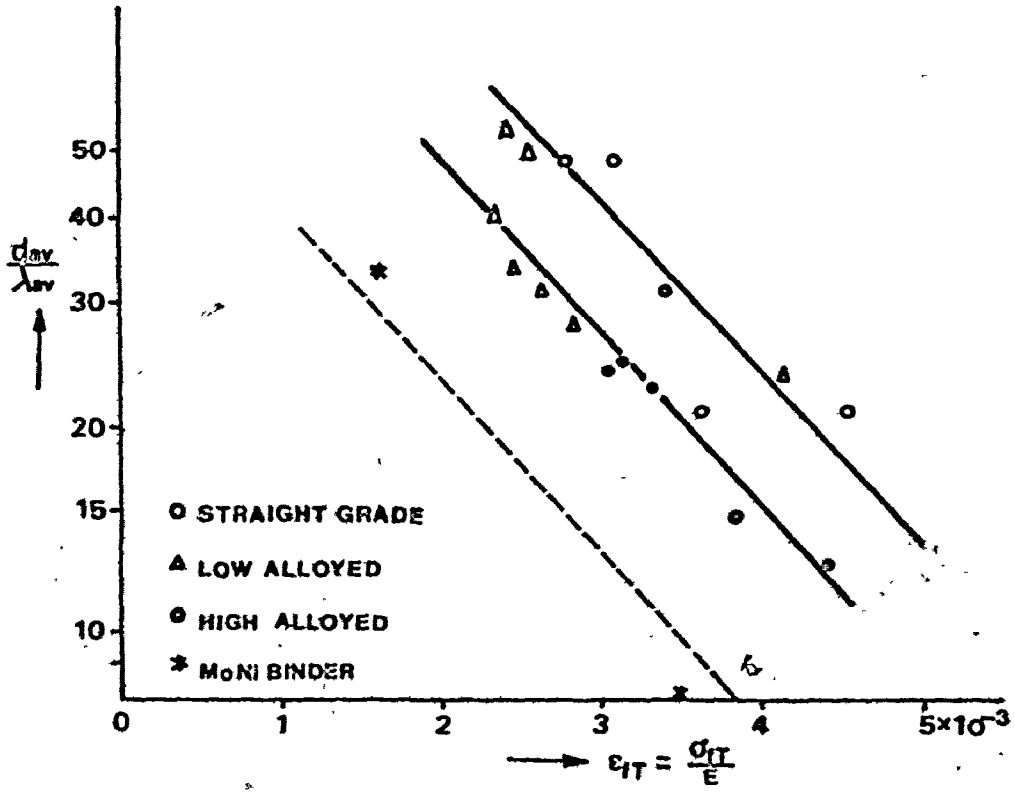

Figure 16. The Ultimate Uniaxial Strain (ε_{ft}, Bending Test) vs. the Ratio d_{av}/λ_{av} for a Number of Commercial Grades.

method for testing toughness of cemented carbides in which a disc-type specimen is compressed [7]. It is based upon the phenomenon that a tensile stress is acting across the loaded diameter of a diametrical loaded disc. Except for the regions quite near the strip loadings, this stress is uniformly distributed over the loaded diameter and is equal to

$$\sigma_3 = \frac{2F}{\pi dt} \qquad (2.9)$$

where F = applied load

d = diameter of the disc

t = thickness of the disc

The stresses in such a case are shown to be as given in Figure 17.

In the region of the load the stress condition is biaxial compressive which means that the material there can resist much greater stresses. The fact that compression shows a minimum at the centre of the disc specimens may explain why the specimens rupture at the centre. Also, the volume under stress is rather well specified. For these reasons, this test may become more important than the classical test.

2.3.5 The Development of Test Method

The development of the test method based on the diametrical compression test was carried out by H. Kals and W. Nollet [16]. Square specimens are ground flat at the two diagonally opposed corners till the resulting faces

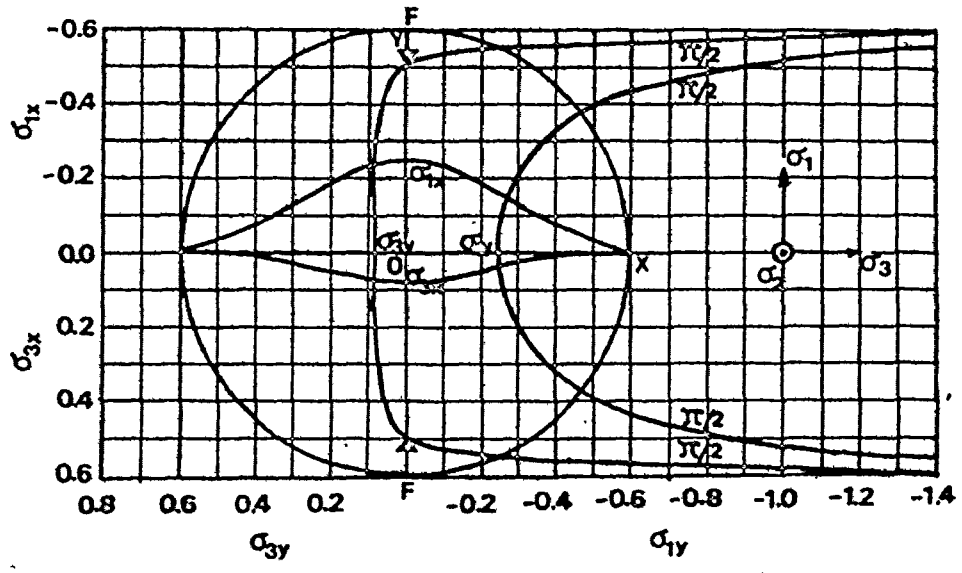

Figure 17. Distribution of Stresses of a Diametrical Loaded Circular Disk.

attain a length of 0.1 D, where D is the length of the diagonal. The test specimen is placed upright, the two small faces touching between the dies of an adapted pillar die set. The results of stress-analysis (plane stress) made with the aid of the finite element is given in Figure 18. Figure 18-a shows the principle stresses across the diagonals and Figure 18-b shows the mesh distribution in the quarter of the specimen.

2.3.6 Introduction of Tool Fracture Classification System

Keiji Okushima and Tetsutaro Hashi [17] classified the tool fractures into three major categories according primarily to the outside appearance and association with any preceding crack. They are:

Category 1	Chipping at low cutting speed.
Category 2	Chipping of large size without a preceding crack.
Category 3	Fractures at high cutting speed: it occurred as a result of fatigue damage to the tool tip.

The tests were carried out in the face-milling operations on carbon steel work materials.

Features of Category 1 and Category 2

Category 1: The chipping occurred along the cutting edge, and the thickness of the fractured portion was rather small

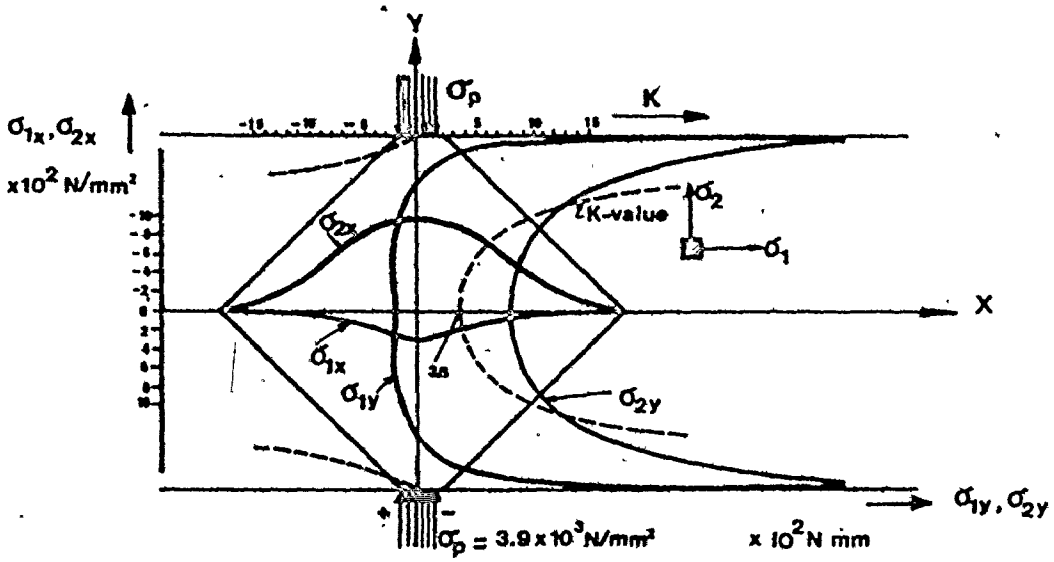

(a)

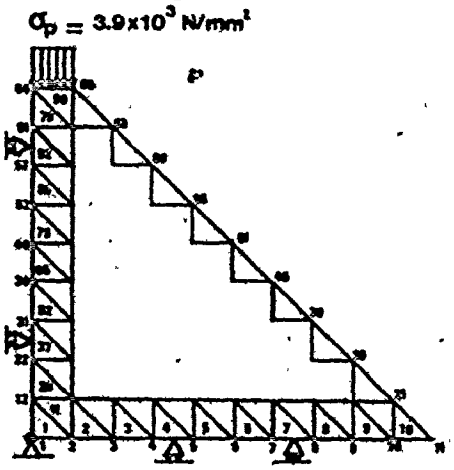

(b)

Figure 18. Stress Distribution across the Diagonals of a Diagonally Loaded Square Specimen.

on the rake face but somewhat larger on the flank. No crack was inferred. This type of chipping occurred a short time after a new tool tip was put into operation. A tougher tool grade was safer from this type of chipping. Also it was commonly experienced that machining of a harder steel was accompanied by more danger due to this type of chipping. The experiments showed the chipping at low cutting speeds is caused by mechanical impacts of intermittent cutting and the brittleness of tool material when subjected to the impact loading (Figure 19).

Category 2: This is the fracture which occurs in a fairly large size. The fracture is supposed to start on the rake face and develop nearly parallel to the flank so that a large fracture is observed on the flank. No crack is precedingly recognized as causing the fracture. This breakage occurs occasionally at any early stage after a new tool is started.

Features of Category 3

This category is the most important one and it consists of several types of breakage which occur due to preceding cracks, therefore, they are fatigue fractures. Each type of fracture is caused by different types of cracks. They occur earlier at high cutting speeds. Fractures of this category are classified into five types. The first three types are most common in operations without cutting fluids.

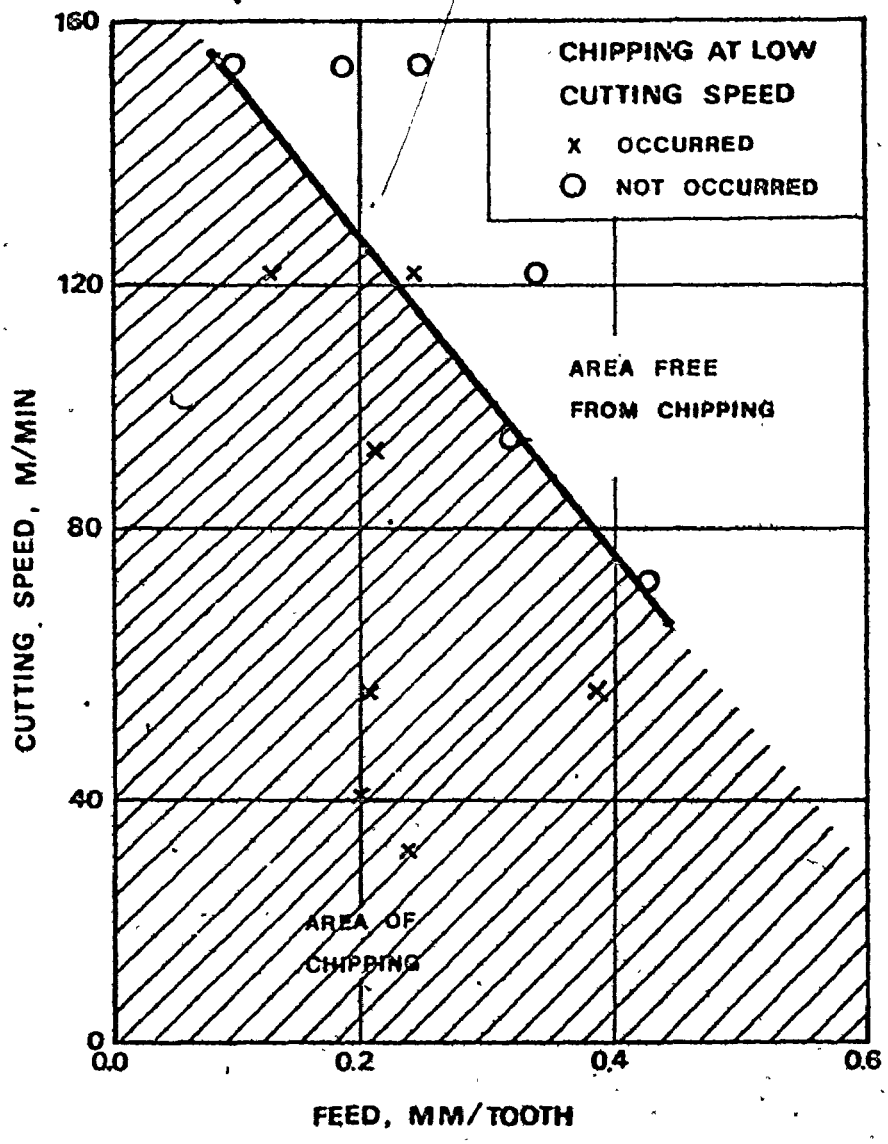

Figure 19. Safety Chart of the Chipping at Low Cutting Speed.

Fracture starting on the rake face is the first type and it is caused by cracks parallel to the cutting edge starting on the rake face. With repetition of the intermittent cutting, the crack gradually propagates into the tool material, nearly parallel to the flank surface and finally causes the breakage (Figure 20-I).

Fracture starting on the flank or land is the second type and it is caused by cross cracks starting on the flank or land (Figures 20-IIA, IIB).

The third type is fracture starting both on the rake face and on the flank and it is caused by combined propagation of the above two cracks (Figures 20-IIIA,B,C,D).

Figure 21 shows that the fracture starting on the flank occurs below a certain cutting speed and the chipping starting on the rake face occurs at high cutting speeds.

Breakage is a fourth type of fracture at high cutting speeds. This is a fracture caused by a crack in the direction nearly perpendicular to the cutting edge which propagates and finally splits the tool tip (Figure 22).

Occasionally, thermal cracks occur also in the direction parallel to the cutting edge.

Pitting is a fifth type of fracture at high cutting speeds. This is segregation of a thin layer of tool material from the localized portion of the tool chip contact area. Pitting occurs adjacent to thermal cracks both perpendicular and parallel to the cutting edge (Figure 20-IV).

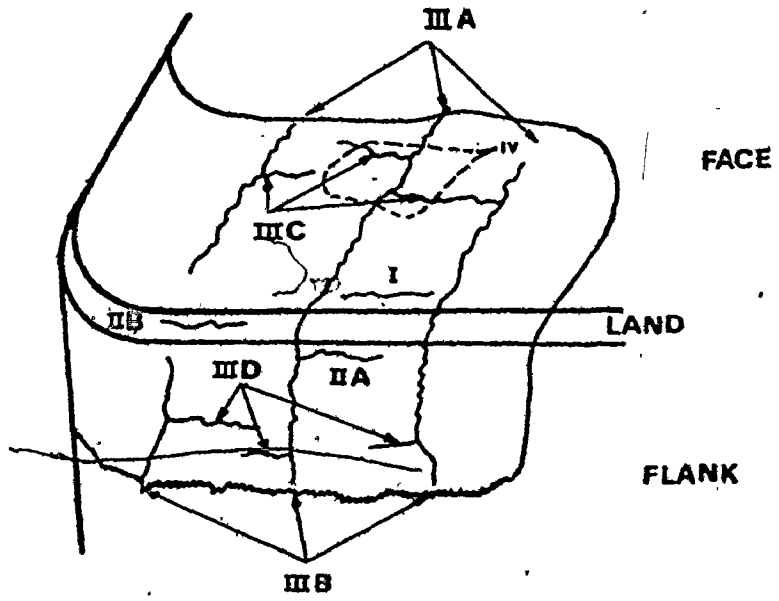

Figure 20. Typical Location and Appearance of Various Types of Fatigue Cracks.

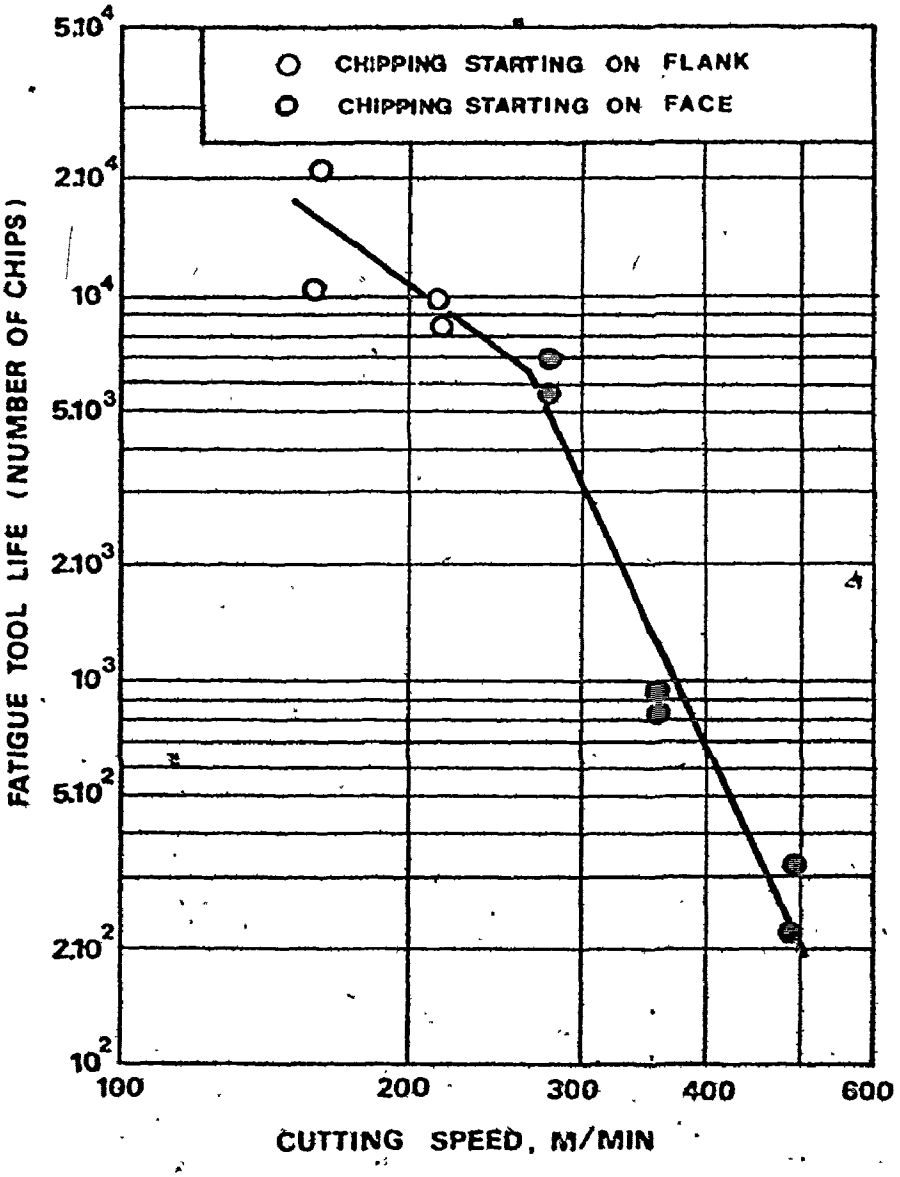

Figure 21. Fatigue Tool Life of P20 Tungsten Carbide Determined by the Chipping Starting on the Flank and/or the Chipping Starting on the Rake Face.

Figure 22. Example of Breakage. Tool Grade K7H, Rake Angle +ve 5°, Work Material Steel 4340 (217 BHN), Initial Diameter 3 inches, Depth of Cut 0.1 inch, Feed .035 inch/rev., Cutting Speed 250 ft./min.

CHAPTER 3

EXPERIMENTAL RESULTS

3.1 Introduction

Failures of tungsten and titanium carbide tools due to fracture of the cutting edge were investigated in turning operations using alloy steel 4340 for work material. The purpose was to classify what is generally called fracture of the tool edge into several definite types and to reveal the cause and mechanism of each type.

The study consisted of metal cutting tests in which tools were tested until they fail due to fracture. The fractured tool was inspected under a scanning electron microscope to analyze the location, size, direction and other characteristics of the fracture.

3.2 Test Equipment and Materials

3.2.1 Machine tool

All turning tests were performed on a Mazak-Rex heavy duty lathe rated at 25 HP of main motor. The spindle speed ranged from 12 to 1200 rev./min. (stepless speed drive) and the feed ranged from (0.0021 inch - 0.265 inch).

3.2.2 Tool

Tool holders for triangular negative rake inserts

and triangular positive rake inserts were used. They had 4.5 in. length, 3/4 in. x 3/4 in. cross section and 30° side cutting edge angle. Figure 23 shows the dimensions of the inserts used and mounted in the tool holder. They had negative 5° and positive 5° rake angles. Steel machining grades of tungsten-titanium carbide Kennametal K7H (93.5 R_wA) and K45 (92.5 R_wA) and Wickaloy WP6 (92.2 R_wA) and WP5 (91.0 R_wA) were used.

They have a three-phase structure as shown in Figures 24, 25, 26 and 27 showing the angular grey grains of tungsten carbide (WC), round dark grey grains of complex (WC + TiC + TaC) carbide and the white phase (Co).

The exact composition of the Kennametal grades was not available. Hardness and chemical composition of the Wickaloy grades (WP6 and WP5) are listed in Table 3.

Table 3

Grade	Chemical Composition				Hardness
	Co	WC	TiC	TaC	R_wA
WP5	8	72	9	11	91.0
WP6	4.5	71	12.5	12	92.2

3.2.3 Workpiece

Three kinds of steel were used: 4340 alloy steel normalized with hardness 217 BHN, 4340 hardened and tempered to about 380 BHN and 1040 carbon steel. Their compositions

LC.	D	T	R
3/8	.539	1/8	1/32

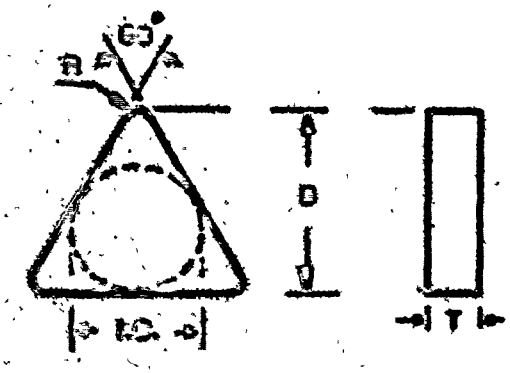

Figure 23: Dimensions of the tool

Figure 24: Microstructure of K7H Carbide grade (X2000)

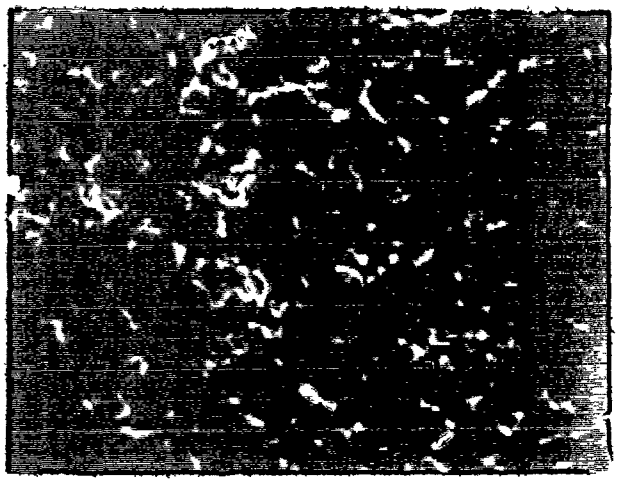

Figure 25: Microstructure of K45 Carbide grade (X2000)

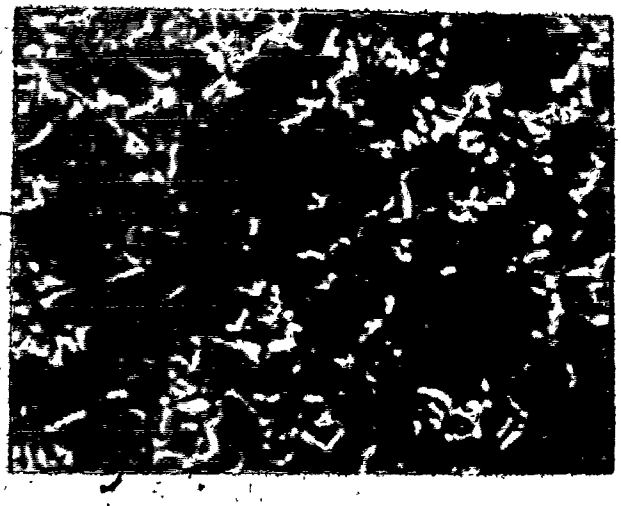

Figure 26: Microstructure of WP5 Carbide grade (X2000)

Figure 27: Microstructure of WP6 Carbide grade (X2000)

are listed in Table 4

Table 4

Steel	Chemical Composition (percent) C	Mn	S	Si	Cr	Ni	Mo	P	Brinell Hardness BHN
4340	.4	.7	0.02	.25	.8	1.75	.25	0.04	217
1040	.4	.6-.7	0.04	-	-	-	-	0.04	210

3.3 Cutting Tests

Two types of cutting tests were carried out. The first type was continuous cutting, where K7H and K45 tool grades and the three kinds of steel workpieces were used. The second type was interrupted cutting. Tool grades WP5 and WP6 and 4340 hardened and tempered steel workpiece were used.

For every tool the test was carried out by increasing the feed in steps from 0.010 inch up to 0.043 inch and using 0.05 inch or 0.1 inch depth of cut. The cutting speed also changed due to the change in workpiece diameter starting from 250 ft./min. down to 100 ft./min.

The tests were periodically interrupted and the tools were examined using the tool maker's microscope. The test results of continuous cutting were recorded in Tables 5 to 18.

For interrupted cutting the test results were recorded in Tables 19, 20 and 21.

a. Continuous Cutting tests

Table 5 : Cutting test results using tool number (1-a)

Tool number (1)

Tool material : K7H
Geometry of tool : positive 5° rake angle
Workpiece material : steel 4340, 217 BHN, initial diameter 3.0 in., length 18.0 in.
Depth of cut : 0.05 in.

Cutting time (min.)	Cutting speed (ft/min)	feed (in./rev.)	Sketch of the figure Shown under the microscope	Comment
1	260	.010	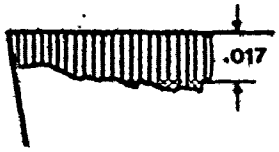	Flank wear
2	260	.010		Flank wear + chipping
3.5	260	.010	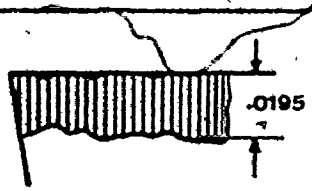	Flank wear + chipping
5.5	225	.018	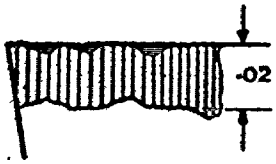	Flank wear + chipping

Cont. Table 5

Cutting time (min.)	Cutting speed (ft/min)	feed (in./rev.)	Sketch of the figure Shown under the microscope	Comment
8	190	.024	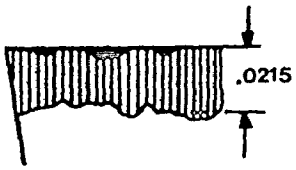	Flank wear + chipping
10	180	.024		Flank wear + chipping
12	160	.024	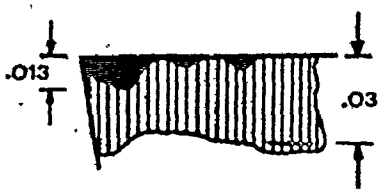	Flank wear + chipping
14	140	.024	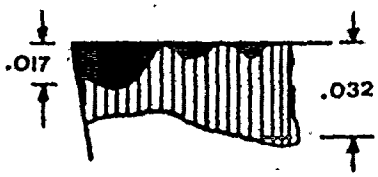	Flank wear + large amount of chipping
16	120	.024	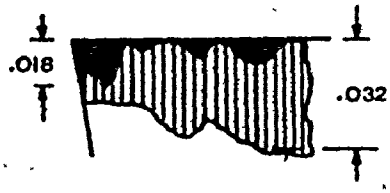	Flank wear + large amount of chipping
18	110	.024	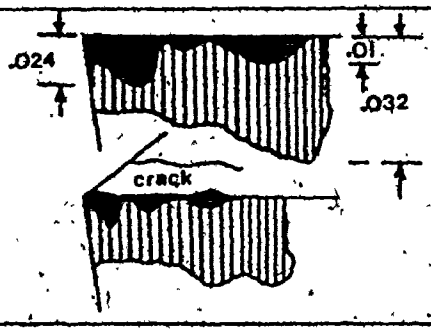	Flank wear + large amount of chipping + crack

Table 6 : Cutting test results using tool number (1-b)

Tool Number 1-b.

Cutting time (min.)	Cutting speed (ft/min)	feed (in./rev.)	Sketch of the figure Shown under the microscope	Comment
5.5	220	.010	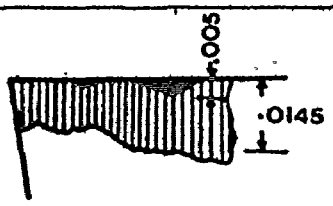	Flank wear + chipping
9.5	160	.024	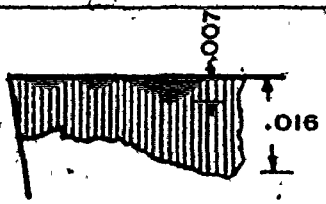	Flank wear + chipping
13	130	.027		Flank wear + chipping
15.5	110	.035	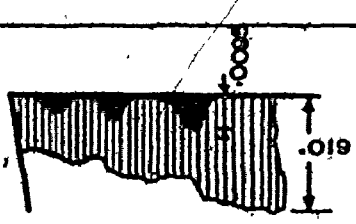	Flank wear + chipping
18	100	.035	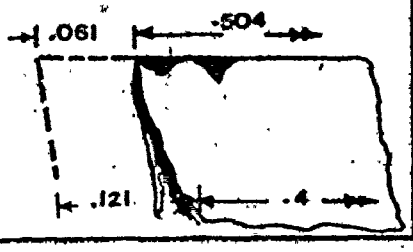	The tool is broken

Tool Number 1-c

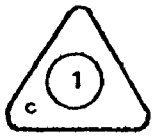

T min.	V ft/min	f in.	Sketch of the figure Shown under the microscope	Comment
1	110	.024		Flank wear + chipping
2.5	110	.024	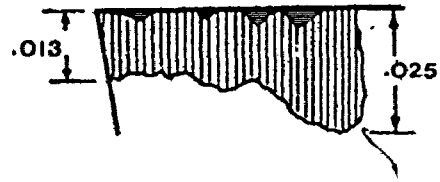	Flank wear + chipping
5.5	100	.024		Flank wear + chipping
7.5	90	.032	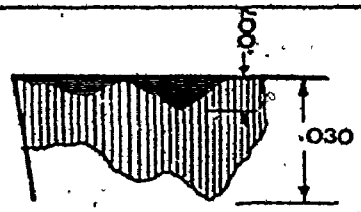	Flank wear + chipping
9.0	90	.043	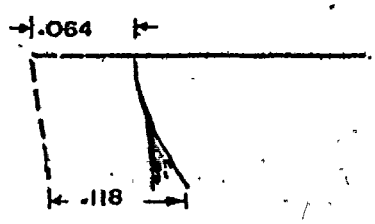	The tool is broken

Table 8 : Cutting test results using tool number (2)

Tool number (2)

Tool material : K7H

Geometry of tool : positive 5^{o} rake angle

Workpiece material : steel 4340, 217 BHN, initial diameter 3.0 in., length 18.0 in.

Depth of cut : 0.05

Cutting time (min.)	Cutting speed (ft/min)	feed (in./rev.)	Sketch of the figure Shown under the microscope	Comment
.5	240	.027	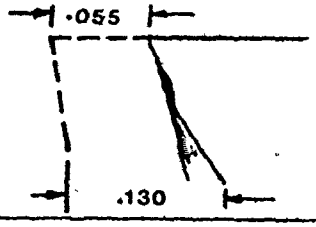	The tool is broken
			Tool number 2-b 	
10	240	.027		Flank wear
20	240	.027		Flank wear + chipping
30	240	.027	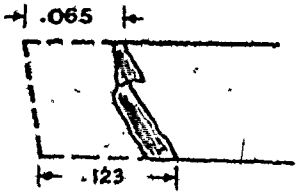	The tool is broken

Table 9 : Cutting test results using tool number (3)

Tool number (3)

Tool material : K7H

Geometry of tool : positive 5^{6} rake angle

Workpiece material : steel 1040, 210 BHN, initial diameter 2.0 in., length 18.0 in.

Depth of cut : 0.05 in.

Cutting time (min.)	Cutting speed (ft/min)	feed (in./rev.)	Sketch of the figure Shown under the microscope	Comment
3	240	.027	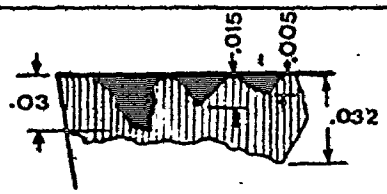	Flank wear + chipping
6.5	240	.027	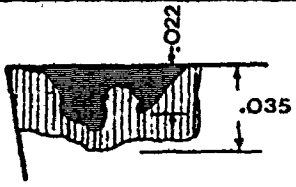	Flank wear + chipping
9.5	240	.027	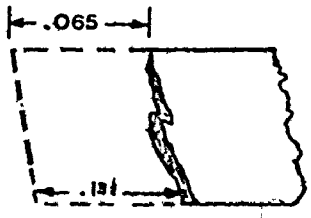	The tool is broken

Table 10 : Cutting test results using tool number (4-a)

Tool number (4)

Tool material : K7H
Geometry of tool : negative 5^{o} rake angle
Workpiece material : steel 3440, 217 BHN, initial diameter 3.0 in., length 18.0 in.
Depth of cut : 0.05 in.

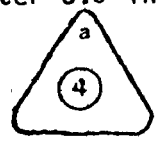

Cutting time (min.)	Cutting speed (ft/min)	feed (in./rev.)	Sketch of the figure Shown under the microscope	Comment
1.5	250	.019		Flank wear
4.5	240	.035	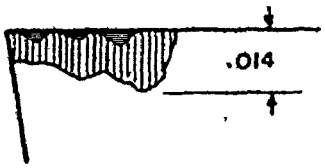	Flank wear + chipping
5.5	230	.043	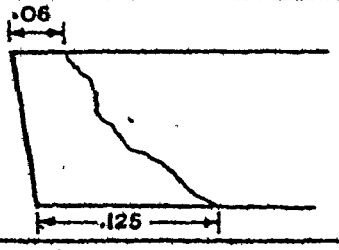	Crack

Table 11 : Cutting test results using tool number (4-b,c)

Tool number 4-b,c 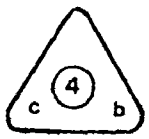				
Cutting time (min.)	Cutting speed (ft/min)	feed (in./rev.)	Sketch of the figure Shown under the microscope	Comment
1.5	220	.019	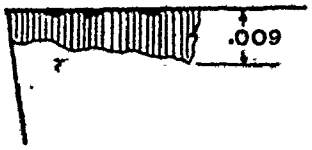	Flank wear + chipping
4.5	200	.035		Flank wear + chipping
6	190	.043	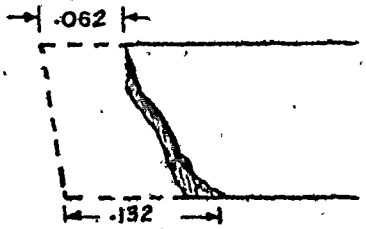	The tool is broken

Table 12 : Cutting test results using tool number (5)

Tool number (5)

Tool material : K45

Geometry of tool : positive 5^{o} rake angle

Workpiece material : steel 4340, 217 BHN, initial diameter 2.0 in., length 18.0 in.

Depth of cut : 0.05 in.

Cutting time (min.)	Cutting speed (ft/min)	feed (in./rev.)	Sketch of the figure Shown under the microscope	Comment
3.5	240	.027	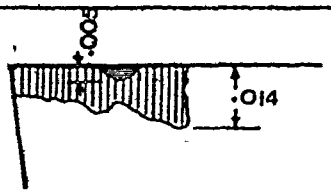	Flank wear + chipping
8.5	240	.027		Flank wear + chipping
13.5	220	.035	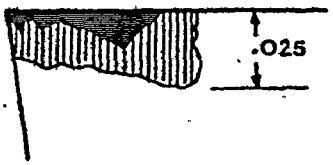	Flank wear + chipping

Table 13 : Cutting test results using tool number (6)

Tool number (6)

Tool material : K45

Geometry of tool : negative 5^{o} rake angle

Workpiece material : 4340 steel hardened and tempered to 380 BHN, initial diameter 2.0 in., length 18.0 in.

Depth of cut : 0.05 in.

Cutting time (min.)	Cutting speed (ft/min)	feed (in./rev.)	Sketch of the figure Shown under the microscope	Comment
1	250	.010	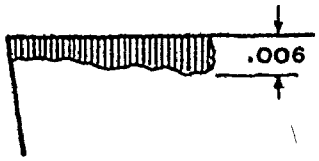	Flank wear
2	250	.024		Flank wear
3	250	.035	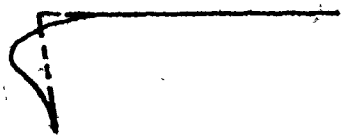	Plastic deformation

Table 14 : Cutting test results using tool number (7-a)

Tool number (7)

Tool material : K45

Geometry of tool : positive 5^{o} rake angle

Workpiece material : 4340 steel hardened and tempered to 380 BHN, initial diameter 2.6 in., length 18.0 in.

Depth of cut : o.1 in.

Cutting time (min.)	Cutting speed (ft/min)	feed (in./rev.)	Sketch of the figure Shown under the microscope	Comment
1	160	.020.	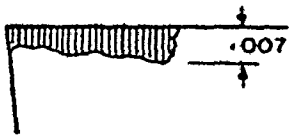	Flank wear
2	160	.027		Flank wear + chipping
5	160	.038	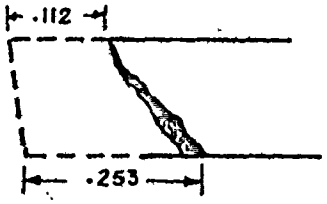	The tool is broken

Table 15 : Cutting test results using tool number (7-b)

Tool number 7-b 				
Cutting time (min.)	Cutting speed (ft/min)	feed (in./rev.)	Sketch of the figure Shown under the microscope	Comment
1	150	.020	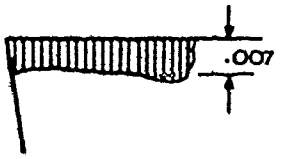	F lank wear
4	150	.030	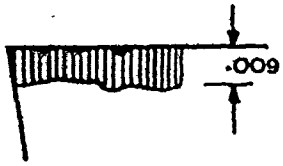	Flank wear + chipping
7	150	.033	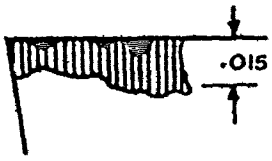	Flank wear + chipping
8	150	.033	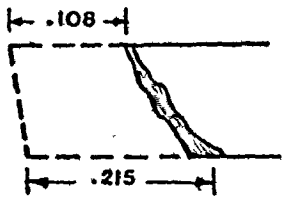	The tool is broken

Table 16 : Cutting test results using tool number (8)

Tool number (8)

Tool material : K45

Geometry of tool : negative 5^{0} rake angle

Workpiece material : steel 4340, 217 BHN, initial diameter 2.3 in., length 18.0 in.

Depth of cut : 0.1 in.

Cutting time (min.)	Cutting speed (ft/min)	feed (in./rev.)	Sketch of the figure Shown under the microscope	Comment
2	250	.018	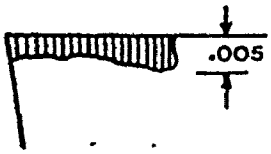	Flank wear
3.5	250	.024	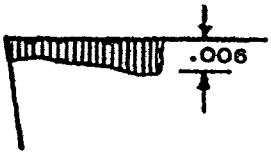	Flank wear + chipping
4.5	250	.030		Flank wear + chipping
5.5	200	.030	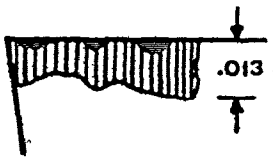	Flank wear + chipping
7.5	200		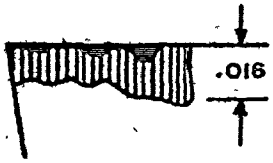	Flank wear + chipping

Cont. Table 16

Cutting time (min.)	Cutting speed (ft/min)	feed (in.rev.)	Sketch of the figure Shown under the microscope	Comment
9.5	160		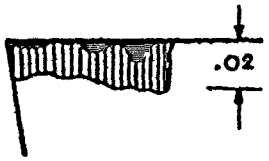	F lank wear + chipping
11.5	160		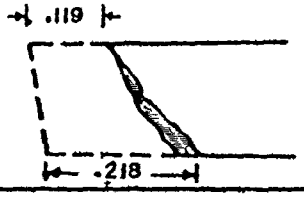	The tool is broken

Table 17 : Cutting test results using tool number (9)

Tool number (9)

Tool material : K45

Geometry of tool : positive 5^{o} rake angle

Workpiece material : 4340 steel hardened and tempered to 380 BHN, initial diameter 1.5 in., length 20.0 in.

Depth of cut : 0.1 in.

Cutting time (min.)	Cutting speed (ft/min)	feed (in./rev.)	Sketch of the figure Shown under the microscope	Comment
.5	150	.033	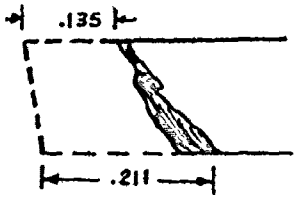	The tool is broken
				
1	150	.03	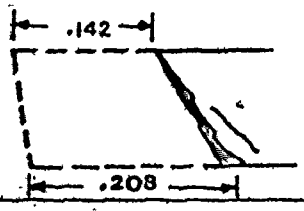	The tool is broken
				
2	150	.02		Good example of chipping

Table 18 : Cutting test results using tools number (10,11)

Tool number (10)

Tool material : K45

Geometry of tool : positive 5^{o} rake angle

Workpiece material : steel 4340, 217 BHN, initial diameter 2.0 in., length 20.0 in.

Depth of cut : 0.1 in.

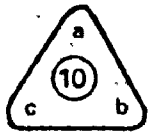

Cutting time (min.)	Cutting speed (ft/min)	feed (in./rev.)	Sketch of the figure Shown under the microscope	Comment
1.0	250	.031	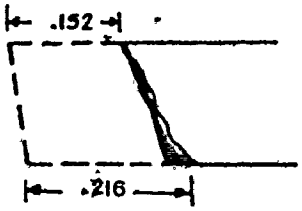	The tool is broken

Tool number (11)

Tool material : K45

Geometry of tool : positive 5^{o} rake angle

Workpiece material : steel 4340, 217 BHN, initial diameter 2.0 in., length 20.0 in.

Depth of cut : 0.1 in.

Cutting time (min.)	Cutting speed (ft/min)	Feed (in./rev.)	Sketch of the figure Shown under the microscope	Comment
1.0	250	.034		The tool is broken

b. Interrupted Cutting tests

Table 19 : Cutting test results using tool number (1)

Tool number (1)

Tool material : WP5

Geometry of tool : positive 5^0 rake angle

Workpiece material : 4340 steel hardened and tempered to 380 BHN, initial diameter 3.5, length 25. in.

Depth of cut : 0.1 in.

Cutting time (min.)	Cutting speed (ft/min)	feed (in./rev.)	Sketch of the figure Shown under the microscope	Comment
.1	250	.020	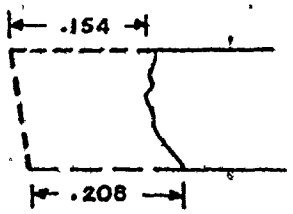	The tool is broken

Table 20 : Cutting test results using tool number (2)

Tool number (2)

Tool material : WP5

Geometry of tool : positive 5^{o} rake angle

Workpiece material : steel 4340 hardened and tempered to 380 BHN, initial diameter 3.5 in., length 25.0 in.

Depth of cut : 0.1 in.

Cutting time (min.)	Cutting speed (ft/min)	feed (in./rev.)	Sketch of the figure Shown under the microscope	Comment
1.5	200	0.022	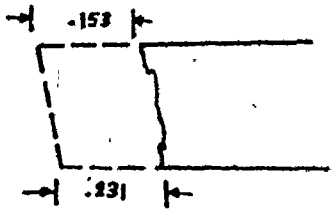	Breakage
Tool number 2-b 				
2	250	0.017	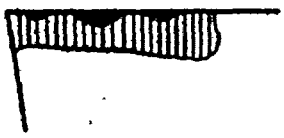	Chipping
5	250	0.017	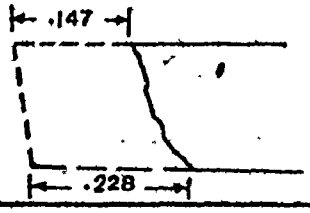	Breakage

Table 21 : Cutting test results using tools number (3,4)

Tool number (3)

Tool material : WP6
Geometry of tool : positive 5^{o} rake angle
Workpiece material : 4340 steel hardened and tempered to 380 BHN, initial diameter 3.0 in., length 25.0
Depth of cut : 0.1 in.

Cutting time (min.)	Cutting speed (ft/min)	feed (in./rev.)	Sketch of the figure Shown under the microscope	Comment
1.0	180	0.0155	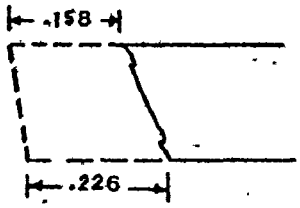	The tool is broken

Tool number (4)

Tool material : WP6
Geometry of tool : positive 5^{o} rake angle
Workpiece material : 4340 steel hardened and tempered to 380 BHN, initial diameter 3.0 in., length 25.0
Depth of cut : 0.1 in.

Cutting time (min.)	Cutting speed (ft/min)	feed (in./rev.)	Sketch of the figure Shown under the microscope	Comment
1.0	200	0.022	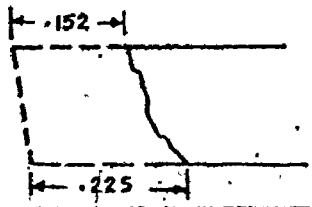	The tool is broken

According to the preceding tables, the results of the tests conducted for both types of cutting are summarized in Tables 22 and 23.

From Table 22 one may conclude that:

1. Complete breakage of the tool occurred starting from a feed rate of 0.027 in./rev. In the case of tool 1-a the only observations were chipping and crack on the rake face at 0.024 in./rev. feed rate.
2. Breakage occurred at a higher feed rate (0.043 in./rev.) when using tools with negative rake angle (tools 4, 6 and 8), than with tools with positive rake angle.
3. An increase in the depth of the cut (0.1 in.) had a similar effect as an increase of feed; it lead to a breakage in a shorter cutting time.
4. For the same cutting conditions tool material and workpiece there was considerable scatter in the time of cutting before breakage. (Tool number 7 was broken after 4 minutes while tool number 9 was broken after 0.5 minute).
5. The difference in breakage observed in cutting the hardened steel (380 BHN) and non-hardened steel (217 BHN) was rather small.
6. In general breakage occurred at heavy loads on the tool tip, actually, when a load specified by feeds in the range of 0.027 inch to 0.043 inch at 0.05 and 0.1 inch width of cut was exceeded. Often, it occurred first after some amount of chipping had

Table (22) : Cutting test results in case of continuous cutting

Tool No.	Tool grade	Work piece material	Cutting speed (ft/min)	Maximum feed (inch)	Depth of cut (inch)	Total time (min.)	Time at max. feed (min.)	Speed at max. feed (ft/min.)	Comment
1-a	K7H positive 5° RAKE ANGLE	4340 STEEL 217 BHN	260	0.024	0.05	18	12.5	110	Chipping, crack
1-b			220	0.035	0.05	18	5	100	Chipping, break
1-c			110	0.043	0.05	9	1.5	90	Chipping, break
2-a	K7H positive 5° RAKE	4340 STEEL 217 BHN	240	0.027	0.05	0.5	0.5	240	Break
2-b			240	0.027	0.05	9.5	9.5	240	Break
3	K7H +ve 5 RAKE	1040 STEEL 210 BHN	240	0.027	0.05	9.5	9.5	240	Break
4-a	K7H negative 5° RAKE	4340 STEEL 217 BHN	250	0.043	0.05	5.5	1.0	230	Break
4-b,c			220	0.043	0.05	6	1.5	190	Break
5	K45 +ve 5° RAKE	4340 STEEL 217 BHN	240	0.036	0.05	13.5	5	220	Chipping

Cont. Table (22)

Tool No.	Tool grade	Work piece material	Cutting speed (ft/min)	Maximum feed (inch)	Depth of cut (inch)	Total time (min.)	Time at max. feed (min.)	Speed at max. feed (ft/min.)	Comment
6	K45 −ve 5° RAKE	hardened 4340 380 BHN	250	0.035	0.05	3	1	250	Plastic deformation
7-a	K45 positive 5° RAKE	hardened 4340 380 BHN	160	0.038	0.1	5	3	160	Break
7-b			150	0.033	0.1	8	4	150	Break
8	K45 −ve 5° RAKE	4340 STEEL 217 BHN	250	0.03	0.1	11.5	8	160	Break
9-a	K45 positive 5 RAKE ANGLE	hardened 4340 STEEL 380 BHN	150	0.033	0.1	.5	.5	150	Break
9-b			150	0.03	0.1	1.0	1.0	150	Break
9-c			150	0.02	0.1	2.0	2.0	150	Chipping
10 a,b,c	K45 +ve 5 RAKE	4340 STEEL 217 BHN	250	0.031	0.1	1.0	1.0	250	Break
11 a,b,c	K45 +ve 5 RAKE	4340 STEEL 217 BHN	250	0.039	0.1	1.0	1.0	250	Break

Table (23) : Cutting tests results in case of interrupted cutting

Tool		Work piece material	Cutting speed (ft/min)	Maximum feed (inch)	Depth of cut (inch)	Total time (min.)	Time at max. feed (min.)	Speed at max. feed (ft/min.)	Comment
No.	grade								
1	WP5 −ve 5° RAKE	HARDENED 4340 STEEL (380 BHN)	180	0.02	0.1	2.0	2.0	180	Break
2-a	WP5 −ve 5° RAKE		250	0.017	0.1	3.0	3.0	250	Break
2-b			200	0.022	0.1	1.5	1.5	200	Break
3	WP6 −ve 5° RAKE		200	0.022	0.1	.5	.5	200	Break
4	WP6 −ve 5° RAKE		180	0.0155	0.1	0.5	0.5	180	Break

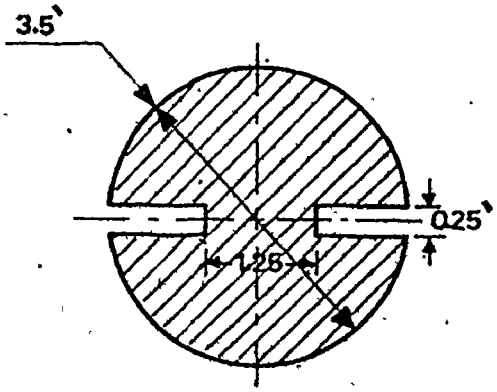

accummulated on the cutting edge (thus obviously contributing to the increase in the cutting force). Sometimes, however, it occurred after a very short time.

Comparing the results of tests carried out in interrupted cutting, Table 23 with those of continuous cutting the most significant difference is found in the fact that in interrupted cutting, complete breakage occurred at feeds of 0.015 inch to 0.022 inch at which it did not occur at all in the continuous cut. Again, the times before breakage were rather short.

The tests were carried out by turning a workpiece with two slots .25 inch wide as indicated by the diagram in Table 23. The side cutting edge angle of the tool was 30^{o}. The diameter of the workpiece was about 3.5 inches and, on average, the spindle speed was about 220 r.p.m.

This means that the increased tendency to breakage in the interrupted cutting cannot be explained by fatigue because the number of impacts before breakage was between 100 and 400. Therefore, the reason should be related rather to either special loading conditions on the edge of the tool at the entrance or at the exit of the cut or to the interference of the chip adhering to the tool at the end of every cutting period. Thermal cycling is not a probable influence because the slots are rather narrow and the tool does not have enough time to cool down between the cutting periods.

3.4 Fractography

The study of fracture in sintered carbides on a microscope scale has been limited mainly to the optical examination of surface cracks on the intersections of fracture surfaces with polished surfaces. The large depth of focus of the scanning electron microscope has permitted the examination of fracture surfaces of many different materials. There appears, however, to have been few applications of the technique to the sintered carbides.

3.5 Fracture Mechanisms for Sintered Carbides

3.5.1 Transgranular Fracture

If the fracture through the tool followed a random surface, the fraction of the surface represented by transgranular fracture would be equal to the volume fraction of carbide in the tool. The actual fractions observed were always much smaller than expected on this basis [1].

Figure 28 shows a transgranular crack at a WC-15% Co specimen [2]. The fraction of transgranular fracture was found to depend on the grain size rather than the cobalt content.

Kreimer and Alekseyva [3] report that no fracture of grains smaller than 2 μm was observed in the cracked specimens.

3.5.2 Intergranular Fracture

The two types of intergranular fracture, namely ductile rupture of the cobalt (which means that the fracture

Figure 28: Optical micrograph showing a transgranular crack in one of the sides of a WC-15 wt%Co specimen. The trains transversed by the crack have been indicated by arrows [2].

occurs through the cobalt layer) and interfacial fracture (which means that the fracture occurs tangent to the grain boundaries) will be discussed together (Figure 29). The fraction of intergranular fracture area represented by interfacial fracture was found to correlate with the cobalt content of the tools but not with their grain size [1].

Figure 30 shows an intergranular crack of the same specimen as Figure 28 [2]. The interfacial fracture area decreased rapidly as the cobalt volume fraction increased from about .1 to .4 [1].

It is concluded, therefore, that intergranular fracture does not follow a random intergranular path and produce one or other mode of fracture according to the thickness of cobalt encountered locally.

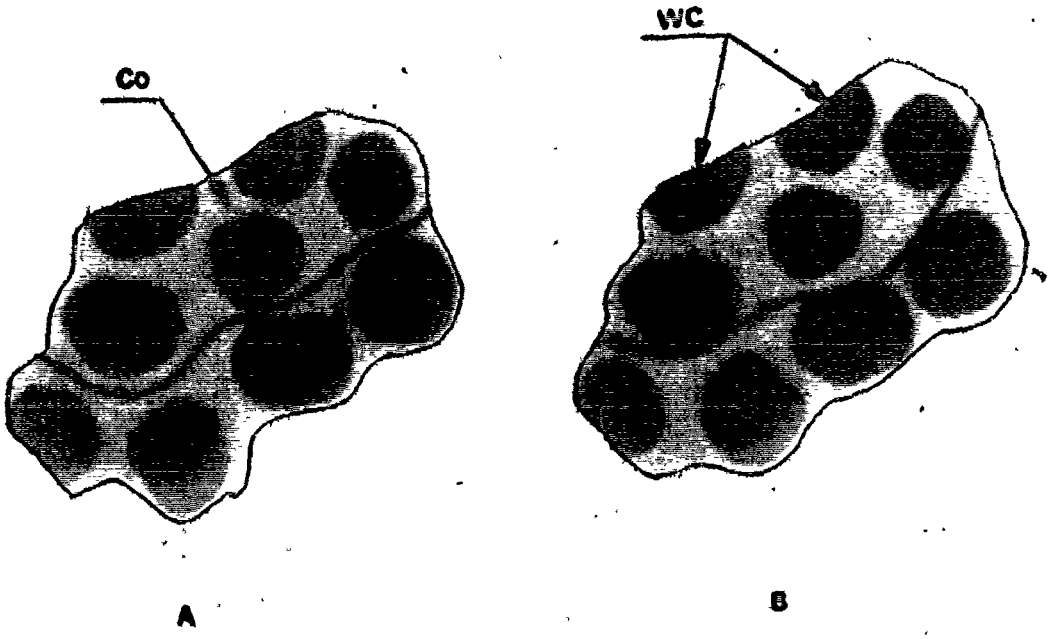

Figure 29: Types of intergranular fracture.
A - Ductile rupture of carbide
B - Interfacial fracture

Figure 30: Optical micrograph showing an intergranular crack in one of the sides of the same specimen as figure 28.

3.6 Evaluation of Test Results

3.6.1 Type of Fracture

On a macroscopic scale, the fracture of all the tools tested had the characteristic features of brittle fracture except in the region where chipping occurred.

No reduction in thickness was observed, and the fragments into which the tools broke fitted one another exactly, so that they could be put together restoring the tools to their original shape and size.

The tool fractures were classified into two major categories according primarily to the outside appearance and the feature of the fracture. They are:

3.6.2 Chipping

Chipping occurs along the cutting edge. Figure 31 shows the chipping area with low magnification. The appearance of the chipped away surfaces makes it obvious that it occurred gradually. Due to the high temperature generated from the cutting operation, the binder (Cobalt) starts to lose a part of its strength which results in some plastic deformation.

Also a portion of the work metal could be adhered to the cutting edge. The tool edge was examined under the ESM using the X-ray to determine its composition. At the nose it is found that a steel layer is spread over the carbide grains (Figure 32-a). It is interesting to note that it is generally inclined at 45° to the rake face. At the area near the nose a small amount of iron was found (Figure 32-b).

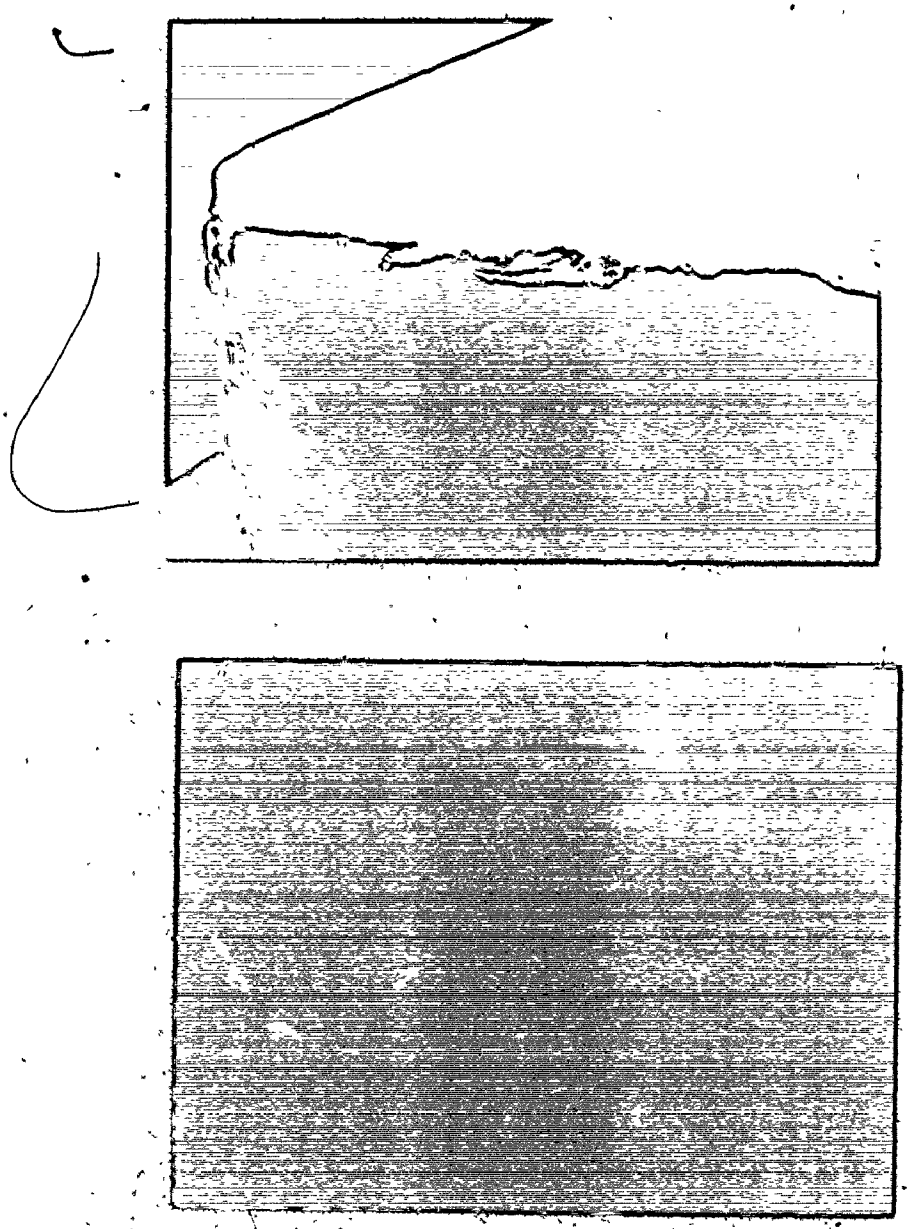

Figure 31: Chipping of the edge in continuous cutting using K45 carbide grade for machining 4340 steel hardened and tempered to 380 BHN (X65).

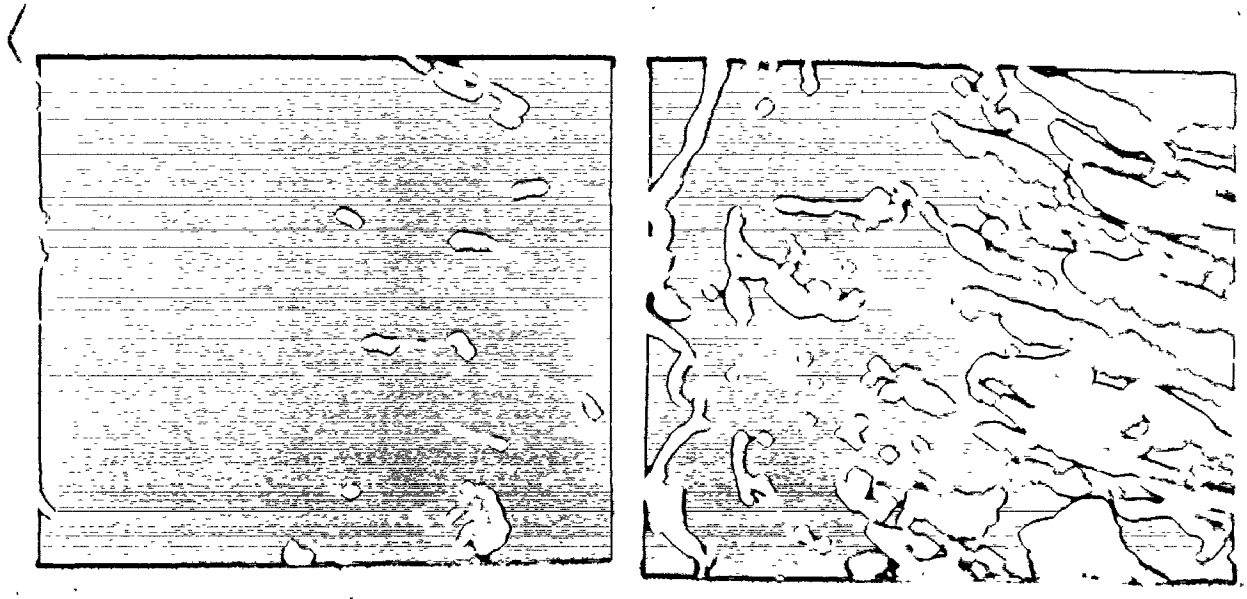

Figure 32-a: Stereo picture of chipping area covered with a steel layer at the tool nose in case of interrupted cutting using WP6 tool grade (X2200).

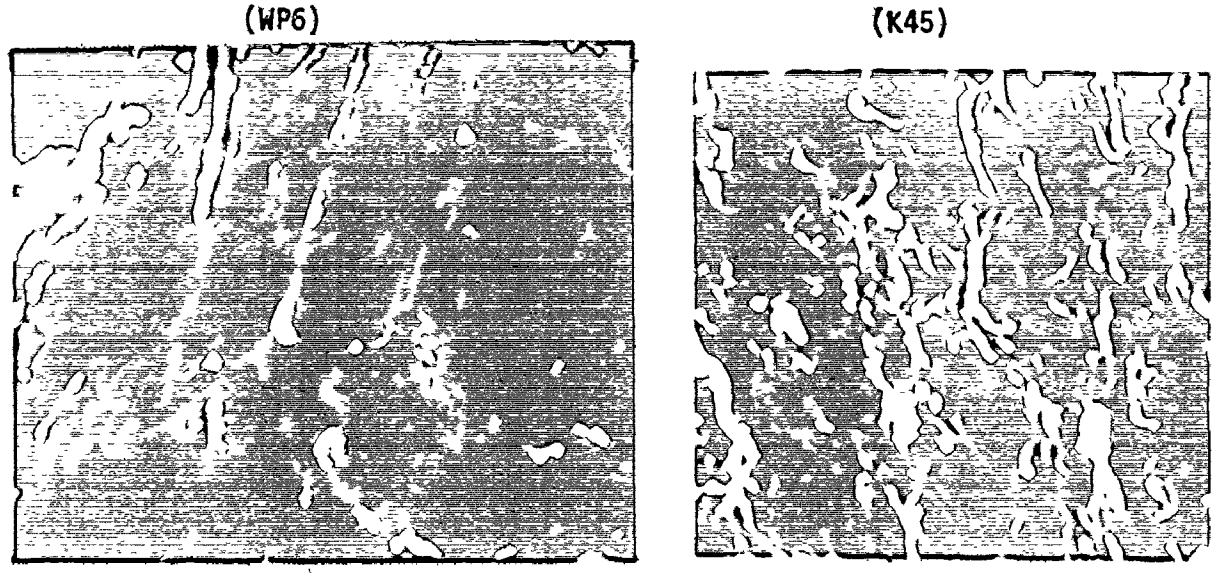

Figure 32-b: Chipping area near to the tool nose in case of interrupted cutting using WP6 tool grade and in case of continuous cutting using K45 grade for machining steel 4340 (380 BHN) (X2000).

Table 24 shows a typical composition of the etcher used to remove the steel.

Table 24

Component	Volume %
nitric acid	30
hyperchloride acid (HCl)	15
hyperfloric acid HF	10

Typical electro scanning micrographs of the chipped surfaces after etching away any steel coating and smears are shown in Figure 33-a for WP6 tool grade and in Figure 33-b for K45 tool grade at 2000 magnification.

3.6.3 Breakage

Breakage is the most dangerous type of fracture because in metal cutting, as mentioned before, it may lead to damage of the workpiece and/or the machine. It occurs due to preceding cracks. The direction of these cracks is nearly perpendicular to the cutting edge which propagates and finally splits the tool tip.

Figure 34 shows the crack which starts on the rake face and gradually propagates into the tool material nearly parallel to the flank surface.

Cracks running from the cutting edge were examined in the present work and found to be mainly intergranular fractures

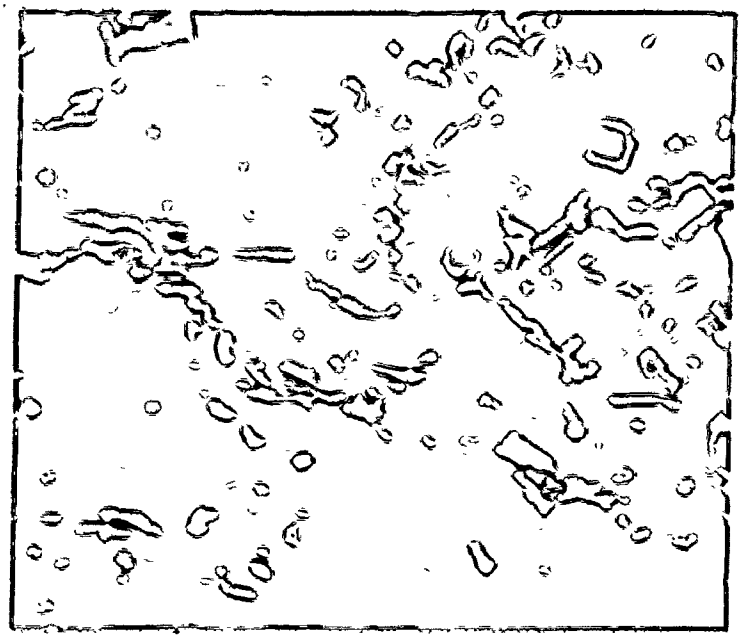

Figure 33-a: Chipping area after etching, WP6, (X2000).

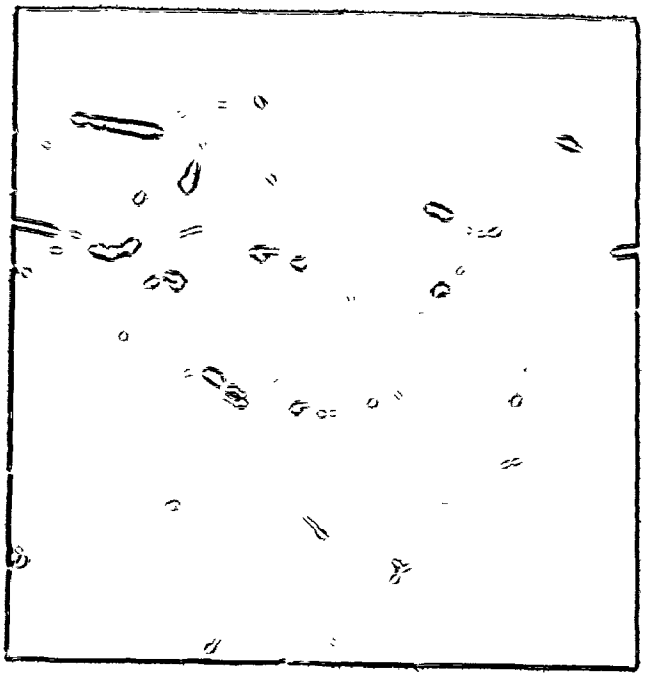

Figure 33-b: Chipping area after etching, K45, (X2000).

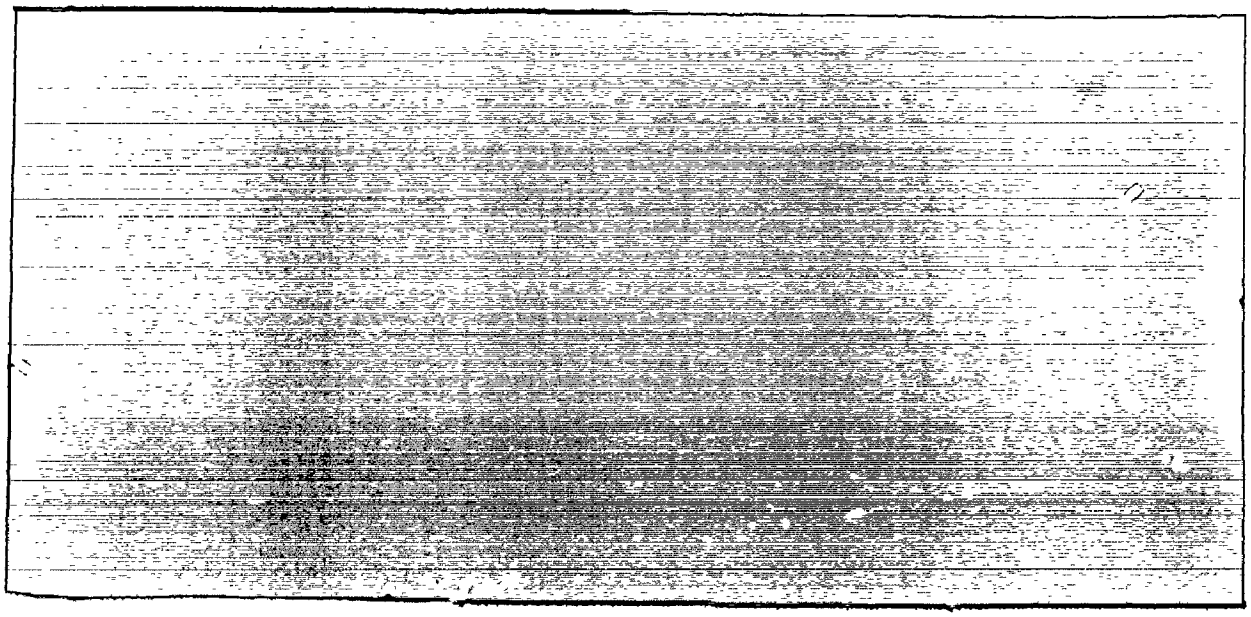

Figure 34-a: Crack on the rake face of K7H carbide grade tool used for machining 4340 steel (217 BHN), (X55).

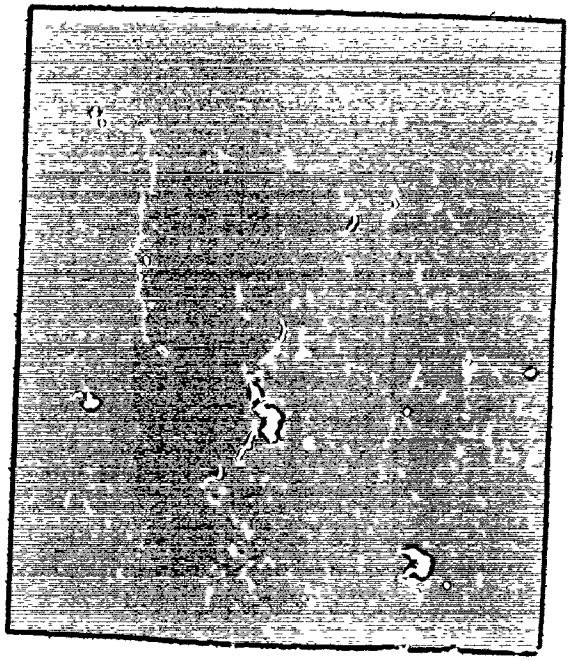

Figure 34-b: End of the same crack with high magnification (X550).

(Figure 35). Transgranular fracture was occasionally observed usually when a large carbide grain was situated across the path of the crack.

Figure 35-a shows the microcrack with low magnification and Figure 35-b shows a stereo view for the same microcrack with high magnification. Figure 36 shows another microcrack which was found in the same tool.

Breakageswith high magnification are illustrated in the following photographs. Figure 37, 38, 39 and 40 are low magnification (X20) views of K7H tool grade and Figure 40 is a low magnification (X23) view of K45 tool grade. The broken surfaces have many sharp edges and other cleavage fracture features of brittle materials. Figures 41 and 42 show the fractured surface of K45 tool grade at high magnification. Figure 43 shows the fractured surface of WP6 tool grade at a 1300 magnification and the same spot again at 2700 magnification. Figure 44 shows the fractured surface of another WP6 tool at 1700 magnification. Figure 45 shows the fractured surface of WP5 tool grade at 1700 magnification and the same spot again at 3300 magnification.

In all these micrographs sharp contours of individual carbide grains are visible. The large grain in the centre of Figure 43 shows ridge markings of intergranular fracture.

Comparing the fracture surfaces in the case of breakage (Figures 44 and 45) with those obtained in the case of chipping (Figures 33), it is seen that there is a significant difference between the two cases.

In the case of breakage it is found that the particles

Figure 35-a: Microcrackon the rake face of K45 carbide grade tool used for machining 4340 steel hardened and tempered to 380 BHN, (X2300).

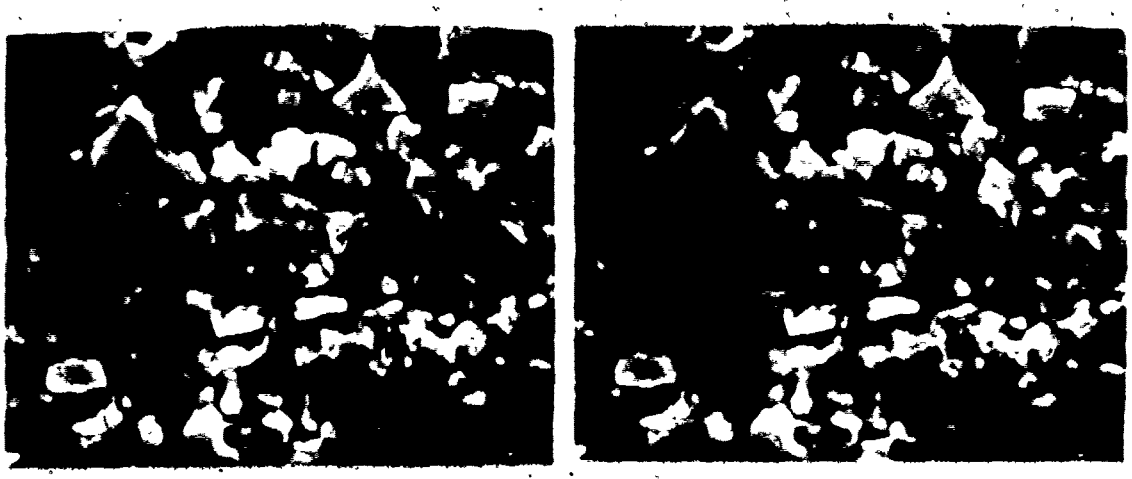

Figure 35-b: Stereo view of the same microcrack as figure 35-a, (X5300).

Figure 36-a: Microcrack on the rake face of the same tool as figure 35, (X2300).

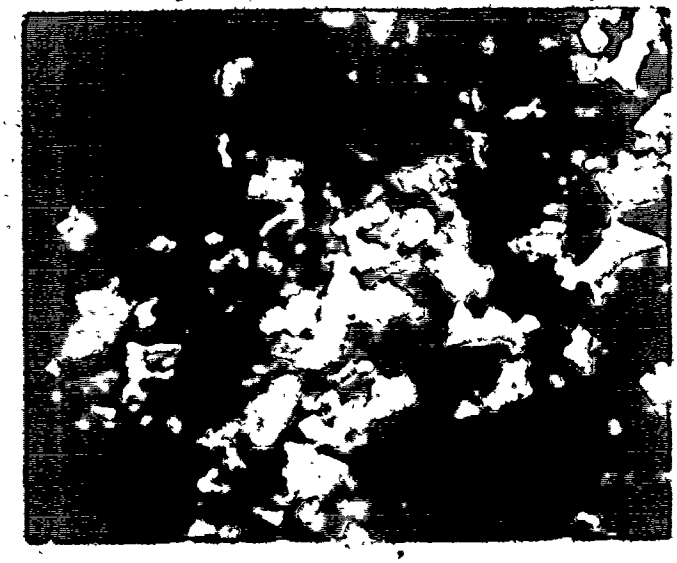

Figure 36-b: Microcrack with high magnification, (X5300).

Figure 37: Fracture surface of K7H carbide grade tool used for machining 4340 steel (217 BHN), (X20).

Figure 38: Fracture surface of the same tool as figure 37 taken from another view, (X20).

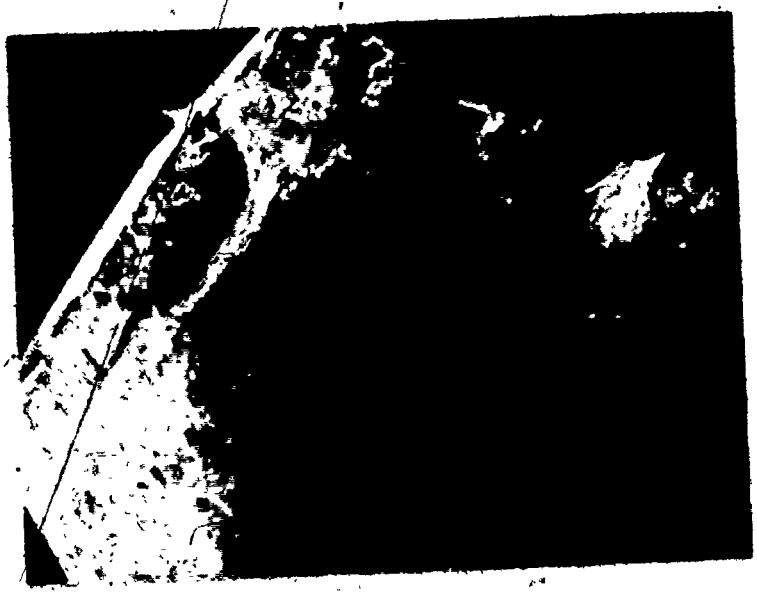

Figure 39: Fracture surface of K7H carbide grade tool used for machining 4340 hardened and tempered to 380 BHN, (X30).

Figure 40: Fracture surface of K45 carbide grade tool used for machining 4340 hardened and tempered to 380 BHN, (X23).

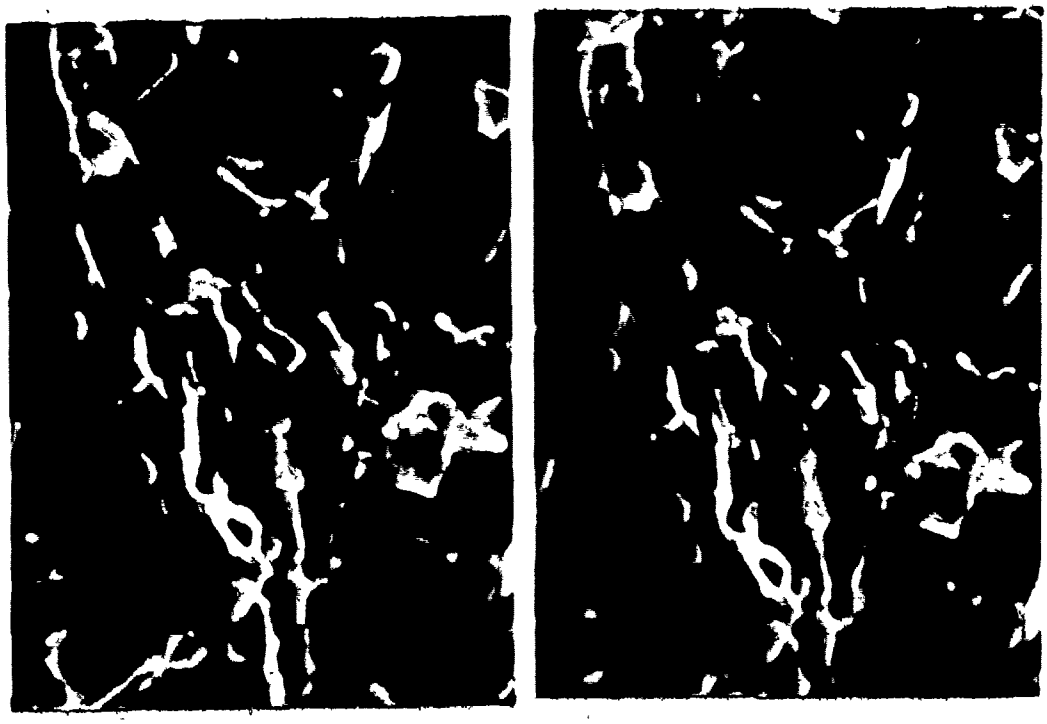

Figure 41: Stereo picture of fracture surface of K45 carbide grade tool used for machining 4340 steel (217 BHN), (X5900).

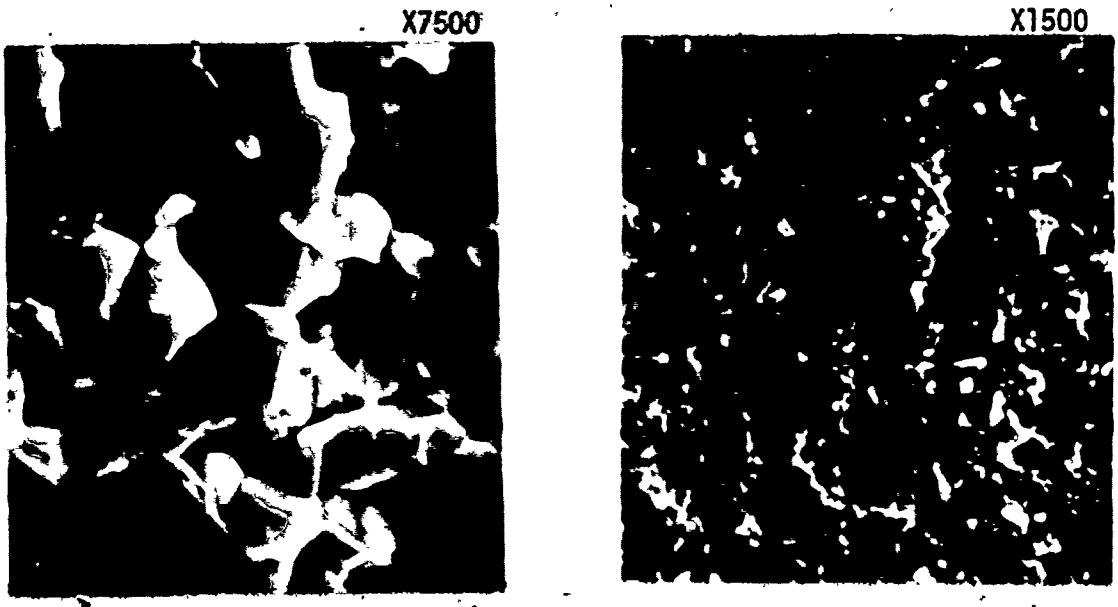

Figure 42: Fracture surface of K45 carbide grade tool used for machining 4340 steel hardened and tempered to 380 BHN.

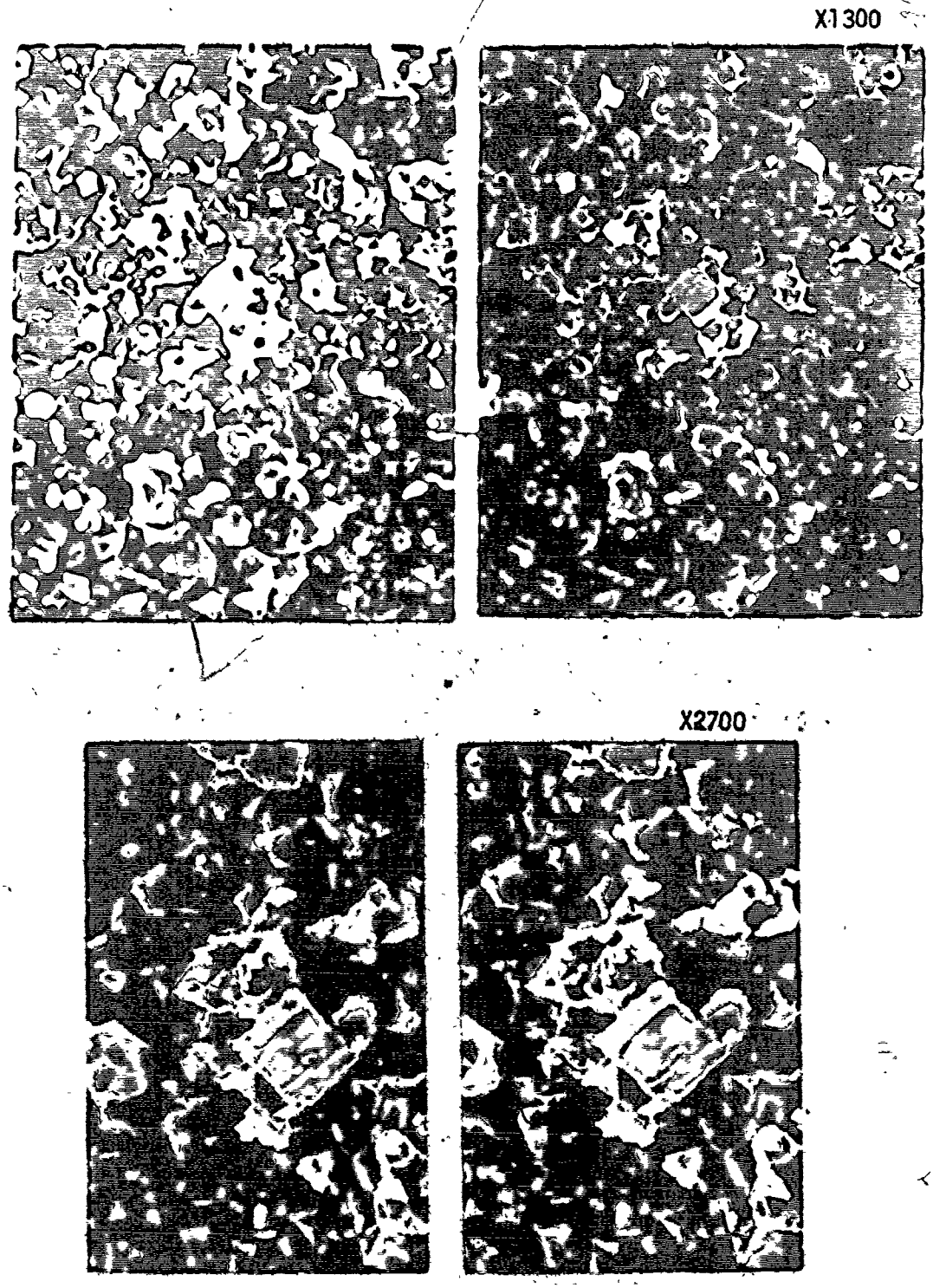

Figure 43: Stereo picture of fracture surface of WC carbide tool used for machining 4340 steel hardened and tempered to 380 BHN (interrupted cutting case).

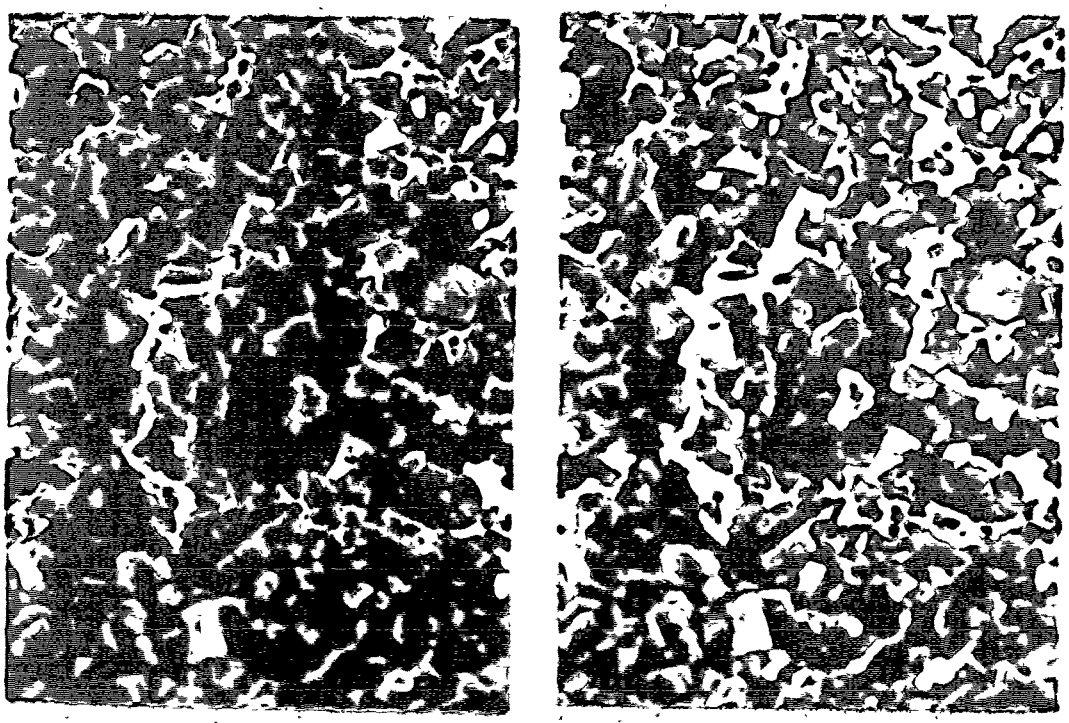

Figure 44: Stereo view of fracture surface of WP5 carbide grade used for machining 4340 steel hardened and tempered to 390 BHN X170 (interrupted cutting case).

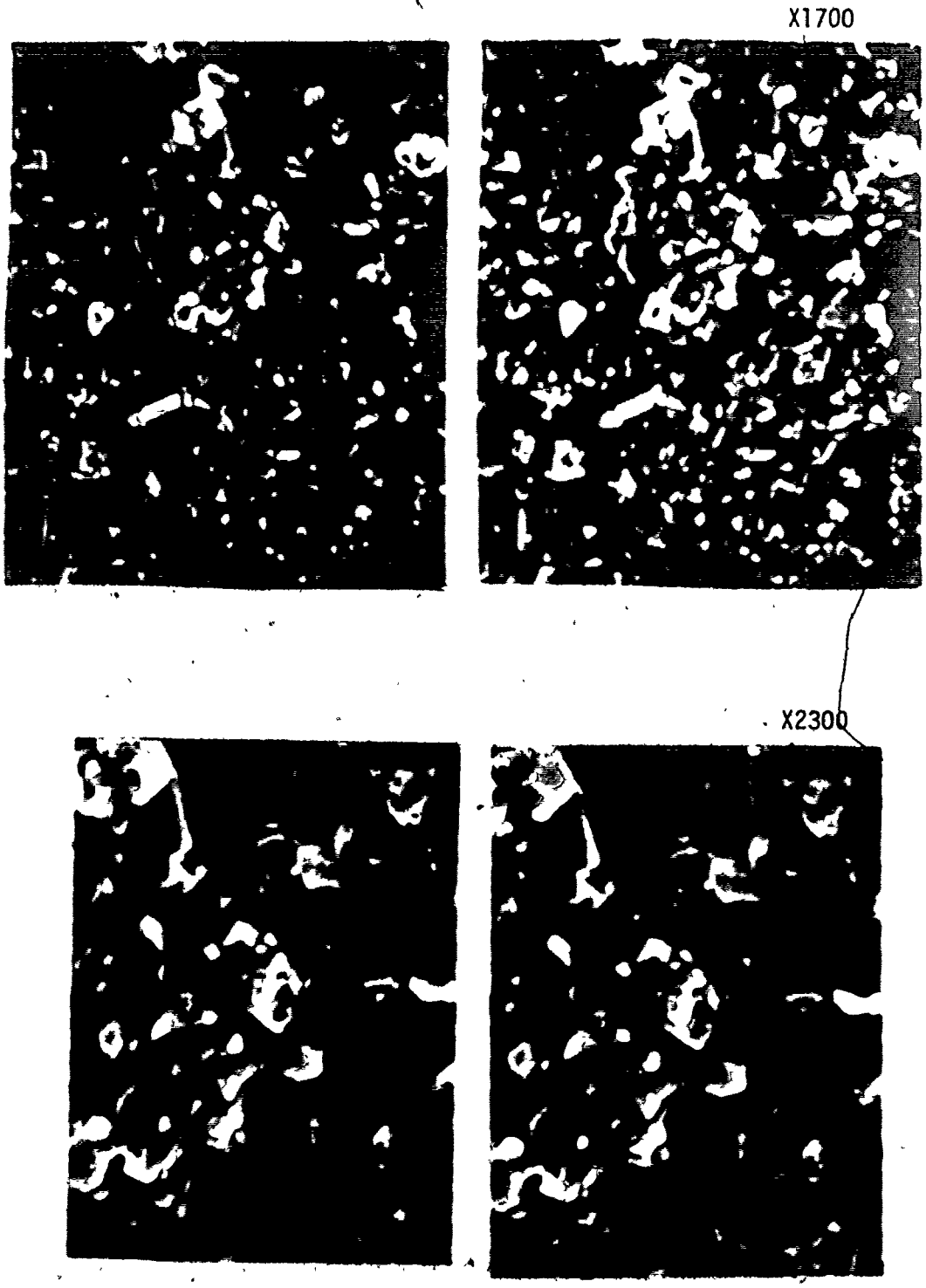

Figure 45: Stereo view of fracture surface of WP5 carbide grade used for machining 4340 steel hardened and tempered to 380 BHN (interrupted cutting case).

are substanding out of the surface and one could easily distinguish between individual grains. But in the case of chipping the fracture surface looks more smooth and it could be considered as a shear mode of failure. However it is obvious that one had to deal with a brittle fracture in the case of breakage and a ductile fracture in the case of chipping.

CHAPTER 4

ANALYSIS OF STRESSES

4.1 Introduction

The finite element method has been used to solve many varied and complex engineering problems. By this method a continuous body is idealized by a number of discrete elements, continuous forces are discretized and the problem is then solved by the methods of structural analysis.

The method is especially useful for stress analysis problems which cannot be solved by classical theory. One such problem which is of special interest in this report concerns the analysis of local stresses in the tool wedge.

4.2 Definition of the Problem

Using the findings of Primus [8] about the actual load distribution on the tip of a cutting tool it should be possible to utilize recent developments in finite elements computing methods to determine stresses in the tool wedge for various geometries and assuming various loadings under various cutting conditions. The case represents a three-dimensional problem due to the rather short length of the loaded edge and to the load on the tip. However for simplifying the computations, a plane strain (2-dimensional) case was assumed. This assumption is considered justifiable in about the middle of the width of

the cut, assuming rather large width to thickness ratio of the chip. This ratio may often in practice be between 10 and 20. At this stage no temperature induced stresses are considered.

Figure 46-a shows the load distribution of normal and shear loads on the rake and on the flank. The length of contact of the chip with the rake face is .040 in. and the length of contact on the flank (a) is taken as 0.0, 0.006 in. and 0.015 in.

Both normal and frictional loads are maximum at the tip of the tool and are assumed to decrease linearly towards the end of the contact area with the exception of the normal force on the rake face which differs slightly by being constant over the distance of half of the undeformed chip thickness.

The size of the insert considered was .5625 in. length and .125 in. thickness. The width may be assumed of any large dimension.

The computation work has been carried out for various tool geometries: zero rake angle, positive 5^{o} rake angle, and negative 5^{o} rake angle, with 8^{o} relief angle in all cases.

Two different methods were used. Figures 46-a and 46-b show the mesh used in the first method. The main characteristic of this method is that the mesh is getting finer the closer it approaches the cutting edge at which the load is concentrated on a small area. Computation of stresses is based on one single large stiffness matrix encompassing the whole tool. This method will be henceforth refered to as "the single step method". A detailed explanation of this method is found in Appendices A and B.

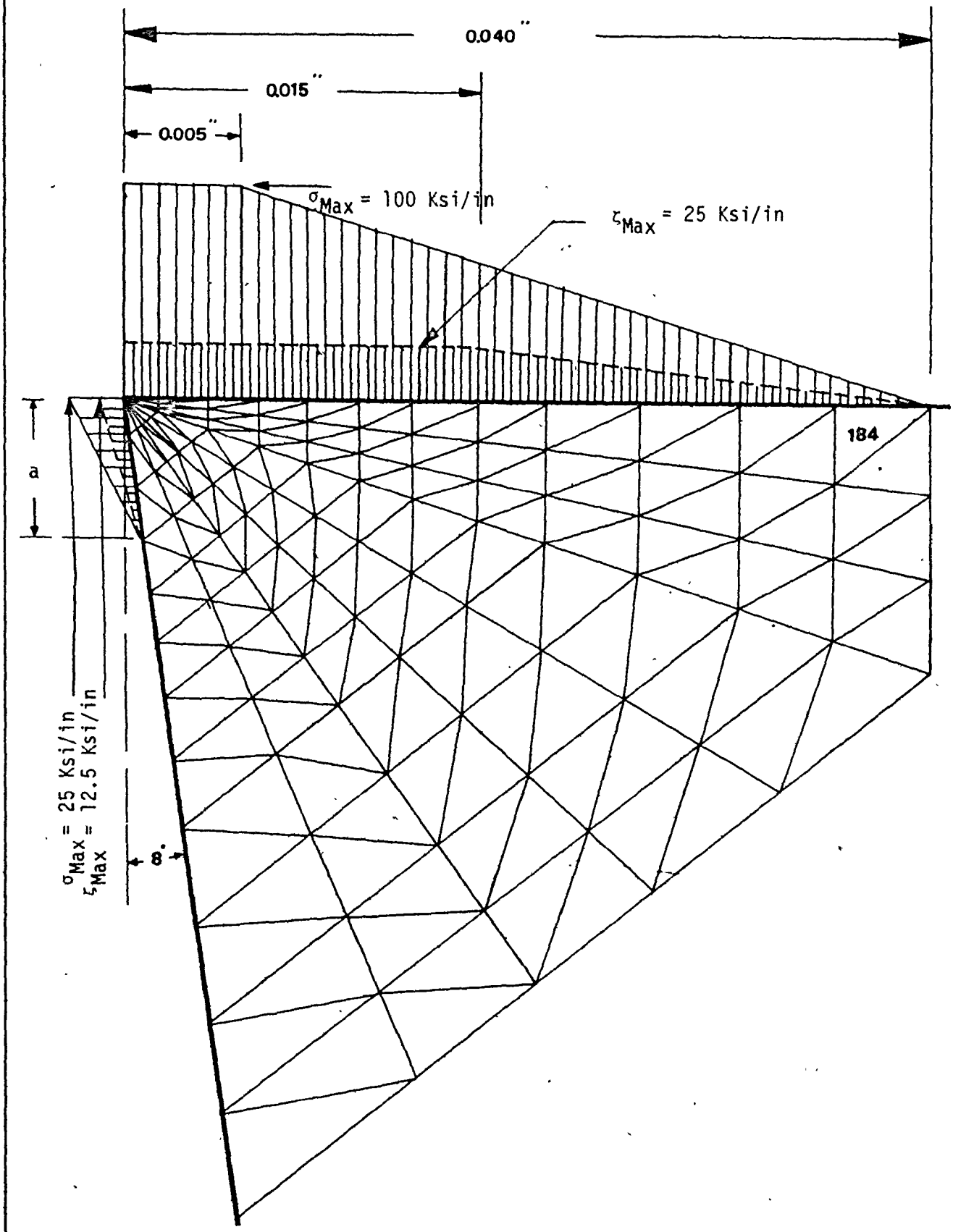

Figure 46-a

Load distribution (normal and shear loads) on the rake face and on the flank (area A in figure 46-b enlarged 175 times).

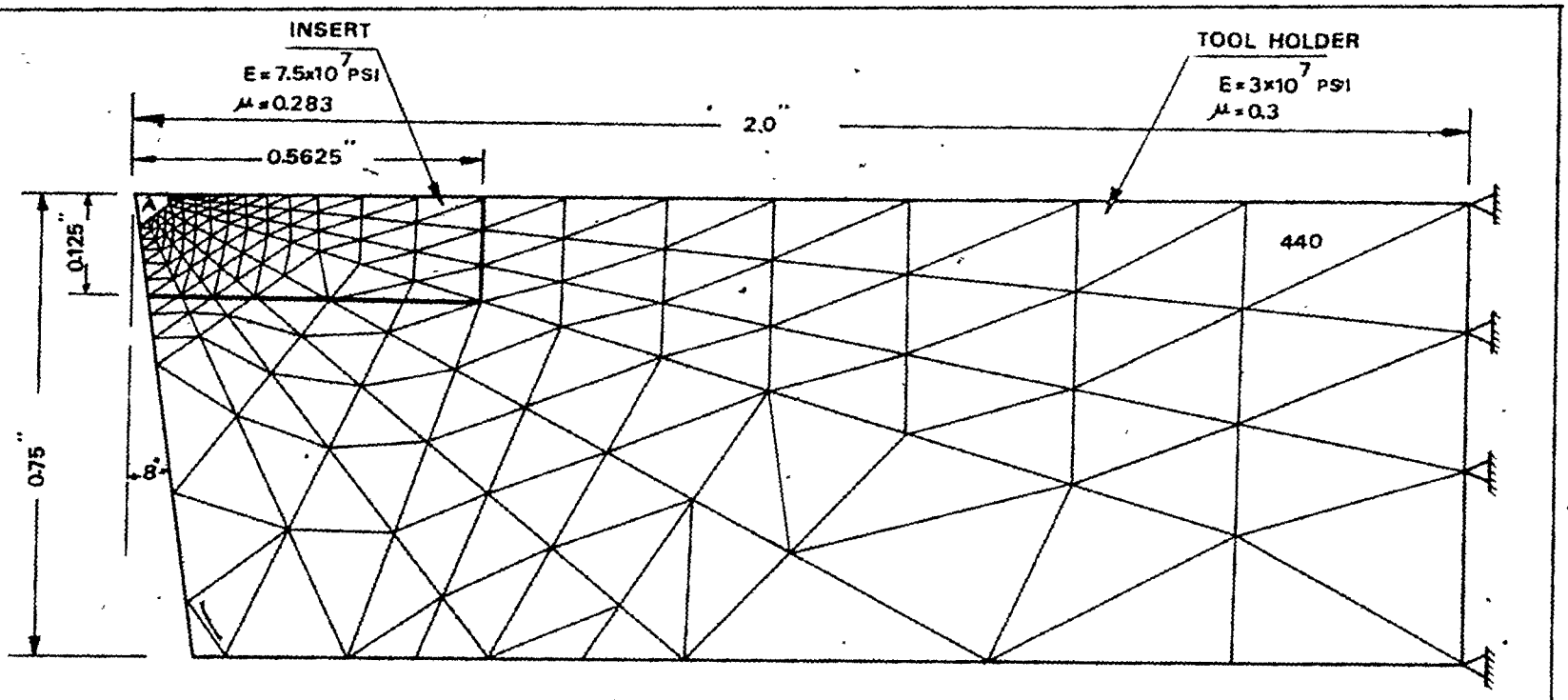

Figure 46-b. Mesh used in finite element computation (single step method).

In this method it is known that the region of high stress gradients necessitates a finer finite element mesh than the other regions of the tool. This gives rise to the following two major difficulties:

i) there will be a great variation in element size resulting in great variations in the terms of the stiffness matrix. This causes computational errors such as rounding errors.

ii) because of limitations on computer memory size the mesh cannot be made as fine as desired.

It is possible to use methods with uniform mesh such that repeatedly, stepwise smaller and smaller areas are considered and mesh refined.

Considering the structure in Figure 47 as a diagrammatical representation of the problem investigated in the present work, the total structure is considered consisting of two areas: A (large) and B (small). The load is concentrated on a part of area B which is the area of interest in which a detailed stress analysis is required. This diagram will represent one step in the gradual narrowing down and refining of a small part of the structure.

The most straightforward of such methods is the one described by Mahomed [18]. For example, in Figure 47 the governing matrix equation for the analysis of the structure (A + B) without imposing the boundary conditions is:

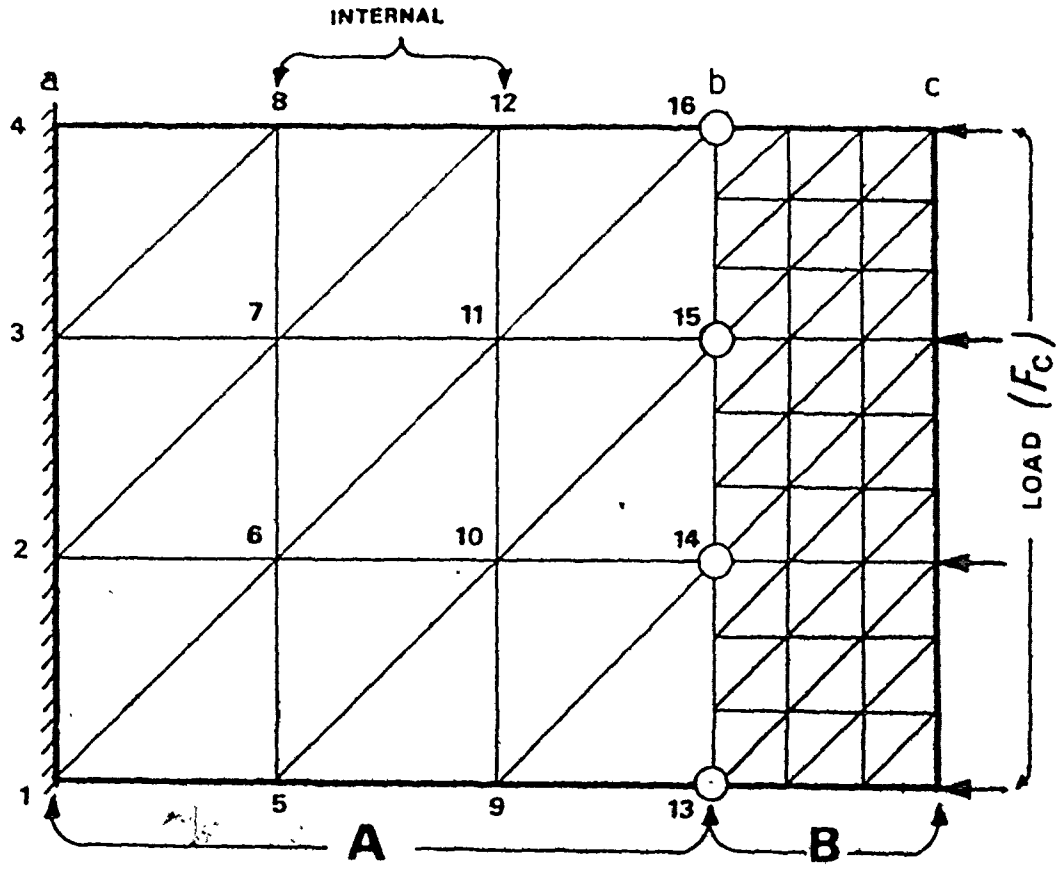

Figure 47. Diagrammatical representation of the problem.

$$\begin{bmatrix} K_a & \\ & K_{(A+B)} \end{bmatrix}_{40\times40} \begin{Bmatrix} \delta_a \\ \delta \end{Bmatrix}_{40\times1} = \begin{Bmatrix} F_a \\ F \end{Bmatrix}_{40\times1} \qquad (4.1)$$

Figure 47 shows that the structure has imposed boundary conditions on a but these are zero displacements (boundary a is fixed). Because the primary interest is in the analysis of stresses not of the forces, Equation (4.1) can be reduced to Equation (4.2).

$$\begin{bmatrix} K_{(A+B)} \text{ less } K_a \end{bmatrix}_{32\times32} \begin{Bmatrix} \delta \text{ less } \delta_a \end{Bmatrix}_{32\times1} = \begin{Bmatrix} 0 \\ 0 \\ 0 \\ \hline F_c \end{Bmatrix}_{32\times1} \qquad (4.2)$$

So, in all the following the structure (A+B) without the terms relating to the boundary a is considered.

In reference [18] a first approximation is made by performing a coarse analysis of the structure (A+B) without particular attention to the mesh size of the region of interest B and solving for the displacements δ_b between A and B.

$$[K_{A+B}] \cdot \{\delta_{A+B}\} = \{F_{A+B}\} ,$$

i.e., in more detail:

$$\begin{bmatrix} K_{AA} & K_{AB} \\ \hline & K_{bb} \; K_{bc} \\ & K_{BB} \\ K_{BA} & K_{cb} \; K_{cc} \end{bmatrix}_{32x32} \cdot \begin{Bmatrix} \delta \\ \hline \delta_b \\ \hline \end{Bmatrix}_{32x1} = \begin{Bmatrix} 0 \\ 0 \\ 0 \\ 0 \\ 0 \\ 0 \\ \hline F_c \end{Bmatrix}_{32x1} \qquad (4.3)$$

where K_{bb} and K_{cc} are sub-matrices representing direct stiffness on boundary b and on the loading nodes c respectively.

The region B is then isolated from the main structure (A+B) and a refined mesh (e.g., three times) applied to this isolated region which is termed a "sub-region". The sub-region B is now treated as a separate problem and the displacements δ_b obtained in the previous step are imposed as displacement conditions on the part B of the outer boundary (Figure 48). The load may now be more uniformly distributed accordingly:

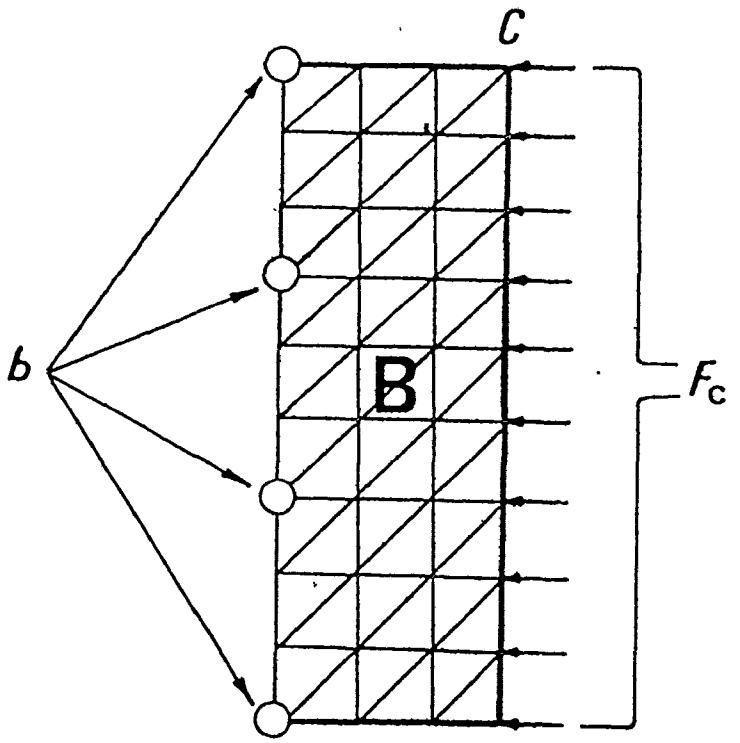

Figure 48. The area of interest (B) with refined mesh and imposed the displacement boundary conditions (δ_b).

$$\begin{bmatrix} K_{bb} & & \\ \hline & K_B & \\ & & K_{cc} \end{bmatrix}_{80\times80} \cdot \begin{Bmatrix} \delta_b \\ \hline \delta \end{Bmatrix}_{80\times1} = \begin{Bmatrix} 0 \\ 0 \\ 0 \\ 0 \\ 0 \\ \hline F_c \end{Bmatrix}_{80\times1} \qquad (4.4)$$

This has now to be solved for displacements δ, and further for strains and stresses with δ_b imposed as boundary conditions. This needs a special computational technique described in [18].

The refined analysis gives a more detailed picture of the stress distribution in the area under special consideration. If the solution by the first sub-region is not as detailed as desired, a second sub-region can be isolated from the first sub-region. A number of sub-regions may be isolated successively in this manner until convergence occurs or until a desired accuracy is attained.

A similar method was proposed by Emery [22]. He wanted to use package programs for stress analysis which, however, do not provide for imposed displacement boundary conditions. Therefore he used a technique which amounts to the same purpose but is formally different.

The first step in the solution is identical with that

in the preceding method [18]; the total structure A and B (B is the part to be subsequently refined in mesh and it contains all the external forces) was solved with coarse mesh for displacements.

Subsequently, as shown in Figure 49, part B is solved with a refined mesh while attaching springs at the original boundary b which are very stiff (several orders stiffer than the elements of the stiffness matrix) and adding external forces at the same boundary b which would give the displacements δ_b as calculated in the first step. These added springs and forces, actually, enforce displacements δ_b with a very good approximation (due to the very high stiffness of the springs). The problem now looks formally different from the preceding one:

$$\begin{bmatrix} K_{bb}+k_b & & \\ & K_B & \\ & & K_{cc} \end{bmatrix}_{80\times 80} \begin{Bmatrix} \\ \delta \\ \\ \end{Bmatrix}_{80\times 1} = \begin{Bmatrix} B_b \\ \\ F_c \end{Bmatrix}_{80\times 1} \qquad (4.5)$$

In both previous methods all steps will have to be repeated for the same structure if the loading is changed. However, the problem investigated in the present work is such that while the region of loading remains confined to always

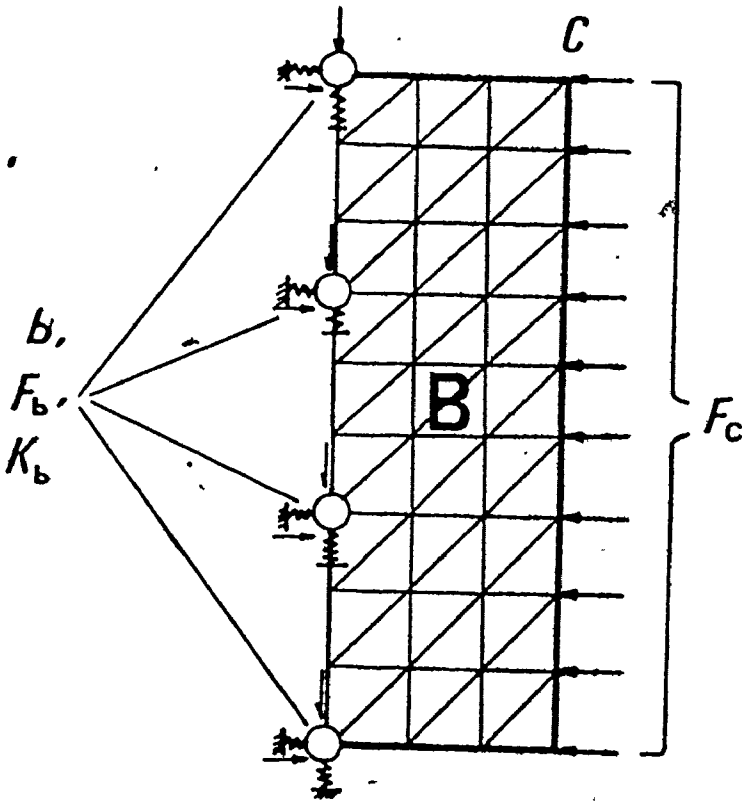

Figure 49. The area of interest (B) with refined mesh and imposed very stiff springs (K_b) and external force (F_b) on boundary b.

the same rather small part of the structure, the actual load distribution varies with cutting conditions. Therefore another method was proposed by Tlusty [23] in which all but the last step may be carried out once only for all the various loadings.

In this method already the first step is different from that in the two previous methods.

Referring to Figure 47 in the first step only part A of the structure is considered and such a structure is sought which would replace A by giving the same relationship between displacements and forces on the boundary b but be much simpler. In other words, the whole structure is considered as a sum of two substructures A and B (Figure 50). The original internal boundary b is split into an external boundary b_A on part A and an external boundary b_B on part B. The original "internal" forces on b may be considered as external forces F_{bA} and F_{bB} acting on these new boundaries. In this way the original structure is a sum of A and B, while

$$\delta_{bA} = \delta_{bB} \quad \text{and} \quad F_{bA} = F_{bB}$$

The task is now to formulate a stiffness matrix K_A^* which would replace the stiffness matrix K_A and be much smaller while it would still give the same relationships between forces F_{bA} and displacements δ_{bA}:

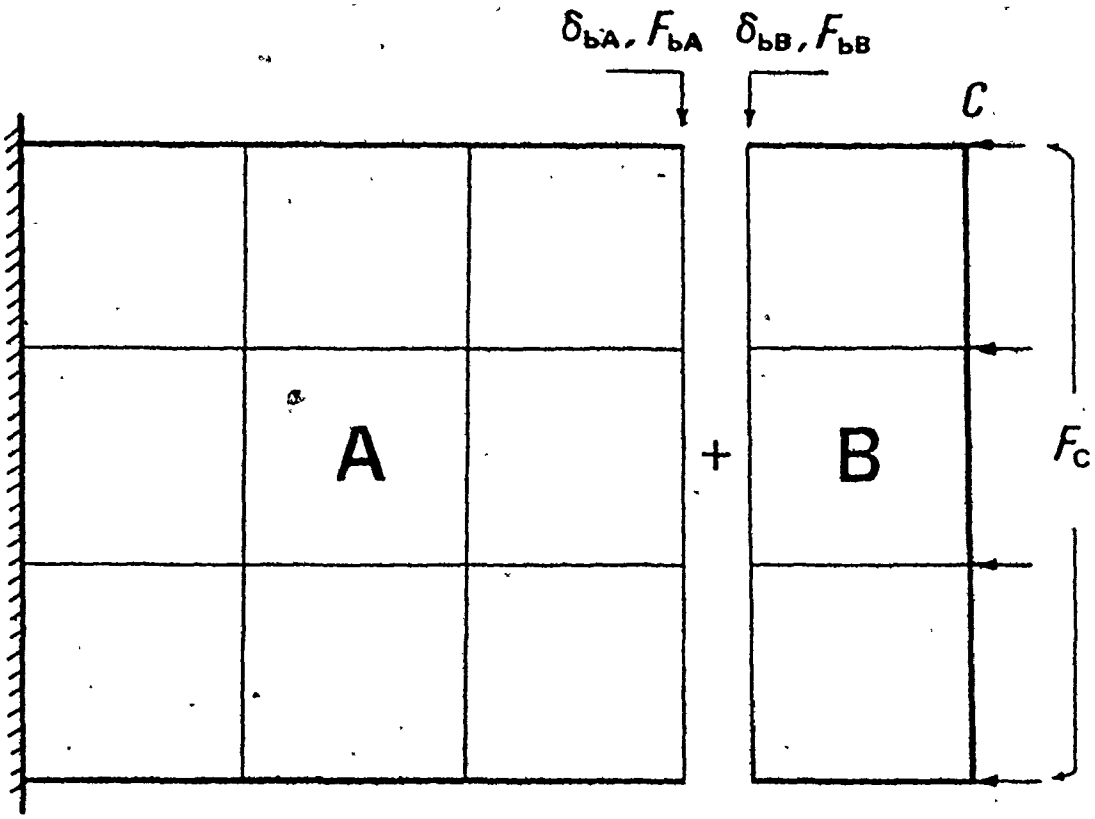

Figure 50. Substructures A and B

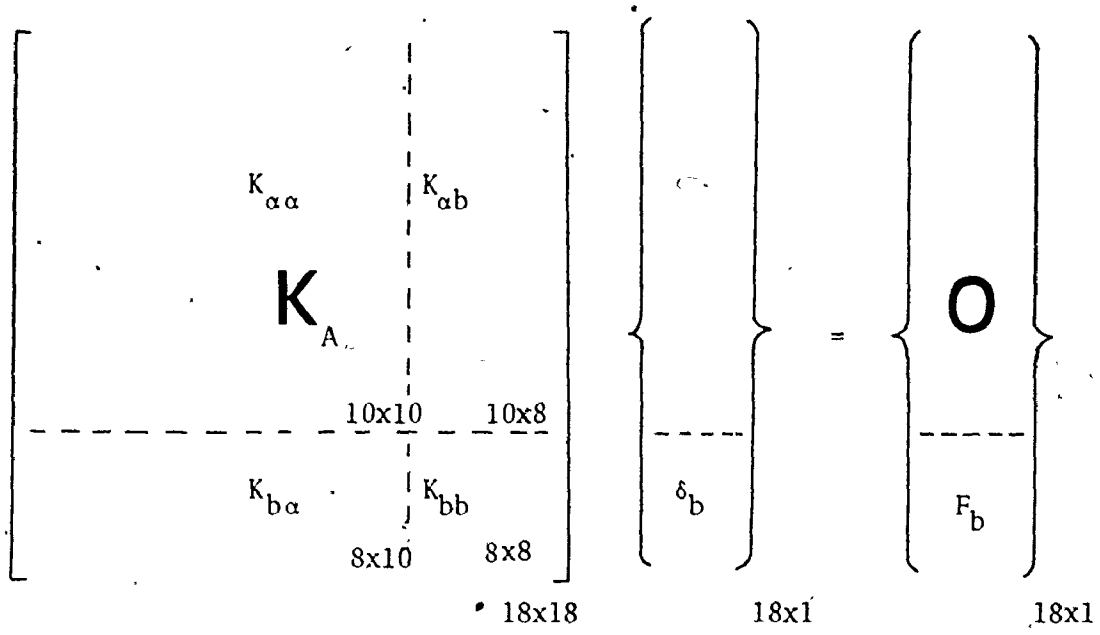

$$[K_A^*]_{8x8} \{\delta_b\}_{8x1} = \{F_b\}_{8x1} \tag{4.6}$$

Actually, as shown in Appendix B, such a replacement matrix can be determined which will have a size of the original K_{bbA} of Equation (4.6), eg., for example in Figure 47 it will be 8 x 8 only instead of 32 x 32. Practically, of course, the saving is much bigger because the number of the boundary nodes is much smaller than the total number of nodes in structure A.

In the next step, solving for part B only, a refined K_B matrix is formulated and combined with the replacement matrix K_A^*. As a result, the displacements could be obtained from Equation (4.7), and accordingly the strains and stresses.

$$\left([K_A^*] + \begin{bmatrix} & & \\ & K_{BB} & \\ & & \end{bmatrix} \right) \cdot \begin{Bmatrix} \\ \delta \\ \\ \end{Bmatrix} = \begin{Bmatrix} 0 \\ \hline F_C \end{Bmatrix} \tag{4.7}$$

In this method again, the refining of the mesh could be carried out in a number of steps.

Applying this method to the problem investigated in the present work, the computations were carried out in a number of steps. Referring to Figure 51, excluding the area ABC which includes the loading region JKC, a large mesh was used. Accordingly, the corresponding stiffness matrix was calculated using a mathematical technique which is explained in detail in Appendix C.

As a result, the effect of both the remaining part of the tool and the tool holder on the region ABC could be found. Proceeding with the same technique and taking into consideration the effect of the previous step, a smaller mesh was used for the area ABED and its effect on the remaining region DEC was calculated.

The same technique is repeatedly used until a very fine mesh is reached for the loading region.

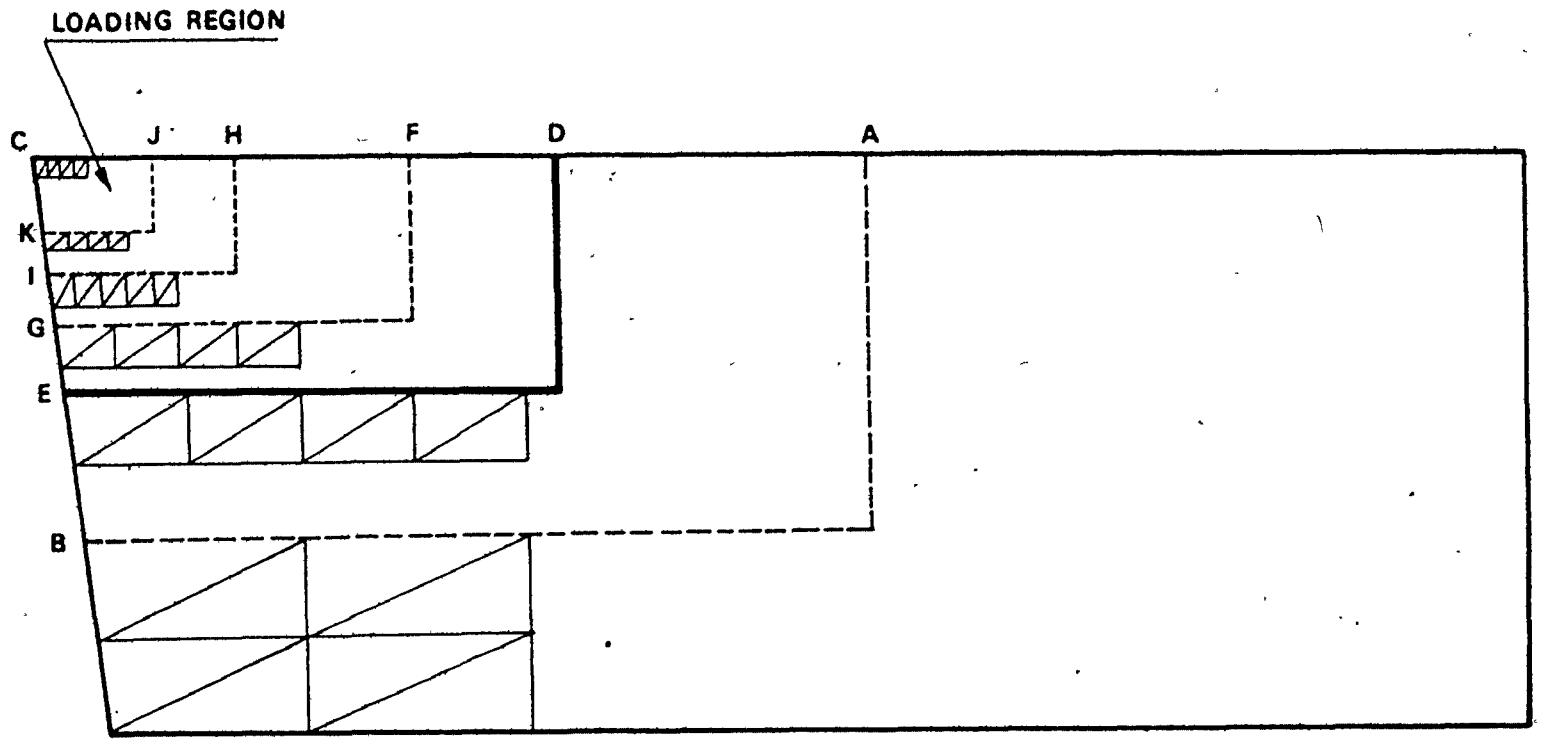

Figure 51. Stepwise and subdividing and refining method.

The stiffness matrix replacing the area KJHI and, in this way replacing all the remaining part of the structure outside of the area of consideration is independent of loading as long as loading is confined to the area of consideration. Once this replacement matrix is derived and combined with the refined matrix of area CJK it may be repeatedly used in the various cases of loading as they correspond to the various combinations of cutting conditions.

4.3 Stress Analysis of the Tool

4.3.1 Solution Using Elementary Beam Theory (Cantiliver Beam in Bending)

The tool and tool holder were treated as a square section cantiliver of 2 inches length and 0.75 inch in depth. A concentrated normal load of 2250 pounds acting at the tip of the free end, which is equivalent to the load acting on the tool tip, was considered.

Figures 52-a, 52-b, 52-c, 52-d and 52-e show the contours of normal stresses (σ_x), the contours of maximum principal stress, the contours of minimum principal stress, the contours of maximum shear stress and the direction of maximum principal and shear stresses respectively.

This approximation cannot, of course, solve the local stresses in the loading region (the tip of the tool). From Figures 52, this analysis would lead to a conclusion that as the tip of the tool is approached, bothprincipal stresses and also the maximum shear stress are all approaching zero and this is obviously incorrect. On the other hand, in regions

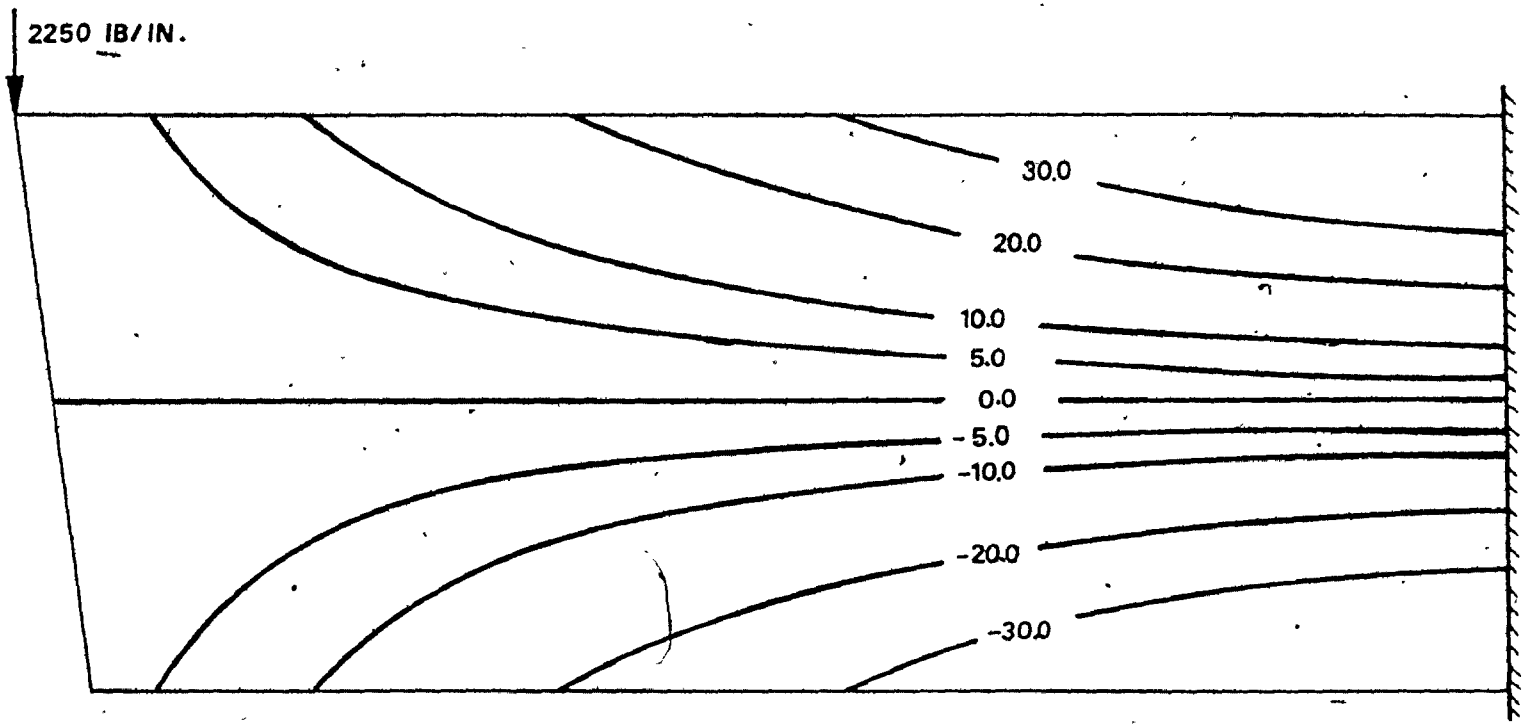

Figure 52-a. Normal stress contours using the classical solution (σ_x Ksi).

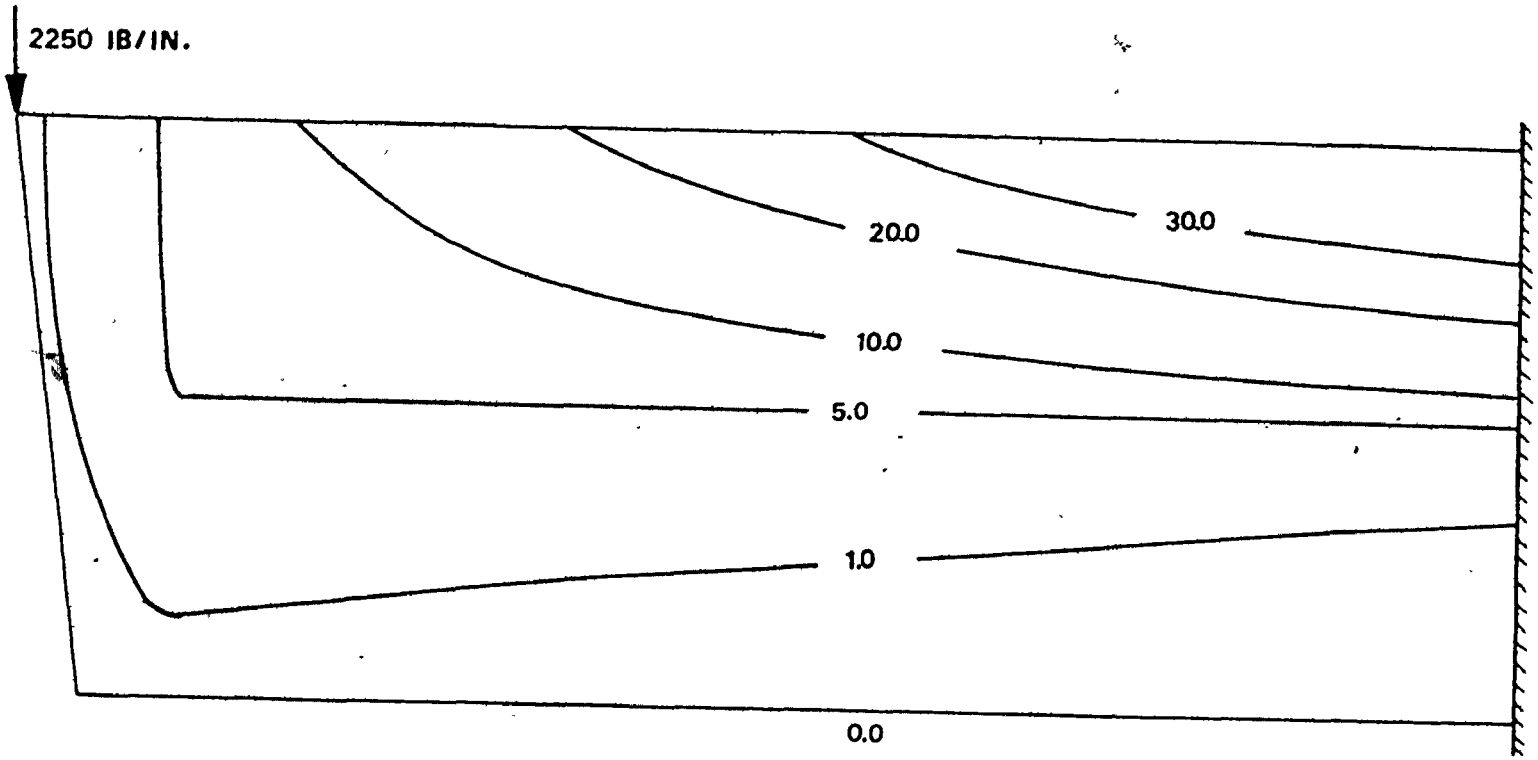

Figure 52-b. Maximum principal stress contours using the classical solution (σ_1 Ksi).

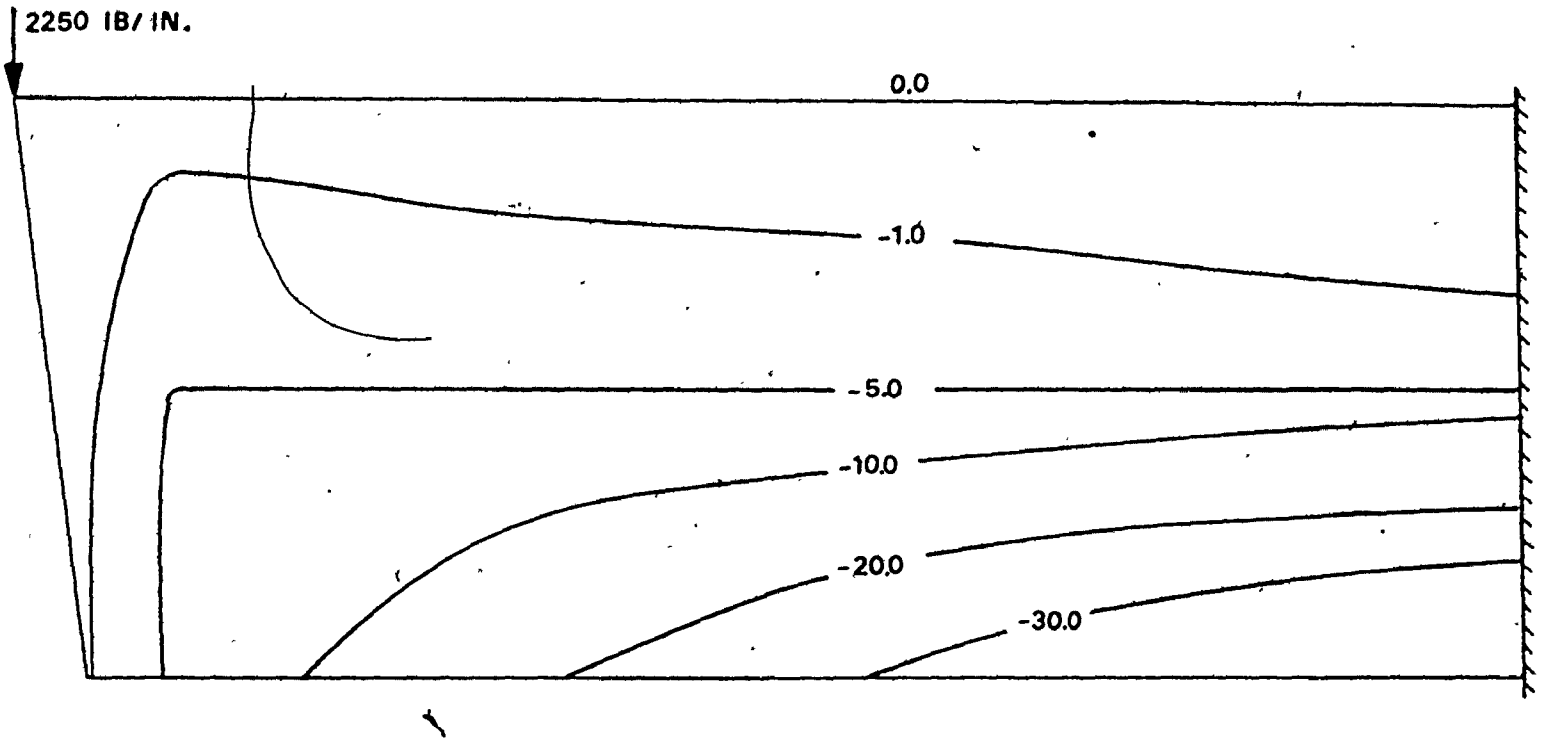

Figure 52-c. Minimum principal stress contours using the classical solution (σ_2 Ksi).

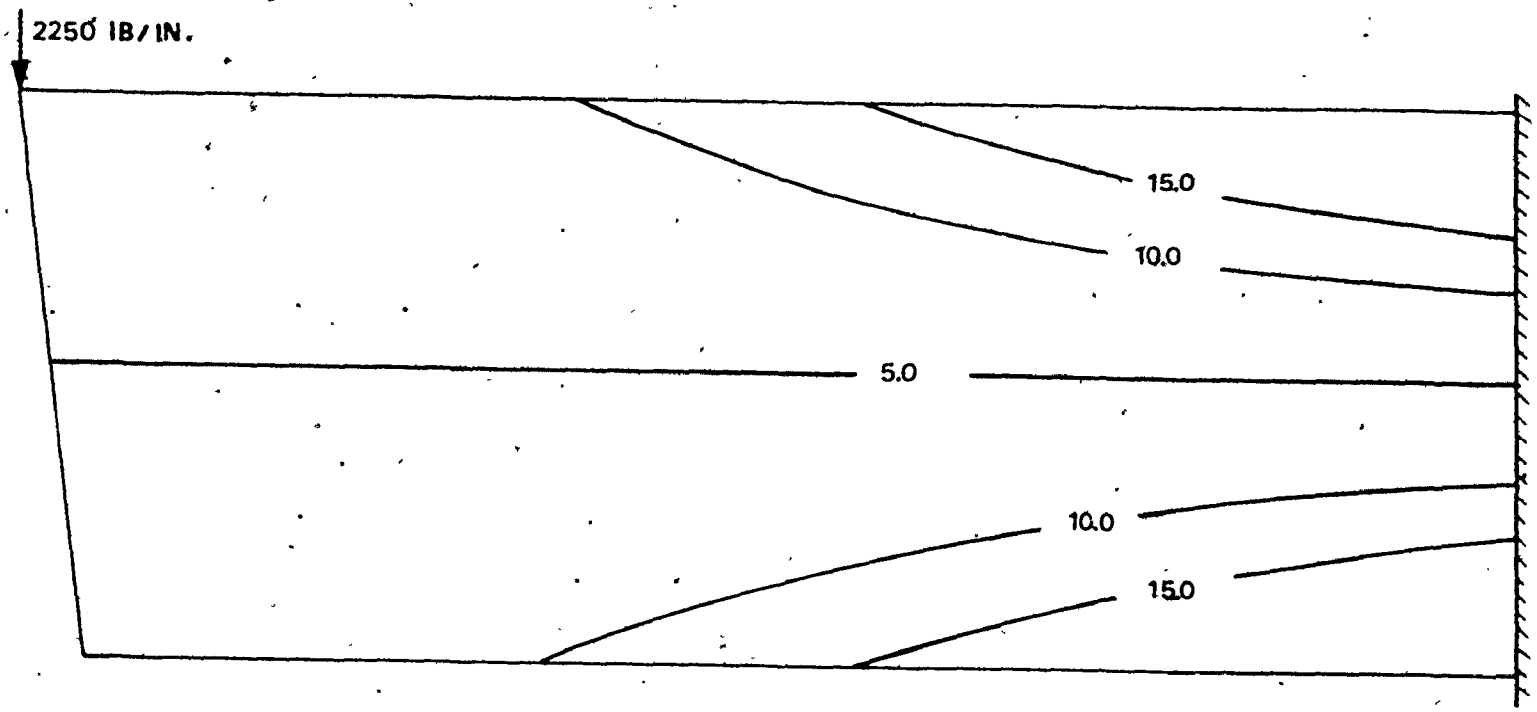

Figure 52-d. Maximum shear stress contours using the classical solution (τ_{Max} Ksi).

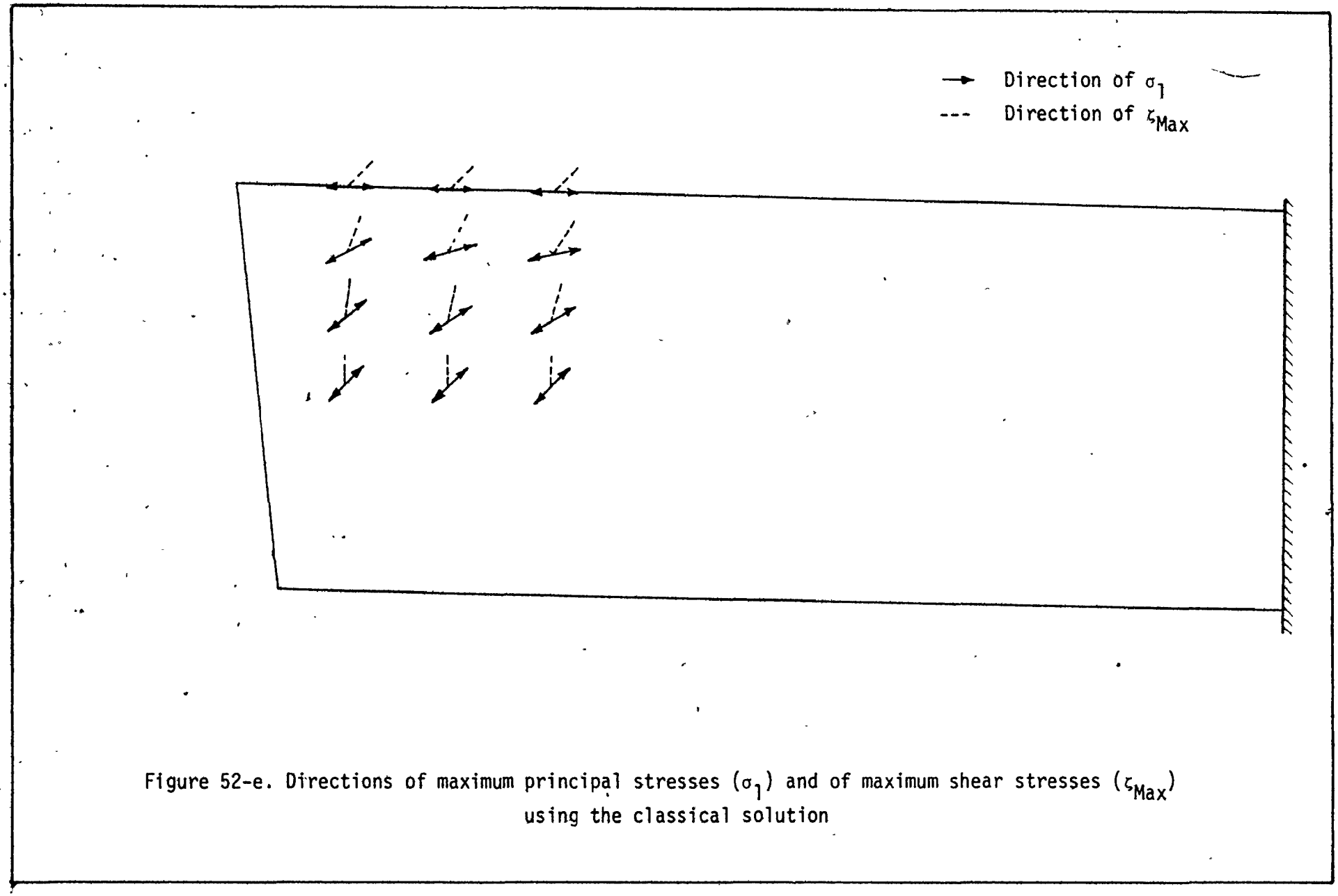

Figure 52-e. Directions of maximum principal stresses (σ_1) and of maximum shear stresses (ζ_{Max}) using the classical solution

remote from the load the stress distribution obtained in this way should approach the actual one. Therefore it will be possible to use these regions for comparing the results obtained by the finite element technique with this classical solution.

4.3.2 Solutions Using the Finite Element Technique

A. Single Step Method

The computations have been carried out for various tool geometries. Three different cases were considered: zero rake angle, positive 5^{o} rake angle and negative 5^{o} rake angle.

The flank wear is considered one of the important failure mechanisms and accordingly in each of the previously mentioned cases three different values of flank wear width "a" were considered: a = 0.0 inch, a = 0.006 inch and a = 0.015 inch, and the corresponding maximum and minimum principal stresses as well as the maximum shear stress were plotted.

The discussion of the results will include the effect of rake angle and the effect of flank wear on the distribution of stresses in the tool with special interest in the tool wedge.

The effect of rake angle:

In the case of zero rake angle ($\alpha = 0^{o}$) with no flank wear, the contours of principal stresses and of maximum shear stress are shown in Figures 53, 54 and 55 respectively.

By inspecting the maximum principal stress contours it can be seen that there are no tensile stresses in the immediate loading area (close to the cutting edge) Figure 53-a.

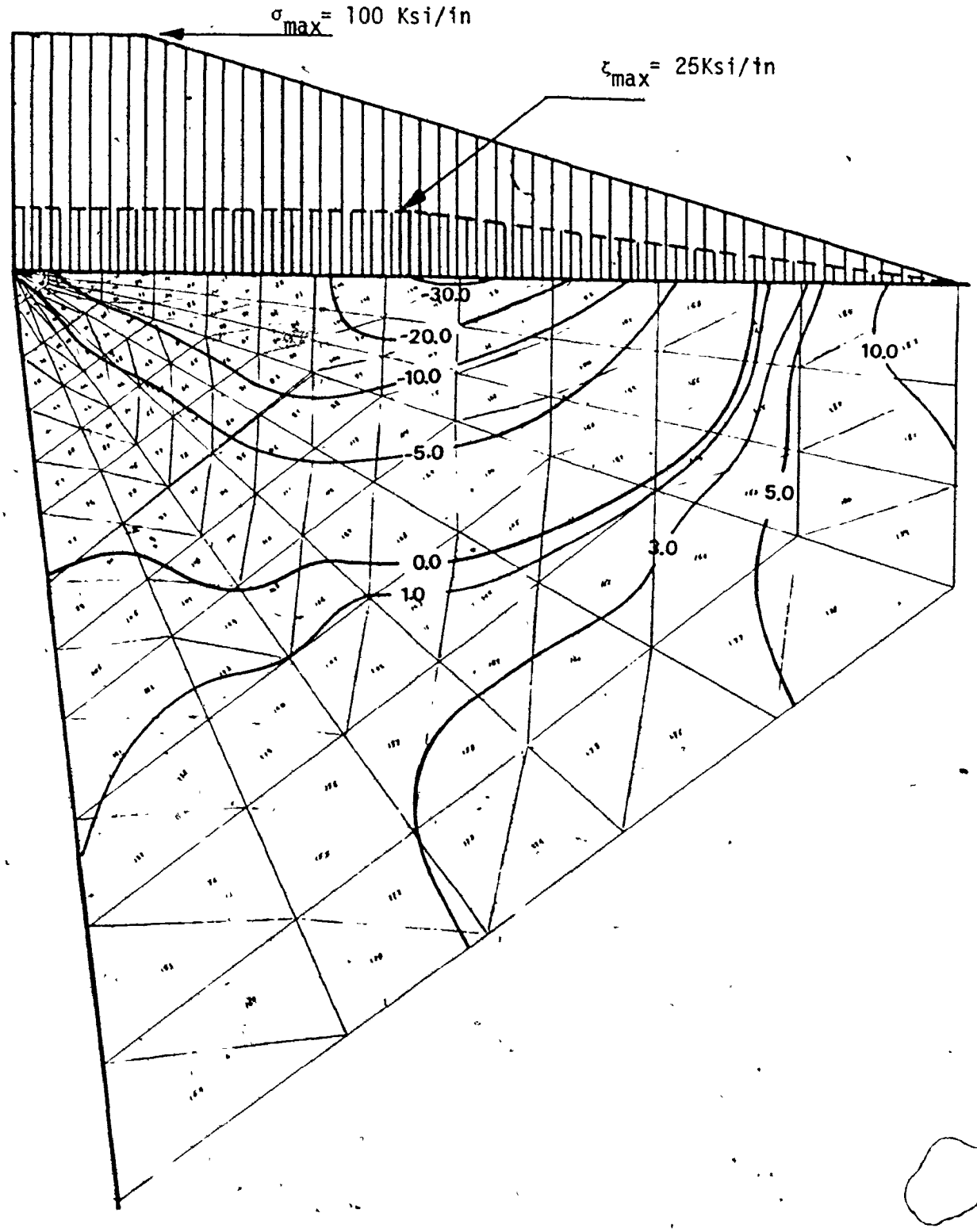

Figure 53-a	Maximum principal stress contours in the loading region (σ_1 Ksi).	$\alpha = 0^o$ a = 0.0 inch

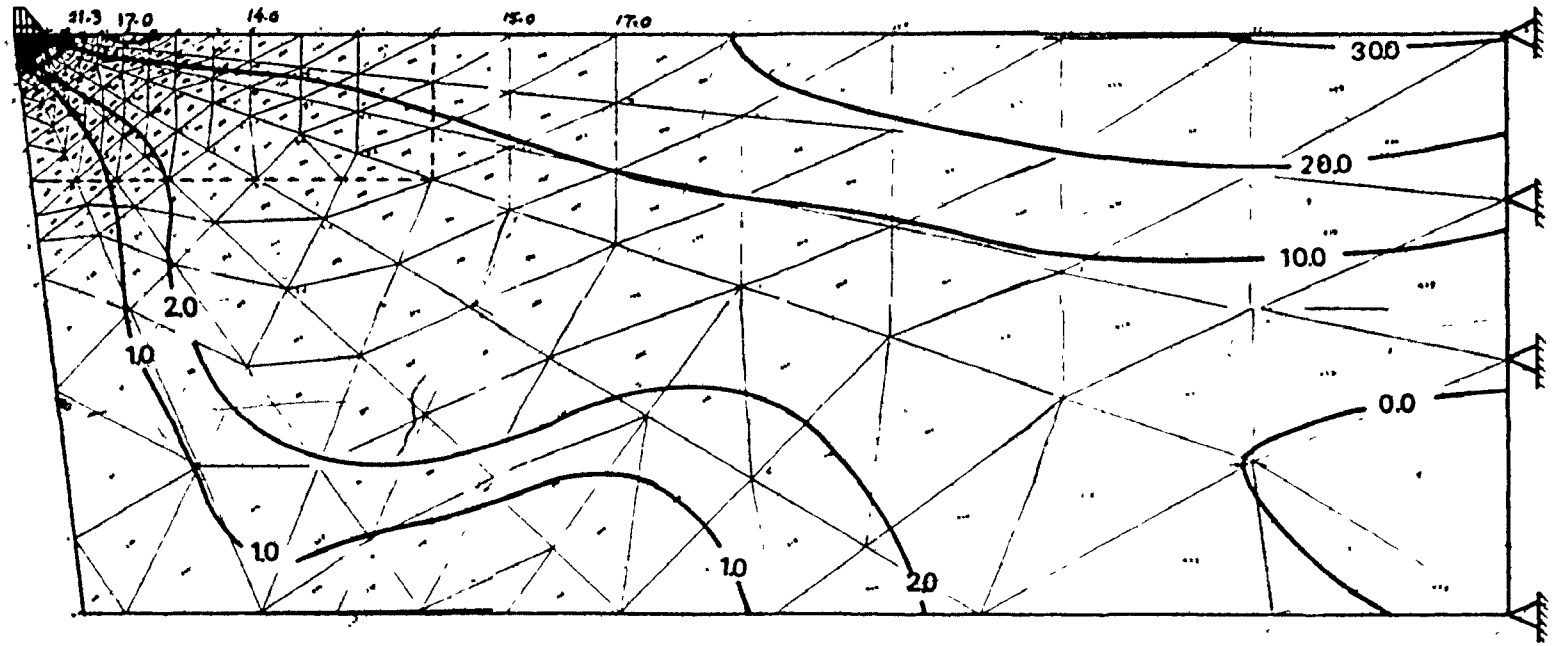

Figure 53-b. Maximum principal stress contours in the tool and tool holder (σ_1 Ksi).

$\alpha = 0^0$

a = 0.0 inch

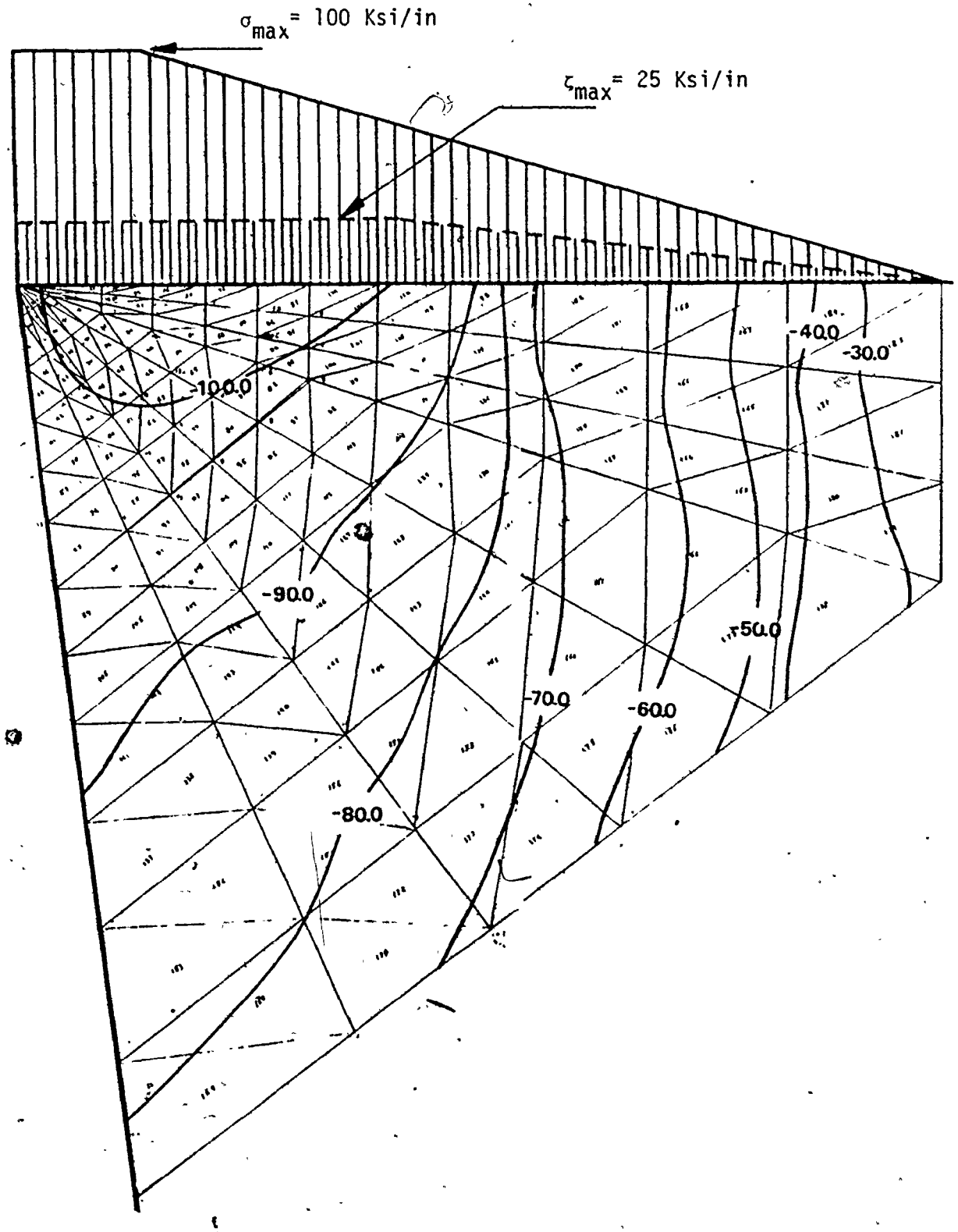

Figure 54	Minimum principal stress contours in the loading region (σ_2 Ksi).	$\alpha = 0^o$ a = 0.0 inch

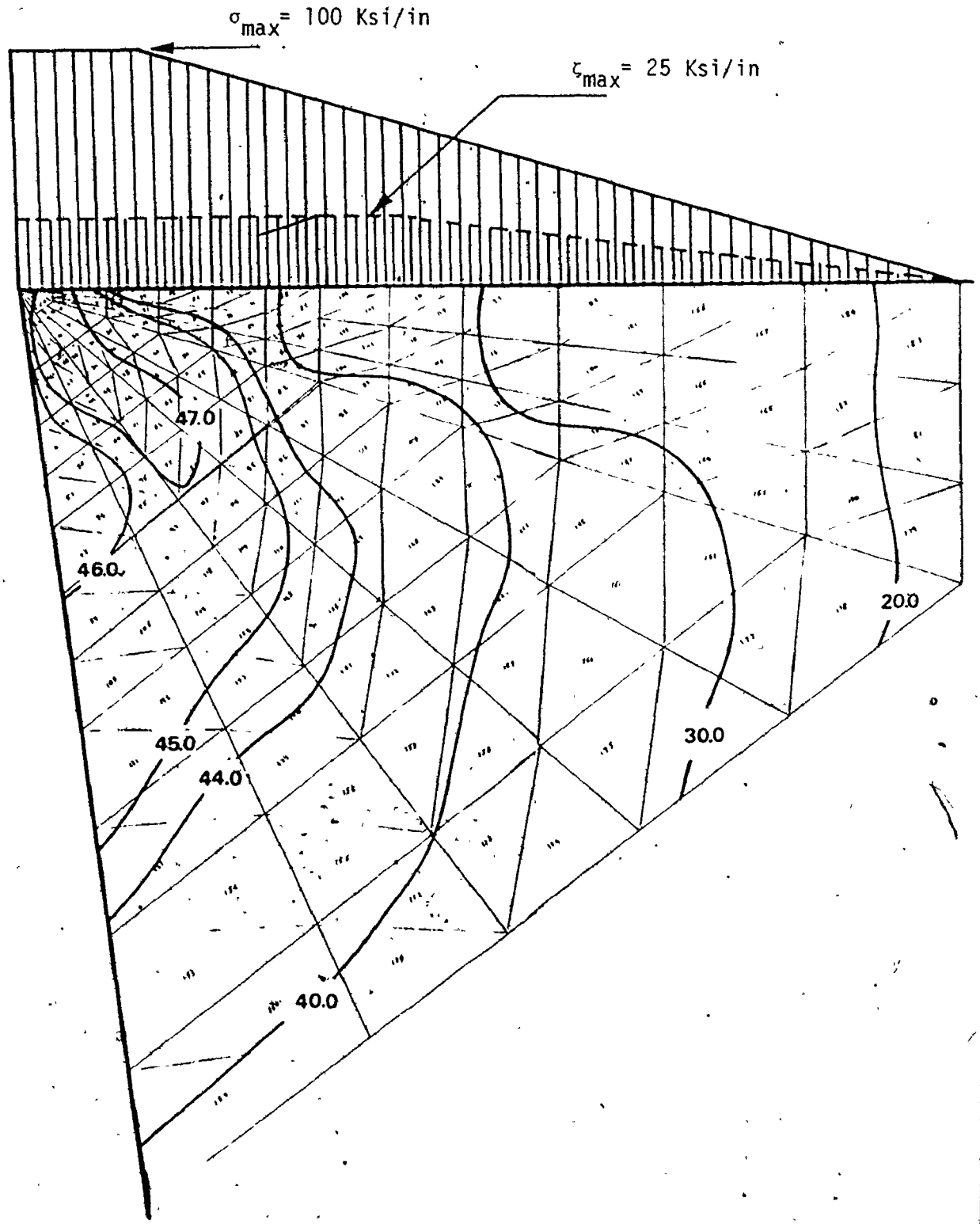

Figure 55	Maximum shear stress contours in the loading region (ζ_{max} Ksi)	$\alpha = 0^0$ a = 0.0 inch

Checking with Figure 53-b it is seen that a local maximum of tensile stress in the carbide insert occurred at the rake face at a distance from the tip slightly greater than two times the length of chip contact, which agrees rather well with the results obtained by Loladze [6].

The value of the local maximum tensile stress is 21.3 Ksi and it starts to decrease moving away from the tool tip and starts to increase again in the tool holder and reaches the maximum value of about 30 Ksi near the fixed end. The area of the local maximum tensile stress is rather small and it is confined to the immediate vicinity of the rake face. From there into the insert the stress decreases rapidly.

The values of the local maximum tensile stress in the insert are rather small. The usual values of the transverse rupture strength of carbides are between 100 Ksi and 400 Ksi. The feed assumed in calculating the forces on the tip of the tool was 0.010 in./rev. In the cutting tests no breakage of the tool was obtained at this feed. The tools were broken at the values of feeds between 0.030 in./rev. and 0.043 in./rev. which are larger by about four times than those used in the computations. For these feeds the computation would give a maximum tensile stress on the rake face of the insert of about 85 Ksi. The difference between this value and the transverse rupture strength may be due to the simplification of the computations to a two-dimensional case. Actually, this value would be expected to be higher if the computations were carried out as a three-dimensional finite element problem which would

better express the real case. Also, in the computations, a homogeneous and isotropic material was assumed. However, actually, in the case of sintered material (carbide), the structure is anisotropic and not homogeneous. The structure consists of two or three phases (Figures 25, 27). Local stresses in such a structure may be much higher than those computed above and this would further account for the discrepancy between computation and experiment. It is however very important that the computations show the location of the point of the highest tensile stress on the rake face of the tool (Figures 53-b, 63-b and 66-b) and this location agrees with the location of breakages found experimentally (Tables 14, 15 and 16)

The point of highest tensile stress found in the computations was at a distance from the tip of between 0.1 inch and 0.13 inch and the distance of breakage from the tip was found to be about 0.15 inch in the cutting tests.

These findings may interpret the breakage of the tool as a brittle fracture phenomenon but in the case of chipping of the edge, these could not explain the chipping phenomenon as caused by tensile stresses because no tensile stresses were found close to the edge of the tool.

Figure 54 shows the contours of the minimum principal stress at the cutting edge. It is seen that high compressive stresses were found with a maximum value of 100 Ksi close to the tip of the tool and they decrease when moving from the tip.

From Figure 55, which shows the contours of the maximum shear stress, it is found that the shear stress increases as

we move towards the tool wedge with a maximum value of 47 Ksi.

These high values of shear stress especially when combined with high temperatures in this area resulting from the cutting operation (400°C), could be the possible cause of chipping as a ductile failure in a shear flow mode. The strength of cobalt starts decreasing to some extent and its ductility increases. The cobalt deforms plastically and spreads over the carbide grains. These results agree with those obtained experimentally. Figures 32, 33 show this kind of fracture and the direction of shear flow of the cobalt matrix is shown too.

There are several other aspects to consider regarding chipping of the edge. One of them is that often the sintering process will not have the same result at the edge as in the bulk of the insert and the edge itself has lower strength. Hence, the purpose of honing the edge. Another one is the opinion that chipping is due to the mechanism of adhesion between the tool and the workpiece material [4].

Figure 56 shows the direction of maximum principal stresses and the maximum shear stresses (the lines with arrows represent the direction of the maximum principal stresses while the simple lines represent the direction of the maximum shear stresses). Comparing these directions with those shown in the photomicrographs of breakage (Figures 37, 40), it is seen that the direction of breakage in the cutting tests was rather the same as the normal to the directions of maximum tensile stresses obtained from the computations. This agrees with the

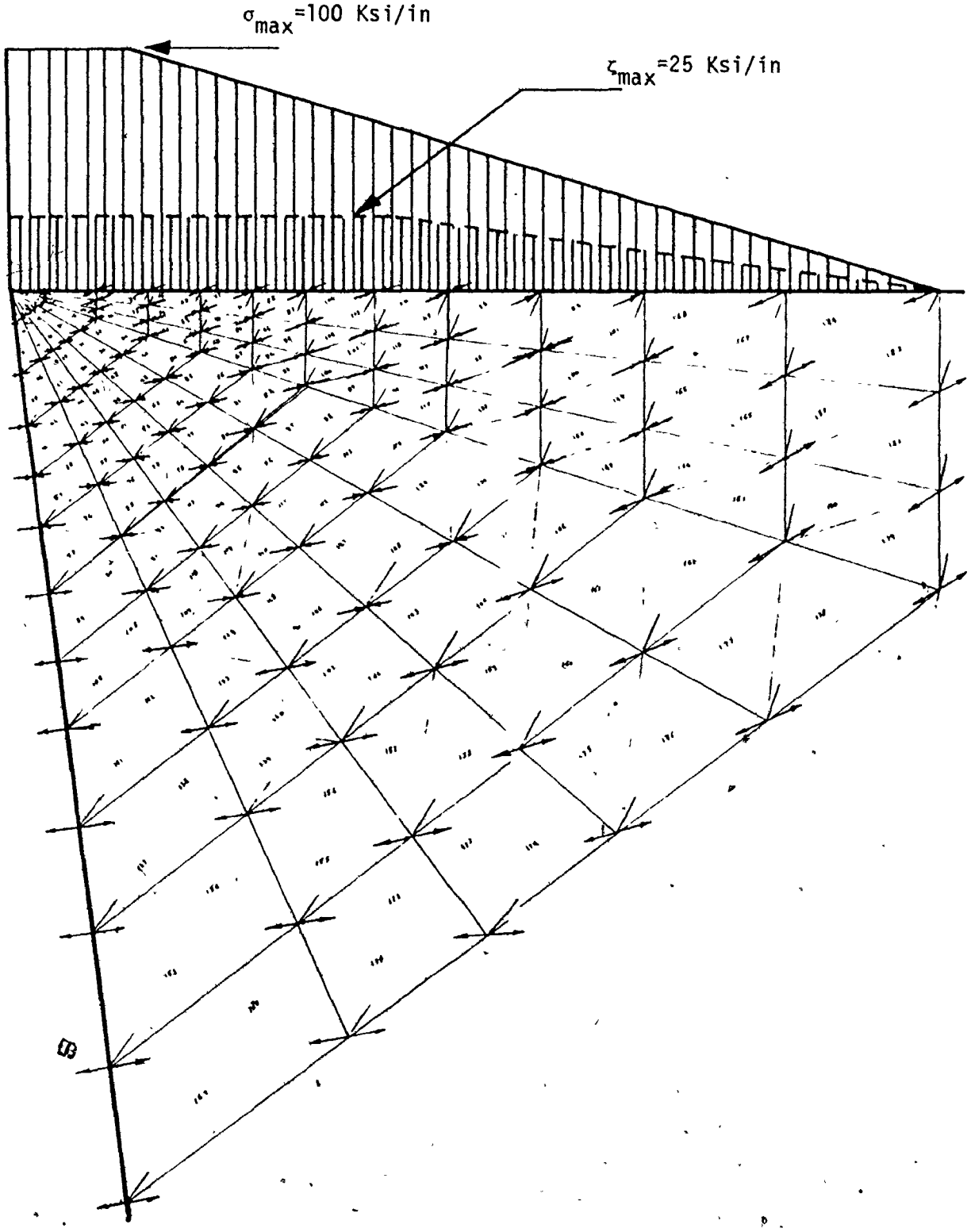

Figure 56-a	Directions of maximum principal stress and of maximum shear stress in the loading region → Direction of σ_1 —— Direction of ζ_{max}.	$\alpha = 0^o$ a = 0.0 inch

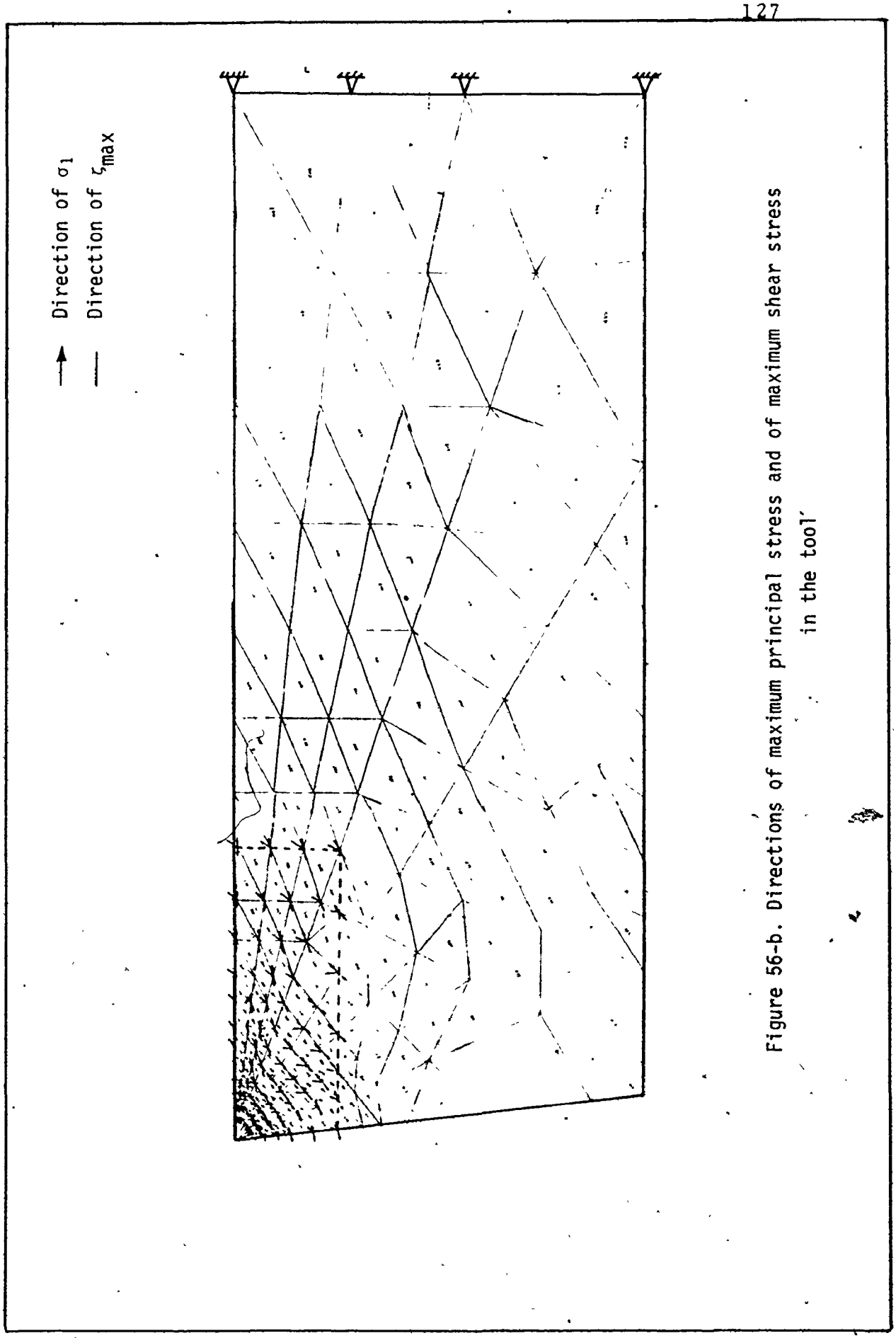

Figure 56-b. Directions of maximum principal stress and of maximum shear stress in the tool

assumption of brittle fracture phenomenon which means that the breakage initiates by crack starts and propagates at the point of maximum tensile stresses and at the direction normal to these stresses.

Comparing the stresses obtained by the classical solution with those resulting from using the finite element technique, a strong difference at the tip of the tool was found. In Figure 53-a a compressive stress area was shown close to the tip when using the finite element method while zero stresses were found at the same area when using the classical solution (Figure 52-b).

Some differences were also found at the fixed boundary. A maximum tensile stress (30 Ksi) was found very close to the top by using the finite element method, but the location of this value using the classical solution was at a distance from the top. Also the end of the stress contours are different in both methods. These differences are understood because the classical solution, similarly to the area under the external load, cannot express the local effects of the fixed boundary reaction stresses.

The contours of 20 Ksi, 10 Ksi and 5 Ksi are almost identical in values and locations but at the area near to the bottom of the tool holder, there are some differences at very low stress values and these can be neglected.

Comparing the contours of the minimum principal stress resulted from both methods, tensile stresses were found in the area close to the top of the fixed end when using the finite

element method (Figure 53-b). The values of these stresses are from 1 Ksi to 3 Ksi. In Figure 52-c it is seen that there are no tensile stresses when using the classical solution.

In the other regions the values of the compressive stress are almost the same in both solutions and it reaches the maximum (30 Ksi) in the area near to the bottom of the fixed end.

Figures 55 and 52-d show the contours of the maximum shear stress resulting from the solution using the above mentioned two methods. The maximum values of shear stress were found in both solutions at the area near to the top and bottom of the fixed end. These values are smaller in the solution using the finite element method in the area near to the upper fixed end than those obtained by using the classical solution. This is mainly due to the difference between the values of the minimum principal stress which were obtained by the finite element method and those of the classical solution.

It is shown that the value of the shear stress is 5.0 Ksi in the middle of the tool holder using the classical solution. This value is the same and approximately at the same area with using the finite element method. The other values of the shear stress are the same in both solutions.

From the above discussion it can be concluded that a comparison of the finite element results with those obtained by the classical method verifies that the finite element results are correct since they agree in general with those obtained from the classical solution in areas remote from

localized stresses.

From investigating the resulting stresses in the case of zero rake angle and comparing with those obtained in the case of -5^{o} and $+5^{o}$ rake angles, it can be concluded that there is no significant difference in the values of stresses of the three cases.

Figures 53-a, 57 and 60 show the maximum principal stress contours at the tool wedge for the cases of $\alpha = 0^{o}$, $\alpha = +5^{o}$ and $\alpha = -5^{o}$ respectively (with flank wear a = 0.0). In all these three cases there are practically no tensile stresses in the vicinity of the tip of the tool.

The value of the maximum compressive stress is almost the same (100 Ksi) and it decreases when moving from the tool wedge in all three cases (Figures 54, 58 and 61). The contours of the maximum shear stress at the tool wedge in the case of $\alpha = 0^{o}$, $\alpha = 5^{o}$ and $\alpha = -5^{o}$ with no flank wear (a = 0.0) are shown in Figures 55, 59 and 62 respectively. The maximum value of the shear stress is 46 Ksi in the case of $\alpha = 5^{o}$, 47 Ksi in the case of $\alpha = 0^{o}$ and 48 Ksi in the case of $\alpha = +5^{o}$. The maximum shear stress increases slightly with decreasing the tool wedge angle but the difference between these values is only about 4%.

The results obtained by using the finite element technique are in agreement with the results obtained from the experimental work in both $+5^{o}$ and -5^{o} rake angle tests. In Table 22, it is seen that in both $+5^{o}$ and -5^{o} rake angles tools and for the same cutting conditions, the breakage occurred approximately at the same cutting time in both tools.

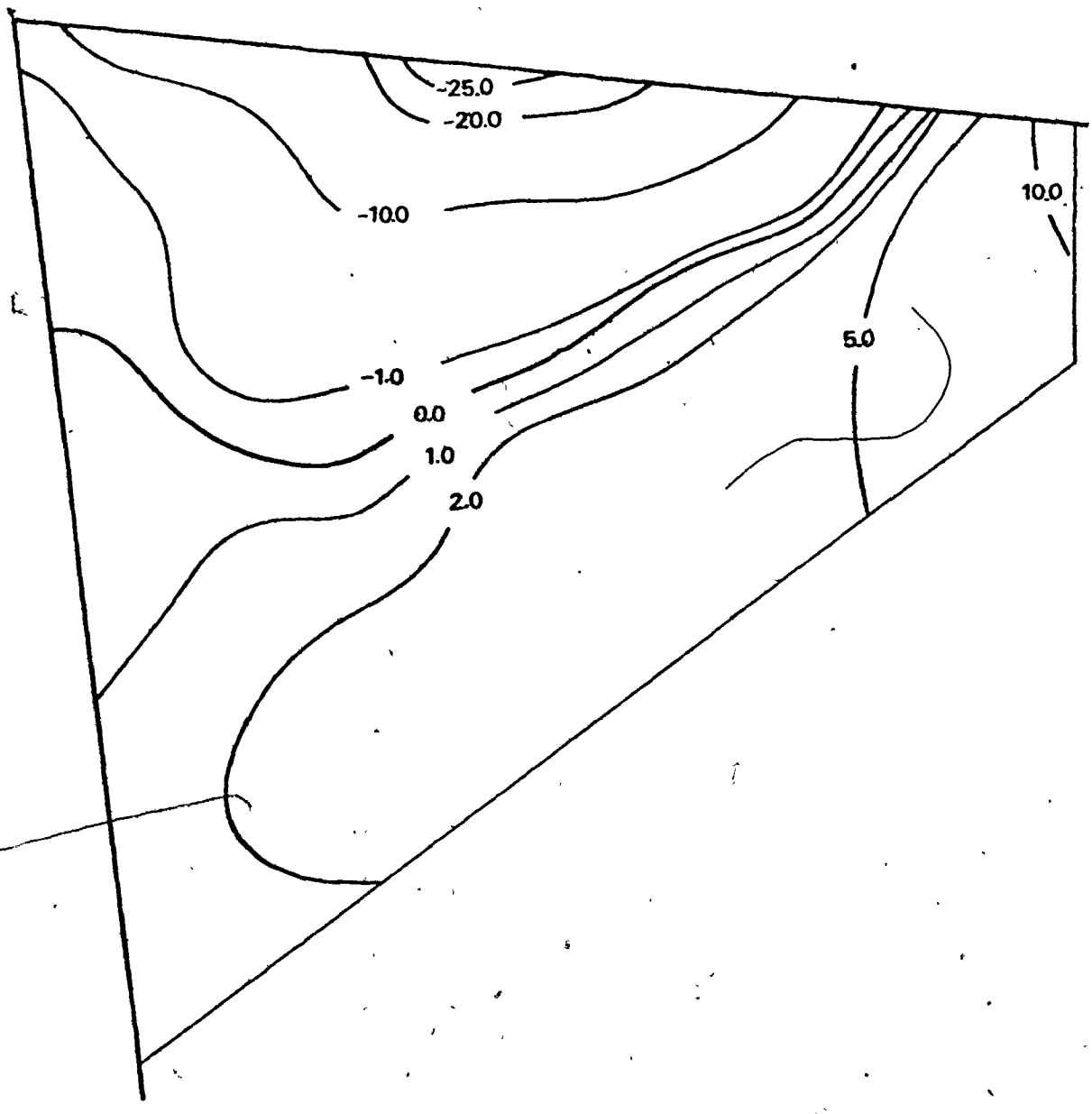

Figure 57	Maximum principal stress contours in the loading region (σ_1 Ksi).	$\alpha = +5^{o}$ a = 0.0 inch

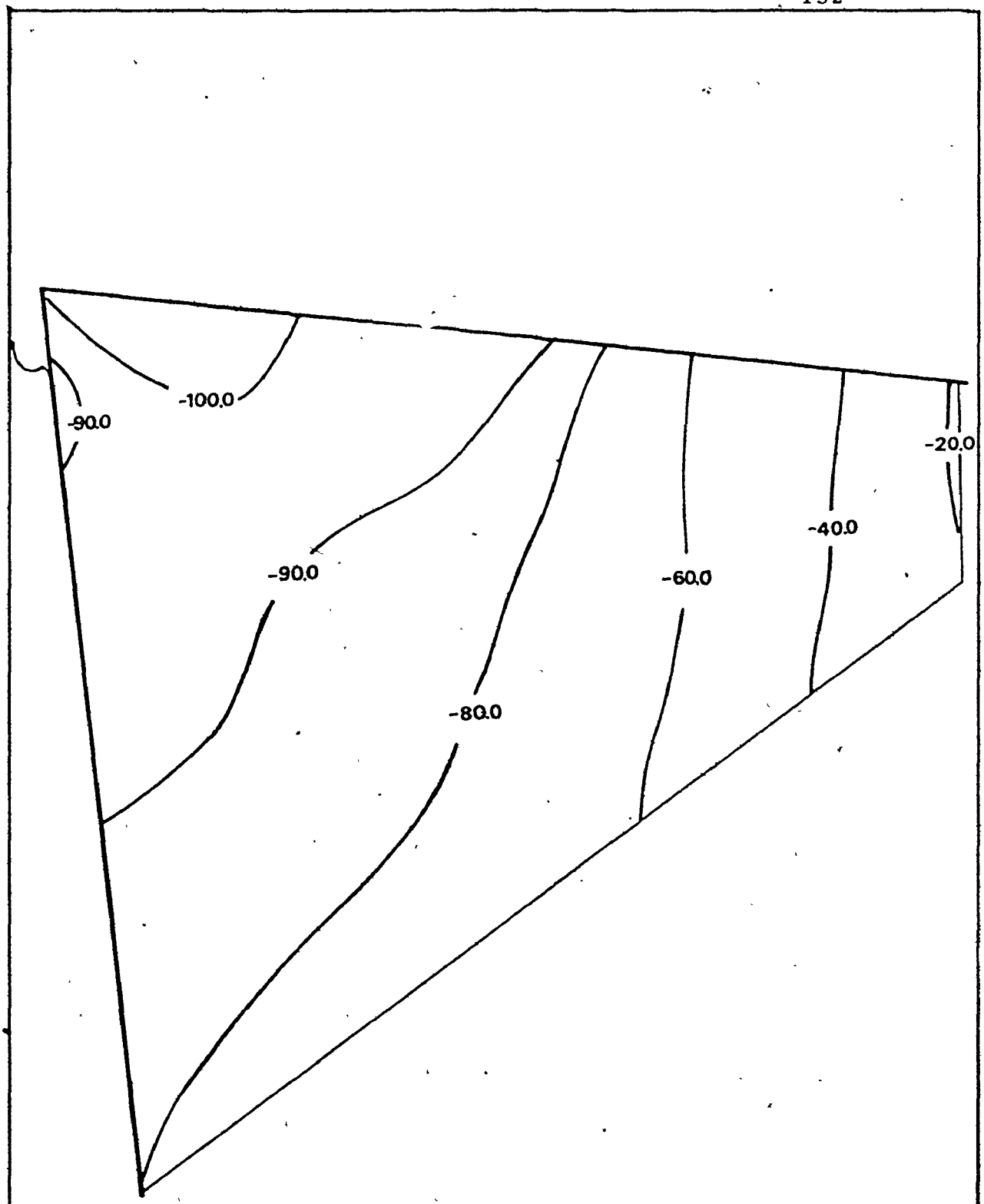

Figure 58	Minimum principal stress contours in the loading region (σ_2 Ksi)	$\alpha = +5^0$ a = 0.0 inch

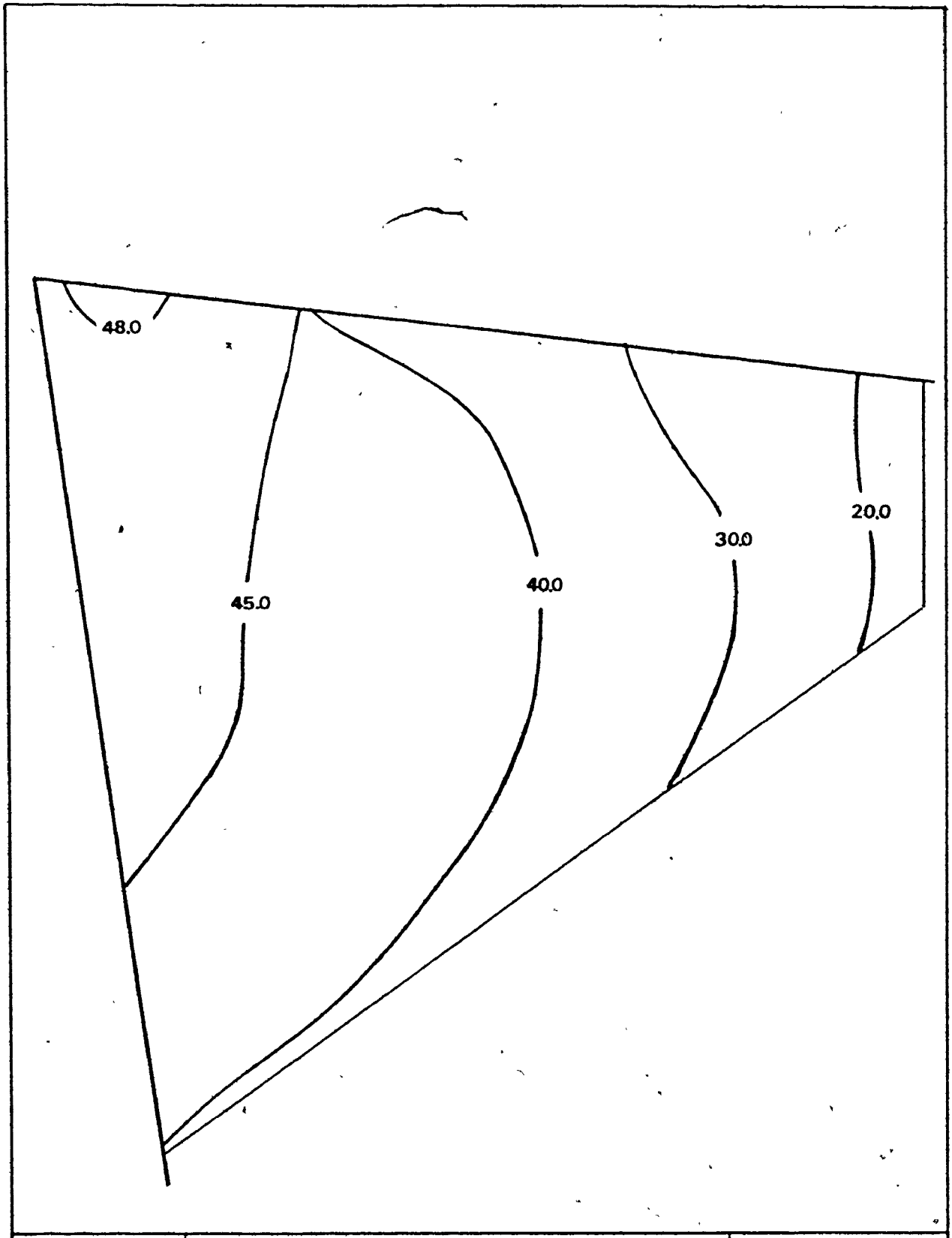

Figure 59	Maximum shear stress contours in the loading region (τ_{max} Ksi)	$\alpha = +5^{o}$ a = 0.0 inch

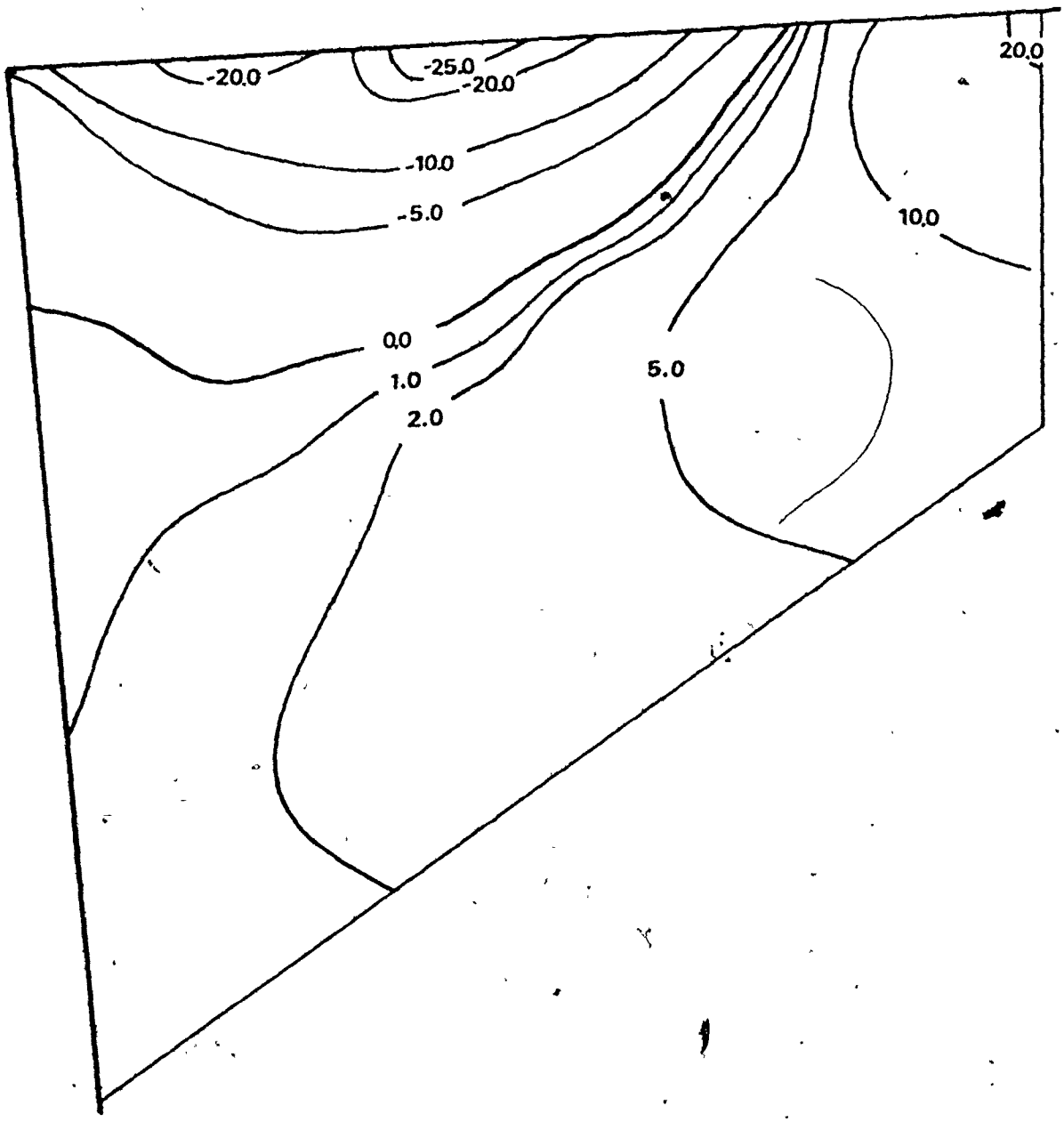

Figure 60	Maximum principal stress contours in the loading region (σ, Ksi)	$\alpha = -5^0$ a = 0.0 inch

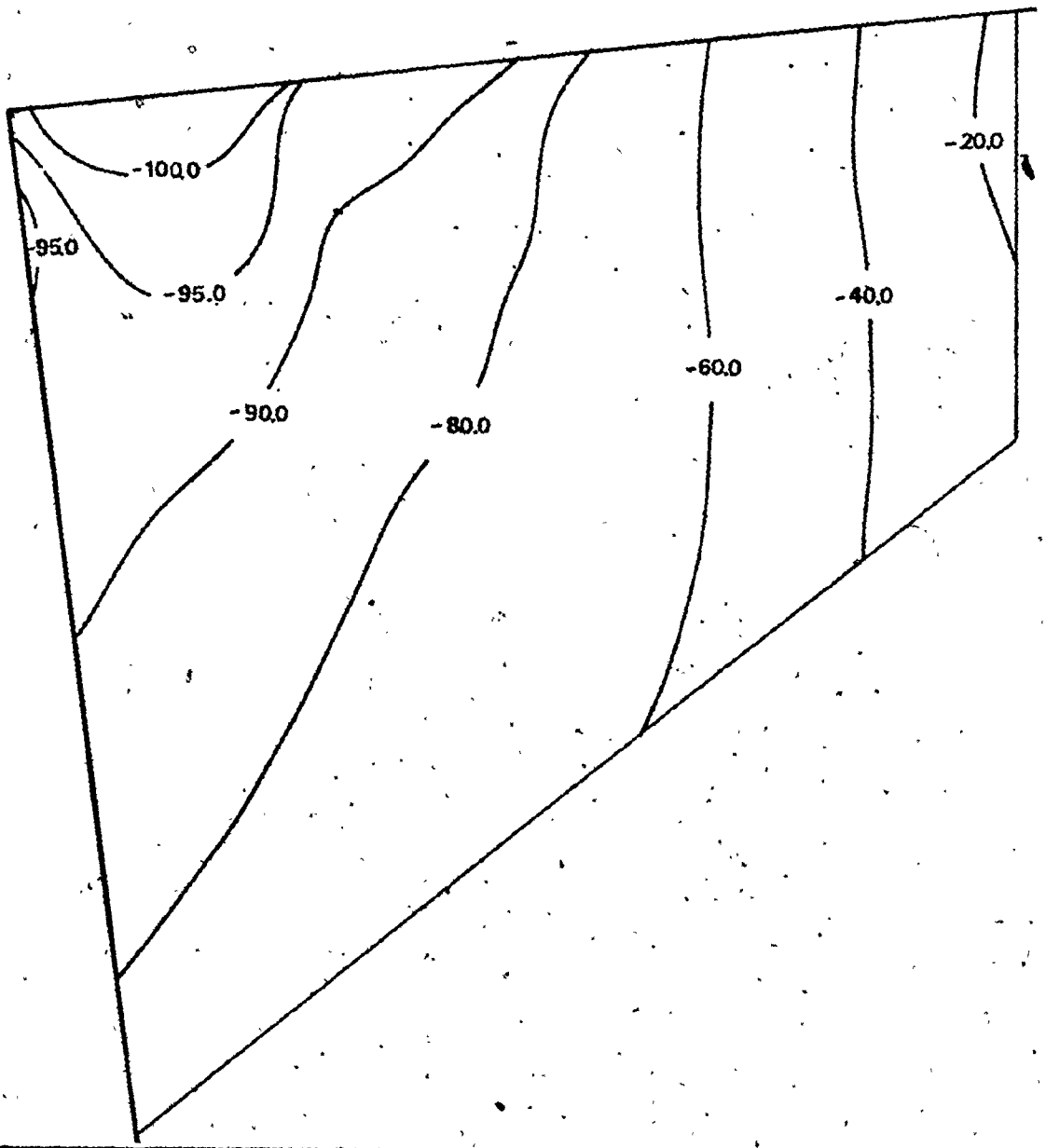

Figure 61	Minimum principal stress contours in the loading region (σ_2 Ksi)	$\alpha = -5^0$ a = 0.0 inch

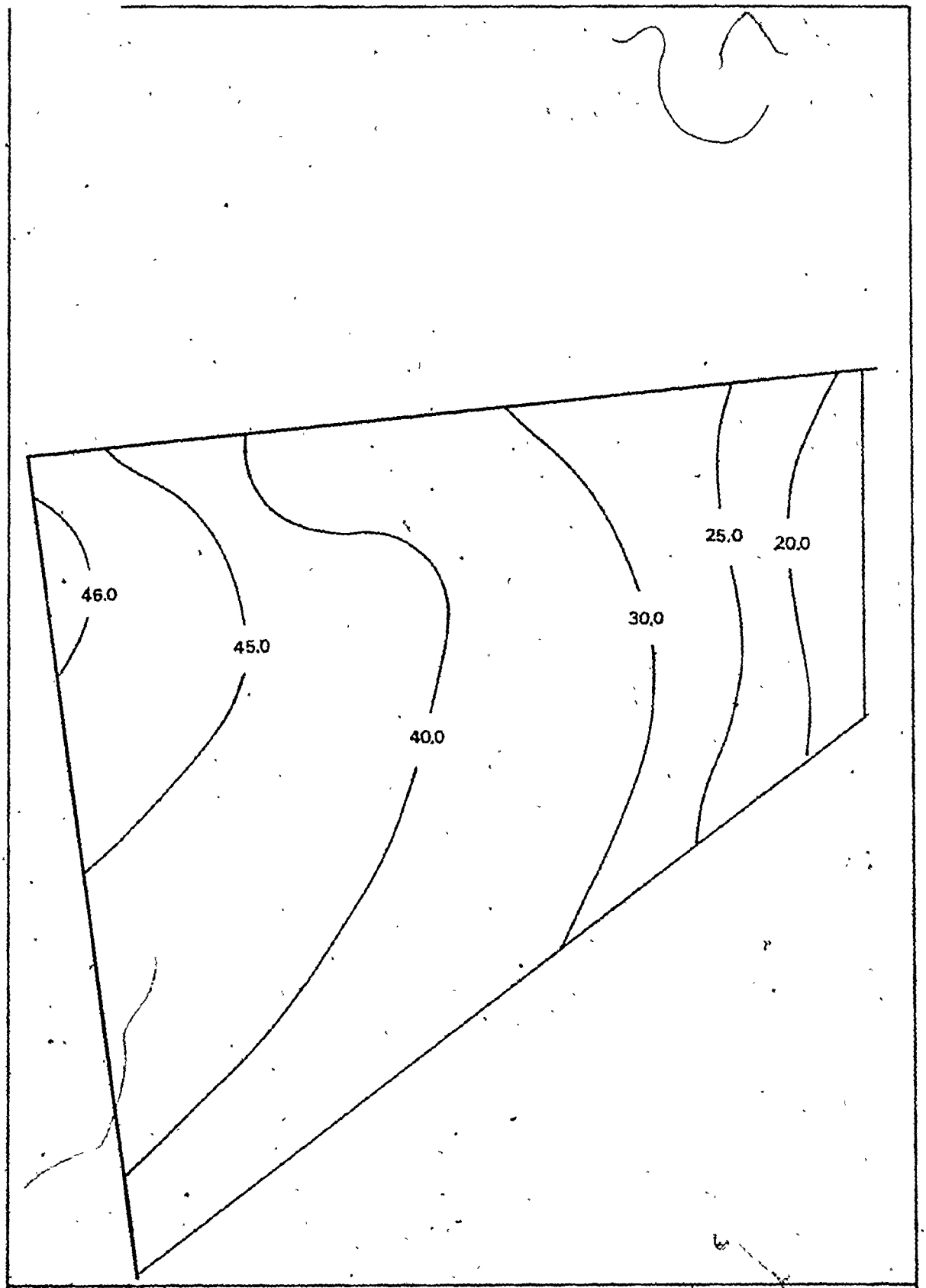

Figure 62	Maximum shear stress contours in the loading region (τ_{max} Ksi)	$\alpha = -5^0$ a = 0.0 inch

Effect of the flank wear:

The discussion of the effect of flank wear will be restricted to the case of zero rake angle.

From Figures 53, 63 and 66 which represent the contours of the maximum principal stress in the three cases of flank wear (a = 0.0, a = 0.006 inch and a = 0.015 inch) respectively, it can be seen that as the flank wear increases the friction load will increase too and consequently the area of the minor compressive stresses at the tool wedge increases (Figures 53-a, 63-a and 66-a).

The value of the local maximum tensile stress in the case of a = 0.0 is 21.3 Ksi and it decreases to 18 Ksi and 17 Ksi as the flank wear increases (Figures 53-b, 63-b and 66-b).

Figures 54, 64 and 67 illustrate the contours of the minimum principal stress of the three values of flank wear width respectively. In these figures there is not any recognizable change in the values of the stress with flank wear growth.

A slight difference in values of the maximum shear stress was found when comparing the three cases of flank wear. It is seen that as the flank wear increases, the shear stress slightly decreases (Figures 55, 65, 68). Its value is 47 Ksi in the case of no flank wear (a = 0.0) and 45 Ksi in the case of flank wear width a = 0.015 inch.

This is mainly so because of the increase in compressive stress in the horizontal direction due to the increasing normal load on the flank which, to some extent,

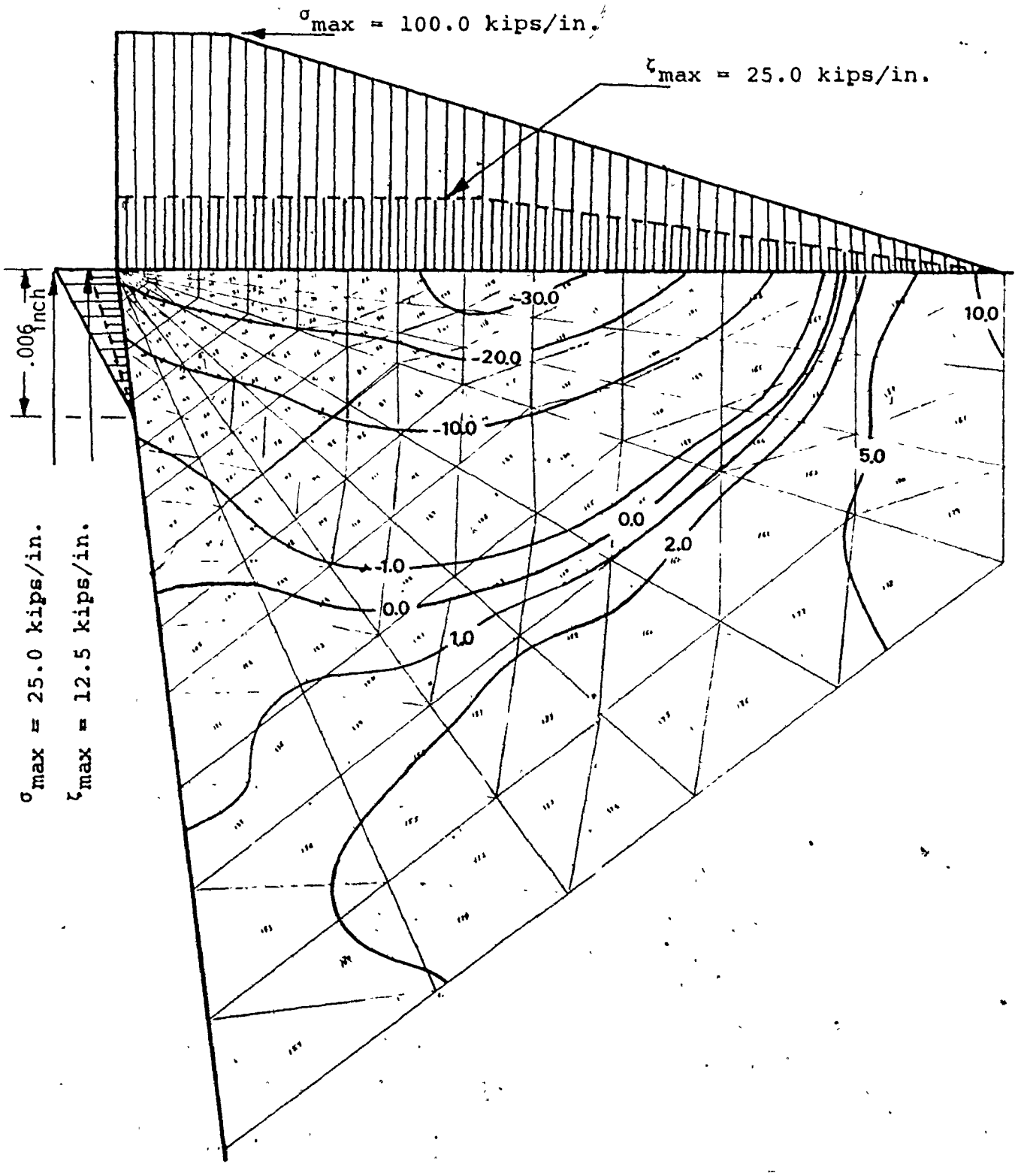

Figure 63a	Maximum principal stress contours in the loading region (σ, Ksi)	α = 0° a = 0.006 inch

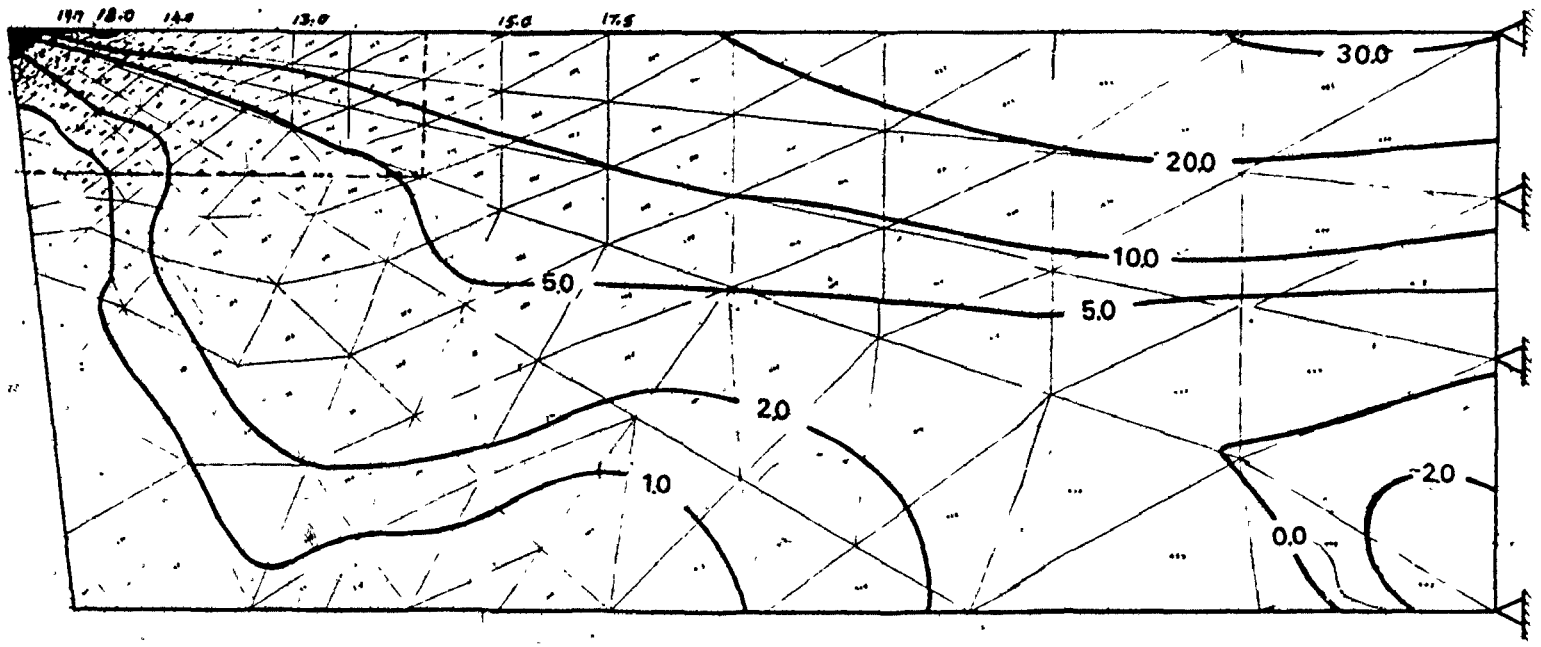

Figure 63b. Maximum principal stress contours in the tool and tool holder (σ_1 Ksi) $\alpha = 0^0$
$a = 0.006$ inch

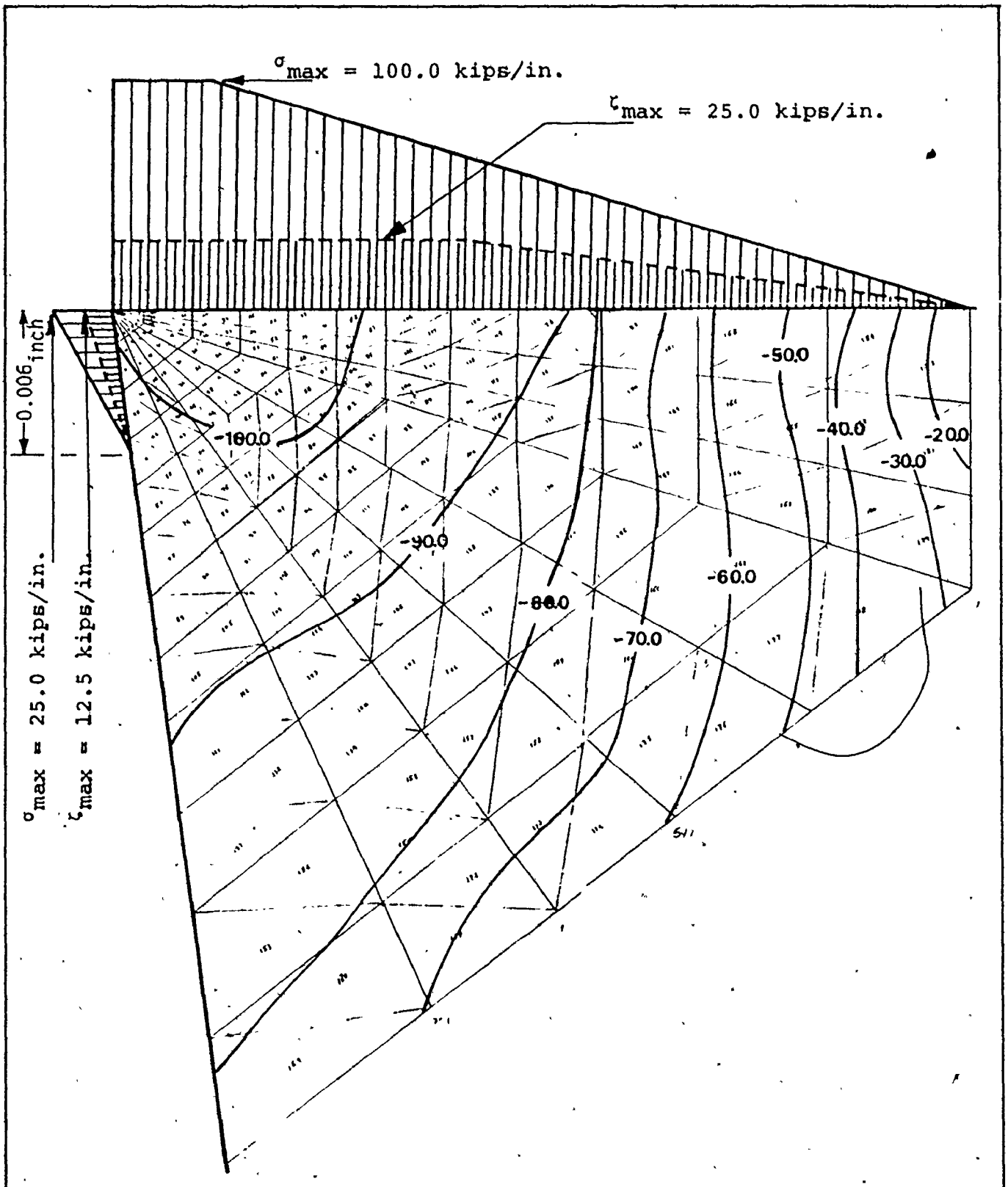

Figure 64	Minimum principal stress contours in the loading region (σ_2 Ksi)	$\alpha = 0^0$ a = 0.006 inch

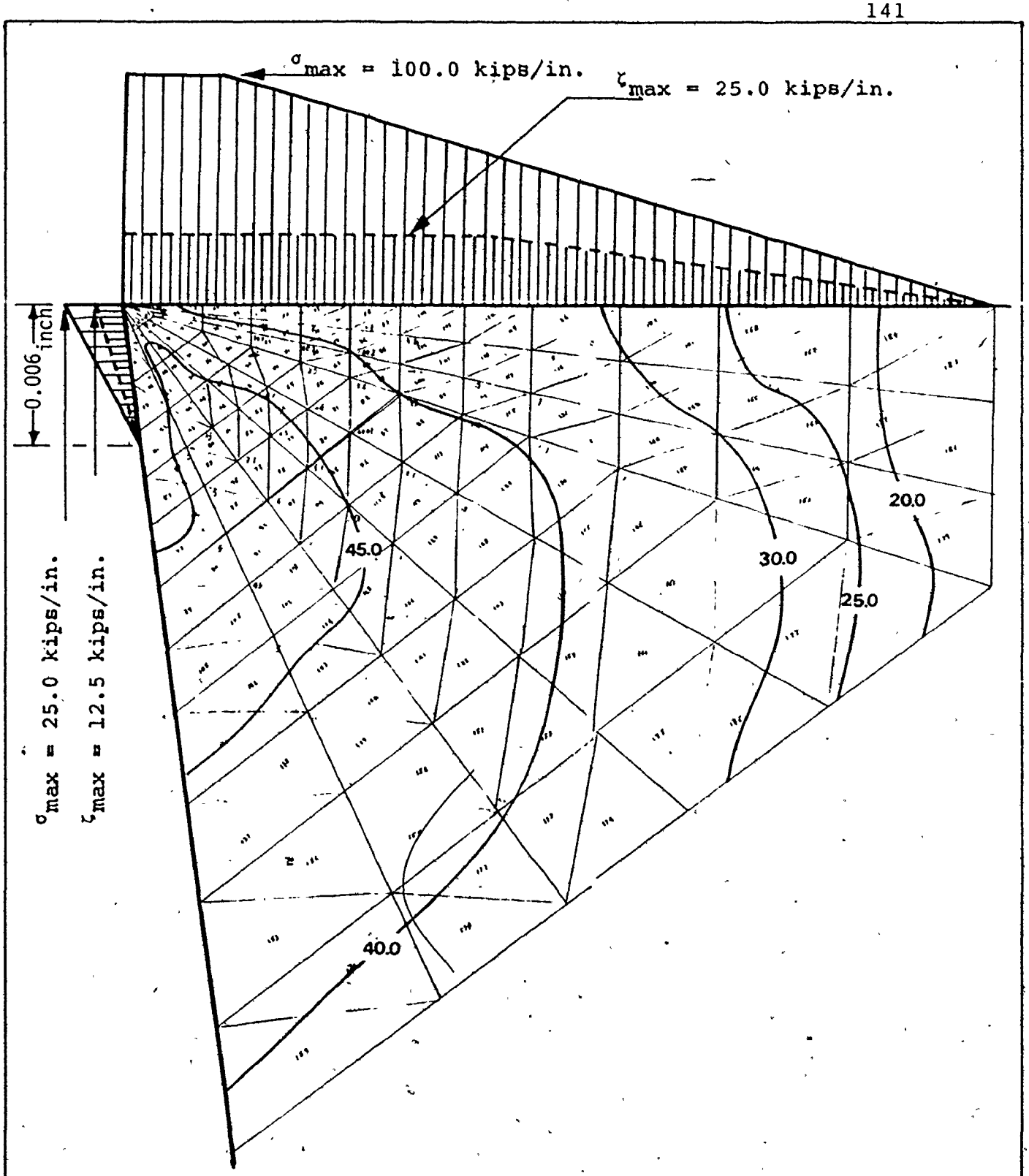

Figure 65	Maximum shear stress contours in the loading region (τ_{max} Ksi)	$\alpha = 0^0$ a = 0.006 inch

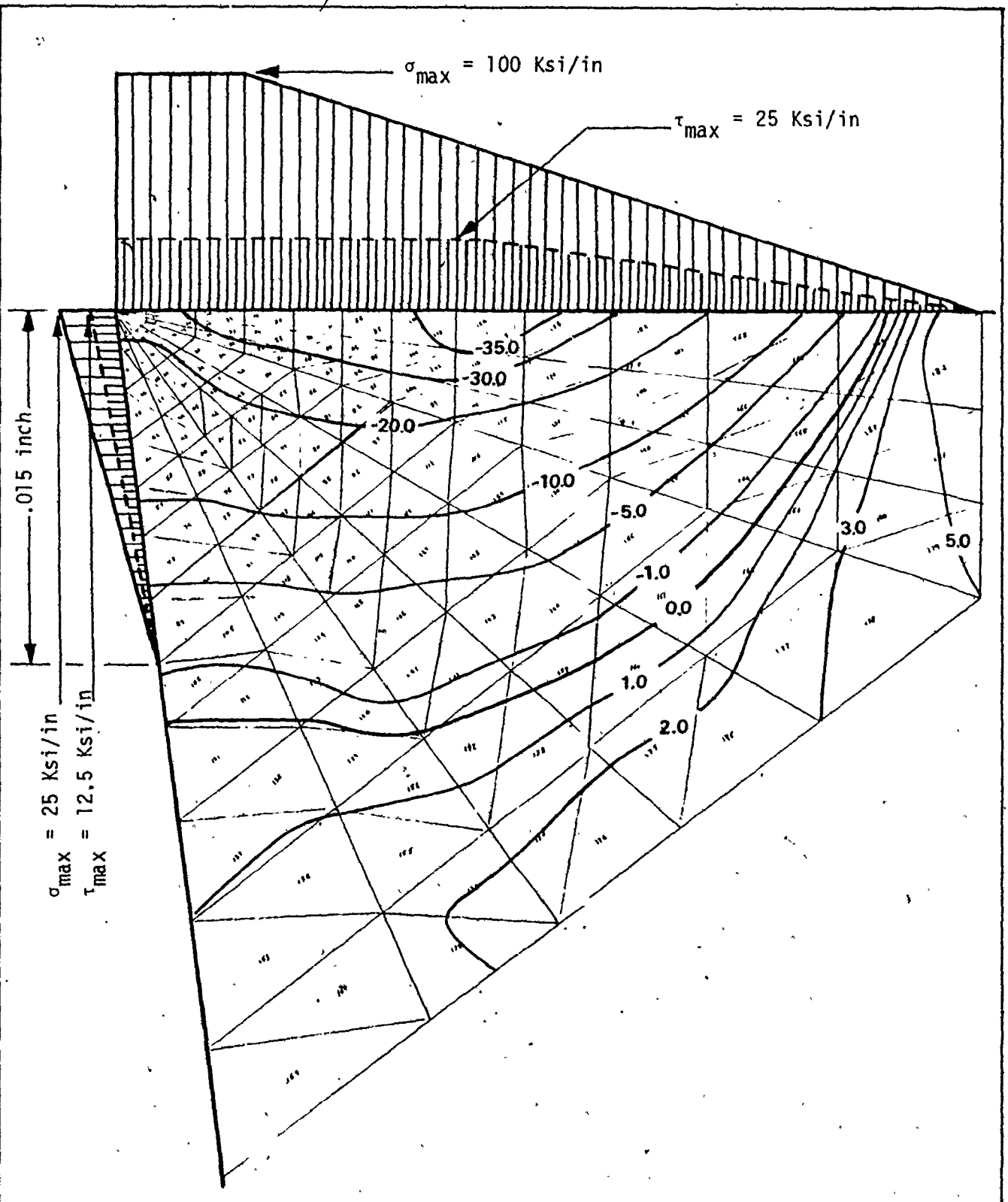

Figure 66a	Maximum principal stress contours in the loading region (σ_1 .Ksi)	$\alpha = 0^o$ a = 0.015 inch

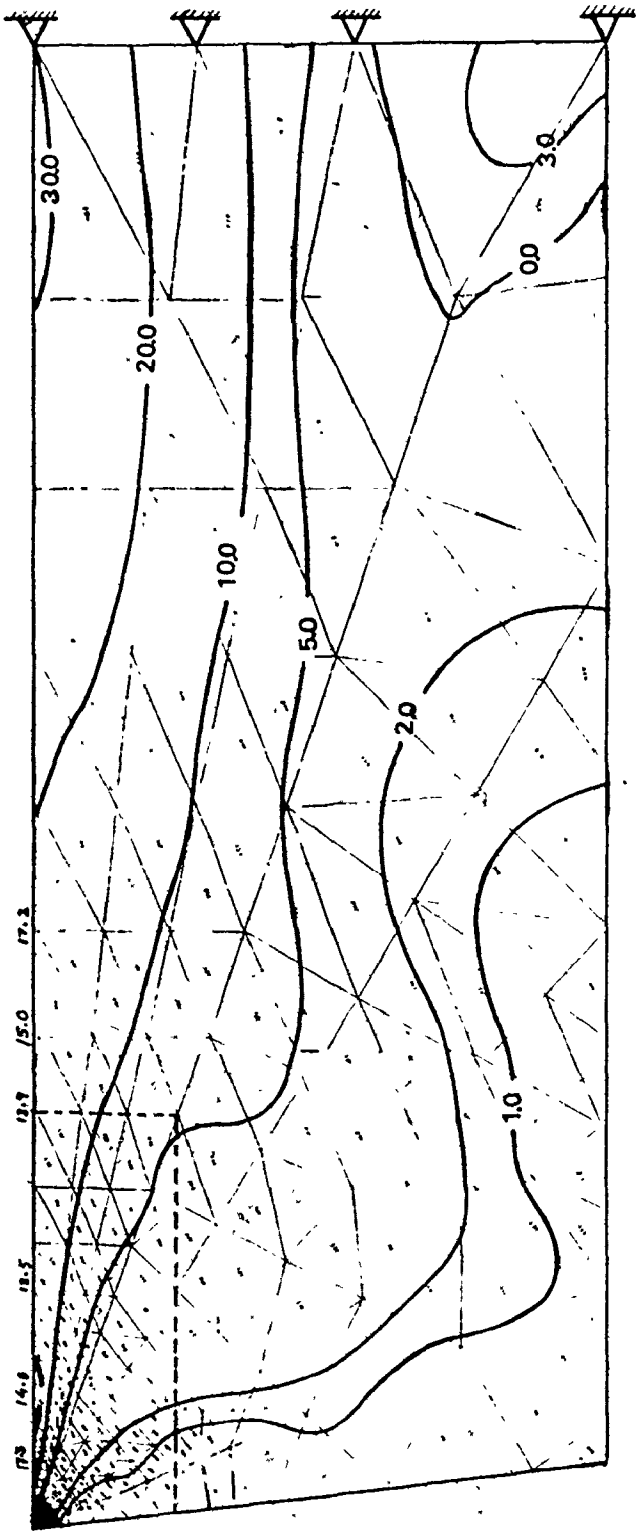

Figure 66b. Maximum principal stress contours in the tool and tool holder (σ_1 Ksi) $\alpha = 0^0$
$a = 0.015$ inch

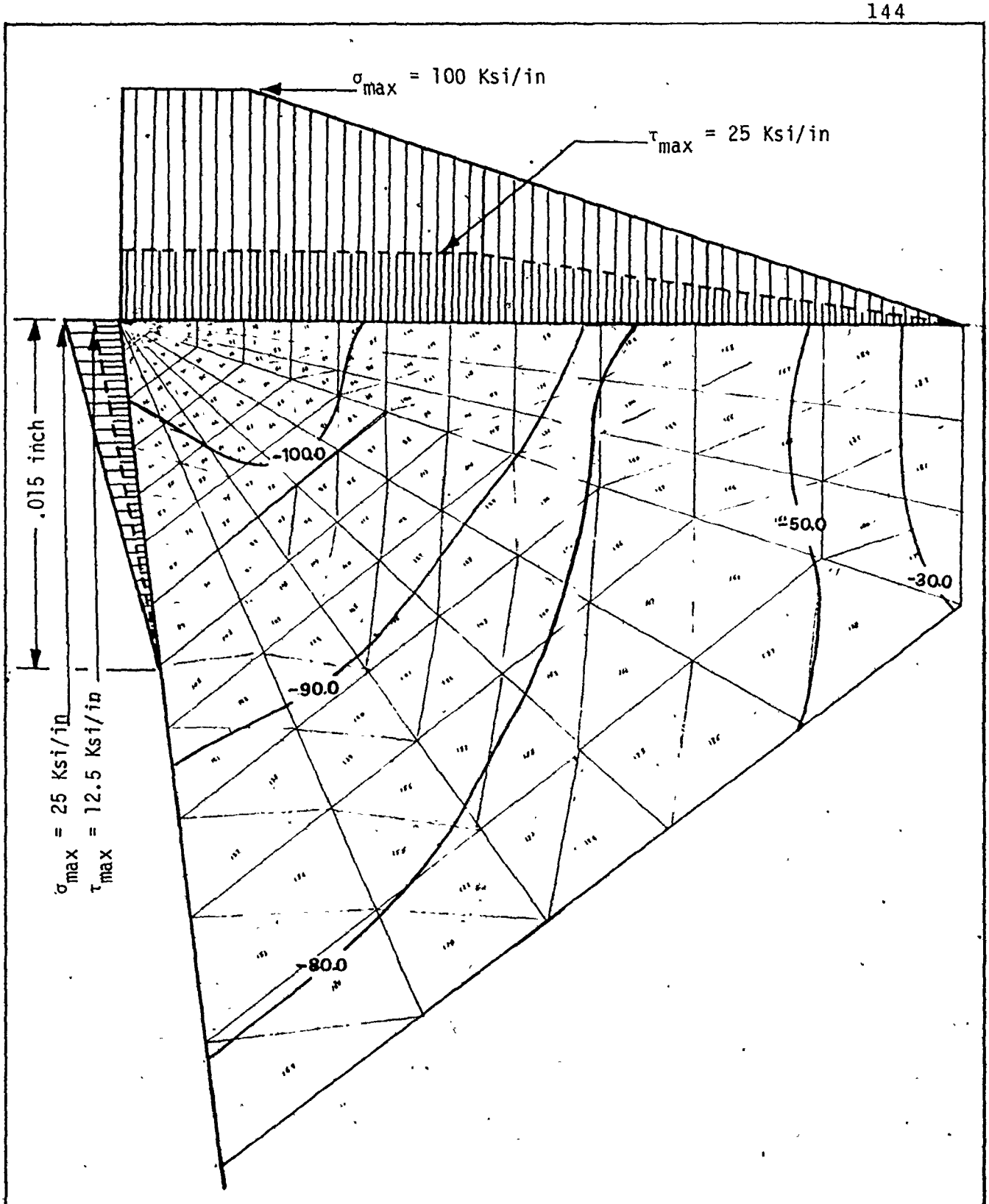

Figure 67	Minimum principal stress contours in the loading region (σ_2 Ksi)	$\alpha = 0^0$ a = 0.015 inch

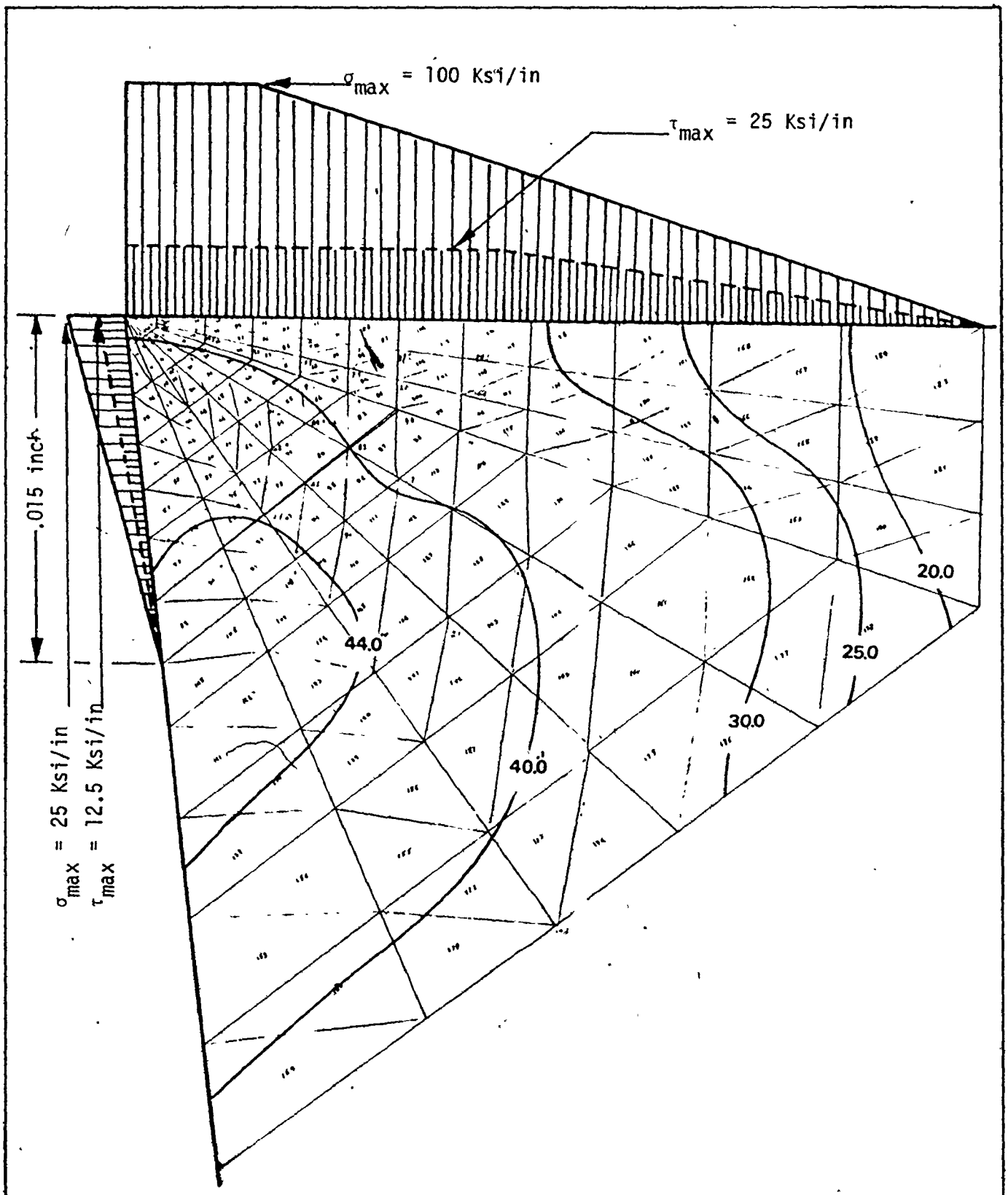

Figure 68	Maximum shear stress contours in the loading region (τ_{max} Ksi)	$\alpha = 0^o$ a = 0.015 inch

"supports" the edge against being sheared off by the effect of normal force acting on the rake face.

In reality, however, an increase of edge wear leads to more chipping and eventually breakage. This is because the initial chipping of the normal load on the rake face increases further with increased chipping, etc. This aspect was not considered in the computations just described where normal load on the rake face was kept constant and independent of the wear on the flank.

B. Stepwise Sub-dividing and Refining Method

The computation work was carried out in five steps using the method suggested by Tlusty [23] for the case of zero rake angle with no flank wear (a = 0.0 inch) and with flank wear width a = 0.006 inch. Figure 69 shows the dimensions of the fifth step (loading region) using the same load values as in the single step method. The area considered in detail overlaps with only a part of the area considered in the preceding, the latter one is shown in a broken line.

The contours of the principal stresses and the maximum shear stresses at the tool edge (loading region) in the case of no flank wear are next shown in Figures 70, 71 and 72.

Figure 70 shows the maximum principal stress contours at the tip of the tool. The stresses were shown in great detail and it is seen that the stresses in this area are compressive stresses. These results agree with those obtained from the single step method (Figure 53-a).

The contours of the minimum principal stress are

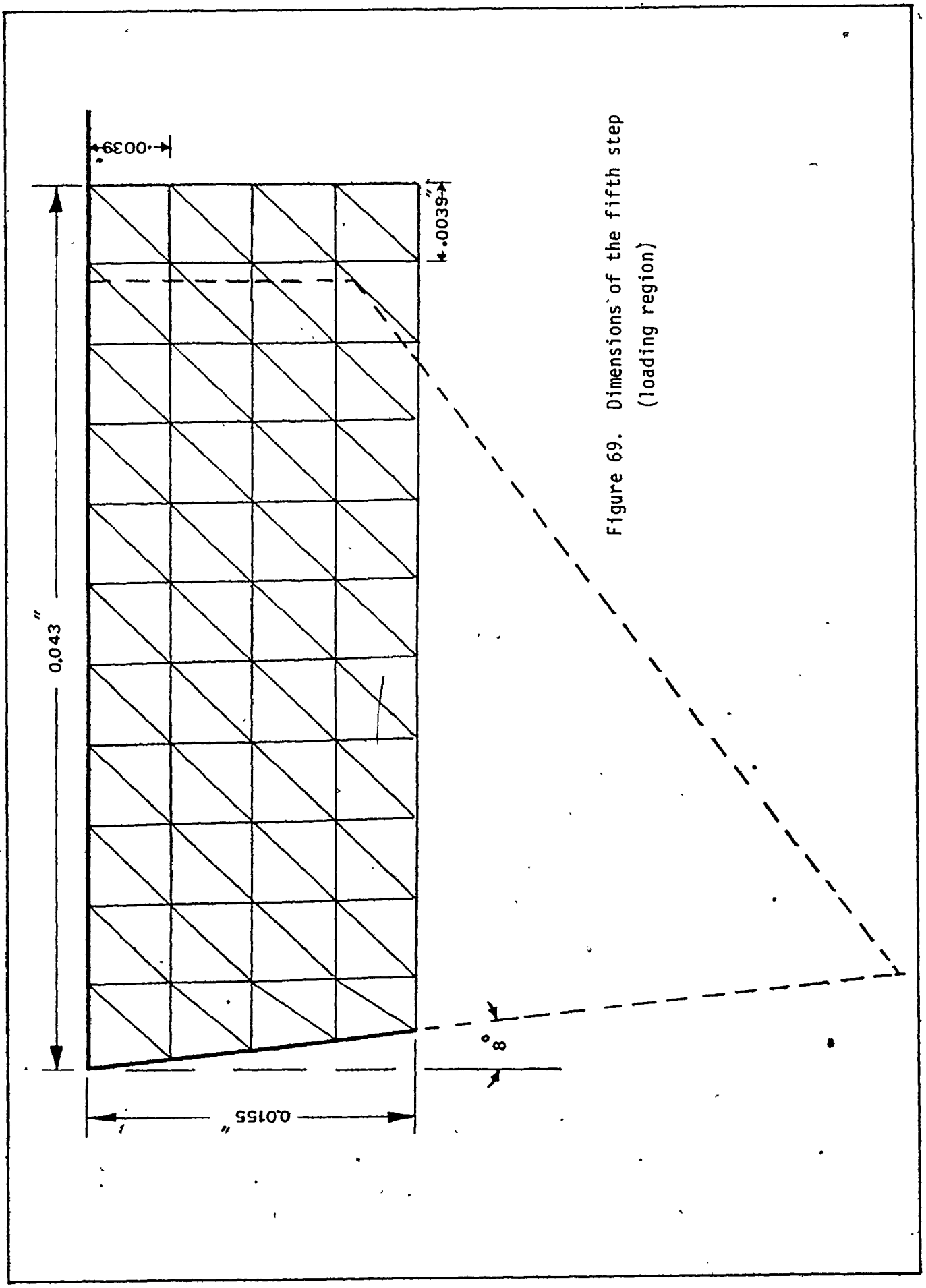

Figure 69. Dimensions of the fifth step (loading region)

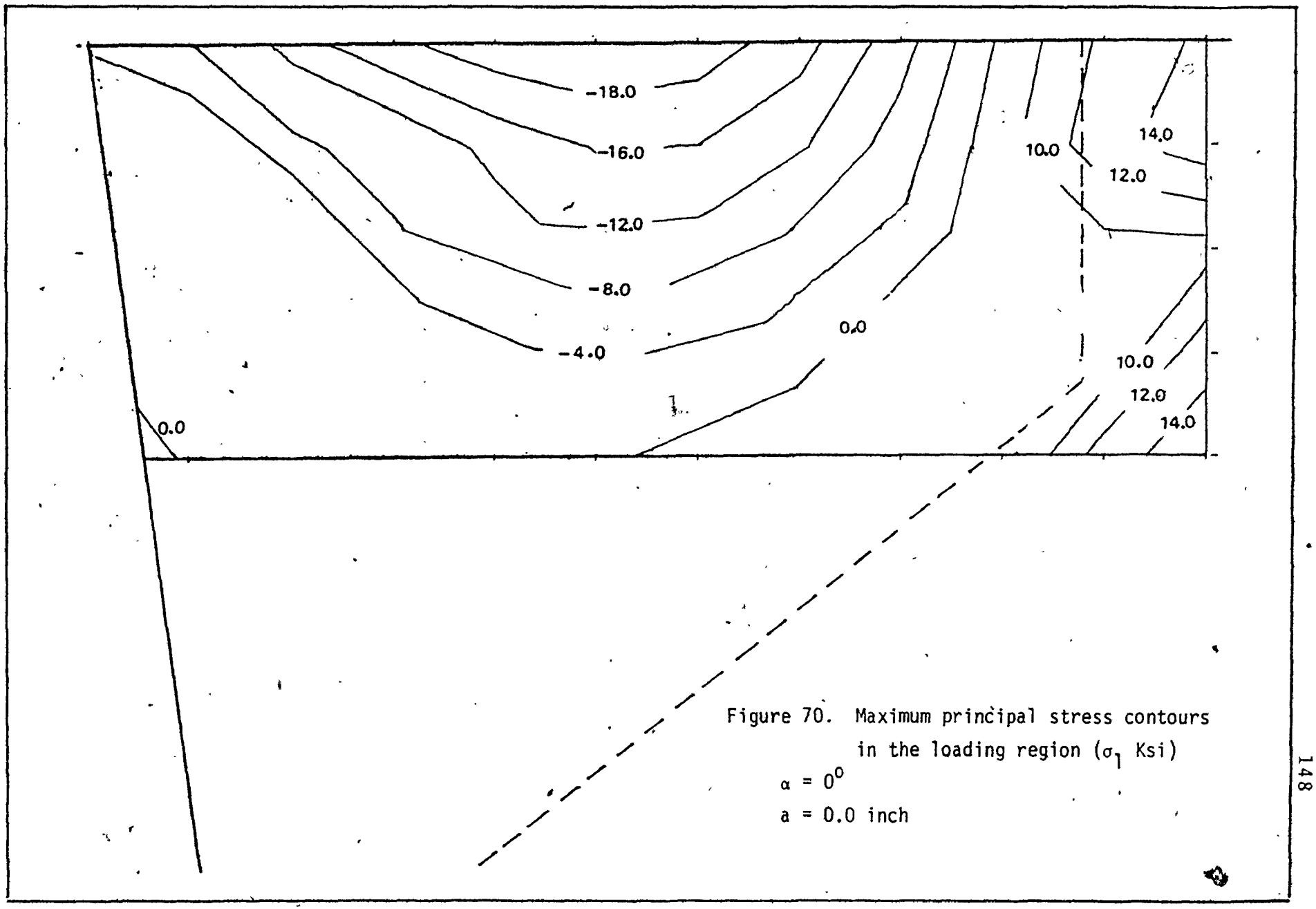

Figure 70. Maximum principal stress contours in the loading region (σ_1 Ksi)

$\alpha = 0^0$

a = 0.0 inch

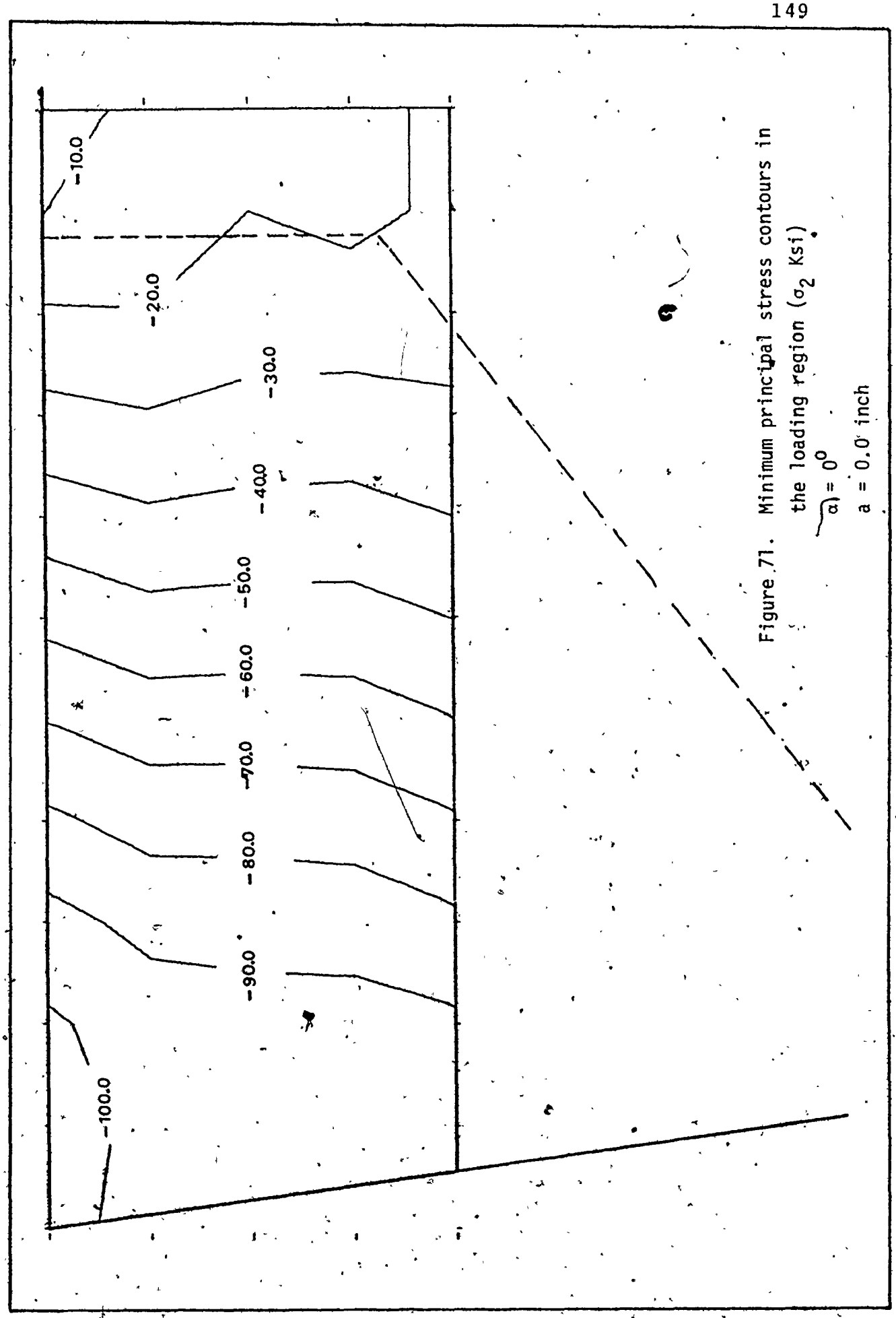

Figure 71. Minimum principal stress contours in the loading region (σ_2 Ksi)
$\alpha = 0^0$
a = 0.0 inch

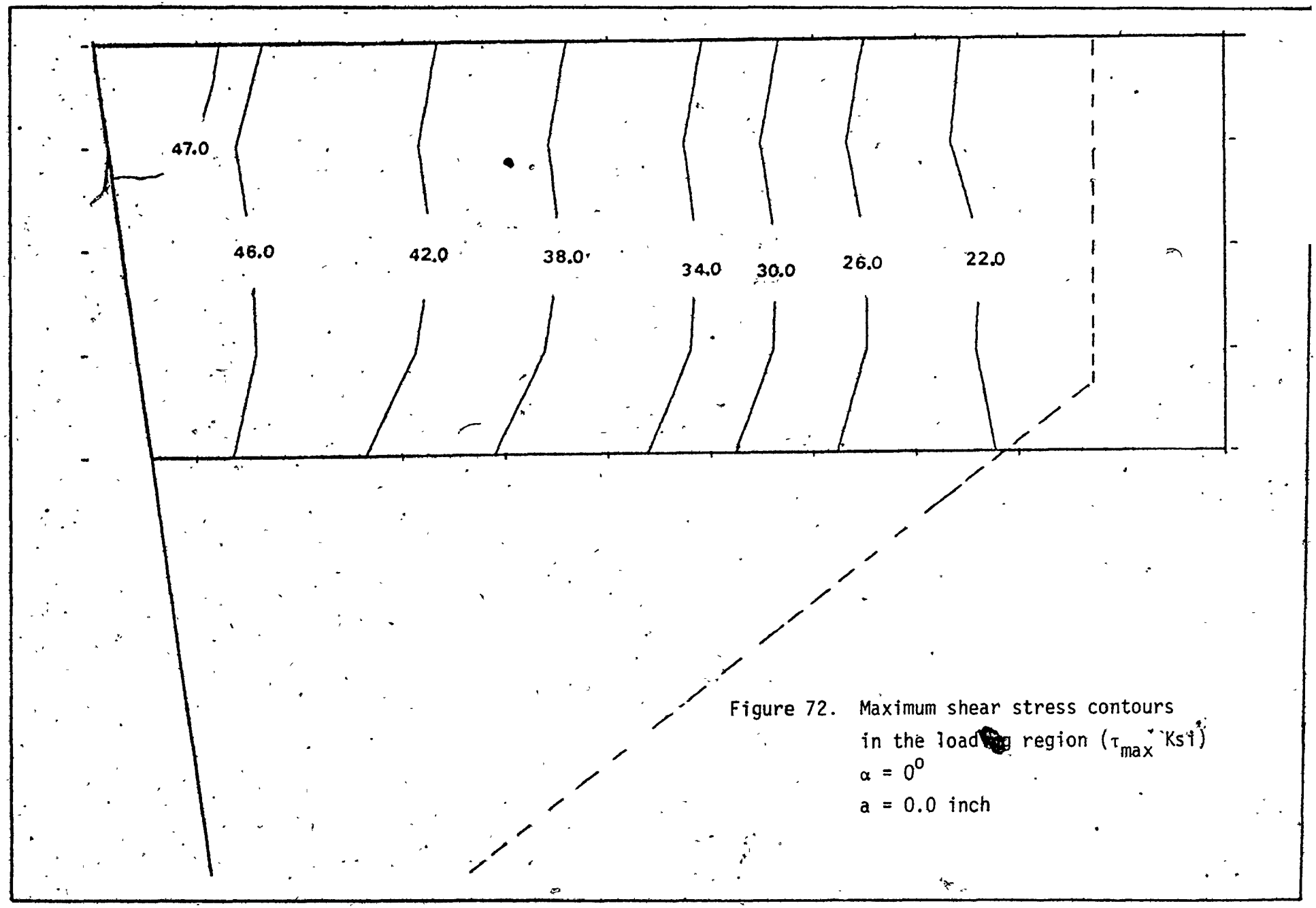

Figure 72. Maximum shear stress contours in the loading region (τ_{max} Ksi)
$\alpha = 0^{o}$
a = 0.0 inch

shown in Figure 71 for the same area. The maximum value of the compressive stress is 100 Ksi which agrees with the results obtained when using the single step method (Figure 54).

The maximum value of the shear stress is 46 Ksi (Figure 72) and the difference between this value and the value obtained by using the finite element method is very small and is equal to 1 Ksi (Figure 55).

In the case of a = 0.006 inch, only the load values of the preceding case were changed and the computation work was carried out for the fifth step only (the loading region).

Figures 73, 74 and 75 show the contours of the principal stresses and the maximum shear stresses resulting in the case of zero rake angle with 0.006 inch flank wear width.

Figure 73 shows the contours of the maximum principal stress (minor compressive stress). It is seen that the stresses near the flank are increased by about 1.5 times the case of no flank wear (a = 0.0). This, actually, is due to increasing the load values resulting from the present flank wear, a = .006 inch.

Comparing these results with those obtained by using the single step method, it is seen that there is no significant difference between the values of the stresses in the case of no flank wear (a = 0.0) and those in the case of a = .006 inch (Figures 53-a,63-a).

From Figure 74 it is seen that the maximum value of the compressive stress is 100 Ksi which agrees with the value

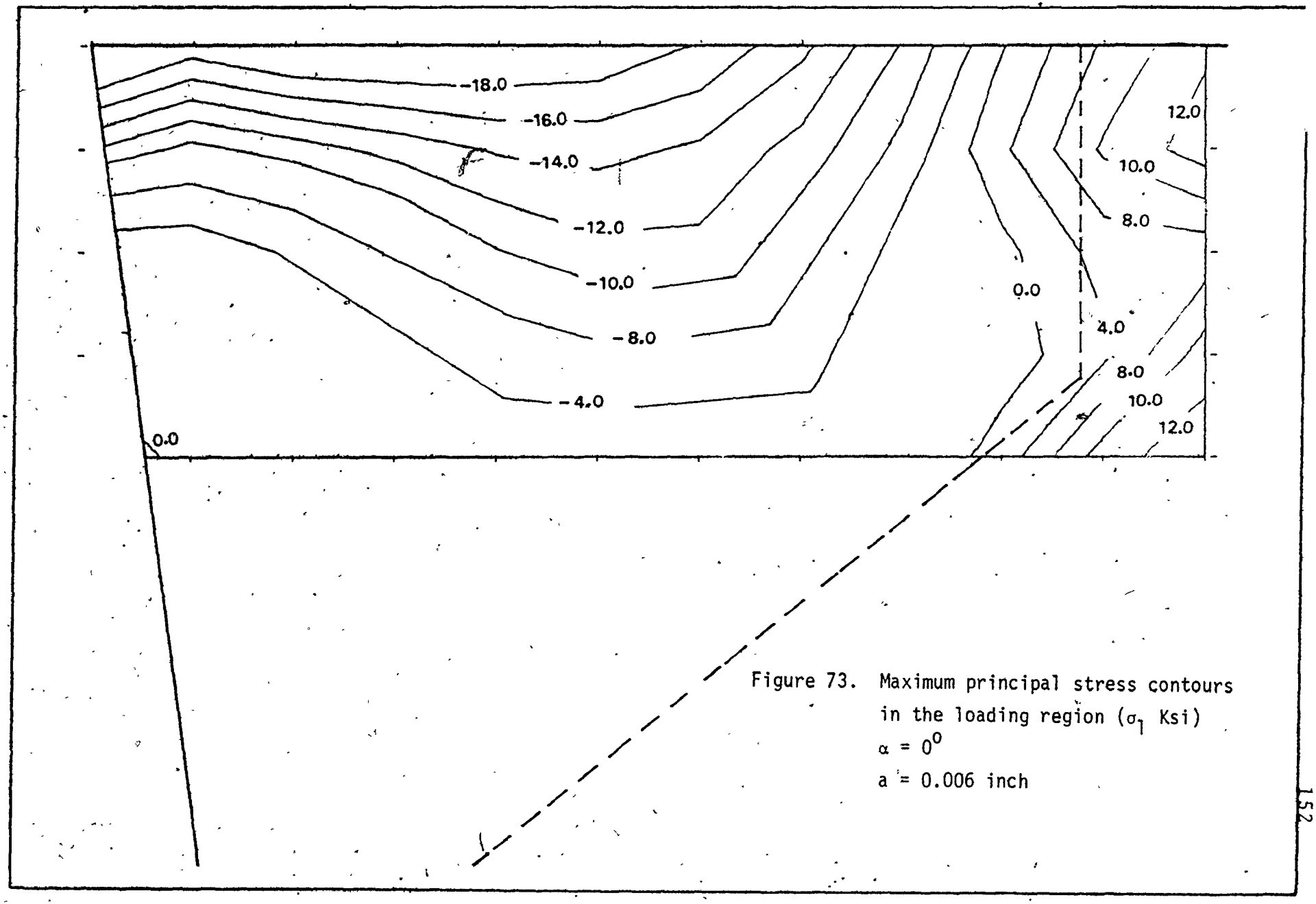

Figure 73. Maximum principal stress contours in the loading region (σ_1 Ksi)
$\alpha = 0^0$
a = 0.006 inch

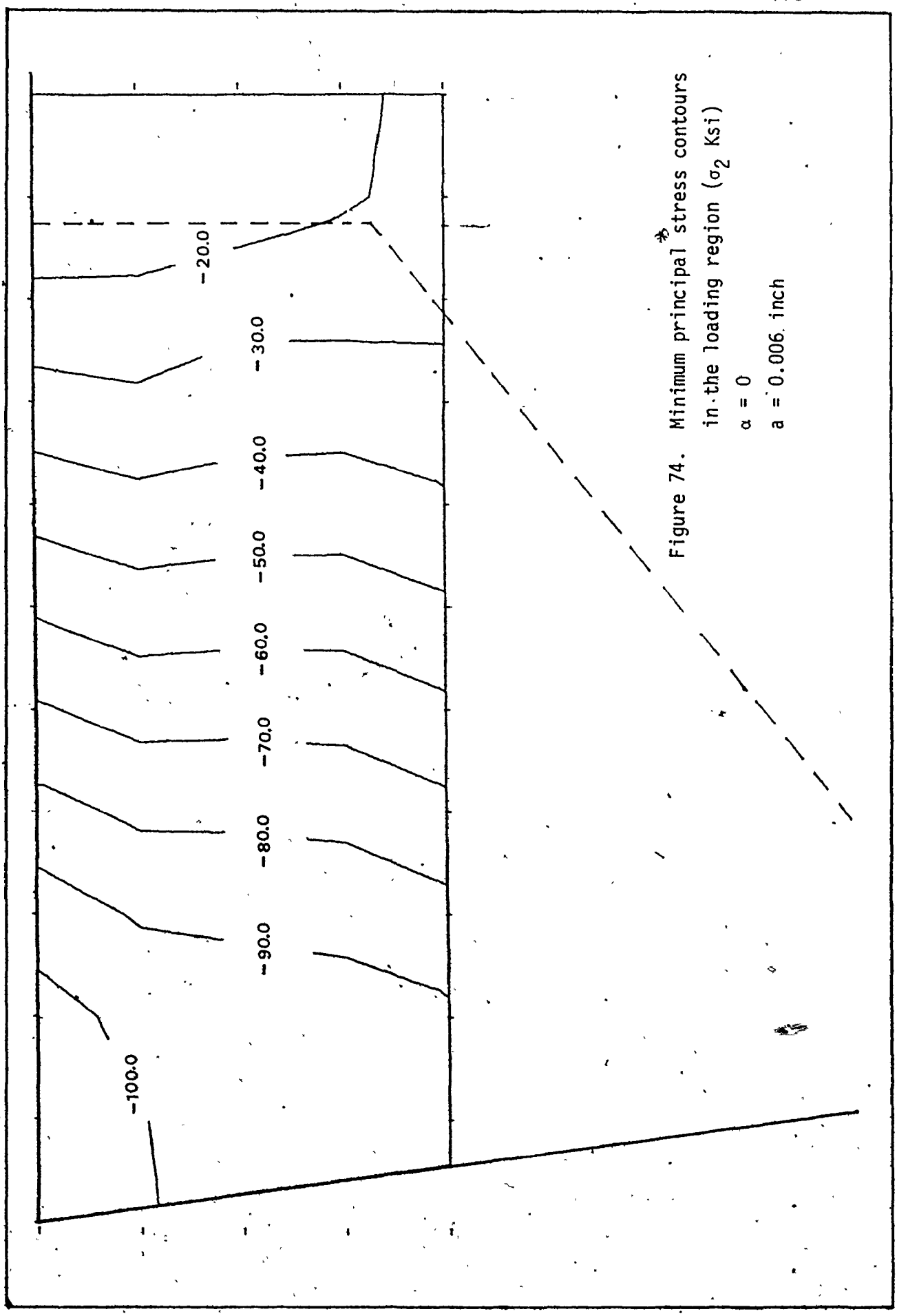

Figure 74. Minimum principal stress contours in the loading region (σ_2 Ksi)
$\alpha = 0$
$a = 0.006$ inch

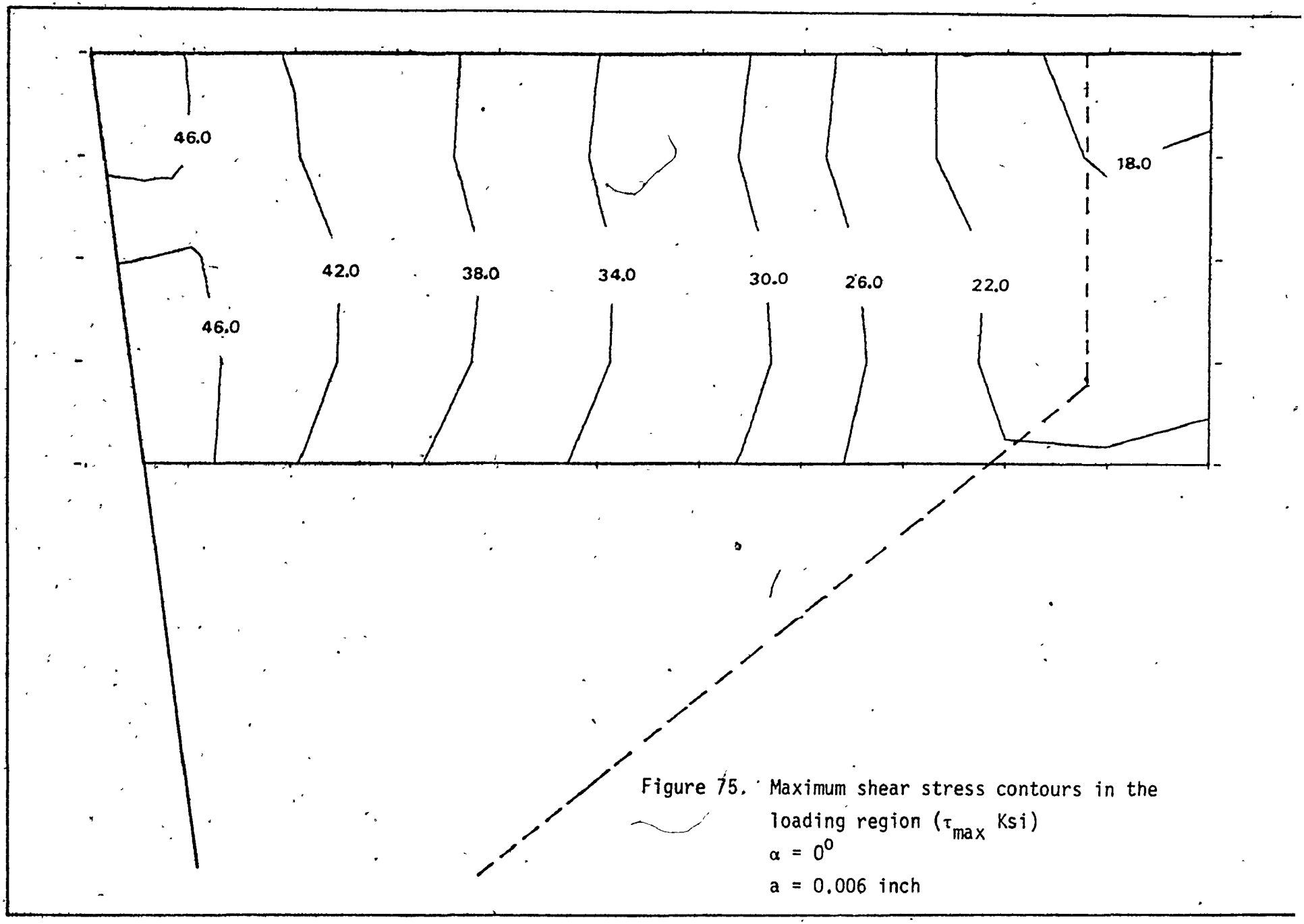

Figure 75. Maximum shear stress contours in the loading region (τ_{max} Ksi)
$\alpha = 0^{o}$
a = 0.006 inch

obtained when using the single step method (Figure 58).

The shear stress has a maximum value of 46 Ksi which occurred close to the flank (Figure 75). These results too agree with those obtained by using the single step method (Figure 10-b).

From the preceding discussion, it can be concluded that comparing the results obtained by using the stepwise method, a negligible difference was found. This difference may be due to variations in grid distribution.

CHAPTER 5

CONCLUSIONS

The investigation concentrated on chipping (gradual damage to the cutting edge) and on breakage (fracture of a rather large portion of the tool wedge) of carbide tools.

Experiments conducted by turning 1040, 4340/217 BHN, and 4340/380 BHN in continuous and interrupted cutting, the latter with very short interruptions so as not to induce cyclic thermal stresses have confirmed general experience in that chipping was observed at medium feeds of .012 to .024 in:/rev. and breakage at heavy feeds of .027 to .043 in./rev. in continuous cutting. Breakage occurred either after some accumulation of chipping (and consequent increase of cutting force) or outright after a very short cutting time. In interrupted cutting breakage occurred at lower feeds about 0.02 inch after very short cutting times. Therefore, fatigue was excluded as an explanation. Occurrence of breakage at lower feeds in interrupted cutting is believed to be due to a change in the loading mode (shock wave at the exit of the cut or chip interference at the entrance into the cut. The nature of this change was not investigated. Both the above mentioned types of fractured surfaces were inspected under a scanning electron microscope. The chipped surfaces appear to have failed in the middle of the cobalt layer and the failure was accompanied by an amount of plastic flow. The broken surfaces

appear as brittle fractures occurring at the cobalt carbide interfaces as a result of tensile stresses.

Stress analysis simplified to a two-dimensional plane strain problem confirmed these conclusions. A local maximum of tensile stress was identifed on the rake face at a distance between .08 to .15 inch from the cutting edge which coincides with the origin of the observed brittle fracture. The level of the stress roughly corresponds to the TRS of the sintered carbide. Shear stress maxima were found close to the cutting edge at levels corresponding to the shear flow strength of the sintered carbide.

Although all three modes of investigation, experimental, fractographic and stress analysis lead to the same conclusion, explaining breakage as brittle failure and chipping as ductile failure it is necessary to be very cautious in accepting these conclusions as absolute. Too many aspects were neglected like thermally induced stresses, anisotropy and nonhomogeneity of the sintered carbide and the three-dimensional nature of the stresses. It is quite possible that on a microscopic scale when considering the individual grains as distinct from the binder, tensile stresses could be found at the cutting edge. As well, adhesive forces could produce tensile stresses at the cutting edge. A large amount of work based on a multifaceted effort will be necessary to really clarify these phenomena. However, the conclusion presented here may remain valid to a good degree.

On the side of methodology an efficient method was presented in applying finite element analysis to a problem with various loads concentrated to one small area of the body.

REFERENCES

1. H.L. Patts,"Understanding Micrograin Cemented Carbides", Proceedings of the 7th Carbide Cutting and Forming Seminar, McMaster University, Hamilton, Canada, June 1975.

2. H.S. Kalish, "Some Plain Talk about Carbides", Proceedings of the 7th Carbide Cutting and Forming Seminar, McMaster University, Hamilton, Canada, June 1975.

3. I.D. Murray, "The Titanium Carbide Coating Concept", Proceedings of the 7th Carbide Cutting and Forming Seminar, McMaster University, Hamilton, Canada, June 1975.

4. J. Tlusty, "Breakage of Carbide Tools", Proceedings of the 7th Carbide Cutting and Forming Seminar, McMaster University, Hamilton, Canada, June 1975.

5. G.S. Kreimer, "Strength of Hard Alloys", Scientific Research Institute for Hard Alloys, Moscow, translated from Russian, Consultants Bureau, New York, 1968.

6. T.N. LoLadze, "Requirements of Tool Materials", Proceedings of the 9th M.T.D.R. Conference, Manchester, England, 1968, Pergamon Press, Oxford.

7. Kals, H.J.J. and P.C. Veenstra, "Proposal for Cooperative Research on Testing and Classification of Cemented Carbide tool materials", Report WT0333, Eindhoven University of Technology, Presented at the meeting of the STC - "Toughness", C.I.R.P., Kyoto, Japan, Aug. 1974.

8. I.F. Primus, "Beitrag zur Kenntnis der Spannungsverteilugen in den Kontaktzonen von Drehwerkzeugen", Dr.-Ing Dissertation, Tech. University Aachen, W. Germany, November, 1969.

9. Kals, H.J.J., Gielisse, P.J., 'The significance of structure parameters in failure of cemented carbides", Report WT0347, Eindhoven University of Technology, Published in the Annals of C.I.R.P. Vol. 24 (1975).

10. Shaw, M.C., Braiden, P.M., DeSalvo, G.J., ASME Paper No. 73-Wa/Prod-17 (1973).

11. Liebowitz, H., "Fracture", Vol. 111 Academic Press (1972).

12. Hatano, T., Int. J. of Fracture Mechanics, Vol. 5, 1 (1969) 73.

13. Brandes, M., Int. J. of Fracture Mechanics, Vol. 1, 1(1965)56.

14. Doi H. Fujiwara, Y., Oosawa, Y., Proc. of the Int. Conf. on Mech. Behaviour of Materials, Kyoto, Vol. V (1972)209.

15. Bridgman, P.W., Trans. Am. Soc. Metals, 32 (1943)553.

16. Kals, H.J.J. Nollet, W.A., "The Testing of Cemented Carbide Tools", Report WT0372, Eindhoven University of Technology, Presented at the meeting of the STC-subgroup "Toughness of tool materials", C.I.R.P., January 1976.

17. Okushima, K., Tetsutaro, H., "Tool Fracture in Face-milling Operation", Kyoto University, Annals of the C.I.R.P. Vol. XV pp. 309-329 (1967).

18. M. Mahomed, M.Eng. Thesis "The finite element method used for the stress analysis of a diamond impregnated circular saw blade", McMaster University, July 1971.

19. A. Mason and P. Kenny, "The structure and fractography of cemented tungsten carbide", Metallurgia, December 1970.

20. S.B. Luyckx, "Microscopic aspects of fracture in WC-Co alloys", Department of Physics, University of the Witwatersrand, Johannesburg, South Africa, ACTA Metallurgica, Vol. 16, April 1968.

21. G.S. Kreimer and N.A. Alekseyeva, "Mechanism of fracture in sintered tungsten-cobalt carbides", Phys. of Metal and Metallography, 13, 117-121, 1962.

22. J.J. Emery, Associate Professor of Civil Engineering and Engineering Mechanics, McMaster University, Personal Communication, 1975.

23. J. Tlusty, MWRG Memorandum of December, 1975.

24. O.C. Zienkiewicz, "The Finite Element Method in Engineering Science", McGraw-Hill, 2nd Edition, 1971

APPENDIX A

ANALYSIS OF STRESSES USING THE SINGLE STEP METHOD

APPENDIX A

The analysis of the problem by using the finite element technique will follow the following logic [24]:

1. The idealization of the structure is shown in Figure 46. Four hundred and forty triangular elements and two hundred and fifty four nodes are used for the mesh generation.
2. The geometric dimensions and elastic properties of the tool and tool holder are shown in Figure 46-b.
3. The boundary condition is defined by the fixity of the side which has nodes number 251, 252, 253 and 254. Therefore, the displacements of these nodes are zero.
4. This is a plane strain analysis problem. The elements used are constant-strain triangles.
5. The governing matrix equation for the analysis of this problem is given by:

$$[K]\ \{\delta\} = \{F\} \tag{A-1}$$

where the stiffness matrix [K] is defined by the equation:

$$[K] = \sum_{1}^{n} [K]_e \tag{A-2}$$

The expression which defines the element stiffness matrix $[K]_e$ is given by the expression:

$$[K]_e = (\text{Area})_e . (\text{thickness})_e . \{B\}_e^T . [D]_e . \{B\}_e \tag{A-3}$$

The displacement strain matrix {B} is defined by Equation (A-4). For a triangular element defined by the nodes i, j, m, the general matrix $\{B\}_e$ is written as:

$$\{B\}_e = \{C\}\,[A^{-1}] \tag{A-4}$$

where

$$\{C\} = \begin{bmatrix} 0 & 1 & 0 & 0 & 0 & 0 \\ 0 & 0 & 0 & 0 & 0 & 1 \\ 0 & 0 & 1 & 0 & 1 & 0 \end{bmatrix} \tag{A-5}$$

and

$$[A] = \begin{bmatrix} 1 & x_i & y_i & 0 & 0 & 0 \\ 1 & x_j & y_j & 0 & 0 & 0 \\ 1 & x_m & y_m & 0 & 0 & 0 \\ 0 & 0 & 0 & 1 & x_i & y_i \\ 0 & 0 & 0 & 1 & x_j & x_j \\ 0 & 0 & 0 & 1 & x_m & y_m \end{bmatrix} \tag{A-6}$$

and the inversion of [A] is:

$$[A^{-1}] = \frac{1}{|A|}\begin{bmatrix} (x_j y_m - x_m y_j) & (x_m y_i - x_i y_m) & (x_i y_i - x_j y_i) & 0 & 0 & 0 \\ (y_i - y_m) & (y_m - y_i) & (y_i - y_i) & 0 & 0 & 0 \\ (x_m - x_j) & (x_i - x_m) & (x_j - x_i) & 0 & 0 & 0 \\ 0 & 0 & 0 & (x_j y_m - x_m y_j) & (x_m y_i - x_i y_m) & (x_i y_i - x_j y_i) \\ 0 & 0 & 0 & (y_j - y_m) & (y_m - y_i) & (y_i - y_j) \\ 0 & 0 & 0 & (x_m - x_j) & (x_i - x_m) & (x_j - x_i) \end{bmatrix} \quad (A\text{-}7)$$

and

$$|A| = |2 \text{ times the area of the element}|$$

$$= x_i(y_j - y_m) + x_j(y_m - y_i) + x_m(y_i - y_j) \quad (A\text{-}8)$$

The elasticity matrix for plane strain analysis problems is given by the expression:

$$[D]_e = \frac{E}{(1+\mu)(1-2\mu)}\begin{bmatrix} (1-\mu) & \mu & 0 \\ \mu & (1-\mu) & 0 \\ 0 & 0 & \frac{1-2\mu}{2} \end{bmatrix} \quad (A\text{-}9)$$

where E = Modulus of elasticity

μ = Poisson's ratio

The general nodal displacement matrix for this particular problem can be written as follows:

$$\{\delta\} = \begin{Bmatrix} u_1 \\ u_2 \\ \\ \\ u_{254} \\ v_1 \\ v_2 \\ \\ \\ v_{254} \end{Bmatrix} \qquad \text{(A-10)}$$

The external loads are applied only at the tip of the tool at nodes 1, 10, 19, 28, 37, 46, 55, 64, 73, 82, 91, 100 and 109 after calculation of the equivalent loads from the distributed load and these external loads are illustrated by the following matrix:

$$
\{F\} = \begin{Bmatrix}
F_{x1} & 19 & \text{node 1} \\
 & 0.0 & \\
 & \vdots & \\
F_{x10} & 46.9 & \text{node 2} \\
 & 0.0 & \\
 & \vdots & \\
F_{x19} & 56.0 & \text{node 19} \\
 & 0.0 & \\
 & \vdots & \\
F_{y1} & -75.0 & \text{node 1} \\
 & 0.0 & \\
 & \vdots & \\
F_{y10} & -187.5 & \text{node 10} \\
 & 0.0 & \\
 & \vdots & \\
F_{y19} & -225.0 & \text{node 19} \\
 & 0.0 &
\end{Bmatrix} \qquad \text{(A-11)}
$$

6. The total stiffness matrix for the tool and tool holder is obtained by the superposition of the element stiffness matrices. The general form of the total matrix will be in the following form:

$$[K]_{total} = \left[\begin{array}{cc|cc} \Sigma K_{11} & \Sigma K_{1,254} & \Sigma K_{11} & \Sigma K_{1,254} \\ \Sigma K_{2,1}\ \Sigma K_{22} & & & \\ & K_{UU} & & K_{UV} \\ & & & \\ \Sigma K_{254,1} & \Sigma K_{254,254} & & \\ \hline \Sigma K_{11} & \Sigma K_{1,254} & \Sigma K_{11} & \\ \Sigma K_{21} & & & \\ & K_{VU} & & K_{VV} \\ & & & \\ \Sigma K_{2541} & & & \Sigma K_{254,254} \end{array}\right] \quad \text{(A-12)}$$

508x508

7. The computation of the nodal displacement $\{\delta\}$ is based on the general equation:

$$\{\delta\} = [K^{-1}]\ \{F\} \qquad \text{(A-13)}$$

The displacement matrix $\{\delta\}$ has 508 possible elements in which the elements u_{251}, v_{251}, u_{252}, v_{252}, u_{253}, v_{253}, u_{254} and v_{254} are zero, due to the fixed boundary condition at

nodes 251, 252, 253 and 254 respectively. This will reduce the stiffness matrix [K] to 500 x 500 instead of 508 x 508. The remaining unknown displacements are computed by the use of Equation (A-13).

8. The calculation of the element strains are performed by the use of the equation:

$$\{\varepsilon\} = \{B\}\{\delta\} \tag{A-14}$$

which relate strains to displacement.

9. The calculation of the element stresses are performed by the use of the equation:

$$\{\sigma\} = [D]\{\varepsilon\} \tag{A-15}$$

Since all the values of the matrices are located at the right-hand side of the above equation, the stresses are readily obtained. The computations are done for each element.

The principal stresses and maximum shear stresses are also readily computed using expressions (A-16), (A-17) and (A-18).

$$\sigma_{max} = \frac{\sigma_x+\sigma_y}{2} + \sqrt{\left(\frac{\sigma_x-\sigma_y}{2}\right)^2 + \tau_{xy}^2} \tag{A-16}$$

$$\sigma_{min} = \frac{\sigma_x+\sigma_y}{2} - \sqrt{\left(\frac{\sigma_x-\sigma_y}{2}\right)^2 + \tau_{xy}^2} \tag{A-17}$$

$$\tau_{max} = \frac{\sigma_{max} - \sigma_{min}}{2} \tag{A-18}$$

and the direction of principal stresses is given by the equation:

$$\tan 2\theta = \frac{-\tau_{xy}}{(\sigma_x-\sigma_y)/2} \tag{A-19}$$

APPENDIX B

RESULTING STRESSES IN THE CASE OF ZERO RAKE ANGLE AND NO FLANK WEAR (a=0.0)

FIRST LINE FOR EACH NODE GIVES INCREMENT, SECOND GIVES TOTAL

NO.	X STRESS	Y STRESS	XY STRESS	MAX STRESS	MIN STRESS	MAX SH-STR	DIRECTION
1	-9147.0779	-94346.7975	18509.2698	-5207.6933	-98220.1821	46479.2444	11.1317
	-9147.0779	-94346.7975	18509.2698	-5207.6933	-98220.1821	46479.2444	11.1077
2	-3013.8338	-91772.9476	13427.6978	-1026.9358	-93759.8455	46366.4549	8.4170
	-3013.8338	-91772.9476	13427.6978	-1026.9358	-93759.8455	46366.4549	8.4170
3	-3098.0163	-94143.0366	14727.6366	-774.9184	-96460.1344	47842.6080	8.9038
	-3098.0163	-94143.0366	14727.6366	-774.9184	-96460.1344	47842.6080	8.9038
4	-5526.8243	-94547.6655	17016.9029	-2366.0511	-97690.4367	47652.1938	10.4020
	-5526.8243	-94547.6655	17018.9029	-2366.0511	-97690.4367	47652.1938	10.4526
5	-6213.4478	-95231.6117	18067.7599	-4377.7785	-99067.2810	47344.7512	11.6110
	-6213.4478	-95231.6117	18067.7599	-4377.7785	-99067.2810	47344.7512	11.6110
6	-6744.1374	-97142.2567	19979.5807	-4438.1404	-101448.2536	48505.0566	12.1023
	-6744.1374	-97142.2567	19979.5807	-4438.1404	-101448.2536	48505.0566	12.1023
7	-12374.4088	-97866.4757	20542.6966	-7694.4393	-102546.4452	47426.0030	12.6339
	-12374.4088	-97866.4757	20542.6966	-7694.4393	-102546.4452	47426.0030	12.6339
8	-14586.6923	-98928.0907	21883.7917	-9246.6748	-104268.1083	47510.7168	13.7132
	-14586.6923	-98928.0907	21883.7917	-9246.6748	-104268.1083	47510.7168	13.7132
9	-15780.7754	-98833.5916	22656.8963	-10001.9824	-104612.3846	47305.2011	14.3065
	-15780.7754	-98833.5916	22656.8963	-10001.9824	-104612.3846	47305.2011	14.3065
10	-15622.1593	-99046.4812	23496.2427	-9646.8181	-105221.8224	47787.5022	14.7256
	-15622.1593	-99046.4812	23496.2427	-9646.8181	-105221.8224	47787.5022	14.7256
11	-1959.9962	-89249.6701	12038.9167	-330.0369	-90879.6314	45274.7973	7.7104
	-1959.9962	-89249.6701	12038.9167	-330.0369	-90879.6314	45274.7973	7.7104
12	-2296.3463	-94052.1666	13592.3070	-325.1889	-96023.3259	47849.0685	8.2515
	-2296.3463	-94052.1666	13592.3070	-325.1889	-96023.3259	47849.0682	8.2515
13	-3716.8303	-98515.4746	16019.4406	-1082.9787	-101149.3262	50033.1737	9.3308
	-3716.8303	-98515.4746	16019.4486	-1082.9787	-101149.3262	50033.1737	9.3308
14	-5948.6244	-97990.9507	17044.3646	-2893.7463	-101045.8288	49076.0412	10.1613
	-5948.6244	-97990.9507	17044.3646	-2893.7463	-101045.8288	49076.0412	10.1613
15	-10400.3743	-99019.3249	18802.4174	-6576.0725	-102843.6268	48133.7771	11.4908
	-10400.3743	-99019.3249	18602.4174	-6576.0725	-102843.6268	48133.7771	11.4908
16	-15831.2167	-98816.3982	20766.7045	-10924.5499	-103723.0650	46399.2576	13.2936
	-15831.2167	-98816.3982	20766.7045	-10924.5499	-103723.0650	46399.2576	13.2936
17	-16361.2317	-99385.2366	22983.3851	-12295.7897	-105450.6766	46577.4445	14.7036
	-16361.2317	-99385.2366	22983.3851	-12295.7897	-105450.6765	46577.4445	14.7836
18	-21160.9644	-99549.9506	23902.3246	-14447.6214	-106263.2935	45907.8361	15.0002
	-21160.9644	-99549.9506	23902.3246	-14447.6214	-106263.2935	45907.8361	15.0002
19	-22454.4034	-100265.4492	25273.0602	-14966.3029	-107753.5497	46393.6234	16.5039
	-22454.4034	-100265.4492	25273.0802	-14966.3029	-107753.5497	46393.6234	16.5034
20	-1780.5063	-86778.3508	11264.7857	-312.9209	-88245.9361	43966.5076	7.4227
	-1780.5063	-86778.3508	11264.7857	-312.9209	-88245.9361	43966.5076	7.4227
21	-2068.0275	-89439.9447	12457.8136	-326.4603	-91181.5119	45427.5258	7.9302
	-2068.0275	-89439.9447	12457.8136	-326.4603	-91181.5119	45427.5258	7.9302
22	-3577.9227	-98818.9892	14174.0026	-1513.2717	-100883.6402	49685.1842	8.2877
	-3577.9227	-98818.9892	14174.0026	-1513.2717	-100883.6402	49685.1842	8.2877
23	-7232.1635	-99190.4422	14395.6970	-5031.2515	-101391.3542	46180.0513	8.6925
	-7232.1635	-99190.4422	14395.6970	-5031.2515	-101391.3542	46180.0513	8.6925
24	-11540.4436	-99262.8451	18535.3051	-7790.5781	-103018.7106	47614.0662	11.4549
	-11540.4436	-99262.8451	18535.3051	-7790.5761	-103016.7106	47614.0662	11.4549

25	-16969.4185	-99267.9618	20625.4353	-12089.6652	-104147.7151	40029.0250	13.3106
	-16969.4185	-99267.9618	20625.4353	-12089.6652	-104147.7151	40029.0250	13.3106
26	-20599.0831	-99415.8384	22525.2503	-14616.5004	-105399.2212	40391.3004	14.0729
	-20599.0831	-99415.8384	22525.2503	-14616.5004	-105399.2212	40391.3004	14.0729
27	-24733.4581	-99683.6153	23749.0407	-17841.9000	-106575.1734	44366.6367	15.1018
	-24733.4581	-99683.6153	23749.0407	-17841.9000	-106575.1734	44366.6367	15.1018
28	-27071.1516	-100384.4283	25269.9802	-19204.9752	-108250.6047	44522.8148	17.2306
	-27071.1516	-100384.4283	25269.9802	-19204.9752	-108250.6047	44522.8148	17.2306
29	-1755.5346	-88319.7105	10606.6152	-474.8643	-89600.3608	44562.7563	0.0047
	-1755.5346	-88319.7105	10606.6152	-474.8643	-89600.3808	44562.7583	0.0047
30	-2440.3081	-90124.2559	11286.7567	-1010.2736	-91554.2905	40272.0084	7.2196
	-2440.3081	-90124.2559	11286.7587	-1010.2736	-91554.2905	40272.0084	7.2196
31	-3280.9403	-94410.8418	11572.6826	-1840.1369	-95857.6452	47008.7242	9.1260
	-3280.9403	-94410.8418	11572.6826	-1840.1369	-95857.6452	47008.7242	9.1260
32	-6660.9653	-97923.8596	15286.4648	-4167.9267	-100416.6962	46124.4827	9.2015
	-6660.9653	-97923.8596	15286.4648	-4167.9267	-100416.8962	46124.4827	9.2015
33	-11389.5997	-98297.1733	18069.2949	-7774.7751	-101911.9979	47068.6114	11.3007
	-11389.5997	-98297.1733	18069.2949	-7774.7751	-101911.9979	47068.6114	11.3007
	-17391.4601	-97426.0587	21013.6932	-12209.5504	-102607.9624	42199.2030	13.6224
35	-22232.8469	-98582.7079	22485.2602	-16103.0079	-104712.5469	44304.7693	15.2492
	-22232.8469	-98582.7079	22485.2602	-16103.0079	-104712.5469	44304.7693	15.2492
36	-26603.3908	-99299.0158	22943.9267	-19967.6338	-105934.7726	42963.5693	15.1307
	-26603.3908	-99299.0158	22943.9267	-19967.6338	-105934.7726	42963.5693	15.1307
37	-29996.8342	-100261.7347	24901.7544	-22066.6970	-108191.8718	43062.5874	17.6044
	-29996.8342	-100261.7347	24901.7544	-22066.6970	-108191.8718	43062.5874	17.6044
38	-1276.0165	-90005.1274	10388.3747	-77.9548	-91205.1911	42563.6161	0.5896
	-1276.0165	-90005.1274	10388.3747	-77.9548	-91205.1911	42563.6161	0.5896
39	-1777.0679	-91124.3477	11009.1562	-440.5387	-92460.8770	46010.1692	0.9219
	-1777.0679	-91124.3477	11009.1562	-440.5387	-92460.8770	46010.1692	0.9219
40	-2773.4213	-94402.3899	12344.7214	-1139.4165	-96036.3947	47448.4891	1.2401
	-2773.4213	-94402.3899	12344.7214	-1139.4165	-96036.3947	47448.4891	1.2401
41	-6156.4245	-95849.3053	15169.6197	-3653.8653	-98351.8645	47348.9990	3.3057
	-6156.4245	-95849.3053	15169.6197	-3653.8653	-98351.8645	47348.9990	3.3057
42	-11236.2612	-95613.3558	18327.6850	-7427.2264	-99422.3906	45997.5021	11.7406
	-11236.2612	-95613.3558	18327.6850	-7427.2264	-99422.3906	45997.5021	11.7406
43	-17633.5850	-92334.1662	21457.4138	-12095.4499	-98072.3033	42988.4267	14.9717
	-17633.5850	-92334.1662	21457.4138	-12095.4499	-98072.3033	42988.4267	14.9717
44	-22627.5737	-93105.1403	24247.1415	-15091.4144	-100641.2997	42774.9420	17.2056
	-22627.5737	-93105.1403	24247.1415	-15091.4144	-100641.2997	42774.9420	17.2056
45	-28606.8660	-94275.9216	26370.1804	-19328.5379	-103554.2497	42112.8559	19.3844
	-28606.8660	-94275.9216	26370.1804	-19328.5379	-103554.2497	42112.8559	19.3844
46	-32245.5676	-100994.2754	26333.7921	-23317.9030	-109921.9400	43302.0185	18.7270
	-32245.5676	-100994.2754	26333.7921	-23317.9030	-109921.9400	43302.0185	18.7270
47	-1086.4066	-91206.9997	10465.0649	112.8679	-92406.2742	40259.5710	0.0375
	-1086.4066	-91206.9997	10465.0649	112.8679	-92406.2742	40259.5710	0.0375
48	-1477.5654	-91190.0998	11014.1985	-145.1188	-92522.5464	40188.7138	0.0979
	-1477.5654	-91190.0998	11014.1985	-145.1188	-92522.5464	40188.7138	0.0979
49	-2672.2600	-93305.8886	12562.1160	-903.3322	-95014.8163	47025.7420	7.7459
	-2672.2600	-93305.8886	12562.1160	-963.3322	-95014.8163	47025.7420	7.7459
50	-5741.2780	-93451.4848	15370.0635	-3125.8644	-96066.8984	46470.5170	9.6571
	-5741.2780	-93451.4848	15370.0635	-3125.8644	-96066.8984	46470.5170	9.6571
51	-11099.1706	-91609.5330	18319.0687	-7126.8955	-95581.8061	44227.4263	12.2345
	-11099.1706	-91609.5330	18319.0687	-7126.8955	-95581.8061	44227.4263	12.2345

52	-16281.0988	-87087.4144	17949.9146	-11990.6423	-91377.8708	39693.6143	13.4426
	-16281.0988	-87087.4144	17949.9146	-11990.6423	-91377.8708	39693.6143	13.4426
53	-20361.3902	-84506.5530	18755.7848	-15279.8340	-89588.1092	37154.1376	15.1594
	-20361.3902	-84506.5530	18755.7848	-15279.8340	-89588.1092	37154.1376	15.1594
54	-24180.3078	-80602.4451	19320.0225	-18198.8676	-86583.8853	34192.5089	17.2024
	-24180.3078	-80602.4451	19320.0225	-18198.8676	-86583.8853	34192.5089	17.2024
55	-28481.6190	-80196.2474	23016.9448	-19319.4989	-89358.3675	35019.4343	21.2036
	-28481.6190	-80196.2474	23016.9448	-19319.4989	-89358.3675	35019.4343	21.2036
56	-971.5564	-91534.3871	10676.9778	270.1884	-92776.1319	40523.1601	0.6338
	-971.5564	-91534.3871	10676.9778	270.1884	-92776.1319	40523.1001	0.6336
57	-1167.5833	-90584.9020	11207.9610	215.8075	-91968.3526	40092.1101	1.0307
	-1167.5833	-90584.9020	11207.9610	215.8075	-91966.3526	40092.1101	1.0307
58	-2487.4462	-91470.4907	12807.9073	-680.6095	-93277.3274	40298.3589	3.0298
	-2487.4462	-91470.4907	12807.9073	-680.6095	-93277.3274	40298.3589	3.0298
59	-5182.7023	-90373.0592	15420.1693	-2474.7061	-93081.0554	40303.1740	3.9333
	-5182.7023	-90373.0592	15420.1693	-2474.7061	-93081.0554	40303.1740	3.9333
60	-9587.5880	-87734.6675	16915.6822	-6083.1779	-91239.0776	42577.9499	11.7043
	-9587.5860	-87734.6675	16915.6822	-6083.1779	-91239.0776	42577.9499	11.7043
61	-14470.2884	-87830.8868	17828.2084	-10367.1430	-91934.0343	40783.4456	12.9609
	-14470.2884	-87830.8868	17828.2084	-10367.1430	-91934.0343	40783.4456	12.9609
62	-20775.7806	-89503.1879	17474.0776	-16588.1222	-93690.8463	38551.3620	13.4706
	-20775.7806	-89503.1879	17474.0776	-16588.1222	-93690.8463	38551.3620	13.4706
63	-28686.5870	-90695.3775	17202.1645	-24421.5509	-95160.4056	35369.4234	14.2307
	-28686.5870	-90695.3775	17202.1645	-24421.5509	-95160.4056	35369.4234	14.2307
64	-32009.9404	-87958.3763	15030.1700	-28227.8538	-91740.4629	31756.3046	14.1243
	-32009.9404	-87958.3763	15030.1700	-28227.8538	-91740.4629	31756.3046	14.1243
65	-816.2174	-90538.5819	11106.2757	538.1204	-91892.9277	40219.5260	0.9520
	-816.2174	-90538.5819	11106.2757	538.1204	-91892.9277	40219.5260	0.9520
66	-800.4517	-88966.3903	11664.9952	710.9013	-90483.7434	39597.3224	1.4113
	-800.4517	-88966.3903	11664.9952	710.9013	-90483.7434	39597.3224	1.4113
67	-2057.0296	-88930.1699	13249.5304	-81.2041	-90905.9954	40412.3957	3.4817
	-2057.0296	-88930.1699	13249.5304	-81.2041	-90905.9954	40412.3957	3.4817
68	-3653.0641	-86769.8660	15707.0000	-977.4052	-89645.5249	44334.0598	10.3749
	-3653.0641	-86769.8660	15707.0000	-977.4052	-89645.5249	44334.0598	10.3749
69	-7489.9796	-85324.5765	17854.6996	-3589.6834	-89224.8727	42617.5947	12.3225
	-7489.9796	-85324.5765	17854.6996	-3589.6834	-89224.8727	42617.5947	12.3225
70	-11937.7870	-81019.2639	21416.5301	-5837.0396	-87120.0113	40641.4659	15.9002
	-11937.7870	-81019.2639	21416.5301	-5837.0396	-87120.0113	40641.4659	15.9002
71	-17669.6421	-82758.2026	21356.3367	-11288.2357	-89139.6090	38925.7867	16.6310
	-17669.8421	-82758.2026	21356.3367	-11288.2357	-89139.6090	38925.7867	16.6310
72	-26677.0251	-83769.5844	20955.8599	-19811.6262	-90635.7833	35412.0788	18.1414
	-26677.0251	-83769.5844	20955.8599	-19811.6262	-90635.7833	35412.0766	18.1414
73	-37336.3032	-90526.5220	22980.3677	-26784.9524	-99079.6728	35147.4002	20.4124
	-37336.3032	-90526.5220	22980.3677	-26784.9524	-99079.6728	35147.4602	20.4124
74	-645.7088	-88316.9650	11871.7822	933.4349	-89896.1068	40414.7719	1.5708
	-645.7088	-88316.9650	11871.7822	933.4349	-89696.1068	40414.7719	1.5708
75	-430.2071	-86132.5204	12533.3420	1305.0302	-87927.8296	44640.4329	8.1517
	-430.2071	-86132.5204	12533.3420	1305.0362	-87927.8296	44640.4329	8.1517
76	-1380.2901	-84961.6470	14266.6261	986.3520	-87336.4891	44161.5205	9.4378
	-1380.2901	-84961.6470	14266.6261	986.3520	-87336.4891	44161.5205	9.4378
77	-2219.1349	-81632.0260	17344.4470	1116.3426	-85267.5055	43191.9241	11.0361
	-2219.1349	-81632.0260	17344.4470	1116.3426	-85267.5055	43191.9241	11.0361
78	-5092.7203	-77456.5779	20659.5020	-219.1941	-83090.1041	41435.4250	15.1133
	-5092.7203	-77456.5779	20659.5020	-219.1941	-83090.1041	41435.4250	15.1133

79	-9372.3246	-67743.1813	23750.7179	-929.4946	-76186.0113	37628.2583	19.5091
	-9372.3246	-67743.1813	23750.7179	-929.4946	-76186.0113	37628.2583	19.5091
80	-14973.2700	-69104.6995	22794.4386	-6053.4037	-77424.5658	35365.5610	20.0518
	-14973.2700	-69104.6995	22794.4386	-6053.4037	-77424.5658	35365.5610	20.0518
81	-21063.4089	-68671.2160	20688.3064	-13329.5280	-76405.0969	31537.7044	20.4972
	-21063.4089	-68671.2160	20688.3064	-13329.5280	-76405.0969	31537.7044	20.4972
82	-30752.6895	-74600.8427	21487.7856	-21978.5652	-83375.1670	30698.3009	22.2122
	-30752.6895	-74600.8427	21487.7856	-21978.5652	-83375.1670	30698.3009	22.2122
83	-777.0160	-84955.2246	12782.7567	1121.2821	-86853.5227	43987.4024	8.4409
	-777.0160	-84955.2246	12782.7567	1121.2821	-86853.5227	43987.4024	8.4409
84	-331.9847	-82219.3245	13639.2114	1880.0193	-84431.3266	43155.6740	8.2120
	-331.9847	-82219.3245	13639.2114	1880.0193	-84431.3266	43155.6740	8.2120
85	-1076.6129	-79749.1847	15817.4841	1984.4619	-82810.2595	42397.3607	10.9926
	-1076.6129	-79749.1847	15817.4841	1984.4619	-82810.2595	42397.3607	10.9926
86	-2025.4912	-74326.2976	19531.5129	2913.4166	-79265.2074	41089.3130	14.1908
	-2025.4912	-74326.2976	19531.5129	2913.4166	-79265.2074	41089.3130	14.1908
87	-4664.4652	-66267.0675	22921.2078	2748.0909	-73879.6236	38313.8973	18.3723
	-4664.4652	-66267.0675	22921.2078	2748.0909	-73879.6236	38313.8973	18.3723
88	-6909.5370	-52280.7180	24299.3807	3647.8555	-62838.1105	33242.9830	23.4830
	-6909.5370	-52280.7180	24299.3807	3647.8555	-62838.1105	33242.9830	23.4830
89	-9699.5975	-52036.7045	22598.9077	96.6401	-61832.9421	30964.7911	23.4329
	-9699.5975	-52036.7045	22598.9077	96.6401	-61832.9421	30964.7911	23.4329
90	-13406.4159	-52226.5764	19135.6148	-5559.8826	-60073.1095	27256.6133	22.2900
	-13406.4159	-52226.5764	19135.6148	-5559.8826	-60073.1095	27256.6133	22.2900
91	-19113.3738	-57270.7837	18363.3361	-11711.7258	-64672.4317	26480.3930	21.9227
	-19113.3738	-57270.7837	18363.3361	-11711.7258	-64672.4317	26480.3930	21.9227
92	-1120.6715	-80157.1737	13670.5866	1171.2333	-82455.0765	41813.1559	8.5417
	-1120.6715	-80157.1737	13670.5866	1171.2333	-82455.0765	41813.1559	8.5417
93	-2883.6033	-77205.3576	14956.3145	2522.0391	-80011.0599	41266.5499	10.9218
	-2883.6033	-77205.3576	14956.3145	2522.0391	-80011.0599	41266.5499	10.9218
94	-902.0506	-73144.8265	17426.0539	3061.9592	-77128.8364	40102.3970	12.8774
	-902.0506	-73144.8265	17426.0539	3061.9592	-77128.8364	40102.3970	12.8774
95	2072.4102	-65017.4102	21074.1950	4331.7311	-71421.5514	37870.6412	16.9033
	2072.4102	-65017.4102	21074.1950	4331.7311	-71421.5514	37870.6412	16.9033
96	-479.0369	-53365.0756	23402.1675	4645.9975	-62805.7120	33725.8247	21.9096
	-479.0369	-53365.0756	23402.1675	4645.9975	-62805.7120	33725.8247	21.9096
97	-3004.0780	-34291.5502	22431.0210	6407.4036	-46063.8317	26035.6177	20.6836
	-3004.0780	-34291.5502	22431.0210	6407.4036	-46063.8317	26035.6177	20.6836
98	-5206.2420	-32177.4586	21279.0349	6436.6124	-43882.3129	25229.4921	20.0327
99	-2221.8426	-31134.0041	18245.4962	6600.3155	-39950.1621	23278.2306	20.0049
	-2221.8426	-31134.0041	18245.4962	6600.3155	-39950.1621	23278.2306	20.0049
100	-4166.4383	-38343.9248	15722.5834	1966.0323	-44470.3954	23221.2139	21.3079
	-4166.4383	-38343.9248	15722.5834	1966.0323	-44470.3954	23221.2139	21.3079
101	-2332.8551	-75123.9886	14022.5510	275.0295	-77731.8734	39003.4515	10.5324
	-2332.8551	-75123.9888	14022.5510	275.0295	-77731.8734	39003.4515	10.5324
102	-1423.1051	-71216.9674	15586.8933	1899.6844	-74539.7569	38219.7206	12.0341
	-1423.1051	-71216.9674	15586.8933	1899.6844	-74539.7569	38219.7206	12.0341
103	-1839.2538	-63480.5775	18487.5339	3260.3418	-68600.1731	35940.2574	13.4765
	-1839.2538	-63480.5775	18487.5339	3260.3418	-68600.1731	35940.2574	13.4765
104	-3646.6947	-50858.1380	20671.3585	4257.0061	-56761.8387	31509.4224	20.7410
	-3646.6947	-50858.1380	20671.3585	4257.0061	-58761.8387	31509.4224	20.7410
105	-5602.9741	-35574.4901	20620.0913	4854.7022	-46092.1664	29473.4343	21.0236
	-5602.9741	-35574.4901	20620.0913	4854.7022	-46092.1664	29473.4343	21.0236

106	-2210.5256	-16980.3513	15017.4983	7139.6203	-26330.4972	16735.0563	31.9071
	-2210.5256	-16980.3513	15017.4983	7139.6203	-26330.4972	16735.0568	31.9071
107	962.2642	-12684.1865	13028.4777	8848.5152	-20567.1375	14707.8263	31.1702
	962.2642	-12684.1865	13028.4777	8848.5152	-20567.1375	14707.8263	31.1702
108	6608.0233	-10014.0971	10555.0425	11893.4388	-15099.5126	13496.4757	29.7247
	6608.0233	-10014.0971	10555.0425	11893.4388	-15099.5126	13496.4757	29.7247
109	11573.4268	-12625.7208	9796.2743	15041.9831	-16094.2771	15568.1301	19.4975
	11573.4268	-12625.7208	9796.2743	15041.9831	-16094.2771	15568.1301	19.4975
110	-2719.2358	-65446.2479	12334.8930	-380.8265	-67784.6572	33701.9153	10.7366
	-2719.2358	-65446.2479	12334.8930	-380.8265	-67784.6572	33701.9153	10.7366
111	-3258.3754	-62017.2835	15346.5239	508.3335	-65783.9923	33146.1629	13.7903
	-3258.3754	-62017.2835	15346.5239	508.3335	-65783.9923	33146.1629	13.7903
112	-4435.4220	-47195.1111	17987.4492	2124.7779	-53755.3110	27940.0445	20.0374
	-4435.4220	-47195.1111	17987.4492	2124.7779	-53755.3110	27940.0445	20.0374
113	-5683.2550	-34048.0422	16595.8043	3521.1901	-43252.4874	23386.8388	20.3342
	-5683.2550	-34048.0422	16595.8043	3521.1901	-43252.4874	23386.8388	20.3342
114	-4973.7968	-19616.7725	15104.8150	4490.4122	-29080.9815	16785.6968	32.0700
	-4973.7968	-19616.7725	15104.8150	4490.4122	-29080.9815	16785.6968	32.0700
115	1732.1639	-7926.2221	7680.0173	5975.1135	-12169.1717	9072.1426	28.9192
	1732.1639	-7926.2221	7680.0173	5975.1135	-12169.1717	9072.1426	28.9192
116	6777.5911	-4508.1825	4945.4965	8638.0454	-6368.6367	7503.3411	20.6199
	6777.5911	-4508.1825	4945.4965	8638.0454	-6368.6367	7503.3411	20.6199
117	13497.2857	-2647.4180	2761.6870	13956.6265	-3106.7588	6531.6926	9.4433
	13497.2857	-2647.4180	2761.6870	13956.6265	-3106.7586	6531.6926	9.4433
118	19157.6121	-1359.7006	76.2397	19157.8954	-1359.9839	10258.9397	.2129
	19157.6121	-1359.7006	76.2397	19157.8954	-1359.9639	10258.9397	.2129
119	-1868.9007	-51175.0693	10540.6837	289.9635	-53333.9334	26811.9484	11.5746
	-1868.9007	-51175.0693	10540.6837	289.9635	-53333.9334	26811.9484	11.5746
120	-3404.4847	-48084.2947	13695.9704	459.6360	-51948.4154	26204.0257	19.7556
	-3404.4847	-48084.2947	13695.9704	459.6360	-51948.4154	26204.0257	19.7556
121	-5299.9358	-34735.7045	16059.4328	1765.6943	-41601.3346	21783.5145	23.7479
	-5299.9358	-34735.7045	16059.4328	1765.6943	-41601.3346	21783.5145	23.7479
122	-6210.4346	-22761.7536	14956.2176	2607.0327	-31579.2209	17093.1268	30.5215
	-6210.4346	-22761.7536	14956.2176	2607.0327	-31579.2209	17093.1268	30.5215
123	-3397.2299	-10442.4941	9912.8012	3600.2409	-17439.9649	10520.1029	35.2163
	-3397.2299	-10442.4941	9912.8012	3600.2409	-17439.9649	10520.1029	35.2163
124	3295.6787	-3411.9731	3878.1707	5069.0700	-5185.3644	5127.2172	24.5734
	3295.6787	-3411.9731	3878.1707	5069.0700	-5185.3644	5127.2172	24.5734
125	8573.2557	-1670.3532	1223.8396	8717.4426	-1814.5400	5265.9913	8.7193
	8573.2557	-1670.3532	1223.8396	8717.4426	-1814.5400	5265.9913	8.7193
126	15319.8817	-692.5558	227.8126	15323.1222	-695.7963	8009.4593	.8149
	15319.8817	-692.5558	227.8126	15323.1222	-695.7963	8009.4593	.8149
127	21175.0396	258.7009	-1578.1955	21293.4485	140.2920	10576.5783	-4.2907
	21175.0396	258.7009	-1578.1955	21293.4485	140.2920	10576.5783	-4.2907
128	-2120.9543	-40983.3601	9280.4142	-18.5153	-43085.7991	21533.6419	12.1047
	-2120.9543	-40983.3601	9280.4142	-18.5153	-43085.7991	21533.6419	12.1047
129	-3346.1773	-37418.7246	12094.2926	508.4724	-41275.3742	20691.9233	17.6865
	-3346.1773	-37418.7246	12094.2926	508.4724	-41275.3742	20691.9233	17.6865
130	-5517.1509	-25818.1804	13462.9014	1193.0183	-32528.3496	15660.6340	20.4929
	-5517.1509	-25818.1804	13462.9014	1193.0183	-32528.3496	15660.6340	20.4929

131	-5669.7037	-14883.1947	11552.1005	2160.3161	-22713.2145	12436.7053	34.1234
	-5669.7037	-14883.1947	11552.1005	2160.3161	-22713.2145	12436.7053	34.1234
132	-2289.5763	-5808.4508	6777.9911	2956.1160	-11050.1432	7003.1290	37.7102
	-2289.5763	-5808.4508	6777.9911	2956.1160	-11050.1432	7003.1290	37.7102
133	3767.8060	-1656.6855	2442.2045	4722.7429	-2591.6224	3657.1825	20.9461
	3767.8060	-1656.6855	2442.2045	4722.7429	-2591.6224	3657.1825	20.9461
134	8619.1180	-576.8754	256.4606	8626.2047	-584.0221	4605.1434	1.9962
	8619.1180	-576.8754	256.4606	8626.2047	-584.0221	4605.1434	1.9962
135	14212.6586	-204.8750	-341.1922	14220.7284	-212.9449	7216.8366	-1.3249
	14212.6586	-204.8750	-341.1922	14220.7284	-212.9449	7216.8366	-1.3249
136	19317.9411	317.4746	-1316.0574	19406.2659	226.7498	9590.7560	-3.9435
	19317.9411	317.4746	-1316.0574	19406.2659	226.7498	9590.7560	-3.9435
137	-1472.6037	-32387.5965	7715.1233	345.6278	-34206.0280	17275.8279	13.2024
	-1472.6037	-32387.5965	7715.1233	345.6278	-34206.0280	17275.8279	13.2024
138	-3486.0469	-29161.3092	10041.2156	-25.5031	-32621.9330	16298.2149	14.0157
	-3486.0469	-29161.3092	10041.2156	-25.5031	-32621.9330	16298.2149	14.0157
139	-5530.2161	-18272.7939	11196.4486	980.7987	-24783.8108	12662.3047	30.1741
	-5530.2181	-18272.7939	11196.4486	980.7987	-24783.8108	12662.3047	30.1741
140	-5124.6965	-9843.3634	9208.4185	2021.7079	-16989.9678	9505.8378	37.0146
	-5124.6965	-9843.3634	9208.4185	2021.7079	-16989.9678	9505.8378	37.0146
141	-1696.2347	-3992.8490	5337.0826	2614.6750	-8303.7602	5459.2160	30.9266
	-1696.2347	-3992.8498	5337.0826	2614.6758	-8303.7602	5459.2160	30.9266
142	4309.6719	-925.7832	1687.7579	4919.3469	-1535.4582	3227.4026	17.6302
	4309.6719	-925.7832	1687.7579	4919.3469	-1535.4582	3227.4026	17.6302
143	8751.0459	-192.9180	189.2819	8755.0499	-196.9220	4475.9059	1.2116
	8751.0459	-192.9180	189.2819	8755.0499	-196.9220	4475.9059	1.2116
144	13048.9132	-89.9953	-273.1786	13054.5906	-95.6727	6575.1315	-1.1906
	13048.9132	-89.9953	-273.1788	13054.5906	-95.6727	6575.1315	-1.1906
145	16914.4378	141.5827	-919.1202	16964.6534	91.3670	8436.6432	-3.1212
	16914.4378	141.5827	-919.1202	16964.6534	91.3670	8436.6432	-3.1212
146	-875.8866	-24113.1054	6556.9553	1034.8060	-25823.7801	13429.2930	14.6179
	-875.8866	-24113.1054	6558.9553	1034.8060	-25823.7801	13429.2930	14.6179
147	-2021.4506	-21598.1986	8357.6467	1061.1706	-24680.8202	12870.9952	20.2429
	-2021.4506	-21598.1986	8357.6467	1061.1706	-24680.8202	12870.9952	20.2429
148	-4863.9011	-13068.6229	9562.4084	1438.9780	-19371.5020	10405.2400	33.3901
	-4863.9011	-13068.6229	9562.4084	1438.9780	-19371.5020	10405.2400	33.3901
149	-4622.5263	-6971.9053	7619.7415	2110.2633	-13704.6974	7907.4805	40.7264
	-4622.5263	-6971.9053	7619.7415	2110.2633	-13704.6974	7907.4805	40.7264
150	-940.1814	-2606.5737	4526.1659	2825.2964	-6378.0515	4601.6739	39.6031
	-940.1814	-2606.5737	4526.1659	2825.2964	-6378.0515	4601.6739	39.6031
151	4147.9717	-386.2473	1702.3255	4715.7453	-956.0206	2635.6031	10.4470
	4147.9717	-386.2473	1702.3255	4715.7453	-956.0206	2635.6031	10.4470
152	8565.7331	82.6218	176.8764	8569.4108	78.9441	4255.2333	1.1911
	8565.7331	82.6218	176.8764	8569.4108	78.9441	4255.2333	1.1911
153	12296.7738	3.0640	-190.5524	12299.7266	.1112	6149.6077	-.0878
	12296.7738	3.0640	-190.5524	12299.7266	.1112	6149.6077	-.0878
154	15566.5247	179.5067	-564.0277	15568.6602	157.3732	7719.6435	-2.1705
	15566.5247	179.5067	-564.0277	15568.6602	157.3732	7719.6435	-2.1705
155	-2795.7450	-18623.9715	5699.3549	-957.1235	-20462.2930	9752.7347	17.0736
	-2795.7450	-18623.9715	5699.3549	-957.1235	-20462.2930	9752.7347	17.0736
156	-2523.9240	-15830.8519	7126.4303	573.0685	-16928.4444	9751.0964	23.4009
	-2523.9240	-15830.8519	7126.4303	573.0685	-18928.4444	9751.0964	23.4009
157	-4654.0044	-9853.1299	8251.4992	1593.9804	-15801.1147	8697.5476	33.7024
	-4654.0044	-9853.1299	8251.4992	1593.9804	-15801.1147	8697.5476	33.7024

158	-4093.6899	-5499.3373	6662.3889	1922.7336	-11515.7606	6719.2472	41.9300
	-4093.6899	-5499.3373	6662.3889	1922.7336	-11515.7606	6719.2472	41.9300
159	-671.3600	-2024.8597	4071.6465	2779.3969	-5472.6166	4127.5067	70.2013
	-671.3600	-2024.8597	4071.6465	2779.3969	-5472.6166	4127.5067	70.2013
160	4133.3465	-235.2740	1690.9326	4713.1564	-813.0839	2763.1212	10.0000
	4133.3465	-235.2740	1690.9326	4713.1564	-813.0839	2763.1212	10.0000
161	6070.4819	7.5657	390.4676	6089.3472	-11.2996	4050.3234	2.7021
	6070.4819	7.5657	390.4676	6089.3472	-11.2996	4050.3234	2.7021
162	11792.4311	-104.8598	-37.5765	11792.5496	-104.8720	7946.7641	-.1310
	11792.4311	-104.8598	-37.5765	11792.5496	-104.8720	7946.7641	-.1310
	14285.8271	168.3243	-494.1549	14602.7442	151.4122	9225.6860	-1.9007
164	-1445.6639	-14633.0352	4629.4135	17.2106	-16093.9096	8056.5600	17.5363
	-1445.6639	-14633.0352	4629.4135	17.2106	-16093.9096	8056.5600	17.5363
165	-2754.2470	-13093.9855	5874.2167	-96.9010	-15749.3315	7825.2152	24.3246
	-2754.2470	-13093.9855	5874.2167	-96.9010	-15749.3315	7825.2152	24.3246
166	-4278.3481	-8102.9883	6664.4618	935.1864	-13316.5228	7125.8540	37.2165
	-4278.3481	-8102.9883	6664.4618	935.1864	-13316.5228	7125.8540	37.2165
167	-4142.5469	-4092.8138	5714.9934	1597.3672	-9832.7218	6715.0472	42.1240
	-4142.5469	-4092.8138	5714.9934	1597.3672	-9832.7218	6715.0472	42.1240
168	-911.0745	-1817.8205	3654.7669	2318.3324	-5047.2274	3682.7799	41.4043
	-911.0745	-1817.8205	3654.7669	2318.3324	-5047.2274	3682.7799	41.4043
169	4013.6151	-2.2560	1955.6603	4808.7481	-797.3909	2803.0095	22.1236
	4013.6151	-2.2560	1955.6603	4808.7481	-797.3909	2803.0095	22.1236
170	7628.2326	116.4413	781.1293	7906.5579	38.1160	3934.2209	5.7200
	7628.2326	116.4413	781.1293	7906.5579	38.1160	3934.2209	5.7200
171	11428.5017	-74.6802	338.4582	11438.4515	-84.6300	5761.5408	1.6839
	11428.5017	-74.6802	338.4582	11438.4515	-84.6300	5761.5408	1.6839
172	13970.2142	155.2711	-187.7873	13972.7663	152.7190	6910.0237	-.7760
	13970.2142	155.2711	-187.7873	13972.7663	152.7190	6910.0237	-.7760
173	-1003.4282	-10299.9731	3979.9974	467.6797	-11771.0810	6119.3803	20.2026
	-1003.4282	-10299.9731	3979.9974	467.6797	-11771.0810	6119.3803	20.2026
174	-2074.0537	-9885.3400	5265.6909	576.3347	-12535.7284	6556.0315	26.1175
	-2074.0537	-9885.3400	5265.6909	576.3347	-12535.7284	6556.0315	26.1175
175	-3385.9639	-6414.3822	6210.7264	1492.4752	-11292.8213	6392.6482	30.1491
	-3385.9639	-6414.3822	6210.7264	1492.4752	-11292.8213	6392.6482	30.1491
176	-3733.8005	-3152.3227	5141.4387	1706.5910	-8592.7141	5149.6526	40.6102
	-3733.8005	-3152.3227	5141.4387	1706.5910	-8592.7141	5149.6526	40.6102
177	-803.6401	-548.1693	3259.4838	2586.0811	-3937.8905	3261.9858	40.1221
	-803.6401	-548.1693	3259.4838	2586.0811	-3937.8905	3261.9858	40.1221
178	3609.8378	-220.1178	2276.8725	4669.9715	-1280.2515	2975.1115	24.9071
	3609.8378	-220.1178	2276.8725	4669.9715	-1280.2515	2975.1115	24.9071
179	7640.1119	-120.9779	1060.2519	7782.3475	-263.2135	4022.7805	7.6408
	7640.1119	-120.9779	1060.2519	7782.3475	-263.2135	4022.7805	7.6408
180	11300.1400	-200.5826	551.1961	11326.4966	-226.9395	5776.7181	2.7377
	11300.1400	-200.5826	551.1961	11326.4968	-226.9395	5776.7181	2.7377
181	14042.8349	117.6841	-20.8958	14042.8665	117.6525	5962.6070	-.0004
	14042.8349	117.6841	-20.8958	14042.8665	117.6525	5962.6070	-.0004
182	-1170.9387	-5112.9072	2849.4149	322.7480	-6606.5939	3464.6709	27.6039
	-1170.9387	-5112.9072	2849.4149	322.7480	-6606.5939	3464.6709	27.6039
183	-1660.6254	-5761.8466	4479.5700	1215.3807	-8637.8526	4926.6167	32.7016
	-1660.6254	-5761.8466	4479.5700	1215.3807	-8637.8526	4926.6167	32.7016
184	-2741.4406	-3935.5756	5784.0509	2476.2777	-9153.2941	5814.7659	42.0532
	-2741.4406	-3935.5756	5784.0509	2476.2777	-9153.2941	5814.7659	42.0532
185	-2725.7262	-2100.2171	5370.3514	2966.4790	-7792.4223	5379.4507	40.6005
	-2725.7262	-2100.2171	5370.3514	2966.4790	-7792.4223	5379.4507	40.6005

186	-1021.9176	-775.7938	3601.6965	2890.3488	-4716.0603	3804.2046	40.0399
	-1021.9176	-775.7938	3601.6965	2890.3486	-4716.0603	3804.2046	40.0399
187	4051.7476	-353.1754	2209.3279	4968.8960	-1270.3239	3119.6100	22.5446
	4051.7476	-353.1754	2209.3279	4968.8960	-1270.3239	3119.6100	22.5446
188	7700.7049	-165.2873	1192.4865	7877.5120	-342.0944	4109.8032	8.4331
	7700.7049	-165.2873	1192.4865	7877.5120	-342.0944	4109.8032	8.4331
189	11438.5414	-186.3696	675.3980	11537.4504	-225.2786	2881.3045	3.2911
	11438.5414	-186.3696	675.3980	11537.4504	-225.2786	2881.3045	3.2911
190	14210.0567	96.4834	64.4251	14210.3508	96.1893	7057.0308	.2015
	14210.0567	96.4834	64.4251	14210.3508	96.1893	7057.0308	.2015
191	-862.4774	-1378.2968	1338.6711	242.9023	-2483.6764	1363.2893	33.5476
	-862.4774	-1378.2968	1338.6711	242.9023	-2483.6764	1363.2893	33.5476
192	-2078.2341	-1808.6363	2687.2876	946.9973	-4833.8678	2890.4325	40.3305
	-2078.2341	-1808.6363	2687.2876	946.9973	-4833.8678	2890.4325	40.3305
193	-3057.3398	-1728.1495	5213.2910	2862.7372	-7648.2265	2255.4815	43.6324
	-3057.3398	-1728.1495	5213.2910	2862.7372	-7648.2265	2255.4815	43.6324
194	-2541.7589	-1031.7298	5362.1009	3628.2567	-7201.7455	2415.0011	44.0014
	-2541.7589	-1031.7298	5362.1009	3628.2567	-7201.7455	2415.0011	44.0014
195	-890.6318	-779.9081	4561.7941	3726.8601	-5397.4000	1562.1300	42.3470
	-890.6318	-779.9081	4561.7941	3726.8601	-5397.4000	1562.1300	42.3476
196	1699.2521	-388.6890	3084.6486	3909.1637	-2602.5965	3255.8801	32.6077
	1699.2521	-388.6890	3084.6486	3909.1637	-2602.5965	3255.8801	32.6077
197	5089.3723	-797.7520	2358.0979	5917.4390	-1025.8167	3771.6266	19.3492
	5089.3723	-797.7520	2358.0979	5917.4390	-1025.8167	3771.6266	19.3492
198	6041.0488	-699.9433	1359.5799	8247.6362	-906.5308	4577.0833	8.6400
	6041.0488	-699.9433	1359.5799	8247.6362	-906.5308	4577.0833	8.6400
199	11611.7529	-881.8954	680.9695	11648.7619	-918.9044	8263.8332	5.1107
	11611.7529	-881.8954	680.9695	11648.7619	-918.9044	8263.8332	5.1107
200	14568.2376	56.2276	60.7956	14568.4923	55.9729	7256.2597	.2400
	14568.2376	56.2276	60.7956	14568.4923	55.9729	7256.2597	.2400
201	-509.1000	-1193.7003	779.5594	.0000	-1702.6003	851.4002	33.1470
	-509.1000	-1193.7003	779.5594	.0000	-1702.6003	851.4002	33.1470
202	-874.8758	-853.8690	1191.4420	327.1159	-2055.8607	1191.4883	42.2525
	-874.8758	-853.8690	1191.4420	327.1159	-2055.8607	1191.4883	42.2525
203	-4265.4953	-445.5267	2383.7925	699.0752	-5410.0952	3054.5872	64.3515
	-4265.4953	-445.5267	2383.7925	699.0752	-5410.0952	3054.5872	64.3515
204	-4540.6027	-459.9827	4080.4647	2060.2006	-7066.7860	4563.4933	50.2987
	-4540.6027	-459.9827	4080.4647	2060.2006	-7066.7860	4563.4933	50.2987
205	-3314.0975	-344.2839	5312.4031	3686.8382	-7345.2196	2516.0269	22.0863
	-3314.0975	-344.2839	5312.4031	3686.8382	-7345.2196	2516.0269	22.0863
206	-402.8499	-616.1562	4849.1346	4339.2705	-5361.2766	4850.2746	44.3700
	-402.8499	-616.1562	4849.1346	4339.2705	-5361.2766	4850.2746	44.3700
207	3582.2687	-194.4938	3097.3814	5321.5252	-1933.7503	3627.6377	23.3123
	3582.2687	-194.4938	3097.3814	5321.5252	-1933.7503	3627.6377	23.3123
208	8371.8441	-290.1229	1710.5488	8697.4039	-615.6827	4656.5433	10.7729
	8371.8441	-290.1229	1710.5488	8697.4039	-615.6827	4656.5433	10.7729
209	12033.9758	-445.2303	644.9826	12090.9307	-502.1852	6296.5500	3.8501
	12033.9758	-445.2303	644.9826	12090.9307	-502.1852	6296.5500	3.8501
210	14662.0227	-97.4952	34.6159	14662.1039	-97.5764	7379.8401	.1354
	14662.0227	-97.4952	34.6159	14662.1039	-97.5764	7379.8401	.1354
211	-7179.4288	-300.3709	2001.6429	280.7828	-7756.5865	4018.6857	74.7011
	-7179.4288	-300.3709	2001.6429	280.7828	-7756.5865	4018.6857	74.7011
212	-7069.4439	-199.8214	2999.7353	925.6678	-8194.9331	4560.3005	69.4341
	-7069.4439	-199.8214	2999.7353	925.6678	-8194.9331	4560.3005	69.4341

213	-5122.3478	86.5943	4697.3605	2845.5070	-7911.2605	2378.3837	59.5730
	-5122.3478	86.5943	4697.3805	2845.5070	-7911.2605	2378.3837	59.5730
214	-1112.0564	-273.2648	5132.7379	4456.9075	-5842.8291	2149.8263	47.3373
	-1112.0564	-273.2648	5132.7379	4456.9075	-5842.8291	2149.8263	47.3373
215	4000.3551	351.9116	3089.6747	6476.6104	-2118.3435	4297.4769	32.4166
	4000.3551	351.9116	3089.6747	6476.6104	-2118.3435	4297.4769	32.4166
216	8561.0935	473.6421	2269.5585	9154.4288	-119.7233	4637.0910	14.0517
	8561.0935	473.6421	2269.5585	9154.4288	-119.7233	4637.0910	14.0517
217	12952.2462	173.6365	1299.8957	13083.1365	42.7462	6520.1942	5.7499
	12952.2462	173.6365	1299.8957	13083.1365	42.7462	6520.1942	5.7499
218	15649.9813	1143.7323	311.1863	15056.6538	1137.0599	7259.7970	1.2263
	15649.9813	1143.7323	311.1863	15056.6538	1137.0599	7259.7970	1.2263
219	-10467.2285	-167.8898	2288.4269	317.6872	-10952.8059	2639.2463	79.8202
	-10467.2285	-167.8898	2288.4269	317.6872	-10952.8059	2639.2463	79.8202
220	-6486.5886	170.5937	3992.7868	1467.3752	-9783.3701	2625.3727	70.1554
	-6486.5886	170.5937	3992.7868	1467.3752	-9783.3701	2625.3727	70.1554
221	-3102.5488	122.0954	4903.4792	3671.5260	-6651.9795	5161.7927	54.1007
	-3102.5488	122.0954	4903.4792	3671.5260	-6651.9795	5161.7927	54.1007
222	3460.3869	446.7994	4500.3633	6712.6913	-2785.3044	4749.0961	39.6371
	3460.3869	446.7994	4500.3633	6712.6913	-2785.3044	4749.0961	39.6371
223	9056.7662	288.4751	3283.7600	10150.1942	-804.9529	5477.5733	13.4167
	9056.7662	288.4751	3283.7600	10150.1942	-804.9529	5477.5733	13.4167
224	14356.5565	-280.0081	2078.1337	14647.8590	-569.3066	6808.5036	1.9203
	14356.5585	-280.0081	2078.1337	14647.8590	-569.3066	6808.5036	1.9203
225	17739.8076	294.8911	828.8066	17776.8772	255.8215	8761.8279	2.7133
	17739.8076	294.8911	828.8066	17776.8772	255.8215	8761.8279	2.7133
226	-15112.8532	35.8173	1804.9345	247.9052	-15324.7411	7786.3231	83.2962
	-15112.8532	35.8173	1804.9345	247.9052	-15324.7411	7700.3231	83.2962
227	-12690.5861	-121.6659	2000.2720	307.2535	-13407.4807	6697.3595	70.9201
228	-9091.4858	-506.1353	4355.2819	1316.5925	-10914.2136	6115.4030	67.2916
	-9091.4858	-506.1353	4355.2819	1316.5925	-10914.2136	6115.4030	67.2916
229	263.3349	-215.4855	4831.1328	4860.9860	-4813.1360	4837.0513	43.5815
	263.3349	-215.4855	4831.1328	4860.9860	-4813.1360	4837.0513	43.5815
230	8921.0495	-382.0905	3799.2736	10275.4419	-1736.4828	6005.9023	13.6205
	8921.0495	-382.0905	3799.2736	10275.4419	-1736.4828	6005.9623	13.6205
231	15949.5651	-674.4049	2612.2259	16350.3764	-1075.2161	8712.7962	0.7232
	15949.5651	-674.4049	2612.2259	16350.3764	-1075.2161	8712.7962	0.7232
232	20515.6564	163.7958	1140.8664	20579.4103	100.0419	10239.6842	3.1985
	20515.6564	163.7958	1140.8664	20579.4103	100.0419	10239.6842	3.1985
233	-16595.6733	71.9409	2610.7138	533.1582	-17056.8905	8795.0243	80.6812
	-16595.6733	71.9409	2610.7138	533.1582	-17056.8905	8795.0243	80.6812
234	-13424.3703	-769.7604	3351.3140	62.9691	-14257.0999	7160.0345	70.0428
	-13424.3703	-769.7604	3351.3140	62.9691	-14257.0999	7160.0345	70.0428
235	-3400.0748	-134.6902	4132.3119	2675.7792	-6210.5441	4443.1617	22.7796
	-3400.0748	-134.6902	4132.3119	2675.7792	-6210.5441	4443.1617	22.7796
236	8000.5380	-484.5610	3976.2319	9572.5949	-2056.6178	2814.6063	21.5720
	8000.5380	-484.5610	3976.2319	9572.5949	-2056.6178	2814.6063	21.5720
237	17530.3273	-830.8651	2878.4205	17970.9915	-1271.5293	9621.2604	0.1040
	17530.3273	-830.8651	2878.4205	17970.9915	-1271.5293	9621.2004	0.1040
238	23724.4285	231.8926	1144.6107	23780.0648	176.2563	11801.9043	2.7826
	23724.4285	231.8926	1144.6107	23780.0646	176.2563	11801.9043	2.7826
239	-23628.1089	1045.8849	1521.4840	1139.3508	-23721.5748	12430.4628	80.4847
	-23628.1089	1045.8849	1521.4840	1139.3508	-23721.5748	12430.4628	80.4847
240	-16667.6185	-654.9618	2575.8593	-293.8465	-19028.7338	9367.4437	82.0116
	-16667.6185	-654.9618	2575.8593	-293.8465	-19028.7338	9367.4437	82.0116

241	-10770.6991	-569.2537	4051.1513	843.7936	-12183.7464	6513.7700	70.7711
	-10770.6991	-569.2537	4051.1513	843.7936	-12183.7464	6513.7700	70.7711
242	5756.5294	-379.1364	4623.1155	8237.1013	-2859.7083	5548.4048	28.2161
	5756.5294	-379.1364	4623.1155	8237.1013	-2859.7083	5548.4048	28.2161
243	18919.3086	-977.7600	3306.2197	19454.3054	-1512.7567	10483.5311	9.1917
	18919.3086	-977.7600	3306.2197	19454.3054	-1512.7567	10483.5311	9.1917
244	27153.4168	443.7936	1247.5312	27211.5609	385.6515	13412.9547	2.6624
	27153.4168	443.7936	1247.5312	27211.5609	385.6515	13412.9547	2.6624
245	-25084.9084	1985.4542	2952.2883	2303.6890	-25403.1433	13853.4161	83.6477
	-25084.9084	1985.4542	2952.2883	2303.6890	-25403.1433	13853.4161	83.6477
246	-21793.2524	-692.0553	3367.1556	-167.7784	-22317.5293	11074.8755	61.1499
	-21793.2524	-692.0553	3367.1556	-167.7784	-22317.5293	11074.8755	61.1499
247	480.9741	-349.4526	4166.8397	4253.2368	-4121.7152	4187.4760	42.1547
	480.9741	-349.4526	4166.8397	4253.2368	-4121.7152	4187.4760	42.1547
248	19134.9538	1341.8552	3746.8378	19891.7657	585.0432	9653.3612	11.4133
	19134.9538	1341.8552	3746.8378	19891.7657	585.0432	9653.3612	11.4133
249	30403.6998	393.0876	1305.4686	30460.3809	336.4064	15061.9872	2.4861
	30403.6998	393.0876	1305.4686	30460.3809	336.4064	15061.9872	2.4861
250	-36062.9651	1967.4811	2127.6461	2086.1441	-36181.6281	19133.8861	80.8078
	-36062.9651	1967.4811	2127.6461	2086.1441	-36181.6281	19133.8861	80.8078
251	-30376.8108	-4961.5803	3612.8033	-4457.9946	-30880.3966	13211.2010	82.0647
	-30376.8108	-4961.5803	3612.8033	-4457.9946	-30880.3966	13211.2010	82.0647
252	-8531.2784	-2819.7066	5237.4599	289.9495	-11640.9346	5965.4421	59.3009
	-8531.2784	-2819.7066	5237.4599	289.9495	-11640.9346	5965.4421	59.3009
253	11726.9221	3564.8521	5325.7143	14355.4385	936.3358	6709.5513	26.2667
	11726.9221	3564.8521	5325.7143	14355.4385	936.3358	6709.5513	26.2667
254	29588.8415	6106.4814	3891.0817	30216.8096	5478.5133	12369.1462	9.1077
	29588.8415	6106.4814	3891.0817	30216.8096	5478.5133	12369.1462	9.1077

APPENDIX C

DERIVATION OF THE REPLACEMENT MATRIX USED IN THE METHOD SUGGESTED BY TLUSTY

C. Stepwise Sub-dividing and Refining Method (Tlusty's Method)

The purpose of the problem of stepwise sub-dividing and refining of a structure with loading concentrated on a small part of the outer boundary is to investigate stresses in greater detail in the vicinity of the concentrated load.

In this method, if there is a structure "A and B", Figure 47, where B is the part in which all external loads are applied and which has to be subsequently refined in mesh. Such a structure is sought which would replace A by giving the same relationship between displacements and forces on boundary b but be much simplier. Actually the size of the stiffness matrix of this replacement structure would be 2n x 2n where n is the number of nodes on boundary b, irrespectively of the number of nodes of the original structure A.

As an example, in Figure 47 part A is originally represented by a 24 x 24 stiffness matrix. There are no external forces acting on internal nodal points of A; all external forces are concentrated on boundaries a and b. In addition to this simplifcation, boundary a is fixed.

It can be shown that under these conditions part A can be replaced by another structure A* with a stiffness matrix 8 x 8 only.

The stiffness matrix K_A of the original A structure may be partitioned:

$$\underset{24x24}{\begin{bmatrix} K_A \end{bmatrix}} \cdot \underset{24.1}{\begin{Bmatrix} \delta_{int} \\ \hline \delta_b \end{Bmatrix}} = \underset{24.1}{\begin{Bmatrix} 0 \\ \hline F_b \end{Bmatrix}} \qquad \text{(C-1)}$$

$$\begin{bmatrix} \underset{16x16}{P} & \underset{16x8}{Q} \\ \hline \underset{8x16}{R} & \underset{8x8}{S} \end{bmatrix} \begin{Bmatrix} \delta_{int} \\ \hline \delta_b \end{Bmatrix} = \begin{Bmatrix} 0 \\ \hline F_b \end{Bmatrix} \qquad \text{(C-2)}$$

From (C-2)

$$[P]\{\delta_{int}\} + [Q]\{\delta_b\} = 0 \qquad \text{(C-3)}$$

and

$$[R]\{\delta_{int}\} + [S]\{\delta_b\} = \{F_b\} \qquad \text{(C-4)}$$

From (C-3) and (C-4)

$$[\delta_{int}] = -[P]^{-1}[Q]\{\delta_b\}$$

$$\therefore \quad \left[[S] - [R][P]^{-1}[Q]\right]\{\delta_b\} = \{F_b\} \qquad \text{(C-5)}$$

From (C-5) we can see that

$$[K_A^*] = \left[[S] - [R][P^{-1}][Q]\right] \qquad \text{(C-6)}$$

where K_A^* is the stiffness matrix of the replacement structure and it is 8 x 8.

So now the stiffness matrix of the total original structure (A+B) is replaced by a sum:

$$\left(\underset{8x8}{\left[K_A^* \right]} + \underset{16x16}{\left[K_B \right]} \right) \begin{Bmatrix} \delta_b \\ \hline \delta_c \end{Bmatrix} = \begin{Bmatrix} 0 \\ \hline F_c \end{Bmatrix} \qquad (C\text{-}7)$$

In the next step, area B may be covered by a finer mesh expressed by a corresponding stiffness matrix $K_B^{\#}$. Now,

1.) either $K_B^{\#}$ is arranged so that the points of the original boundary are partitioned:

$$\left[K_A^* \right] + \left[\begin{array}{c|c} & \\ \hline & K_B^{\#} \end{array} \right] \begin{Bmatrix} \delta_b \\ \hline \end{Bmatrix} \qquad (C\text{-}8)$$

2.) or the nodes of the original boundary b are interspersed in $K_B^{\#}$

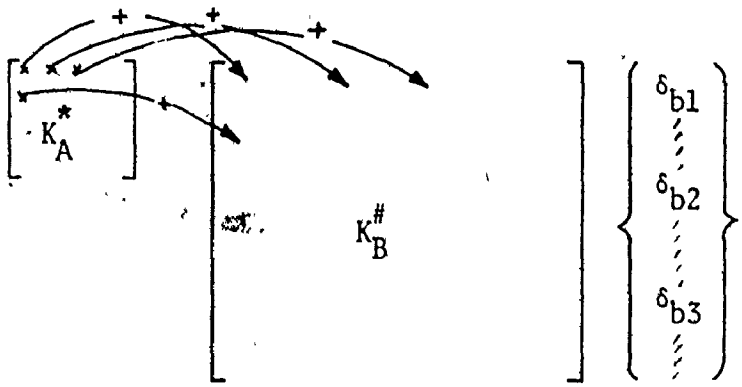

(C-9)

In both cases, the band width of $K_B^\#$ is increased, so generally boundaries b between the parts A and B of a structure would have more than 4 nodes. It will be necessary to do the refining of the mesh in steps in order to keep the band width of a reasonable size.

APPENDIX D

COMPUTER PROGRAM USED FOR CALCULATION OF THE REPLACEMENT MATRIX IN THE FIRST STEP

```
C     ************************************************************************
C     PLANE STRAIN FINITE ELEMENT PROGRAM BY MASOOD Z.
C     ************************************************************************
C
C     SMM IS THE TOTAL STIFFNESS MATRIX
C     BBA TWISE AREA OF ELEMENT
C     NI,NJ,NK NUMBER OF NODES OF ELEMENT IN ANTICLOCKWISE DIRECTION
C     E MODULUS OF ELASTICITY
C     U POSSION RATIO
C     UW SPECIFIC WEIGHT OF ELEMENT
C     ARRWT OWN WEIGHT OF ELEMENT
C     T IS ELEMENT STIFFNESS MATRIX
C     X,Y ARE COORDINATES OF NODES
C     NN NUMBER OF NODES
C     NE NUMBER OF ELEMENTS
C     NLC NUMBER OF LOAD CASES
C     NU NUMBER OF UNKNOWNS
C
      COMMON BBA(100),NI(96),NK(96),NJ(96),E(100),U(100)
     $,ARR(100),T(100,6,6),SMM(108,108),MP(100,6),X(65),Y(65)
      COMMON CC(100,100),N1(100)
      COMMON ND(65,2),FF(2),S(6,6),R(6,6),F(160),SB(6),FN(3),NPN(3),P(
     $100,6,6)
      WRITE(6,1)
    1 FORMAT(1H1,30X,*FINITE ELEMENT PROGRAM FOR SOLVING STRESSES ON
     $CARBIDE TOOL*,//)
      READ(5,3) NN,NE,NLC
      READ(5,3) NU
    3 FORMAT(3I6)
      WRITE(6,4)
    4 FORMAT(1X,4H NO.,4H  NI,4H  NJ,4H  NK,5H   XI,5H   XJ,5H   XK,
     15H   YI,5H   YJ,5H   YK,18H   CODE NUMBERS   ,6H  AREA,12H
     2   E,6H     U,6H  UNWT/)
      DO 19 I=1,NN
      READ(5,2)NM,ND(I,1),ND(I,2),X(I),Y(I)
    2 FORMAT(3I6,2F8.0)
   19 CONTINUE
      ARRT=0.0
      NB=0
C
      DO 11 J=1,NE
      READ(5,724)NI(J),NJ(J),NK(J),E(J),U(J)
  724 FORMAT(3I6,2F12.3)
```

```
C
CC      CALCULATION OF CODE NUMBERS
C
        MP(J,1)=ND(NI(J),1)
        MP(J,2)=ND(NJ(J),1)
        MP(J,3)=ND(NK(J),1)
        MP(J,4)=ND(NI(J),2)
        MP(J,5)=ND(NJ(J),2)
        MP(J,6)=ND(NK(J),2)
C
CC      CALCULATION OF BAND WIDTH
C
        MAX=0
        MIN=3000
        DO 27 II=1,6
        IF(MP(J,II).EQ.0) GO TO 27
        IF(MP(J,II)-MAX) 28,28,29
   29   MAX=MP(J,II)
   28   IF(MP(J,II)-MIN) 30,27,27
   30   MIN=MP(J,II)
   27   CONTINUE
        NB1=MAX-MIN
        IF(NB1.GT.NB) NB=NB1
        DO 15 II=1,6
        DO15 JJ=1,6
        P(J,II,JJ)=0.0
   15   CONTINUE
C
CC      CALCULATION OF ELEMENT STIFFNESS MATRIX
C
        XI=X(NI(J))
        XJ=X(NJ(J))
        XK=X(NK(J))
        YI=Y(NI(J))
        YJ=Y(NJ(J))
        YK=Y(NK(J))
        P(J,1,1)=XJ*YK-XK*YJ
        P(J,1,2)=XK*YI-XI*YK
        P(J,1,3)=XI*YJ-XJ*YI
        P(J,2,1)=YJ-YK
        P(J,2,2)=YK-YI
        P(J,2,3)=YI-YJ
        P(J,3,1)=XK-XJ
        P(J,3,2)=XI-XK
        P(J,3,3)=XJ-XI
        P(J,4,4)=P(J,1,1)
        P(J,4,5)=P(J,1,2)
        P(J,4,6)=P(J,1,3)
        P(J,5,4)=P(J,2,1)
        P(J,5,5)=P(J,2,2)
        P(J,5,6)=P(J,2,3)
        P(J,6,4)=P(J,3,1)
        P(J,6,5)=P(J,3,2)
        P(J,6,6)=P(J,3,3)
        BBA(J)=((XI-XJ)*(YI-YK)-(XI-XK)*(YI-YJ))
        ARR(J)=ABS(BBA(J)/2.)
        WRITE(6,31) J,NI(J),NJ(J),NK(J),XI,XJ,XK,YI,YJ,YK,(MP(J,I),I=1,6),
     $              ARR(J),E(J),U(J)
   31   FORMAT(1X,4I4,6F7.5,6I3,1F8.6,1E10.3,1F5.3)
   11   CONTINUE
```

```
      NB=NB+1
      WRITE(6,34)NN,NE,NB
   34 FORMAT(1H1,3X,14HNO OF NODES IS,I4,3X,17HNO OF ELEMENTS IS,I4,3X,:
     /18HHALF BAND WIDTH IS,I4/)
      NV=NB*NU
      DO 7 IG=1,NU
      F(IG)=0.0
    7 CONTINUE
      NB1=NB -1
      READ(5,3)MX,NX,LX
      DO 90 NIS=1,NLC
      DO 888 JJ=1,MX
      DO 888 II=1,MX
      SMM(JJ,II)=0.0
  888 CONTINUE
      DO 37 L=1,NE
      WRITE(6,681) L
  681 FORMAT(///,* STIFFNESS MATRIX FOR ELEMENT *,I6,//)
      DO 16 II=1,6
      DO 16 JJ=1,6
      S(II,JJ)=0.0
   16 CONTINUE
      EU=E(L)/((1.+U(L))*(1.-2.*U(L)))
      S(2,2)=EU*(1.-U(L))
      S(2,6)=EU*U(L)
      S(3,3)=EU*(1.-2.*U(L))/2.
      S(3,5)=S(3,3)
      S(5,3)=S(3,3)
      S(5,5)=S(3,3)
      S(6,2)=S(2,6)
      S(6,6)=S(2,2)
      DO 21 JA=1,6
      DO 21 IA=1,6
      R(JA,IA)=0.0
      DO 21 KK=1,6
      R(JA,IA)=R(JA,IA)+S(JA,KK)*P(L,KK,IA)
   21 CONTINUE
      DO 22 JJ=1,6
      DO 22 II=1,6
      T(L,JJ,II)=0.0
      DO 22 KK=1,6
      T(L,JJ,II)=T(L,JJ,II)+P(L,KK,JJ)*R(KK,II)/(4.*ARR(L))
   22 CONTINUE
      DO 641 JJ=1,6
      WRITE(6,642) (T(L,JJ,II) ,II=1,6)
  641 CONTINUE
  642 FORMAT(1X,6E10.2)
C     ****************************************************************
C
C     CALCULATION OF TOTAL STIFFNESS MATRIX
C
C     ****************************************************************
C
      DO 522 KK=1,6
      IF(MP(L,KK).EQ.0) GO TO 522
      IS=MP(L,KK)
      DO 523 KJ=1,6
      IF(MP(L,KJ).EQ.0) GO TO 523
      NS=MP(L,KJ)
```

```
      SMM(IS,NS)=SMM(IS,NS)+T(L,KK,KJ)
  523 CONTINUE
  522 CONTINUE
   37 CONTINUE
      WRITE(6,654)
  654 FORMAT(1H1)
   90 CONTINUE
      DO 201 I=1,NX
      DO 201 J=1,NX
      CC(I,J)=SMM(I,J)
  201 CONTINUE
      ZERO=1.E-06
      CALL INVMAT(CC,100,100,ZERO,IERR,N1)
      DO 261 I=1,NX
      DO 261 J=1,LX
      JJ=NX+J
      SMM(I,J)=0.0
      DO 261 K=1,NX
      SMM(I,J)=SMM(I,J)+SMM(JJ,K)*CC(K,I)
  261 CONTINUE
      DO 262 I=1,LX
      DO 262 J=1,LX
      JJ=NX+J
      CC(I,J)=CC(I,J)+SMM(I,K)*SMM(K,JJ)
  262 CONTINUE
      DO 263 I=1,LX
      II=I+NX
      DO 263 J=1,LX
      JJ=J+NX
      SMM(I,J)=SMM(II,JJ)-CC(I,J)
  263 CONTINUE
      DO 264 I=1,LX
      WRITE(6,650)(SMM(I,J),J=1,LX)
      WRITE(7,231)(SMM(I,J),J=1,LX)
  264 CONTINUE
  650 FORMAT(8(1X,E10.4),/)
  231 FORMAT(8E10.4)
  997 STOP
      END
*       6400 END OF RECORD
   61    92      1
  108
    1     0     00.0        0.0
    2     0     00.0        0.125
    3     0     00.0        0.25
    4     0     00.0        0.375
    5     0     00.0        0.5
    6     0     00.0        0.625
    7     0     00.0        0.75
    8     1     21.905      0.0
    9     3     41.75       0.0
   10     5     61.5        0.0
   11     7     81.25       0.0
   12     9    101.0        0.0
   13    11    120.75       0.0
   14    13    140.5        0.0
   15    15    160.25       0.0
   16    17    180.25       0.125
   17    19    200.25       0.25
   18    21    220.25       0.375
```

19	23	240.25	0.5
20	25	260.25	0.625
21	27	280.25	0.75
22	29	301.92	0.125
23	31	321.75	0.125
24	33	341.5	0.125
25	35	361.25	0.125
26	37	381.0	0.125
27	39	400.75	0.125
28	41	420.5	0.125
29	43	440.5	0.25
30	45	460.5	0.375
31	47	480.5	0.5
32	49	500.5	0.625
33	51	520.5	0.75
34	53	541.94	0.25
35	55	561.75	0.25
36	57	581.5	0.25
37	59	601.25	0.25
38	61	621.0	0.25
39	63	640.75	0.25
40	65	660.75	0.375
41	67	680.75	0.5
42	69	700.75	0.625
43	71	720.75	0.75
44	73	741.958	0.375
45	75	761.75	0.375
46	77	781.5	0.375
47	79	801.25	0.375
48	81	821.0	0.375
49	83	841.0	0.5
50	85	861.0	0.625
51	87	881.0	0.75
52	89	901.975	0.5
53	91	921.75	0.5
54	93	941.5	0.5
55	95	961.25	0.5
56	97	981.25	0.625
57	99	1001.25	0.75
58	101	1021.982	0.625
59	103	1041.75	0.625
60	105	1061.5	0.625
61	107	1081.5	0.75
1	15	2300000000.	0.3
2	15	1630000000.	0.3
2	16	330000000.	0.3
3	16	1730000000.	0.3
3	17	430000000.	0.3
4	17	1830000000.	0.3
4	18	530000000.	0.3
5	18	1930000000.	0.3
5	19	630000000.	0.3
6	19	2030000000.	0.3
6	20	730000000.	0.3
7	20	2130000000.	0.3
15	14	1630000000.	0.3
16	14	2830000000.	0.3
16	28	1730000000.	0.3
17	28	2930000000.	0.3
17	29	1830000000.	0.3

18	29	3030000000.	0.3
18	30	1930000000.	0.3
19	30	3130000000.	0.3
19	31	2030000000.	0.3
20	31	3230000000.	0.3
20	32	2130000000.	0.3
21	32	3330000000.	0.3
14	13	2830000000.	0.3
28	13	2730000000.	0.3
28	27	2930000000.	0.3
29	27	3930000000.	0.3
29	39	3030000000.	0.3
30	39	4030000000.	0.3
30	40	3130000000.	0.3
31	40	4130000000.	0.3
31	41	3230000000.	0.3
32	41	4230000000.	0.3
32	42	3330000000.	0.3
33	42	4330000000.	0.3
13	12	2730000000.	0.3
27	12	2630000000.	0.3
27	26	3930000000.	0.3
39	26	3830000000.	0.3
39	38	4030000000.	0.3
40	38	4830000000.	0.3
40	48	4130000000.	0.3
41	48	4930000000.	0.3
41	49	4230000000.	0.3
42	49	5030000000.	0.3
42	50	4330000000.	0.3
43	50	5130000000.	0.3
12	11	2630000000.	0.3
26	11	2530000000.	0.3
26	25	3830000000.	0.3
38	25	3730000000.	0.3
38	37	4830000000.	0.3
48	37	4730000000.	0.3
48	47	4930000000.	0.3
49	47	5530000000.	0.3
49	55	5030000000.	0.3
50	55	5630000000.	0.3
50	56	5130000000.	0.3
51	56	5730000000.	0.3
11	10	2530000000.	0.3
25	10	2430000000.	0.3
25	24	3730000000.	0.3
37	24	3630000000.	0.3
37	36	4730000000.	0.3
47	36	4630000000.	0.3
47	46	5530000000.	0.3
55	46	5430000000.	0.3
55	54	5630000000.	0.3
56	54	6030000000.	0.3
56	60	5730000000.	0.3
57	60	6130000000.	0.3
10	9	2430000000.	0.3
24	9	2330000000.	0.3
24	23	3630000000.	0.3
36	23	3530000000.	0.3
36	35	4630000000.	0.3

46	35	4530000000.	0.3
46	45	5430000000.	0.3
54	45	5330000000.	0.3
54	53	6030000000.	0.3
60	53	5930000000.	0.3
9	8	2330000000.	0.3
23	8	2230000000.	0.3
23	22	3530000000.	0.3
35	22	3430000000.	0.3
35	34	4530000000.	0.3
45	34	4430000000.	0.3
45	44	5330000000.	0.3
53	44	5230000000.	0.3
53	52	5930000000.	0.3
59	52	5830000000.	0.3
108	100	8	

CDTOT 376

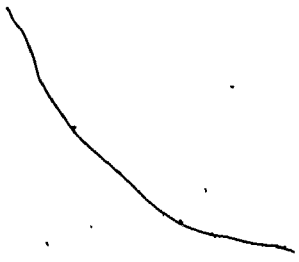

APPENDIX E

COMPUTER PROGRAM FOR THE CALCULATION OF THE STRESSES IN THE FIFTH STEP

```
C     ******************************************************************
C     PLANE STRAIN FINITE ELEMENT PROGRAM BY MASOOD Z.
C     ******************************************************************
C
C     SMM IS THE TOTAL STIFFNESS MATRIX
C     BBA TWISE AREA OF ELEMENT
C     NI,NJ,NK NUMBER OF NODES OF ELEMENT IN ANTICLOCKWISE DIRECTION
C     E MODULUS OF ELASTICITY
C     U POSSION RATIO
C     UW SPECIFIC WEIGHT OF ELEMENT
C     ARRWT OWN WEIGHT OF ELEMENT
C     T IS ELEMENT STIFFNESS MATRIX
C     X,Y ARE COORDINATES OF NODES
C     NN NUMBER OF NODES
C     NE NUMBER OF ELEMENTS
C     NLC NUMBER OF LOAD CASES
C     NU NUMBER OF UNKNOWNS
C
      COMMON SM(5500),BBA(88),NI(88),NJ(88),NK(88),E(88),U(88)
     $,ARR(88),T(88,6,6),SMM(120,120),MP(88,6),X(60),Y(60),EQUV(28,28)
      COMMON ND(60,2),FF(2),S(6,6),R(6,6),F(160),SB(6),FN(3),NPN(3),P(
     $88,6,6)
      WRITE(6,1)
    1 FORMAT(1H1,30X,'FINITE ELEMENT PROGRAM FOR SOLVING STRESSES ON
     $CARBIDE TOOL',//)
      READ(5,3) NN,NE,NLC
      READ(5,3) NU
    3 FORMAT(3I6)
      WRITE(6,4)
    4 FORMAT(1X,4H NO.,4H  NI,4H  NJ,4H  NK,5H   XI,5H   XJ,5H   XK,
     15H   YI,5H   YJ,5H   YK,18H   CODE NUMBERS   ,6H  AREA,12H
     2   E,6H     U,6H  UNWT/)
      DO 19 I=1,NN
      READ(5,2)NM,ND(I,1),ND(I,2),X(I),Y(I)
    2 FORMAT(3I6,2F8.0)
   19 CONTINUE
      ARRT=0.0
      NB=0
C
      DO 11 J=1,NE
      READ(5,724)NI(J),NJ(J),NK(J),E(J),U(J)
  724 FORMAT(3I6,2F12.0)
C
```

```
C     CALCULATION OF CODE NUMBERS
C
      MP(J,1)=ND(NI(J),1)
      MP(J,2)=ND(NJ(J),1)
      MP(J,3)=ND(NK(J),1)
      MP(J,4)=ND(NI(J),2)
      MP(J,5)=ND(NJ(J),2)
      MP(J,6)=ND(NK(J),2)
C
CCC   CALCULATION OF BAND WIDTH
C
      MAX=0
      MIN=3000
      DO 27 II=1,6
      IF(MP(J,II).EQ.0) GO TO 27
      IF(MP(J,II)-MAX) 28,28,29
   29 MAX=MP(J,II)
   28 IF(MP(J,II)-MIN) 30,27,27
   30 MIN=MP(J,II)
   27 CONTINUE
      NB1=MAX-MIN
      IF(NB1.GT.NB) NB=NB1
      DO 15 II=1,6
      DO15 JJ=1,6
      P(J,II,JJ)=0.0
   15 CONTINUE
C
CCC   CALCULATION OF ELEMENT STIFFNESS MATRIX
C
      XI=X(NI(J))
      XJ=X(NJ(J))
      XK=X(NK(J))
      YI=Y(NI(J))
      YJ=Y(NJ(J))
      YK=Y(NK(J))
      P(J,1,1)=XJ*YK-XK*YJ
      P(J,1,2)=XK*YI-XI*YK
      P(J,1,3)=XI*YJ-XJ*YI
      P(J,2,1)=YJ-YK
      P(J,2,2)=YK-YI
      P(J,2,3)=YI-YJ
      P(J,3,1)=XK-XJ
      P(J,3,2)=XI-XK
      P(J,3,3)=XJ-XI
      P(J,4,4)=P(J,1,1)
       P(J,4,5)=P(J,1,2)
      P(J,4,6)=P(J,1,3)
      P(J,5,4)=P(J,2,1)
      P(J,5,5)=P(J,2,2)
      P(J,5,6)=P(J,2,3)
      P(J,6,4)=P(J,3,1)
      P(J,6,5)=P(J,3,2)
      P(J,6,6)=P(J,3,3)
      BBA(J)=((XI-XJ)*(YI-YK)-(XI-XK)*(YI-YJ))
      ARR(J)=ABS(BBA(J)/2.)
      WRITE(6,31)J,NI(J),NJ(J),NK(J),XI,XJ,XK,YI,YJ,YK,(MP(J,I),I=1,6),
     $           ARR(J),E(J),U(J)
   31 FORMAT(1X,4I4,6F7.5,6I3,1F8.6,1E10.3,1F6.3)
   11 END
```

```
      WRITE(6,34)NN,NE,NB
   34 FORMAT(1H1,3X,14HNO OF NODES IS,I4,3X,17HNO OF ELEMENTS IS,I4,3X,1
     18HHALF BAND WIDTH IS,I4/)
      NV=NB*NU
      DO 7 IG=1,NU
      F(IG)=0.0
    7 CONTINUE
      NB1=NB -1
      DO 90 NIS=1,NLC
      DO 888 JJ=1,120
      DO 888 II=1,120
      SMM(JJ,II)=0.0
  888 CONTINUE
      DO 37 L=1,NE
      WRITE(6,661) L
  661 FORMAT(///,* STIFFNESS MATRIX FOR ELEMENT *,I6,//)
      DO 16 II=1,6
      DO 16 JJ=1,6
      S(II,JJ)=0.0
   16 CONTINUE
      EU=E(L)/((1.+U(L))*(1.-2.*U(L)))
      S(2,2)=EU*(1.-U(L))
      S(2,6)=EU*U(L)
      S(3,3)=EU*(1.-2.*U(L))/2.
      S(3,5)=S(3,3)
      S(5,3)=S(3,3)
      S(5,5)=S(3,3)
      S(6,2)=S(2,6)
      S(6,6)=S(2,2)
      DO 21 JA=1,6
      DO 21 IA=1,6
      R(JA,IA)=0.0
      DO 21 KK=1,6
      R(JA,IA)=R(JA,IA)+S(JA,KK)*P(L,KK,IA)
   21 CONTINUE
      DO 22 JJ=1,6
      DO 22 II=1,6
      T(L,JJ,II)=0.0
      DO 22 KK=1,6
      T(L,JJ,II)=T(L,JJ,II)+P(L,KK,JJ)*R(KK,II)/(4.*ARR(L))
   22 CONTINUE
      DO 641 JJ=1,6
      WRITE(6,642) (T(L,JJ,II) ,II=1,6)
  641 CONTINUE
  642 FORMAT(1X,6E10.2)
C     ******************************************************************
C
C     CALCULATION OF TOTAL STIFFNESS MATRIX
C
C     ******************************************************************
      DO 522 KK=1,6
      IF(MP(L,KK).EQ.0) GO TO 522
      IS=MP(L,KK)
      DO 523 KJ=1,6
      IF(MP(L,KJ).EQ.0) GO TO 523
      NS=MP(L,KJ)
      SMM(IS,NS)=SMM(IS,NS)+T(L,KK,KJ)
  523 CONTINUE
```

```
  522 CONTINUE
   37 CONTINUE
      DO 271 I=1,28
      READ(5,272)(EQUV(I,J),J=1,28)
  271 CONTINUE
  272 FORMAT(8E10.4)
      DO 273 I=1,28
      DO 273 J=1,28
      SMM(I,J)=SMM(I,J)+EQUV(I,J)
  273 CONTINUE
      WRITE(6,654)
  654 FORMAT(1H1)
      DO 36 KK=1,5000
      SM(KK)=0.0
   36 CONTINUE
      NBB=NB
      DO 5555 I=1,NU
      DO 5556 J=I,NBB
      IF(I-1) 151,151,152
  152 NA =I-1
      K= NA*NB+J-NA
      GO TO 153
  151 K=J
  153 SM(K)= SMM(J,I)
 5556 CONTINUE
      NBB= NBB+1
 5555 CONTINUE
      WRITE(6,92)NIS
   92 FORMAT(1X,30HNODAL LOADS FOR LOAD CASE  NO.,I4//1X,30HNODE NO.
     $X FORCE      Y FORCE/)
      READ(5,3)NNL
      DO 47 J=1,NNL
      READ(5,48)JNU,FF(1),FF(2)
      DO 50 L=1,2
      IF(ND(JNU,L).EQ.0) GO TO 50
      IK=ND(JNU,L)
      F(IK)=F(IK)+FF(L)
   50 CONTINUE
   47 CONTINUE
      DO 93 II=1,NN
      IF(ND(II,1).NE.0) GO TO 94
      FX=0.0
      GO TO 95
   94 IK=ND(II,1)
      FX=F(IK)
   95 CONTINUE
      IF(NDII,2))NE)0) GO TO 96
      FY=0.0
      GO TO 97
   96 IK=ND(II,2)
      FY=F(IK)
   97 CONTINUE
      WRITE(6,98)II,FX,FY
   98 FORMAT(1X,1I6,2F11.1)
   93 CONTINUE
C
CC    CALCULATION OF DISPLACEMENT
C
      DET=1.E-8
      CALL BAND(SM,F,NU,NB,1,DET)
```

```
      IF(DET)56,57,58
   56 WRITE(6,59)DET
   59 FORMAT(1X,34HMATRIX SM IS NOT POSITIVE-DEFINITE/6H DET= ,E15.7)
      GO TO 997
   57 WRITE(6,60)DET
   60 FORMAT(1X,19HDETERMINANT IS ZERO/6H DET= ,E15.7)
      GO TO 997
   58 CONTINUE
      DO 3336 KKL=1,5000
      SM(KKL)=0.0
 3336 CONTINUE
      WRITE(6,121)NIS
  121 FORMAT(1H1,1X,38HNODAL DISPLACEMENTS FOR LOAD CASE  NO.,I4//1X,40
     $HNODE NO.     X DEFLECTION     Y DEFLECTION/)
      DO 61 K=1,NN
      IF(ND(K,1).NE.0) GO TO 62
      DX=0.0
      GO TO 63
   62 IK=ND(K,1)
      DX=F(IK)
   63 CONTINUE
      IF(ND(K,2).NE.0) GO TO 64
      DY=0.0
      GO TO 67
   64 IK=ND(K,2)
      DY=F(IK)
   67 SM(K)=DX
      SM(K+500)=DY
      WRITE(6,65)K,DX,DY
   65 FORMAT(1X,1I8,2(1PE16.5))
   61 CONTINUE
C
CC    CALCULATION OF STRAINS AND STRESS FOR ELEMENTS
C
      WRITE(6,132)NIS
  132 FORMAT(1H1,1X,47HELEMENT STRAINS AND STRESSES FOR LOAD CADE NO.,I4
     1//)
      WRITE(6,777)
  777 FORMAT(1X,3HNO.,4X,8HX STRAIN,4X,8HY STRAIN,3X,9HXY STRAIN,8X,8HX
     1STRESS,8X,8HY STRESS,7X,9HXY STRESS/)
      DO 68 L=1,NE
      DO 69 JJ=1,6
      SB(JJ)=0.0
      LL=MP(L,JJ)
      IF(LL.EQ.0) GO TO 69
      SB(JJ)=F(LL)
   69 CONTINUE
      RS=(SB(1)*P(L,2,1)+SB(2)*P(L,2,2)+SB(3)*P(L,2,3))/BBA(L)
      SHS=(SB(1)*P(L,3,1)+SB(2)*P(L,3,2)+SB(3)*P(L,3,3)+SB(4)*P(L,2,1)+
     $     SB(5)*P(L,2,2)+SB(6)*P(L,2,3))/BBA(L)
      VS=(SB(4)*P(L,3,1)+SB(5)*P(L,3,2)+SB(6)*P(L,3,3))/BBA(L)
      EU=E(L)/((1.+U(L))*(1.-2.*U(L)))
      SIGR=EU*((1.-U(L))*RS+U(L)*VS)
      SIGS=EU*(((1.-2.*U(L))/2.)*SHS)
      SIGV=EU*(U(L)*RS+(1.-U(L))*VS)
      WRITE(6,81)  L,RS,VS,SHS,SIGR   ,SIGV   ,SIGS
   81 FORMAT(1X,I3,3E12.3,3E16.6)
C
CCC   CALCULATION OF STRESS AT NODES
C
```

```
      NPN(1)=NI(L)
      NPN(2)=NJ(L)
      NPN(3)=NK(L)
      FN(1)=SIGR
      FN(2)=SIGV
      FN(3)=SIGS
      DO 75 NMM=1,3
      IEC=10*NPN(NMM)-9+1000
      SM(IEC)=SM(IEC)+1.
      DO 75 MNN=1,3
      ICC=IEC+MNN
      SM(ICC)=SM(ICC)+FN(MNN)
   75 CONTINUE
   68 CONTINUE
      WRITE(6,144) NIS
  144 FORMAT(1H1,1X,33HNODAL STRESSES FOR LOAD CASE  NO.,I4//)
      WRITE(6,1442)
     $11HMAX. STRESS,5X,11HMIN. STRESS,2X,14HMAX.S. STRESS,8X,4HDIR.//)
 1442 FORMAT(1X,3HNO.,8X,8HX STRESS,8X,8HY STRESS,7X,9HXY STRESS,5X,
      DO 76 KKZ=1,NN
      IOC=10*KKZ-9+1000
      SIGNR=SM(IOC+1)/SM(IOC)
      SIGNV=SM(IOC+2)/SM(IOC)
      SIGNS=SM(IOC+3)/SM(IOC)
      STMAX=.5*((SIGNR+SIGNV)+SQRT((SIGNR-SIGNV)**2+4.*SIGNS**2))
      STMIN=.5*((SIGNR+SIGNV)-SQRT((SIGNR-SIGNV)**2+4.*SIGNS**2))
      SSMN=.5*(STMAX-STMIN)
      RESN=ABS(STMAX-STMIN)
      IF(RESN.GT.0.001) GO TO 141
      DIRRN=999.
      GO TO 142
  141 DIRN=ATAN2(2.*SIGNS,SIGNR-SIGNV)
      DIRRN=(.5/.0174533)*DIRN
  142 WRITE(6,83)KKZ,SIGNR,SIGNV,SIGNS,STMAX,STMIN,SSMN,DIRRN
      WRITE(7,84)STMAX
      WRITE(7,84)STMIN
      WRITE(7,84)SSMN
   84 FORMAT(E16.6)
   83 FORMAT(1X,I3,7E16.6)
   48 FORMAT(I6,2F10.0)
   76 CONTINUE
   90 CONTINUE
  997 STOP
      END
      SUBROUTINE BAND(A,B,N,M,LT,DET)                                   BNDF0010
      DIMENSION A(1),B(1)                                               BNDF0020
      MM=M-1                                                            BNDF0030
      NM=N*M                                                            BNDF0040
      NM1=NM-MM                                                         BNDF0050
      IF (LT.NE.1) GO TO 55                                             BNDF0060
      MP=M+1                                                            BNDF0070
      KK=2                                                              BNDF0080
      FAC=DET                                                           BNDF0090
      A(1)=1./SQRT(A(1))                                                BNDF0100
      BIGL=A(1)                                                         BNDF0110
      SML=A(1)                                                          BNDF0120
      A(2)=A(2)*A(1)                                                    BNDF0130
      A(MP)=1./SQRT(A(MP)-A(2)*A(2))                                    BNDF0140
      IF(A(MP).GT.BIGL)BIGL=A(MP)                                       BNDF0150
      IF(A(MP).LT.SML)SML=A(MP)                                         BNDF0160
```

```
      MP=MP+M                                                          BNDF0170
      DO 62 J=MP,NM1,M                                                 BNDF0180
      JP=J-MM                                                          BNDF0190
      MZC=0                                                            BNDF0200
      IF(KK.GE.M) GO TO 1                                              BNDF0210
      KK=KK+1                                                          BNDF0220
      II=1                                                             BNDF0230
      JC=1                                                             BNDF0240
      GO TO 2                                                          BNDF0250
1     KK=KK+M                                                          BNDF0260
      II=KK-MM                                                         BNDF0270
      JC=KK-MM                                                         BNDF0280
2     DO 65 I=KK,JP,MM                                                 BNDF0290
      IF(A(I).EQ.0.)GO TO 64                                           BNDF0300
      GO TO 66                                                         BNDF0310
64    JC=JC+M                                                          BNDF0320
65    MZC=MZC+1                                                        BNDF0330
      ASUM1=0.                                                         BNDF0340
      GO TO 61                                                         BNDF0350
66    MMZC=MM*MZC                                                      BNDF0360
      II=II+MZC                                                        BNDF0370
      KM=KK+MMZC                                                       BNDF0380
      A(KM)=A(KM)*A(JC)                                                BNDF0390
      IF(KM.GE.JP)GO TO 6                                              BNDF0400
      KJ=KM+MM                                                         BNDF0410
      DO 5 I=KJ,JP,MM                                                  BNDF0420
      ASUM2=0.                                                         BNDF0430
      IM=I-MM                                                          BNDF0440
      II=II+1                                                          BNDF0450
      KI=II+MMZC                                                       BNDF0460
      DO 7 K=KM,IM,MM                                                  BNDF0470
      ASUM2=ASUM2+A(KI)*A(K)                                           BNDF0480
7     KI=KI+MM                                                         BNDF0490
5     A(I)=(A(I)-ASUM2)*A(KI)                                          BNDF0500
6     CONTINUE                                                         BNDF0510
      ASUM1=0.                                                         BNDF0520
      DO 4 K=KM,JP,MM                                                  BNDF0530
4     ASUM1=ASUM1+A(K)*A(K)                                            BNDF0540
61    S=A(J)-ASUM1                                                     BNDF0550
      IF(S.LT.0.)DET=S                                                 BNDF0560
      IF(S.EQ.0.)DET=0.                                                BNDF0570
      IF(S.GT.0.)GO TO 63                                              BNDF0580
      NROW=(J+MM)/M                                                    BNDF0590
      WRITE(6,99) NROW                                                 BNDF0600
99    FORMAT(35H0ERROR CONDITION ENCOJNTERED IN ROW,I6)                BNDF0610
      RETURN                                                           BNDF0620
   63 A(J)=1./SQRT(S)                                                  BNDF0630
      IF(A(J).GT.BIGL)BIGL=A(J)                                        BNDF3640
      IF(A(J).LT.SML)SML=A(J)                                          BNDF0650
   62 CONTINUE                                                         BNDF0660
      IF(SML.LE.FAC*BIGL) GO TO 54                                     BNDF0670
      GO TO 53                                                         BNDF0680
   54 DET=0.                                                           BNDF0690
      RETURN                                                           BNDF0700
   53 DET=SML/BIGL                                                     BNDF0710
   55 B(1)=B(1)*A(1)                                                   BNDF0720
      KK=1                                                             BNDF0730
      K1=1                                                             BNDF0740
      J=1                                                              BNDF0750
      DO 8 L=2,N                                                       BNDF0760
```

```
      BSUM1=0.                                                          BNDF0770
      LM=L-1                                                            BNDF0780
      J=J+M                                                             BNDF0790
      IF(KK.GE.M) GO TO 12                                              BNDF0800
      KK=KK+1                                                           BNDF0810
      GO TO 13                                                          BNDF0820
   12 KK=KK+M                                                           BNDF0830
      K1=K1+1                                                           BNDF0840
   13 JK=KK                                                             BNDF0850
      DO 9 K=K1,LM                                                      BNDF0860
      BSUM1=BSUM1+A(JK)*B(K)                                            BNDF0870
      JK=JK+MM                                                          BNDF0880
    9 CONTINUE                                                          BNDF0890
    8 B(L)=(B(L)-BSUM1)*A(J)                                            BNDF0900
      B(N)=B(N)*A(NM1)                                                  BNDF0910
      NMM=NM1                                                           BNDF0920
      NN=N-1                                                            BNDF0930
      ND=N                                                              BNDF0940
      DO 10 L=1,NN                                                      BNDF0950
      BSUM2=0.                                                          BNDF0960
      NL=N-L                                                            BNDF0970
      NL1=N-L+1                                                         BNDF0980
      NMM=NMM-M                                                         BNDF0990
      NJ1=NMM                                                           BNDF1000
      IF(L.GE.M) ND=ND-1                                                BNDF1010
      DO 11 K=NL1,ND                                                    BNDF1020
      NJ1=NJ1+1                                                         BNDF1030
      BSUM2=BSUM2+A(NJ1)*B(K)                                           BNDF1040
   11 CONTINUE                                                          BNDF1050
   10 B(NL)=(B(NL)-BSUM2)*A(NMM)                                        BNDF1060
      RETURN                                                            BNDF1070
      END                                                               BNDF1080
*       6400 END OF RECORD
   60    88      1
  120
    1     1       2.04468   .0
    2     3       4.04297   .0
    3     5       6.03906   .0
    4     7       8.03515   .0
    5     9      10.03124   .0
    6    11      12.02733   .0
    7    13      14.02343   .0
    8    15      16.01951   .0
    9    17      18.01562   .0
   10    19      20.011715  .0
   11    21      22.00781   .0
   12    23      24.00391   .0
   13    25      26.00391   .00781
   14    27      28.00391   .01562
   15    29      30.00391   .00391
   16    31      32.00391   .011715
   17    33      34.00781   .00391
   18    35      36.04523   .00391
   19    37      38.04297   .00391
   20    39      40.03906   .00391
   21    41      42.03515   .00391
   22    43      44.03124   .00391
   23    45      46.02733   .00391
   24    47      48.02343   .00391
   25    49      50.01951   .00391
```

26	51	52.01562	.00391
27	53	54.011715	.00391
28	55	56.00781	.00781
29	57	58.00781	.011715
30	59	60.00781	.01562
31	61	62.011715	.00781
32	63	64.011715	.011715
33	65	66.04578	.00781
34	67	68.04297	.00781
35	69	70.03906	.00781
36	71	72.03515	.00781
37	73	74.03124	.00781
38	75	76.02733	.00781
39	77	78.02343	.00781
40	79	80.01951	.00781
41	81	82.01562	.00781
42	83	84.01562	.011715
43	85	86.011715	.01562
44	87	88.01562	.01562
45	89	90.01951	.011715
46	91	92.04633	.011715
47	93	94.04297	.011715
48	95	96.03906	.011715
49	97	98.03515	.011715
50	99	100.03124	.011715
51	101	102.02733	.011715
52	103	104.02343	.011715
53	105	106.01951	.01562
54	107	108.02343	.01562
55	109	110.02733	.01562
56	111	112.03124	.01562
57	113	114.03515	.01562
58	115	116.03906	.01562
59	117	118.04297	.01562
60	119	120.04688	.01562
12	11	1575000000.	.283
15	11	1775000000.	.283
15	17	1375000000.	.283
13	17	2875000000.	.283
13	28	1675000000.	.283
16	28	2975000000.	.283
16	29	1475000000.	.283
14	29	3075000000.	.283
11	10	1775000000.	.283
17	10	2775000000.	.283
17	27	2875000000.	.283
28	27	3175000000.	.283
28	31	2975000000.	.283
29	31	3275000000.	.283
29	32	3075000000.	.283
30	32	4375000000.	.283
10	9	2775000000.	.283
27	9	2675000000.	.283
27	26	3175000000.	.283
31	26	4175000000.	.283
31	41	3275000000.	.283
32	41	4275000000.	.283
32	42	4375000000.	.283
43	42	4475000000.	.283
9	8	2675000000.	.283

26	8	2575000000.	.283
26	25	4175000000.	.283
41	25	4075000000.	.283
41	40	4275000000.	.283
42	40	4575000000.	.283
42	45	4475000000.	.283
44	45	5375000000.	.283
8	7	2575000000.	.283
25	7	2475000000.	.283
25	24	4075000000.	.283
40	24	3975000000.	.283
40	39	4575000000.	.283
45	39	5275000000.	.283
45	52	5375000000.	.283
53	52	5475000000.	.283
7	6	2475000000.	.283
24	6	2375000000.	.283
24	23	3975000000.	.283
39	23	3875000000.	.283
39	38	5275000000.	.283
52	38	5175000000.	.283
52	51	5475000000.	.283
54	51	5575000000.	.283
6	5	2375000000.	.283
23	5	2275000000.	.283
23	22	3875000000.	.283
38	22	3775000000.	.283
38	37	5175000000.	.283
51	37	5075000000.	.283
51	50	5575000000.	.283
55	50	5675000000.	.283
5	4	2275000000.	.283
22	4	2175000000.	.283
22	21	3775000000.	.283
37	21	3675000000.	.283
37	36	5075000000.	.283
50	36	4975000000.	.283
50	49	5675000000.	.283
56	49	5775000000.	.283
4	3	2175000000.	.283
21	3	2075000000.	.283
21	20	3675000000.	.283
36	20	3575000000.	.283
36	35	4975000000.	.283
49	35	4875000000.	.283
49	48	5775000000.	.283
57	48	5875000000.	.283
3	2	2075000000.	.283
20	2	1975000000.	.283
20	19	3575000000.	.283
35	19	3475000000.	.283
35	34	4875000000.	.283
48	34	4775000000.	.283
48	47	5875000000.	.283
58	47	5975000000.	.283
2	1	1975000000.	.283
19	1	1875000000.	.283
19	18	3475000000.	.283
34	18	3375000000.	.283
34	33	4775000000.	.283

```
    47     33     4675000000.     .283
    47     46     5975000000.     .283
    47     46     6075000000.     .283
 .2086E+09 .1143E+08-.2279E+09 .7631E+07-.8140E-09-.1032E-09-.2002E-09-.2046E-10
-.4603E-10 .2697E-12-.2465E-10 .1533E-10-.1333E-10 .1833E-10-.1136E-10 .1959E-10
-.1136E-07 .1365E-08-.8003E-08-.6663E-10-.5522E-08-.3299E-09-.3920E-08-.3217E-09
-.1955E-08-.2007E-09-.1288E-08-.1372E-09
 .1143E+08 .7035E+08 .3186E+07-.6689E+08-.1247E-09-.1561E-10-.3066E-10-.3133E-11
-.7045E-11 .4142E-13-.3775E-11 .2348E-11-.2041E-11 .2807E-11-.1739E-11 .3000E-11
 .1488E-08-.6956E-08 .5027E-09-.1928E-08 .7808E-10-.5236E-09-.2008E-09-.1243E-09
-.3155E-09-.1126E-10-.2042E-09-.1635E-10
-.2279E+09 .3186E+07 .3347E+09 .1143E+08-.9645E+08-.1461E+08-.4060E-09-.4149E-10
-.9334E-10 .5491E-12-.4999E-10 .3110E-10-.2703E-10 .3717E-10-.2304E-10 .3973E-10
-.2889E-08-.4033E-09-.2987E-08-.1874E-09-.3527E-08-.7539E-10-.4622E-08 .1069E-09
-.4255E-08-.5715E-10-.2737E-08-.1946E-09
 .7631E+07-.6689E+08 .1143E+08 .1305E+09-.1906E+08-.2919E+08-.6889E-10-.7022E-11
-.1584E-10 .8669E-13-.8479E-11 .5261E-11-.4575E-11 .6286E-11-.3889E-11 .6716E-11
-.2899E-09 .1519E-10-.2027E-09-.8409E-10-.1168E-09-.3086E-09 .7004E-10-.1082E-08
 .1591E-09-.1066E-08-.8671E-10-.2857E-09
-.6140E-09-.1247E-09-.9645E+08-.1906E+08 .2075E+09 .3367E+08-.9645E+08-.1461E+08
-.3009E-09 .2650E-11-.1617E-09 .1024E-09-.8874E-10 .1228E-09-.7694E-10 .1318E-09
-.8054E-09-.1058E-09-.8211E-09-.6009E-10-.9550E-09-.5714E-10-.1225E-08-.1013E-09
-.2621E-08-.5074E-10-.3992E-08 .1433E-09
-.1032E-09-.1561E-10-.1461E+08-.2919E+08 .3367E+08 .1067E+09-.1906E+08-.2919E+08
-.6090E-10-.1813E-11-.3119E-10 .1496E-10-.1366E-10 .1679E-10-.8412E-11 .1676E-10
-.1020E-09-.1326E-10-.1039E-09-.7785E-11-.1204E-09-.8027E-11-.1538E-09-.1569E-10
-.9747E-10-.2755E-09 .1027E-09-.9919E-09
-.2002E-09-.3066E-10-.4060E-09-.6889E-10-.9645E+08-.1906E+08 .2075E+09 .3367E+08
-.9645E+08-.1461E+08-.8418E-09 .5390E-09-.4550E-09 .6482E-09-.3726E-09 .6855E-09
-.1981E-09-.2600E-10-.2019E-09-.1480E-10-.2348E-09-.1415E-10-.3010E-09-.2526E-10
-.6163E-09-.4506E-10-.9083E-09-.8704E-10
-.2046E-10-.3133E-11-.4149E-10-.7022E-11-.1461E+08-.2919E+08 .3367E+08 .1067E+09
-.1906E+08-.2919E+08 .2242E-09-.4321E-09 .2619E-09-.5572E-09 .3360E-09-.5238E-09
-.2024E-10-.2657E-11-.2063E-10-.1512E-11-.2399E-10-.1445E-11-.3076E-10-.2576E-11
-.6337E-10-.4153E-11-.9383E-10-.7201E-11
-.4603E-10-.7048E-11-.9334E-10-.1584E-10-.3009E-09-.6090E-10-.9645E+08-.1906E+08
 .2075E+09 .3367E+08-.9645E+08-.1461E+08-.4734E-09 .5277E-10-.1629E-09 .8047E-11
-.4554E-10-.5978E-11-.4642E-10-.3403E-11-.5398E-10-.3253E-11-.6921E-10-.5807E-11
-.1417E-09-.1039E-10-.2087E-09-.2014E-10
 .2697E-12 .4142E-13 .5491E-12 .8669E-13 .2650E-11-.1813E-11-.1461E+08-.2919E+08
 .3367E+08 .1067E+09-.1906E+08-.2919E+08-.1119E-09-.2155E-08-.1648E-10-.1988E-08
 .2669E-12 .3512E-13 .2722E-12 .1984E-13 .3167E-12 .1859E-13 .4064E-12 .3232E-13
 .9710E-12-.1006E-12 .1588E-11-.4882E-12
-.2465E-10-.3775E-11-.4999E-10-.8479E-11-.1617E-09-.3119E-10-.8418E-09 .2242E-09
-.9645E+08-.1906E+08 .2075E+09 .3367E+08-.9645E+08-.1461E+08-.1050E-08 .5193E-09
-.2439E-10-.3201E-11-.2486E-10-.1822E-11-.2891E-10-.1742E-11-.3707E-10-.3109E-11
-.7596E-10-.5461E-11-.1120E-09-.1039E-10
 .1533E-10 .2348E-11 .3110E-10 .5261E-11 .1024E-09 .1496E-10 .5390E-09-.4321E-09
-.1461E+08-.2919E+08 .3367E+08 .1067E+09-.1906E+08-.2919E+08-.1581E-11-.5388E-08
 .1517E-10 .1991E-11 .1546E-10 .1133E-11 .1798E-10 .1083E-11 .2306E-10 .1930E-11
 .4754E-10 .3066E-11 .7043E-10 .5220E-11
-.1333E-10-.2041E-11-.2703E-10-.4575E-11-.8874E-10-.1366E-10-.4550E-09 .2619E-09
-.4734E-09-.1119E-09-.9645E+08-.1906E+08 .2075E+09 .3367E+08-.9645E+08-.1461E+08
-.1319E-10-.1731E-11-.1344E-10-.9851E-12-.1563E-10-.9411E-12-.2004E-10-.1678E-11
-.4127E-10-.2714E-11-.6110E-10-.4722E-11
 .1833E-10 .2807E-11 .3717E-10 .6286E-11 .1228E-09 .1679E-10 .6482E-09-.5572E-09
 .5277E-10-.2155E-08-.1461E+08-.2919E+08 .3367E+08 .1067E+09-.1906E+08-.2919E+08
 .1813E-10 .2380E-11 .1848E-10 .1355E-11 .2150E-10 .1294E-11 .2756E-10 .2306E-11
 .5689E-10 .3583E-11 .8436E-10 .5935E-11
-.1136E-10-.1739E-11-.2304E-10-.3889E-11-.7694E-10-.8412E-11-.3726E-09 .3360E-09
```

```
-.1629E-09-.1648E-10-.1050E-08-.1581E-11-.9645E+08-.1906E+08 .2075E+09 .3367E+08
-.3645E+08-.1461E+08-.1145E-10-.8393E-12-.1332E-10-.8013E-12-.1708E-10-.1428E-11
-.3538E-10-.2072E-11-.5261E-10-.3121E-11
 .1959E-10 .3000E-11 .3973E-10 .6716E-11 .1318E-09 .1676E-10 .6855E-09-.6238E-09
 .8047E-11-.1988E-08 .5193E-09-.5388E-08-.1461E+08-.2919E+08 .3367E+08 .1067E+09
-.1906E+08-.2919E+08 .1976E-10 .1448E-11 .2298E-10 .1383E-11 .2946E-10 .2464E-11
 .6089E-10 .3742E-11 .9038E-10 .6013E-11
-.1186E-07 .1488E-08-.2889E-08-.2899E-09-.8054E-09-.1020E-09-.1981E-09-.2024E-10
-.4554E-10 .2669E-12-.2439E-10 .1517E-10-.1319E-10 .1813E-10-.9645E+08-.1906E+08
 .2075E+09 .3367E+08-.9645E+08-.1461E+08-.5798E-08-.3499E-09-.4034E-08-.3331E-09
-.1936E-08-.1958E-09-.1275E-08-.1351E-09
 .1365E-08-.6956E-08-.4033E-09 .1519E-10-.1058E-09-.1326E-10-.2600E-10-.2657E-11
-.5978E-11 .3512E-13-.3201E-11 .1991E-11-.1731E-11 .2380E-11-.1461E+08-.2919E+08
 .3367E+08 .1067E+09-.1905E+08-.2919E+08-.2575E-10-.7501E-09-.2198E-09-.1915E-09
-.2660E-09-.1149E-10-.1725E-09-.1433E-10
-.8063E-08 .5027E-09-.2987E-08-.2027E-09-.8211E-09-.1038E-09-.2019E-09-.2063E-10
-.4642E-10 .2722E-12-.2486E-10 .1546E-10-.1344E-10 .1848E-10-.1145E-10 .1976E-10
-.9645E+08-.1906E+08 .2069E+09 .3367E+08-.9572E+08-.1461E+08-.5222E-08-.3203E-09
-.1994E-08-.1748E-09-.1309E-08-.1318E-09
-.6663E-10-.1928E-08-.1874E-09-.8409E-10-.6009E-10-.7785E-11-.1480E-10-.1512E-11
-.3403E-11 .1984E-13-.1822E-11 .1133E-11-.9851E-12 .1355E-11-.8393E-12 .1448E-11
-.1461E+08-.2919E+08 .3367E+08 .1067E+09-.1906E+08-.2897E+08-.4024E-10-.8556E-09
-.1308E-09-.3130E-10-.8934E-10-.1408E-10
-.5522E-08 .7808E-10-.3527E-08-.1168E-09-.9550E-09-.1204E-09-.2348E-09-.2399E-10
-.5398E-10 .3167E-12-.2891E-10 .1798E-10-.1563E-10 .2150E-10-.1332E-10 .2298E-10
-.5798E-08-.2575E-10-.9572E+08-.1906E+08 .2075E+09 .3367E+08-.9720E+08-.1461E+08
-.2346E-08-.1716E-09-.1533E-08-.1457E-09
-.3299E-09-.5236E-09-.7539E-10-.3086E-09-.5714E-10-.8027E-11-.1415E-10-.1445E-11
-.3253E-11 .1859E-13-.1742E-11 .1083E-11-.9411E-12 .1294E-11-.8013E-12 .1383E-11
-.3499E-09-.7501E-09-.1461E+08-.2897E+08 .3367E+08 .1067E+09-.1906E+08-.2942E+08
-.7417E-10-.9086E-10-.6361E-10-.2804E-10
-.3920E-08-.2008E-09-.4622E-08 .7004E-10-.1225E-08-.1538E-09-.3010E-09-.3076E-10
-.6921E-10 .4064E-12-.3707E-10 .2306E-10-.2004E-10 .2756E-10-.1708E-10 .2946E-10
-.4034E-08-.2198E-09-.5222E-08-.4024E-10-.9720E+08-.1906E+08 .3120E+09 .3367E+08
-.7316E+07-.1461E+08-.1987E-08-.1727E-09
-.3217E-09-.1243E-09 .1069E-09-.1082E-08-.1013E-09-.1569E-10-.2526E-10-.2576E-11
-.5807E-11 .3232E-13-.3109E-11 .1930E-11-.1678E-11 .2306E-11-.1428E-11 .2464E-11
-.3331E-09-.1915E-09-.3203E-09-.8556E-09-.1461E+08-.2942E+08 .3367E+08 .1601E+09
-.1906E+08-.2417E+08-.6284E-10-.8398E-10
-.1955E-08-.3155E-09-.4255E-08 .1591E-09-.2621E-08-.9747E-10-.6163E-09-.6337E-10
-.1417E-09 .9710E-12-.7596E-10 .4754E-10-.4127E-10 .5689E-10-.3538E-10 .6089E-10
-.1936E-08-.2660E-09-.1994E-08-.1308E-09-.2346E-08-.7417E-10-.7316E+07-.1906E+08
 .2075E+09 .3367E+08-.7316E+07-.1461E+08
-.2007E-09-.1126E-10-.5715E-10-.1066E-08-.5074E-10-.2755E-09-.4506E-10-.4153E-11
-.1039E-10-.1006E-12-.5461E-11 .3066E-11-.2714E-11 .3583E-11-.2072E-11 .3742E-11
-.1958E-09-.1149E-10-.1748E-09-.3130E-10-.1716E-09-.9086E-10-.1461E+08-.2417E+08
 .3367E+08 .1067E+09-.1906E+08-.2417E+08
-.1288E-08-.2042E-09-.2737E-08-.8671E-10-.3992E-08 .1027E-09-.9083E-09-.9383E-10
-.2087E-09 .1588E-11-.1120E-09 .7043E-10-.6110E-10 .8436E-10-.5261E-10 .9038E-10
-.1275E-08-.1725E-09-.1309E-08-.8934E-10-.1533E-08-.6361E-10-.1987E-08-.6284E-10
-.7316E+07-.1906E+08 .1038E+09 .3367E+08
-.1372E-09-.1635E-10-.1946E-09-.2857E-09 .1433E-09-.9919E-09-.8704E-10-.7201E-11
-.2014E-10-.4882E-12-.1039E-10 .5220E-11-.4722E-11 .5935E-11-.3121E-11 .6013E-11
-.1351E-09-.1433E-10-.1318E-09-.1408E-10-.1457E-09-.2804E-10-.1727E-09-.8398E-10
-.1461E+08-.2417E+08 .3367E+08 .5337E+08
    12
    30-2.0       -7.0
    43-11.0      -44.0
    44-22.25     -89.0
    46-35.0      -8.75
```

```
53-33.8       -134.0
54-45.1       -180.0
55-56.75      -227.0
56-68.0       -272.0
57-79.50      -318.0
58-91.40      -365.0
59-100.0      -396.0
60-90.0       -210.0
```

CDTOT 728